The role of the bioactive lipid mediator sphingosine-1-phosphate in aortic aneurysm formation

Inaugural-Dissertation

Zur Erlangung des Doktorgrades
der Mathematisch-Naturwissenschaftlichen Fakultät
der Heinrich-Heine-Universität Düsseldorf

vorgelegt von
Nathalie Hannelore Schröder
geboren am 16.10.1992 in Kyritz

Düsseldorf, October 25

aus dem Institut für Molekulare Medizin III
der Heinrich-Heine-Universität Düsseldorf

Gedruckt mit der Genehmigung der
Mathematisch-Naturwissenschaftlichen Fakultät der
Heinrich-Heine-Universität Düsseldorf

Berichterstatter:

1. Prof. Dr. Bodo Levkau

2. Prof. Dr. Hubert Schelzig

Tag der mündlichen Prüfung 01.07.2026

Table of Content

List of Figures

List of Tables

List of Abbreviations

AAA	Abdominal aortic aneurysm
AA	Aortic aneurysm
ACER	Alkaline ceramidase
ACh	Acetylcholine
Acta2; ACTA2	Smooth muscle actin
AD	Aortic dissection
Ang II	Angiotensin II
APCI	Atmospheric pressure chemical ionization
ApoM	Apolipoprotein
AUC	Area under the curve
AV	Atrioventricular
BSA	Bovine Serum Albumin
Ca^{2+}	Calcium
$[Ca^{2+}]_i$	Intracellular calcium
CAD	Coronary artery disease
CD	Cluster of differentiation
cDNA	Complementary DNA
Cer	Ceramide
CERT	Ceramide transfer protein
Col	Collagen
CPM	Counts per million
CT	Computed tomography
DAG	Diacylglycerol
DEG	Differential expressed genes
dhCer	Dihydro ceramide
DMSO	Dimethylsulfoxide
DOP	4-Deoxypyridoxin
ECL	Enhanced chemiluminescence solution
ECM	Extracellular matrix

EDTA	Ethylenediaminetetraacetic acid
Eln	Elastin
eNOS	Endothelial nitric oxide synthase
ET-1	Endothelin
EtOH	Ethanol
ER	Endoplasmatic reticulum
ERK1/2	Extracellular signal-regulated protein kinase 1 and 2
ESI	Electrospray ionization
ESI-MS	Electrospray ionization mass spectrometry
EVAR	Endovascular aneurysm repair
FACS	Fluorescence activated cell sorting
FBS	Fetal bovine serum
FDR	False discovery rate
FTY720	Fingolimod
Gapdh;GAPDH	Glyceraldehyde 3-phosphate dehydrogenase
GO	Gene ontology
GPCR	G-protein coupled receptor
GSEA	Gene set enrichment analysis
HDL	High-density lipoprotein
HPLC	High performance liquid chromatography
ICAM-1	Intercellular adhesion molecule
IHC	Immunohistochemistry
IL	Interleukin
Indo	Indomethacin
IP3	Inositol triphosphate
KEGG	Kyoto encyclopaedia of genes and genomes
KLF4	Krüppel-like factor 4
LC-MS/MS	Liquid chromatography coupled with tandem mass spectrometry
LGALS3	Galectin 3
Lox; LOX	Lysyl oxidase
LPC	Lysophosphatidylcholine

LPE	Lysophosphatidylethanolamine
MAPK	Mitogen-activated protein kinase
MeOH	Methanol
MFSD2B	Major facilitator superfamily domain-containing protein 2 B
MLC	Myosin light chain
MLCK	Myosin light chain kinase
MLCP	Myosin light chain phosphatase
MMP	Matrix metalloproteinase
MS	Multiple sclerosis
MS/MS	Tandem mass spectrometry
Myh11; MYH11	Myosin heavy chain 11
NO	Nitric oxide
PAD	Peripheral artery disease
PBS	Phosphate buffered saline
PC	Phosphatidylcholine
PCA	Principal component analysis
PE	Phosphatidylethanolamine
PFA	Paraformaldehyde
p-FTY720	Fingolimod-phosphate
Phe	Phenylephrine
PI3K	Phosphatidylinositol 3-kinase
PKC	Protein kinase C
PLC	Phospholipase C
PVDF	Polyvinylidene fluoride
RBC	Red blood cell
ROC	Receptor-operated channel
ROC curve	Receiver operating characteristic curve
ROS	Reactive oxygen species
RUNX2	Runt-related transcription factor 2
RQN	RNA quality number
S1P	Sphingosine-1-phosphate

S1PR	Sphingosine-1-phosphate receptor
SBP	Systolic blood pressure
SEM	Standard error of mean
SGPL1	Sphingosine-1-phosphate lyase
SM	Sphingomyelin
SOCE	Store-operated calcium channel
SPNS2	Sphinster homolog 2
Sph	Sphingosine
SphK	Sphingosine kinase
SPP	Sphingosine-1-phosphate phosphatase
SRF	Serum response factor
TAA	Thoracic aortic aneurysm
Tagln; TAGLN	Transgelin, Smooth muscle 22 alpha
TEMED	N, N, N', N'-Tetramethylethylendiamin
TFA	Trifluoroacetic acid
TGF	Transforming growth factor
TGFBR	Transforming growth factor beta receptor
TIMP	Tissue inhibitors of metalloproteinases
TNF	Tumor necrosis factor
TPM	Transcripts per million
TRP	Transient receptor potential
UMI	Unique molecular identifiers
VCAM-1	Vascular cell adhesion molecule-1
VOCC	Voltage-operated calcium channel
VSMC	Vascular smooth muscle cell
WT	Wild type
WTD	Western type diet
WB	Western Blot

Summary

The endogenous bioactive sphingolipid sphingosine-1-phosphate (S1P) acts through five G protein-coupled receptors, collectively known as sphingosine-1-phosphate receptors (S1PRs), which regulate various cardiac and vascular functions. Although dysregulated S1P levels have been associated with several cardiovascular diseases, their contribution to aortic aneurysm pathophysiology remains poorly defined.

Experimental approaches of this study included the murine Angiotensin II (Ang II) infusion model which was combined with pharmacological elevation of S1P levels and genetic deletion of specific S1PRs to investigate their contribution to aneurysm formation. Pharmacological interventions comprised inhibition of S1P lyase and treatment with the clinically approved S1PR modulator FTY720. In addition, *in vitro* studies using primary vascular smooth muscle cells (VSMCs) were conducted to delineate S1PR-specific signalling mechanisms. As a translational approach, sphingolipidomic analysis of plasma and aortic tissue samples from patients with abdominal aortic aneurysms was performed to identify disease-associated alterations in sphingolipid profile.

Ang II-infused mice with pharmacologically elevated S1P levels showed a marked increase in mortality due to rupture, severe aortic dissections, loss of contractile VSMC genes, and increased vascular hypercontractility. RNA sequencing and proteomic analyses revealed pronounced downregulation of several molecular pathways associated with vascular homeostasis, smooth muscle contraction, and extracellular matrix organization, collectively contributing to vascular instability.

To identify S1PR-specific mechanisms underlying these effects, *in vitro* experiments using primary VSMCs demonstrated that S1P signalling regulated contractile gene expression in a receptor-dependent manner, with acute S1PR2 activation promoting upregulation, whereas tonic activation of S1PR1 and S1PR3 contributed to downregulation. Consistent with these findings, Ang II-infused S1PR3-deficient mice exhibited protection against rupture-associated mortality, preservation of the contractile VSMC phenotype, and reduced vascular responsiveness to vasoconstrictors. In contrast, S1PR2-deficient mice did not display protection against aneurysm formation, rupture, or alterations in vascular reactivity.

Supporting these *in vivo* observations, *in vitro* studies showed that activation of S1PR3 under elevated S1P conditions sensitized VSMCs to Ang II, resulting in exaggerated

intracellular calcium responses and increased myosin light chain phosphorylation, effects that were abolished upon S1PR3 inhibition. This demonstrates, that S1PR3 is involved in Ang II-induced vascular alterations.

The clinically approved S1PR modulator FTY720, acting as a functional antagonist on multiple S1PRs, was evaluated as a potential therapeutic approach in the murine Ang II model. FTY720 treatment did not alter aneurysm formation, rupture incidence, or vascular function.

As a translational approach, sphingolipid profiles were analysed in plasma and aortic tissue samples from patients with aortic aneurysms. Comprehensive sphingolipidomic profiling revealed distinct alterations in lipid composition in both compartments. S1P levels were significantly elevated in plasma and aortic tissue of aneurysm patients, and in plasma, S1P emerged as a potential discriminatory marker distinguishing individuals with aneurysms from those without. Moreover, increased expression of S1PR1-3 was detected in aortic tissue from patients with aortic aneurysms.

In summary, this study provided comprehensive experimental and translational evidence linking S1P/S1PR signalling to the pathophysiology of aortic aneurysms. Specifically, pharmacological elevation of systemic S1P levels aggravated aneurysm rupture and vascular dysfunction through S1PR3 activation, whereas genetic loss of S1PR3 prevented these effects and preserved vascular integrity. By integrating *in vivo*, *in vitro*, and human data, this study established S1P as a central regulator of vascular integrity and remodelling. These findings advanced the understanding of sphingolipid-mediated mechanisms in aneurysm disease and emphasize the potential of targeting S1P signalling for therapeutic intervention and disease stabilization.

Zusammenfassung

Das endogene bioaktive Sphingolipid Sphingosin-1-Phosphat (S1P) vermittelt über fünf G-Protein-gekoppelte Rezeptoren, die als Sphingosin-1-Phosphat Rezeptoren (S1PRs) bezeichnet werden, eine Vielzahl kardialer und vaskulärer Funktionen.
Obwohl dysregulierte S1P-Spiegel mit verschiedenen kardiovaskulären Erkrankungen assoziiert sind, ist der Einfluss von S1P auf die Pathophysiologie von Aortenaneurysmen bislang unzureichend erforscht.
Experimentelle Ansätze dieser Arbeit umfassten das murine Angiotensin II (Ang II)-Infusionsmodell, das mit einer pharmakologischen Erhöhung der S1P-Spiegel moduliert wurde oder das an verschiedenen S1PR-defizienten Mäusen durchgeführt wurde. Dadurch wurde der Einfluss von S1P und seiner Rezeptoren auf die Aneurysmenbildung untersucht. Zu den untersuchten pharmakologischen Interventionen zählte die Inhibition der S1P-Lyase, sowie die Behandlung mit dem klinisch zugelassenen S1PR-Modulator FTY720. Zusätzlich wurden *in vitro* Studien mit primären Gefäßmuskelzellen (VSMCs) durchgeführt, um S1PR-spezifische Signalmechanismen zu charakterisieren. Als translationaler Ansatz wurde eine Sphingolipidom Analyse von Plasma- und aortalen Gewebeproben von Patient:innen mit abdominalen Aortenaneurysmen durchgeführt, um krankheitsassozierte Veränderungen im Sphingolipidprofil zu identifizieren.
Ang II-behandelte Mäuse mit pharmakologisch erhöhten S1P-Spiegeln zeigten eine deutlich erhöhte Mortalität infolge von Rupturen, ausgeprägtere Aortendissektionen, einen Verlust kontraktiler VSMC-Gene, sowie eine gesteigerte vaskuläre Hyperkontraktilität. Transkriptom- und Proteom-Analysen zeigten eine ausgeprägte Herunterregulation mehrerer molekularer Signalwege, die mit vaskulärer Homöostase, glatter Muskelkontraktion und extrazellulärer Matrixorganisation assoziiert sind und gemeinsam zur Gefäßinstabilität beitragen.
Zur Identifizierung der zugrundeliegenden S1PR-spezifschen Mechanismen zeigten *in vitro* Experimente mit VSMCs, dass S1P die Expression kontraktiler Gene rezeptorabhängig reguliert. Eine akute Aktivierung von S1PR2 führte zu einer Hochregulation, während eine tonische Aktivierung von S1PR1 und S1PR3 eine Herunterregulation bewirkte.
Im Einklang mit diesen Befunden waren Ang II-behandelte S1PR3-defiziente Mäuse vor rupturbedingter Mortalität geschützt. Gleichzeitig zeigten sie einen erhaltenen

kontraktilen VSMC-Phänotyp sowie eine verringerte vaskuläre Reaktivität auf verschiedene Vasokonstriktoren. Im Gegensatz dazu zeigten S1PR2-defiziente Mäuse keinen Schutz vor Aneurysmenbildung, Ruptur oder Veränderungen der vaskulären Reaktivität. Weiterhin zeigten die VSMCs *in vitro* nach Aktivierung von S1PR3 unter erhöhten S1P-Spiegeln eine Sensibilisierung gegenüber Ang II, was sich durch verstärkte intrazelluläre Calciumfreisetzung äußerte und zu einer erhöhten Myosin-Leichtekettenphosphorylierung führte. Die Effekte waren unter Inhibition von S1PR3 aufgehoben. Das zeigt, dass S1PR3 an den durch Ang II induzierten vaskulären Veränderungen beteiligt ist.

Der klinisch zugelassene S1PR-Modulator FTY720, der als funktionaler Antagonist an mehreren S1PRs wirkt, wurde im murinen Angiotensin II Modell als potenzieller therapeutischer Ansatz untersucht. Die Behandlung mit FTY720 beeinflusste jedoch weder die Aneurysmenbildung noch die Rupturrate oder die Gefäßfunktion.

Als translationaler Ansatz wurden Sphingolipidprofile in Plasma- und Aortenproben von Patient:innen mit Aortenaneurysmen analysiert. Die umfassende Sphingolipidom Analyse zeigte in beiden Kompartimenten deutliche Veränderungen der Lipidzusammensetzung. Im Plasma und im Aortengewebe von Aneurysma-Patient:innen waren die S1P-Spiegel signifikant erhöht, wobei S1P im Plasma als potenzieller diskriminierender Marker zur Unterscheidung von Patient:innen mit und ohne Aneurysma identifiziert wurde. Darüber hinaus wurde eine erhöhte Expression von S1PR1-3 im humanen Aortengewebe nachgewiesen.

Zusammenfassend liefert diese Studie umfassende experimentelle und translationale Evidenz für die Beteiligung der S1P/S1PR-Signalgebung an der Pathophysiologie von Aortenaneurysmen. Insbesondere verschärfte eine pharmakologische Erhöhung systemischer S1P-Spiegel die Mortalität durch Rupturen sowie die durch S1PR3-Aktivierung vermittelte vaskuläre Dysfunktion. Der genetische Verlust von S1PR3 verhinderte dagegen diese Effekte und bewahrte die Gefäßintegrität. Durch die Integration von *in vivo*-, *in vitro*- und Humandaten identifiziert die Arbeit S1P als einen zentralen Regulator der Gefäßintegrität. Diese Ergebnisse vertiefen das Verständnis sphingolipid-vermittelter Mechanismen bei Aortenaneurysmen und unterstreichen das Potenzial einer therapeutischen Modulation der S1P-Signalgebung zur Krankheitsintervention und -stabilisierung.

1. Introduction

1.1. Aortic aneurysm and aortic dissection

1.1.1. Definition and classification

In 2024, the aorta was defined as an independent organ[1]. It is the largest artery in the human body that carries oxygen-rich blood from the heart to the rest of the body[1]. Anatomically, the aorta is composed of five distinct sections: the aortic root, the ascending aorta, the aortic arch, the descending thoracic aorta, and the abdominal aorta[1]. At its distal end, the abdominal aorta terminates with the bifurcation into the common iliac arteries[1]. All sections originate from different embryonic sources[1]. Starting from the aortic valve, the aortic root originates from the secondary heart field[1]. The ascending aorta and the aortic arch originate from neural crest-derived structures[1]. In contrast the descending aorta, including the thoracic segment down to the diaphragm and the abdominal aorta, have a mesenchymal origin[1,2] (Figure 1). These segments exhibit distinct physicomechanical properties and differ in their cellular and extracellular composition[2]. Structurally, the aortic wall is composed of three layers[1]. The internal layer, the intima, consists mainly of endothelial cells. The media, the middle layer is composed of elastic fibres and vascular smooth muscle cells (VSMCs), which are the predominant cell population in the aorta. The final layer, the adventitia is mainly composed of collagen and fibroblasts[1]. Endothelial cells regulate vascular tone and immune interactions, VSMCs ensure contractility and wall stability, and adventitial fibroblasts maintain extracellular matrix homeostasis, with collagen fibres providing structural integrity and mechanical support[3].

Highly relevant pathologies of the aorta, are aortic aneurysms (AA) and dissections (ADs) in the different aortic segments. Generally, an aortic aneurysm is defined as a localized dilation of the aorta, characterized by an increase in diameter exceeding 1.5-fold to normal diameter[4]. Classified by their localization, aortic aneurysms can be distinguished into thoracic aortic aneurysms (TAA) and abdominal aortic aneurysms (AAA)[5]. According to their morphology, aortic aneurysms are classified as fusiform, defined as a general dilation of the aorta, or as saccular, where only one side of the aortic wall is dilated[6]. An aortic dissection is defined by a tear in the intimal layer of the aortic wall, allowing blood to enter the media, which ends up forming a false lumen[1]. In recent decades, multiple classification systems for dissections have been

developed[1]. Historically, the DeBakey and Stanford classifications have become well-established, with the Stanford classification being more commonly utilized in clinical settings[7,8]. These classifications primarily rely on the localization of the dissection as the fundamental criterion for definition[7].

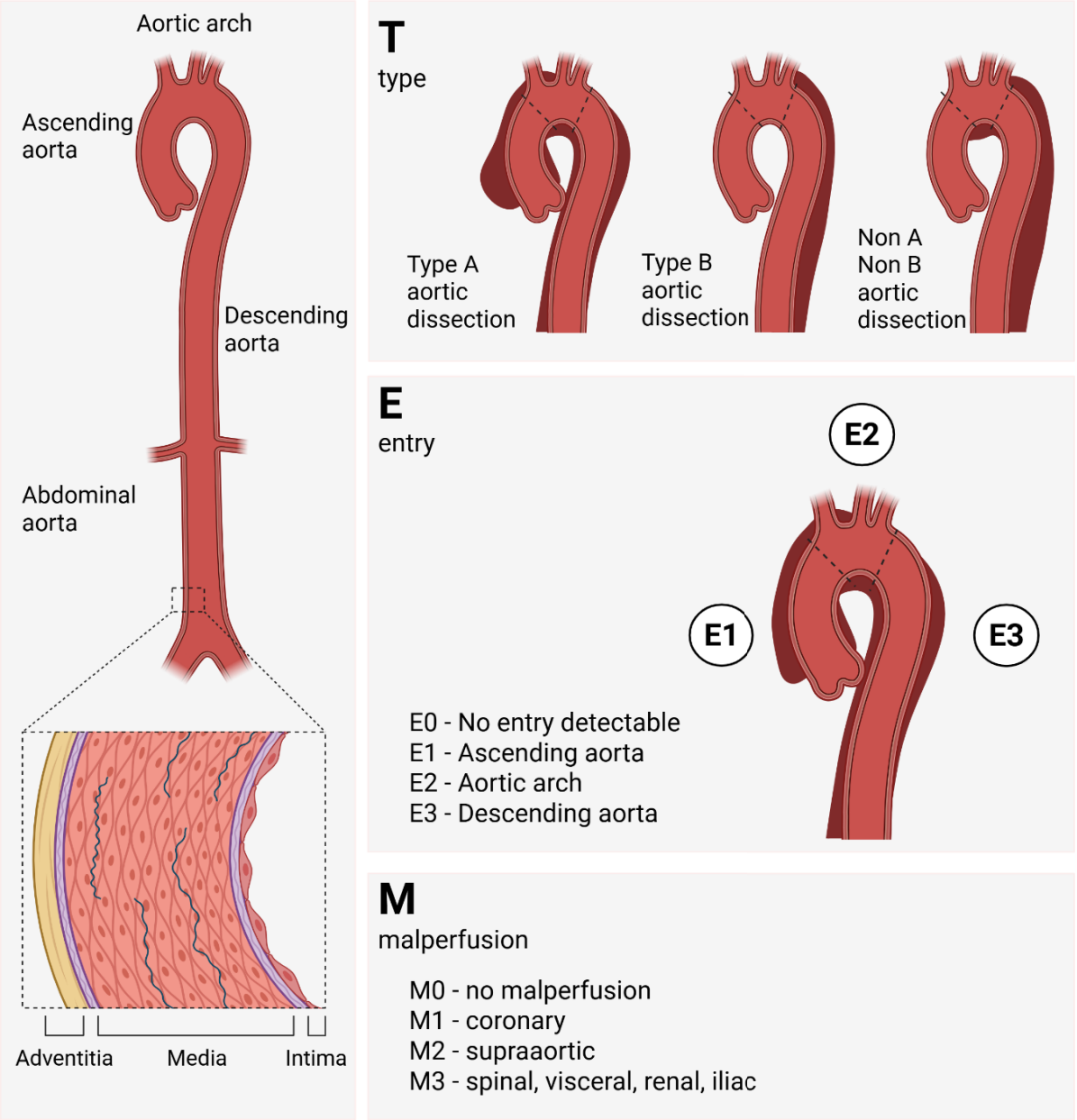

Figure 1: Overview of aortic anatomy and classification of aortic dissection. Anatomical illustration of the aorta with its different sections and its wall layer structure consisting of the adventitia, media and intima (left). TEM (Type/Entry/Malperfusion) classification of aortic dissection illustrated in 3 images (right). T - Classification by dissection type: Type A involves in the ascending aorta, Type B originates in the descending aorta, and Non A/Non B dissection originates in the aortic arch without involving the ascending or descending aorta. E - Classification based on the location of the primary entry tear: E0 (no entry detectable), E1 (ascending aorta), E2 (aortic arch), E3 (descending aorta). M - Status of malperfusion: M0 (no malperfusion), M1 (coronary malperfusion), M2 (supraaortic malperfusion), M3 (malperfusion of spinal, visceral, renal or iliac arteries). Adapted and redrawn from Czerny *et al.*[1]. Created with BioRender.com. Published under BioRender Publication Licence.

In general Stanford Type A is defined as an aortic dissection in the ascending aorta, whereas Stanford Type B dissections are located in the descending aorta often originating distal to the left subclavian artery[9,10]. In addition to the traditional Stanford classification, an intermediate type has been described[9]. The Non-A/Non-B aortic dissection refers to all types that do not fit into the classical categorization[9]. This category includes dissections originating from the aortic arch, which do not conform to the traditional classification scheme[9].

Since the introduction of new guidelines for the diagnosis and treatment of acute and chronic syndromes of the aorta, an extension of the Stanford classification has been recommended, known as the Type/Entry/Malperfusion (TEM) classification[1,11]. The categorization provides a more detailed assessment of aortic dissections[1]. The first component of the TEM classification reflects the anatomical localization of the dissection, following the principle of the Stanford system (T)[1]. Subsequently, it defines the primary entry point (E) based on its location[1]. If the entry point cannot be clearly identified, it is denoted as E0[1]. If located in the ascending aorta, it is classified as E1[1]. An entry point in the aortic arch is designated as E2, and one in the descending aorta is labelled as E3[1]. Furthermore, this classification also considers malperfusion, categorizing it into four subcategories based on the involvement of surrounding vessels[1]. The absence of malperfusion is denoted as M0[1]. If the coronary arteries are affected, it is classified as M1[1]. Involvement of supra-aortic branches is designated as M2[1]. Typically, M3 represents visceral/renal or lower limb malperfusion[1] (Figure 1).

1.1.2. Incidence, diagnosis and treatment

Numerous studies have been conducted on the incidence of aortic aneurysms and dissections. In several industrialized nations, including the United States and Europe, aortic aneurysms are ranked as the 12th to 15th leading cause of death among the elderly population[12,13]. The reported 30-day mortality rate varies from less than 11% to almost 75%[14,15]. A study in Sweden showed that, on average, 15 aortic dissections, 27 AAAs, and 9 TAAs develop in 100,000 high-risk patients[14]. In this study, individuals with pre-existing cardiovascular conditions, such as atherosclerosis or hypertension, are generally considered high-risk patients for vascular complications[14,16]. Furthermore, the study also demonstrated that the acute and hospital mortality rate for ADs was 39%, 41% for ruptured TAAs, and 34% for ruptured AAA[14]. Smoking, a higher age, male sex, or hereditary factors promote the risk of aneurysm formation[14,16,17].

With respect to gender differences, sex-specific disparities in aortic pathology have been reported, showing a higher prevalence of aneurysm formation in men[18-21]. Compared to men, aortic aneurysms of women tend to have higher growth rates, and an increased risk of rupture is usually already present in aneurysms with a smaller diameter[21-24]. Furthermore, there is an elevated risk of mortality among female patients following surgical intervention due to aortic aneurysms[25-27]. However, it should be noted that in many vascular studies, including those on aortic aneurysms, women are underrepresented as a group[28,29].

While gender-specific differences provide important indications of risk factors, the familial background is also crucial for the pathophysiology of aortic aneurysms, especially for thoracic aneurysms[30]. Around 20% of TAAs are hereditary, with the majority being inherited in an autosomal dominant manner[31]. The remaining cases are classified as sporadic aneurysms[31]. Hereditary aneurysms can be further subdivided into syndromic and non-syndromic forms[30]. Syndromic aneurysms include diseases such as Marfan syndrome, Ehlers-Danlos syndrome, and Loeys-Dietz syndrome, in which not only the cardiovascular system is affected, but also other organ systems such as the skin, eyes or skeleton[30]. In addition to these, there are familial, non-syndromic forms in which the cardiovascular system is primarily affected without other organ systems being involved[30]. Here, causative genes, including alpha-smooth muscle actin (ACTA2), myosin heavy chain 11 (MYH11), myosin light chain kinase (MLCK) or lysyl oxidase (LOX) have been identified[32-36]. In general, the genetic changes in hereditary aneurysms can often be linked to specific gene families, especially those involved in the extracellular matrix, the transforming growth factor-beta (TGF-β) signaling pathway or in the composition or function of the cytoskeleton or the smooth muscle contraction apparatus[30,37].

The incidence of aortic aneurysms and dissections varies significantly across studies. One reason is that aortic aneurysms often occu asymptomatically, which makes epidemiological assessment difficult[5,38]. Another reason is that the prevalence is largely attributed to the diagnostic requirements, which necessitate adequate consecutive imaging modalities[39]. Specifically, a minimum of transthoracic echocardiography is essential, while computed tomography (CT) scans or magnetic resonance angiography are considered optimal for accurate diagnosis[40,41]. These imaging techniques are indispensable prerequisites for reliable detection and

characterization of aortic aneurysms and dissections[41]. But despite the importance of early diagnosis, a considerable number of aneurysms and dissections are diagnosed only after the patient develops symptoms like abdominal, chest, or back pain[40,41].

To date, no pharmacological intervention has been identified that can effectively prevent or regress the formation of aortic aneurysms. The present state of therapy primarily focuses on the treatment of associated symptoms and risk factors, such as hyperlipidaemia, obesity, smoking or hypertension[1]. Strict blood pressure control is crucial to mitigate aortic wall stress, thereby slowing aneurysm growth and reducing the risk of rupture[1]. This is typically achieved through antihypertensive therapy, which helps to lower systolic blood pressure to a target range of 100-120 mmHg and maintains a heart rate between 60-80 bpm[1]. In most cases, surgical intervention represents the most effective treatment strategy[1]. However, determining the optimal intervention timing requires a careful anatomical assessment of aortic aneurysms or dissections[42]. The decision to proceed with surgical intervention for aortic aneurysms typically depends on the localization and aneurysm diameter. In general, an intervention is necessary once the diameter reaches 5-5.5 cm[1,42,43]. For hereditary aneurysms, surgical interventions are usually carried out at a smaller diameter, since those aneurysms often show a higher growth rate[1,43]. This typically involves either an open surgical repair or an endovascular aneurysm repair (EVAR)[6]. Open surgical repair replaces the affected aortic segment with a synthetic graft via direct surgery. EVAR, by comparison, is a minimally invasive approach that places a stent graft inside the vessel to exclude the aneurysm from the bloodstream and prevent its progression or rupture[6].

1.1.3. Pathophysiology

The pathophysiology of aortic aneurysms is highly complex, involving endothelial dysfunction, breakdown of the extracellular matrix (ECM), inflammation, oxidative stress, and phenotypic switching of vascular smooth muscle cells (VSMCs)[5,44]. An interplay of these mechanisms drives alterations in aortic wall integrity and stability, which promote aneurysm formation and potential rupture (Figure 2)[5,44].

Endothelial dysfunction is a key initiating and perpetuating factor in the pathophysiology of aortic aneurysms[45]. The endothelium maintains vascular homeostasis by regulating vascular tone, inflammation, and ECM remodelling. In the formation and progression of aneurysms, dysfunction of the endothelial layer

contributes to increased permeability, followed by the infiltration of immune cells and degradation of the aortic wall, ultimately promoting aneurysm expansion and rupture[45]. Endothelial dysfunction can have many causes, including hemodynamic stress or chronic inflammation[46,47]. In line with these alterations, vascular permeability increased further, contributing to the elevation of immune cell infiltration[45,46,48].

One important hallmark of aneurysm formation is the degradation of the extracellular matrix[49]. Under physiological conditions, the ECM plays a fundamental role in maintaining aortic structural integrity, elasticity, and overall vascular function, thereby ensuring the mechanical stability of the aortic wall[49,50]. Major constituents of the ECM network include structural fibres, such as collagen and elastin, together with proteoglycans and various glycoproteins[50]. During aneurysm development, the ECM homeostasis is disrupted, resulting in degradation and loss of organization of all structural components[49,50]. One underlying cause is the imbalance in matrix metalloproteinases (MMPs) and tissue inhibitors of metalloproteinases (TIMPs)[49]. The disruption of elastin, caused by increased MMP-2 and MMP-9 activity, ends up in elastin fragmentation, followed by reduced aortic elasticity, which makes the aorta more prone to rupture[51,52]. Collagen alterations vary depending on the extent of ECM degradation[53]. Increased MMP activity promotes collagen breakdown, while reduced cross-linking further compromises tensile strength of the aortic wall, weakening it. Conversely, as a compensatory response, fibroblasts and VSMCs increase collagen synthesis, leading to aortic stiffening[53-55]. This maladaptive remodelling increases mechanical stress, accelerating aneurysm progression despite the temporary structural reinforcement[53,54].

Next to ECM degradation, vascular inflammation is also involved during aneurysm progression. Initially, immune cells, including macrophages, neutrophils, or T and B cells, infiltrate the vessel wall[56,57]. The release and upregulation of inflammatory cytokines, such as IL-6, TNF-α or IL-1β, drives proteolytic activity, promoting ECM degradation and VSMC apoptosis[44,58,59].

Another important driver of aortic aneurysm formation is oxidative stress[60,61]. As with all the key processes involved in the pathophysiology of aortic aneurysms, the increase in oxidative stress can have multiple causes[60]. For instance, infiltrated immune cells showed increased release of reactive oxygen species (ROS) into the aortic wall[60]. Furthermore, in line with endothelial dysfunction, uncoupled endothelial nitric oxide

synthase (eNOS) shifts from nitric oxide (NO) production to superoxide formation, which further increases oxidative stress[60,62,63].

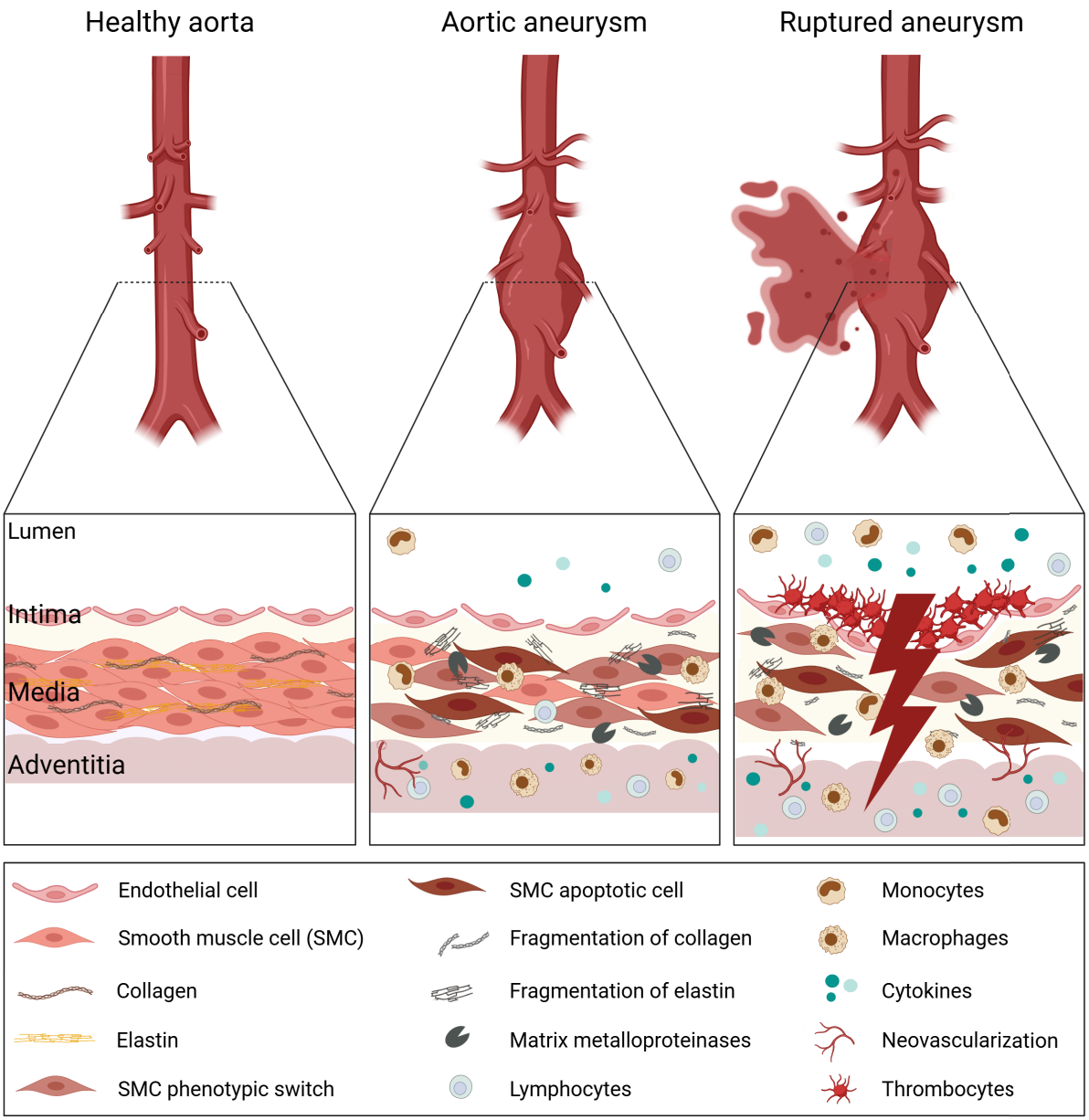

Figure 2: Schematic overview of aneurysm progression. The three panels illustrate the transition from a healthy aorta (left), to early aortic wall changes (middle), to ruptured AAA (right). In the healthy aorta, normal aortic wall structure is maintained with organized vascular smooth muscle cells (SMCs), intact elastin and collagen fibres and absence of inflammation. During aneurysm formation, vascular SMCs undergo phenotypic switch and end up in apoptosis. Extracellular matrix degrades caused by upregulation of matrix metalloproteinases (MMPs) and inflammatory cells enter the vascular wall. In an advanced state, aortic wall could rupture caused by increasing degradation and destabilization of the aortic wall, characterized by the previous cellular processes and increased vascular inflammation, neovascularization and thrombus formation. Adapted from Cho *et al.*[5]. Created with BioRender.com. Published under BioRender Publication Licence.

Under physiological conditions, VSMCs maintain aortic wall integrity by providing mechanical support and regulating vascular tone[64]. One reason for this is the high expression of contractile markers[64]. During aneurysm progression, pathological stimuli such as ECM degradation, chronic inflammation, and oxidative stress trigger VSMC

dysfunction and apoptosis[65]. Furthermore, VSMCs undergo a phenotypic switch, defined by a reduction and loss of their contractile phenotype[64]. As apoptosis increases, the medial layer thins, weakening the structural integrity of the aorta and making it more susceptible to dilation and rupture[65].

1.1.4. The important role of VSMCs in aortic aneurysm pathophysiology

Smooth muscle cells form a key structural element of the aortic wall, with their highest density found in the media[66]. Under physiological conditions, they are essential for maintaining vascular tone, mechanical stability, and structural aortic wall integrity by contributing to ECM synthesis, adaptive remodelling, or vessel contraction[67-72]. VSMCs show high plasticity[71-74]. This is partly due to their different embryonic origins[75,76]. In detail, during vascular homeostasis, VSMCs exhibit a contractile phenotype, defined by their spindle-like morphology and the expression of contractile markers, like ACTA2, MYH11 or smooth muscle 22α (TAGLN)[74,77-80]. The transcriptional control of contractile genes in VSMCs involves several key regulators, notably myocardin, serum response factor (SRF), and Krüppel-like factor 4 (KLF4)[81-83].

Furthermore, a key characteristic of VSMCs is their ability to contract (Figure 3)[84]. This is associated with an increase in intracellular calcium $[Ca^{2+}]_i$[84]. Hereby, vasoconstrictors, such as Ang II or Endothelin-1 (ET-1), bind to G-protein-coupled receptors, which activate phospholipase C (PLC), which drives the production of inositol triphosphate (IP3) and diacylglycerol (DAG)[84,85]. Subsequently, both second messengers induce the mobilisation of calcium (Ca^{2+}) from the sarcoplasmic reticulum and enhance Ca^{2+} entry through plasma membrane channels[86]. This includes the opening of voltage-operated calcium channels (VOCCs), receptor-operated channels (ROCs), store-operated calcium channels (SOCE) pathways, or transient receptor potential (TRP) channels, which further contribute to the increase of $[Ca^{2+}]_i$ levels[86-89]. Afterwards, Ca^{2+} binds to calmodulin and the resulting complex activates MLCK[84,90]. Activated MLCK phosphorylates myosin light chain (MLC), which drives actin polymerization and finally contraction[84].

During aneurysm progression, VSMCs play a central role, as their dysfunction contributes to weakening of the aortic wall through phenotypic switching, increased apoptosis, ECM degradation and hypercontractility[91,92]. It is well known that VSMCs can switch from a contractile state, defined by a high expression of contractile genes,

to a synthetic phenotype in response to various stimuli during vascular diseases like atherosclerosis, hypertension, or restenosis[93,94]. In the context of aortic aneurysm formation, phenotypic switching of VSMCs is an early feature that occurs[95]. To date, several different VSMC phenotypes with distinct gene expression patterns, have been identified under various pathophysiological conditions[96]. From the intermediate synthetic phenotype, VSMCs could end up as mesenchymal, osteogenic, fibroblast, macrophage, and adipocyte-like VSMCs, but further phenotypes are under investigation[96,97]. A mesenchymal-like VSMC is characterized as a cell with higher proliferative potential, lower expression of contractile markers, increased expression of mesenchymal stem cell markers, and the possible capacity to differentiate into other VSMC phenotypes[97-99]. Furthermore, VSMCs can differentiate into osteogenic-like or chondrocyte-like cells under pathophysiological conditions[96]. These cell types are characterized by their upregulation of osteogenic markers, including Runt-related transcription factor 2 (RUNX2) or Osteocalcin, and are key drivers of vascular calcification[100-102]. Furthermore, fibroblast-like or myofibroblast-like VSMCs are described as cells with an increase in a subset of fibroblast-related genes and their involvement in ECM remodelling and fibrotic processes[96,103,104]. Macrophage-like VSMCs are associated with an increase in macrophage markers, including CD68 and Galectin 3 (LGALS3), and show pro-inflammatory properties, such as cytokine release or phagocytic activity[105,106]. Additionally, they are also involved in lipid accumulation, as they internalize cholesterol and differentiate further to foam cells[107,108]. Similarly, VSMCs can also differentiate directly into adipocyte-like VSMCs, which are characterized by lipid accumulation[109].

Next to phenotypic alterations, VSMCs undergo apoptosis during aneurysm progression, which leads to a loss of medial thickness and by that to aortic wall instabity[110-112]. Diverse mechanisms during disease progression can drive VSMC apoptosis[91]. One important aspect is the infiltration of inflammatory cells, and the increasing inflammation status caused by increasing cytokine release[113,114]. Additionally, increasing oxidative stress, such as ROS production, is another factor that drives VSMC death[115,116]. It is important to note that oxidative stress in VSMCs can further drive VSMC inflammation and MMP activation[117]. In detail, VSMCs secrete multiple inflammatory cytokines, such as IL-6 or IL-1β, which promote further infiltration of inflammatory cells[118]. In parallel, oxidative stress and inflammation promote the expression and activation of MMPs[117]. The matrix-metalloproteinases, MMP-2 and

MMP-9, are increased in VSMCs during aortic aneurysm progression and contribute to ECM degradation[119,120].

An important function of VSMCs is the production of ECM components, such as collagens, proteoglycans or elastin[65]. The coordinated interaction between VSMCs and these extracellular matrix elements is crucial for maintaining the architecture, stability, elasticity and function of the vessel wall[91,121]. When this homeostatic balance is disturbed, as observed during aortic aneurysm formation, VSMCs contribute to the pathological remodelling of the vascular wall[91]. In addition to MMPs, VSMCs synthesise further proteolytic enzymes such as cathepsins and A disintegrin and metalloproteases (ADAMs), which degrade ECM components[122-124].

Moreover, transforming growth factor-beta (TGF-β) represents an additional regulatory component that modulates VSMC function and differentiation[125]. VSMC-derived TGF-β contributes to ECM production and maintaining aortic wall integrity[125]. There are three different isoforms of TGF-β (TGF-β1, TGF-β2, TGF-β3), which signal through the formation of complexes between TGF-β type I and type II receptors[126]. Upon activation, TGF-β receptors induce the phosphorylation of downstream mediators of the SMAD family, leading to the formation of different SMAD complexes[126]. These complexes subsequently translocate into the nucleus, where they function as transcription factors to regulate diverse target genes involved in various cellular processes maintaining vascular homeostasis[125,126]. During aortic aneurysm formation TGF-β signaling is dysregulated[127]. These dysregulated signaling can enhance VSMC proliferation, increase the expression of MMPs and proteolytic enzymes, and disorganize ECM production[5]. Moreover, mutations in genes encoding components of the TGF-β signaling pathway, such as transforming growth factor-beta receptors (TGFBR1, TGFBR2) and SMAD3, have been identified in patients with familial thoracic aortic aneurysms, underscoring their relevance in disease pathogenesis[128-132]. In mouse models, both inhibition and overactivation of TGF-β signaling have resulted in aneurysm formation, highlighting its context-dependent and biphasic role[133-136]. Furthermore, it has been shown that mice lacking TGFBR1 or TGFBR2 develop vascular dysfunction and exhibit an increased susceptibility to aortic aneurysm formation[137-139].

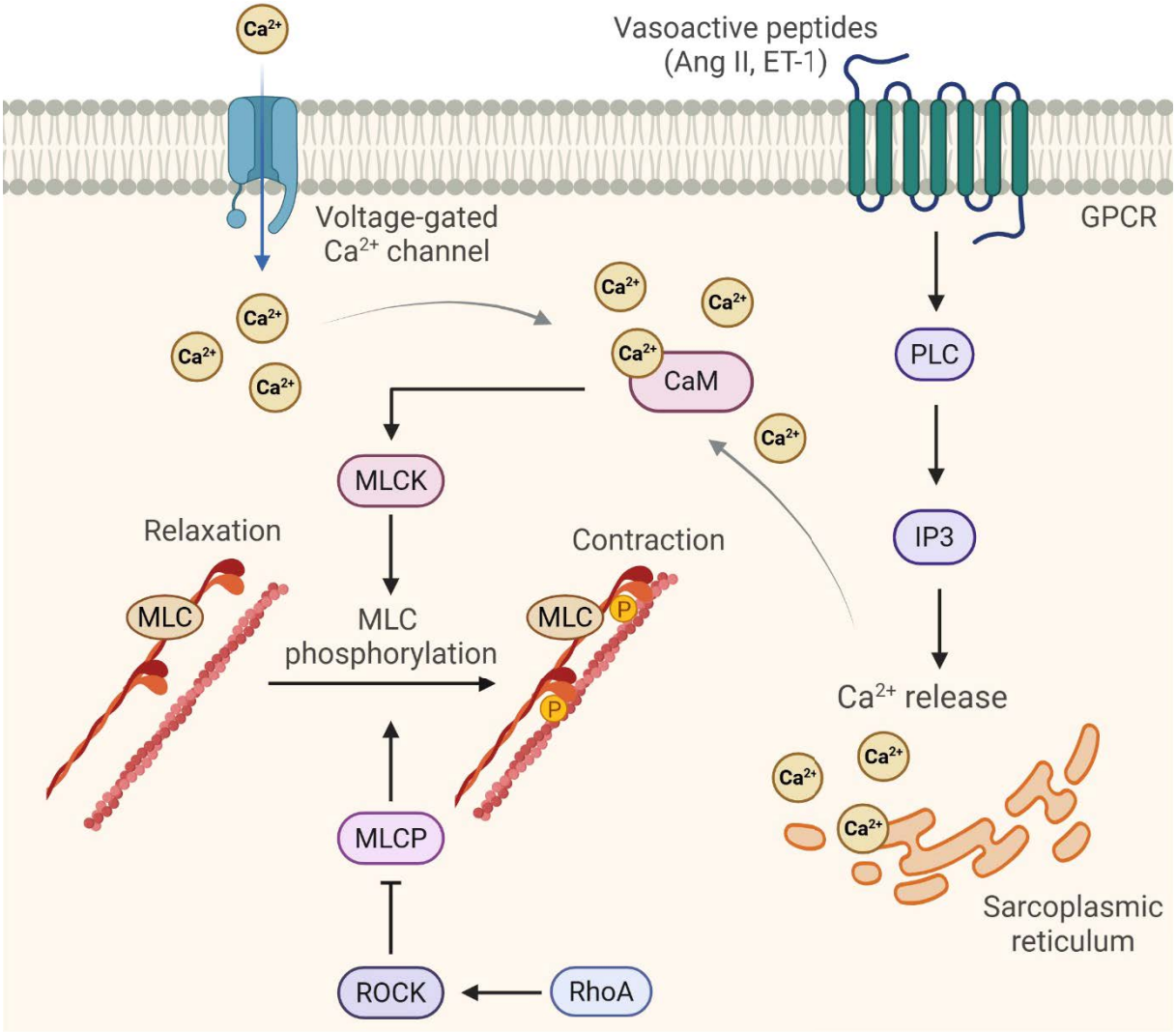

Figure 3: Simplified overview of smooth muscle cell contraction. Binding of vasoactive peptides (e.g. Ang II or ET-1) to G-protein coupled receptors (GPCRs) stimulate phospholipase C (PLC), which catalyses the generation of inositol 1,4,5-trisphosphate (IP3). IP3 induces intracellular calcium (Ca^{2+}) release from sarcoplasmic stores, increasing cytosolic Ca^{2+} levels. Furthermore, opening of voltage-gated Ca^{2+} channels raise also intracellular Ca^{2+} levels. Ca^{2+} binds to calmodulin (CaM), activating myosin light chain kinase (MLCK), which phosphorylates myosin light chains (MLC) and promotes actomyosin-based contraction. Concurrently, activation of the small GTPase RhoA leads to Rho-associated kinase (ROCK) activation, which inhibits myosin light chain phosphatase (MLCP), thereby sustaining MLC phosphorylation and contraction. Reduced intracellular Ca^{2+} levels and MLCP activity (dephosphorylation of MLC) favor relaxation. Created with BioRender.com. Published under BioRender Publication Licence.

Another phenomenon of VSMCs under pathophysiological conditions is their ability to develop a hypercontractile state[92]. In case of hypertension, it has been shown that increased $[Ca^{2+}]_i$ levels enhance calcium-dependent contraction through increased phosphorylation of MLC[92,140-142]. Furthermore, the induction of the RhoA/Rho kinase (ROCK) pathway inhibits myosin light chain phosphatase (MLCP), which leads to sustained MLC phosphorylation and by that to prolonged contraction[92,143]. These alterations in calcium levels contribute to a hypercontractile state of VSMCs.

Vasoconstrictors, such as Ang II and ET-1, could also promote this state by activating G-protein coupled receptors (GPCRs) that further increase intracellular calcium, thereby enhancing MLC phosphorylation[144,145]. Additionally, endothelial dysfunction, a feature of aortic aneurysm progression, leads to reduced nitric oxide (NO) bioavailability, thereby impairing its inhibitory effects on VSMC contractility and promoting vasoconstriction and vessel wall stress[146-148].

In summary, VSMCs constitute the predominant cellular and structural component of the vessel wall and are fundamentally involved in the pathogenesis of aortic aneurysm formation and its complications, including dissection and rupture. At the same time, their remarkable phenotypic plasticity allows them to contribute to vascular remodelling processes, which may initially serve as compensatory or reparative mechanisms but can ultimately promote pathological vessel wall weakening during AA progression.

1.2. Sphingolipids

1.2.1. Sphingolipid metabolism and biosynthesis

Sphingolipids represent a heterogeneous group of lipids with both structural and functional diversity[149]. In the 1880s, Johann Ludwig Wilhelm Thudichum first isolated this novel class of lipids from the human brain. Due to their intricate and poorly understood structure, he named them ‘Sphingolipids’ inspired by the enigmatic nature of the Sphinx[150].

Structurally, sphingolipids consist of a long-chain amino alcohol backbone, typically containing 18 carbon atoms, with an amino group at the C2 position, hydroxyl groups at the C1 and C3 positions, and frequently a trans double bond between the C4 and C5 positions[151]. This characteristic sphingoid backbone, serves as the structural foundation for a diverse variety of sphingolipids[152]. This structural diversity arises primarily from the attachment of fatty acids with varying chain lengths and degrees of saturation via an amide bond at the C2 position. Additionally, the hydroxyl group at the C1 position can undergo further modifications, such as phosphorylation or glycosylation, giving rise to more complex sphingolipids[151,152].

In the *de novo* pathway of sphingolipid biosynthesis, serine and palmitoyl-CoA first condense to generate 3-ketodihydrosphingosine (Figure 4)[153,154]. This intermediate is subsequently reduced to dihydrosphingosine by 3-ketodihydrosphingosine reductase[155,156]. Moreover, dihydrosphingosine is transformed by ceramide synthases

into dihydroceramide, which is further metabolized by the dihydroceramide-reductase to ceramide[156,157]. From there, ceramide can be transported and converted into diverse other lipid species[158]. Via the ceramide transfer protein (CERT), ceramide is transported from the ER to the Golgi apparatus, where it enters the hydrolytic pathway[159,160]. By hydrolysis, ceramide can be formed into sphingomyelin by the neutral and acid sphingomyelinases[161,162]. Furthermore, ceramide, which enters the Golgi, can be modified by glycosylation to more complex glycosphingolipids[151]. While ceramide can be phosphorylated by ceramide kinase at the Golgi network or the plasma membrane to generate ceramide-1-phosphate, it can be hydrolysed by ceramidases to sphingosine[163,164]. In humans, five different ceramidases are known, which differ in their optimal pH, subcellular localization, and substrate specificity[165]. The acid ceramidase is localized to the lysosome and works at a pH value of 4 - 4.5, whereas the neutral ceramidase is more located to the plasma membrane, Golgi, or mitochondria[166-169]. The alkaline ceramidases (ACER1, ACER2, and ACER3), primarily located in the ER and Golgi, function optimally at an alkaline pH and exhibit distinct substrate specificities[165,170]. In detail, ACER1 preferentially hydrolyses very long-chain ceramides, ACER2 acts mainly on unsaturated long-chain ceramides, and ACER3 has broad specificity but higher activity towards ceramides with shorter acyl chains[170-172]. This reaction represents a fundamental step in the sphingolipid salvage pathway, which enables the recycling of sphingolipid metabolites[151]. Sphingosine (Sph) generated through this process can subsequently be reutilized for ceramide resynthesis or phosphorylated to form the potent signaling molecule sphingosine-1-phosphate (S1P)[170]. This phosphorylation is catalysed by two isoforms of sphingosine kinase, SphK1 and SphK2[173-175]. While SphK1 is mainly found in the cytosol and relocates to the plasma membrane upon activation, SphK2 is localized to various intracellular compartments, including the nucleus or mitochondria[176,177]. The generated S1P can be dephosphorylated through three lipid phosphate phosphatases (LPPs) or through two S1P phosphatases (SPPs)[178-180]. LPPs (LPP1-3) are located in the plasma membrane with their catalytic domain facing the extracellular space, enabling the degradation of extracellular S1P at the cell surface[181]. In contrast, SPPs are localized to the endoplasmic reticulum and dephosphorylate intracellular S1P back to Sph, which can subsequently be reutilized for S1P resynthesis by SphKs[182,183].

In addition, the S1P lyase (SGPL1) is the only enzyme that degrades S1P irreversibly to a hexadecenal, a fatty aldehyde, and ethanolamine phosphate.[184] The highly

reactive aldehyde can be further metabolically converted by the fatty aldehyde dehydrogenase to palmitic acid and enter again the sphingolipid synthesis via palmitoyl CoA[149,185].

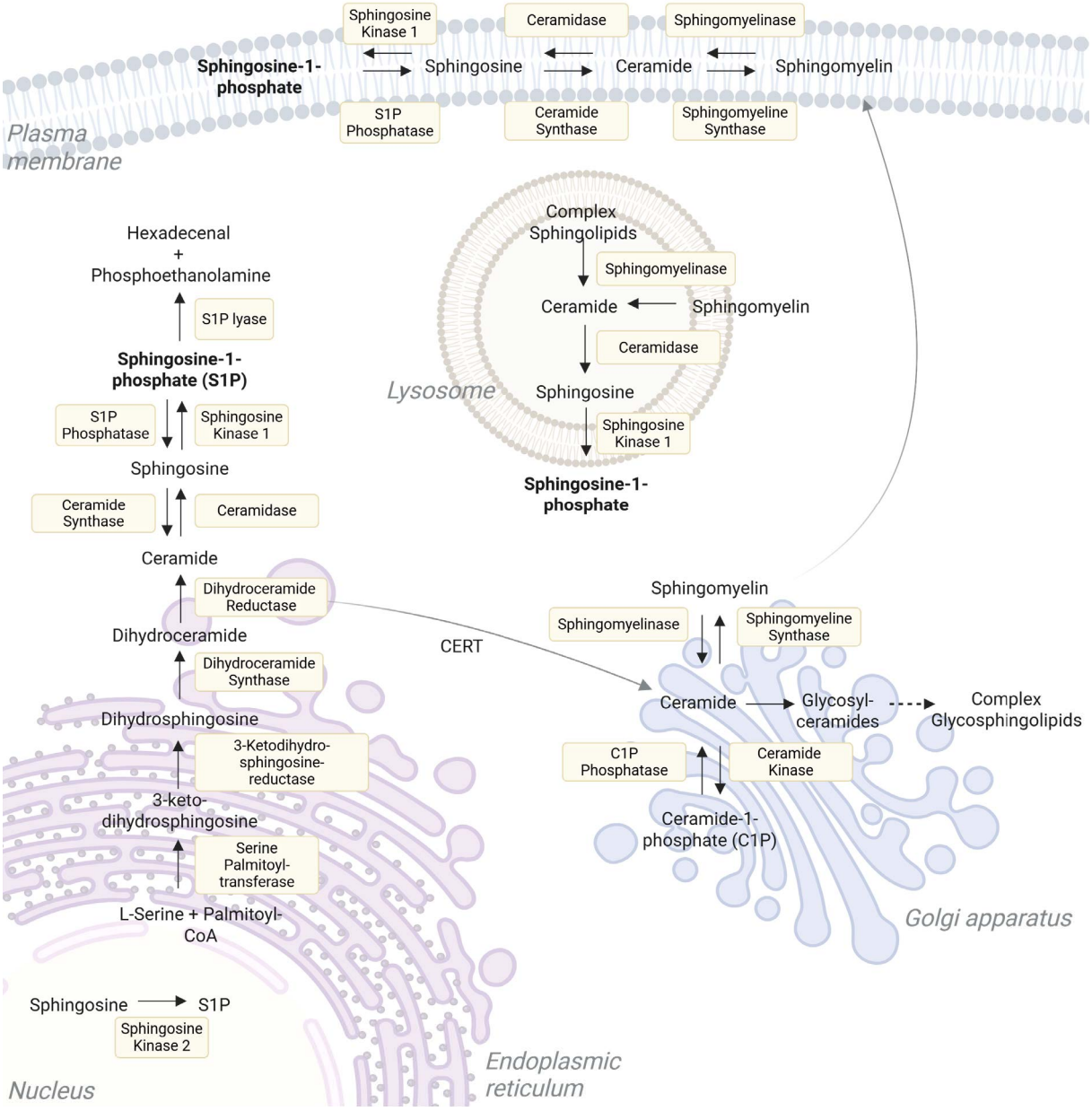

Figure 4: Schematic overview of the sphingolipid metabolism. *De novo* generation of sphingolipids begins in the endoplasmic reticulum with serine and palmitoyl-CoA. These metabolites were further processed into ceramide, sphingosine-1-phosphate (S1P), and complex sphingolipids including sphingomyelin and glycosphingolipids. The reversible interconversion of sphingolipid species is catalysed by multiple enzymes, including sphingosine kinases, ceramidases, and sphingomyelinases. Organelle-specific pathways involve trafficking of intermediates to the Golgi apparatus, lysosomes, and plasma membrane. Adapted from Lee *et al*.[186] Created with BioRender.com. Published under BioRender Publication Licence

Together, the interconnected pathways of sphingolipid metabolism give rise to a broad spectrum of structurally and functionally diverse sphingolipid species (Figure 4)[149]. These lipids are not only integral components of cellular membranes, where they

contribute to membrane organization and compartmentalization, but also act as bioactive signaling molecules that modulate a variety of cellular processes[149]. Through continuous enzymatic interconversion, sphingolipids form a dynamic metabolic network that enables rapid adaptation to cellular demands and ensures tight regulation of key physiological functions[149,158]. Beyond the cellular context, sphingolipids are increasingly recognized as critical mediators of tissue-level homeostasis and pathophysiological mechanisms[149,158].

1.2.2. S1P synthesis, degradation, and cellular trafficking

S1P is one of the most prominent bioactive sphingolipids with diverse cellular and physiological functions[187]. In the plasma, the concentrations range from 0.1 - 1 µM, with a short half-life[188,189]. In the plasma, S1P is usually bound with a high affinity to high-density lipoprotein (HDL) via apolipoprotein (ApoM) or with a lower affinity to albumin[189-191]. ApoM is mainly expressed in hepatocytes and renal tubular epithelial cells, from which it is secreted into the circulation[192]. Experimental evidence shows that S1P is almost exclusively present in ApoM-containing HDL fractions, while ApoM-deficient HDL lacks S1P entirely[190]. Consistently, ApoM knockout mice display markedly reduced HDL-bound S1P levels, whereas ApoM overexpression increases plasma S1P concentrations, underscoring the pivotal role of ApoM and HDL as major S1P carriers in the circulation[190].

S1P-bound carriers can also modulate S1P-mediated biological processes. When complexed with HDL, S1P is presented to endothelial S1PR1 with high efficacy, which stabilises adherens junctions, enhances NO production, and limits vascular leakage[193,194]. ApoM-bound S1P suppresses lymphopoiesis and inflammation[195,196]. Processes mediated by albumin-S1P are shorter-lived than those mediated by HDL-bound S1P[197].

Furthermore, S1P can be generated in diverse cell types, but it is predominantly formed in red blood cells (RBCs), platelets, and endothelial cells[188,198,199]. Under physiological conditions, there exist naturally formed S1P gradients in the body, which are established and maintained by the coordinated activities of SphKs, that synthesize S1P, the degrading enzyme SGPL1, and the S1P transporters[187]. Specific S1P transporters export S1P to the extracellular space, thereby establishing physiologically relevant concentration gradients [187]. The exporter, sphinster homolog 2 (SPNS2), was initially described in the zebrafish, where SPNS2-mediated S1P release generates an

extracellular gradient critical for cardiac development[200,201]. In mice, it has been shown that SPNS2 mediates S1P efflux from endothelial cells, creating a S1P gradient for lymphocytes, which promotes their egress from the lymph nodes into the circulation[202,203]. This gradient, characterized by a high S1P levels in the plasma and a very low levels in the interstitial fluid, acts as a chemotactic agent for the lymphocytes[202,204]. Comparable S1P gradients also exist between blood and lymph, across the cortex-medulla interface of the thymus, and within the bone marrow niche, each involved in trafficking of immune cells[205-207]. In RBCs, the major facilitator superfamily domain-containing protein 2B (MFSD2B) is another S1P transporter, which was discovered[208,209]. Mice lacking this transporter show almost no circulating S1P, indicating that this transporter is highly responsible for S1P efflux into the plasma[208,209]. Other cell types, that express MFSD2B are platelets and megakaryocytes[209]. Disturbances in S1P gradients and the loss of its transporters can result in a number of severe dysfunctions. These range from lymphopenia, increased vascular leakage, anaemia, hearing loss, and defects in embryogenesis[203,210-213].

S1P levels in the circulation are further regulated by dephosphorylation processes[214]. On the surface of hepatocytes, LPPs catalyse the conversion of extracellular S1P to sphingosine, which can subsequently be taken up and rephosphorylated by sphingosine kinases[214]. This reversible cycle contributes to S1P turnover and supports maintaining plasma S1P concentrations under physiological conditions[214].

1.2.3. S1P signaling through membrane receptors and intracellular S1P-binding proteins

Intracellularly produced and exported S1P has been observed to act in an autocrine or paracrine manner, and at the same time, functions as a second messenger, thereby directly inducing intracellular processes[215-218].

Extracellularly, S1P signals via five G-protein-coupled receptors (S1PR1-5), which differ in their signaling cascades and in their localization in the organism (Figure 5)[215]. Depending on the different activation of S1PRs, S1P can initiate several cellular processes, including cell proliferation, migration, survival, differentiation, and many more[219-223].

The S1P receptor, S1PR1, is highly expressed in several organs, including the spleen, brain, lung, kidney, and the cardiovascular system[215,224]. S1PR1 signals only via $G_{i/o,}$

which can further activate numerous signaling cascades, including the activation of the mitogen-activated protein kinase (MAPK) pathway, which in turn activates extracellular signal-regulated protein kinases 1 and 2 (ERK1/2). Moreover, phosphatidylinositol 3-kinase (PI3K) can also be activated through S1PR1, which activates Rac or the Akt pathway[223,225-229]. In contrast to S1PR1, S1PR2 can interact with multiple G proteins, such as $G_{i/o}$, $G_{q,}$ or $G_{12/13}$[230,231]. In accordance with that, S1PR2 can activate multiple cellular processes. Through G_q signaling, PLC can be activated, leading to the activation of IP3 and ultimately resulting in intracellular calcium release. Alternatively, DAG can be activated, which further activates protein kinase C (PKC)[232-235]. Apart from that, via $G_{12/13}$-mediated signaling, the Rho/ ROCK pathway or PTEN could be activated[231,236]. Additionally, this S1PR is also widely expressed in different cell types and organs[215]. S1PR3, which is predominantly expressed in the cardiovascular system, the lungs, the kidneys, or the intestines, acts similarly to S1PR2 through $G_{i/o}$, $G_{q,}$ or $G_{12/13}$[215,230]. The remaining two receptors, S1PR4 and S1PR5, exhibit reduced levels of expression and are exclusively present in specific cell types, including leukocytes, natural killer cells, or diverse cell types of the central nervous system, like oligodendrocytes or astrocytes[237-239]. In addition, both receptors signal through $G_{i/o}$ or $G_{12/13}$[238,240].

Beyond their coupling to distinct G proteins and activation of multiple downstream cascades, S1PRs are tightly regulated to control their activity and availability. Ligand binding leads to receptor phosphorylation, followed by β-arrestin recruitment and internalization[241]. These are important for receptor desensitization, intracellular trafficking, and recycling, as shown for S1PR1[241]. Through these mechanisms, cells can precisely adjust the strength and duration of S1P/S1PR signalling[241,242]. In lymphocytes, internalization and recycling of S1PR1 are key mechanisms controlling cell egress from lymphoid organs by adjusting receptor sensitivity to S1P gradients[242,243]. S1PR3 also undergoes ligand-induced internalization, although this process may occur through distinct regulatory mechanisms compared to S1PR1[244]. These processes enable cells to precisely regulate their S1P signalling.

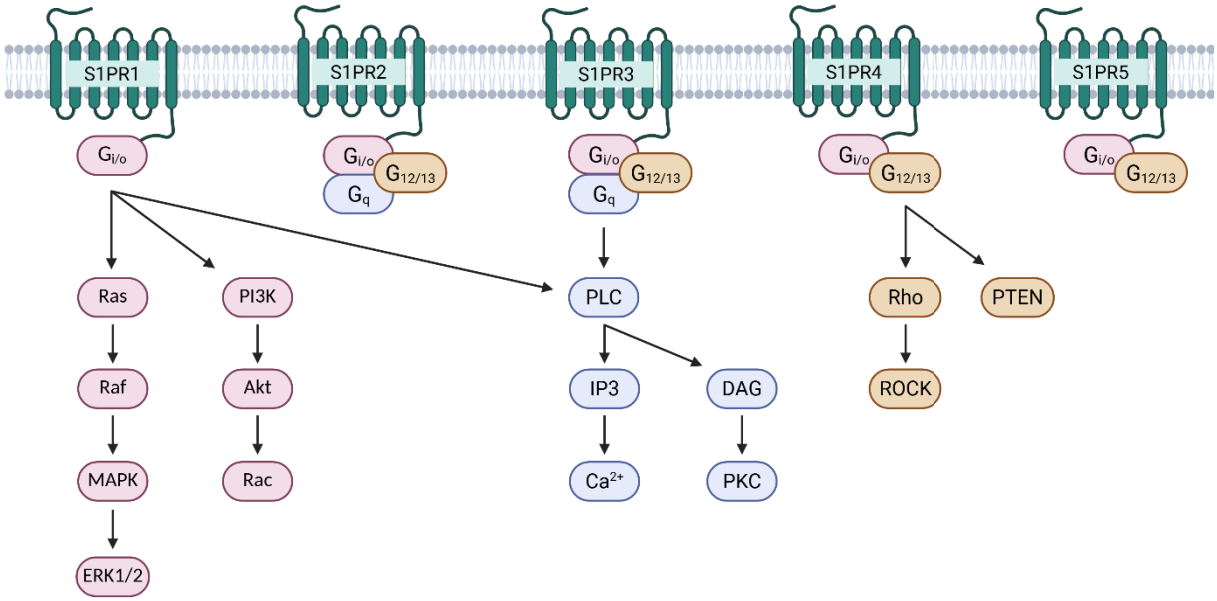

Figure 5: S1P receptor (S1PR) downstream signaling. S1P signals via five G-protein-coupled receptors that mediate diverse intracellular signaling cascades. Each S1PR signals via specific G protein subtypes. S1PR1 exclusively couples to $G_{i/o}$, activating the MAPK/ERK, PI3K/Akt or PLC pathway. S1PR2 and S1PR3 signal through multiple G proteins ($G_{i/o}$, $G_{12/13}$, G_q), enabling activation of PLC, PKC or Rho/ROCK pathway. S1PR4 and S1PR5 signal via $G_{i/o}$ and $G_{12/13}$. Adapted from Limbu *et al.*[245] Created with BioRender.com. Published under BioRender Publication Licence.

Apart from S1PR availability and signalling, S1P can also mediate intracellular processes[215,218]. This is initially due to increased activation of SphKs, which are responsible for the phosphorylation of Sph to form S1P[215]. The S1P, which is not exported to act autocrine or paracrine, could interfere with intracellular targets[215]. Intracellular S1P has been shown to play a role in the regulation of intracellular calcium dynamics[246]. Through activation of PLC and IP_3 signalling cascade, S1P induces calcium release from endoplasmic reticulum by stimulating SOCE[246-248]. The resulting increase in cytosolic calcium can further stimulate the opening of additional plasma membrane calcium channels, thereby amplifying calcium influx[249]. Moreover, S1P can act also on calcium transporter to mediate calcium entry. In VSMCs, S1P promotes calcium influx by activating transient receptor potential canonical 5 (TRPC5) channels, thereby linking S1P signalling to calcium-dependent vascular functions[250].

Beyond its cytosolic functions, intracellular S1P also exerts regulatory roles within various cellular organelles[251,252]. S1P in the nucleus, generated by SphK2, inhibits directly histone deacetylases (HDAC), particularly HDAC1, HDAC2 and HDAC3[252]. This inhibition promotes histone acetylation and thereby enhances gene transcription, which defines a mechanistic link between S1P and epigenetic regulation. Moreover, intracellular S1P also affects mitochondrial biology[251]. It has been demonstrated that

S1P binds to prohibitin-2, which can affect mitochondrial function[251,253,254]. Furthermore, S1P promotes mitochondrial biogenesis through activation of the transcriptional coactivator peroxisome proliferator-activated receptor gamma coactivator 1-alpha (PGC-1α), linking intracellular S1P signalling to the regulation of cellular energy metabolism.[253]

1.2.4. S1PR modulators in clinical application

S1P receptor modulators represent a novel class of immunomodulatory agents that have significantly expanded therapeutic options for patients with relapsing forms of multiple sclerosis (MS)[255]. To date, four S1PR modulators have been approved for clinical use in the European Union[255]. Among them, fingolimod (FTY720), approved in 2011, was the first oral disease-modifying therapy for MS. As a nonselective modulator, FTY720 engages multiple S1PRs, including S1PR1, S1PR3, S1PR4, and S1PR5, while sparing S1PR2[255]. After oral administration, it requires phosphorylation by SphKs to form its active metabolite, fingolimod-phosphate (p-FTY720)[256,257]. The therapeutic mechanism of S1P modulators is based on functional antagonism of S1PR1, which leads to the sequestration of lymphocytes in lymphoid tissues[258]. Upon ligand binding, prolonged receptor activation causes S1PR1 desensitization and internalization, preventing receptor recycling to the cell surface[243]. This process disrupts the physiological S1P gradient between lymph nodes and peripheral blood, thereby reducing the egress of lymphocytes and their infiltration into the central nervous system[258-260]. In MS, this mechanism reduces neuroinflammation and disease activity[260]. The clinical use of FTY720 is often associated with several adverse events, particularly cardiovascular effects such as bradycardia and atrioventricular (AV) block upon initiation[261]. These observations led to the development of more selective second-generation S1PR modulators with enhanced safety profiles. These include ozanimod, ponesimod, siponimod, and etrasimod, all of which were approved from 2020 onwards[262,263]. Unlike FTY720, these newer agents do not require phosphorylation for activation and exhibit greater receptor selectivity[262]. Ozanimod and siponimod primarily target S1PR1 and S1PR5, while ponesimod selectively modulates S1PR1 only[262,264,265]. Etrasimod targets S1PR1, 4 and 5[263].

S1P receptors are broadly expressed across various cell types and tissues, including lymphocytes, endothelial cells, and cardiomyocytes[255]. The expression of S1PR1 and S1PR3 in cardiac tissue is thought to underlie the cardiovascular side effects observed

with this drug class. Clinical trials and post-marketing studies have consistently reported adverse events such as bradycardia, AV conduction abnormalities, and hypertension[261]. A recent meta-analysis estimated that approximately 11% of patients treated with S1PR modulators experience cardiovascular adverse effects[266]. Given these safety concerns, a comprehensive cardiovascular assessment is mandatory before initiating therapy with any S1P modulator[255]. First-dose administration requires close monitoring of heart rate and blood pressure for several hours due to the risk of bradycardia[261]. Laboratory monitoring during treatment should include regular assessment of lymphocyte counts, liver enzymes, and blood pressure[255]. Other adverse effects include serious infections, seizures, and an increased risk of cutaneous malignancies such as basal cell carcinoma[255]. In addition to MS, ozanimod has recently received approval for use in ulcerative colitis, indicating the expanding potential of S1PR modulators beyond neuroimmunological diseases[267].

1.3. Role of S1P in vascular physiology and pathophysiology and its impact on VSMC biology

Under physiological conditions, S1P has diverse functions in the cardiovascular system[268]. The S1PR subtypes, S1PR1 to S1PR3, are predominantly expressed in the vascular system, although their expression varies depending on the cell type[268]. In addition to receptor distribution, the SphKs, the S1P-generating enzymes, and the S1P-degrading enzymes, SGPL1 and SPPs also have an influence on vascular function through their regulation of extra- and intracellular S1P levels[268].

S1P signaling plays an important role in the regulation of vascular development, endothelial barrier integrity or in the modulation of vascular tone[268]. The first finding, which provides evidence for the involvement of S1P in vasculogenesis, was observed in S1PR1-deficient mice, which exhibited subsequent fetal death caused by incomplete development of the vasculature and severe bleeding[269]. Furthermore, the S1PRs (S1PR1-3) and SphK2 were detected in angioblast-rich tissues at an early stage of vascular development[270]. Hereby, S1P promotes the formation of new blood vessels by driving the migration of angioblasts and early endothelial cells[270]. It has been established that the source of S1P during vasculogenesis are RBCs[271].

Besides its role in endothelial cell migration, S1P is also involved in regulating endothelial barrier integrity[268]. Through S1PR1 signaling, S1P has barrier-preserving effects on the endothelial cells by acting on vascular endothelial (VE)-cadherin at

adhesion junctions, which prevents excessive vascular permeability[272]. Furthermore, endothelial-specific S1PR1-deficient mice show vascular leakage and excessive sprouting, which indicates a role of S1PR1 during vascular integrity[273]. In contrast to S1PR1, S1PR2 and S1PR3 signaling was associated with increased vascular permeability[274-277].

Furthermore, under physiological conditions S1P plays an important role in maintaining vascular tone[268,278]. It induces vasodilation through S1PR1 and S1PR3 signaling in endothelial cells, whereas vasoconstriction in VSMCs is mediated through S1PR2 and S1PR3 signaling[279-281]. S1P activates in endothelial cells the endothelial nitric oxide synthase, which leads to the production of NO, which drives vasodilation in VSMCs[280,282,283]. Furthermore, S1P acts directly on VSMCs via the activation of RhoA/Rho kinase signaling, which induces a signaling cascade that includes intracellular calcium release and the final phosphorylation of MLC[284,285]. The interplay of these mechanisms is highly dependent on the vascular bed and the receptor composition in different vessel types[281,286,287].

Given the diverse functions of S1P in maintaining vascular homeostasis, disturbances in S1P levels can have an impact on vascular function[268]. Altered S1P levels or dysregulated receptor signaling have been implicated in the pathogenesis of various cardiovascular diseases, including hypertension and atherosclerosis[268]. Several studies show a link between S1P and hypertension[288]. For instance, chronic administration of S1P was associated with an increase in blood pressure, depending on S1PR3 activation[288,289]. In contrast, the acute generation of S1P induces a temporary reduction in blood pressure[290]. Furthermore, a study demonstrated that SphK1-deficient mice exhibited attenuated Ang II-induced hypertension[291,292]. In contrast, activation of S1PR1 by selective agonists results in a reduction in blood pressure in hypertensive models[293]. Additionally, Nogo-B-deficient mice exhibit a hypotensive phenotype, likely due to increased sphingolipid synthesis caused by the loss of Nogo-B-mediated inhibition of the *de novo* biosynthetic pathway[293]. Chronic administration of FTY720 has been shown to exacerbate hypertension by promoting internalization of S1PR1 and thereby shifting the signaling balance toward vasoconstrictive pathways mediated by S1PR2 and S1PR3[294]. However, these effects appear to be highly vascular bed-specific, as vasodilatory responses to FTY720, in part via S1PR3 activation, have also been reported[295].

Additionally, multiple studies indicate a close association between S1P signaling and the development of atherosclerosis[268]. This is mainly due to the diverse biological functions of S1P, which not only affect vascular cells but also immune cells involved in inflammation[268]. Depending on the context, S1P exerts both pro- and anti-atherogenic effects. On the one hand, S1P promotes macrophage infiltration into atherosclerotic plaques, particularly through signaling via S1PR2 and S1PR3[296,297]. On the other hand, treatment with FTY720 has been associated with reduced plaque formation[298]. In endothelial cells, the loss of S1PR1 has been shown to enhance vascular inflammation by increasing the expression of proinflammatory cytokines and adhesion molecules, such as vascular cell adhesion molecule-1 (VCAM-1) and intercellular adhesion molecule-1 (ICAM-1)[299]. In contrast, activation of S1PR1 and S1PR3 supports vascular integrity by stabilizing the endothelial barrier and promoting NO production, which contributes to vasodilation and an anti-atherogenic environment[300,301]. In VSMCs, S1P signaling via S1PR2 has been reported to reduce inflammatory activation and limit cell migration, which could contribute to plaque stability[302]. However, excessive accumulation of S1P, resulting from the inhibition of its degradation, has also been linked to increased atherosclerosis and plaque vulnerability[303].

1.4. Lipidomics as a tool for cardiovascular risk evaluation

In recent years, lipidomics analyses have gained increasing relevance by enabling the identification of promising target molecules and potential markers for cardiovascular risk and outcome[304]. By combining liquid chromatography with tandem mass spectrometry (LC-MS/MS), it is possible to perform both targeted and untargeted lipidomics, allowing the detection of a broad spectrum of lipid species[304]. This enables the identification of lipid alterations, which have been linked to disease onset, progression, and adverse clinical outcomes in the context of cardiovascular pathology[304]. By that, the resulting specific lipidomic profile could be a promising tool in clinical application, which could offer new possibilities for risk stratification, early diagnosis, or treatment concepts[304].

Since cardiovascular diseases are one of the leading causes of death, prediction and prevention are essential[304-306]. In the context of lipidomics, and especially sphingolipidomic analysis, distinct ceramide species were one of the first sphingolipids, which have been shown to serve as biomarkers for mortality risk in individuals with coronary artery disease (CAD)[307]. Accordingly, further studies followed and identified

several species of sphingolipids and phospholipids in plasma to predict cardiovascular risk. Lipidomics-based scores were developed to enhance predictive potential in patients with CAD[307-311]. The CERT2 score was developed and combined specific ceramide ratios, in detail Cer(d18:1/16:0), Cer(d18:1/18:0), and Cer(d18:1/24:1), which were combined with selected phosphatidylcholines to improve risk stratification for adverse cardiovascular events in patients with CAD[311,312]. Interestingly, the score remained an independent predictor of cardiovascular and all-cause mortality even after comprehensive adjustment for conventional risk factors and established cardiac and inflammatory biomarkers[311,312]. Beyond CAD, lipidomic approaches have additionally been applied to other cardiovascular conditions like atherosclerosis, hypertension, peripheral artery disease (PAD) or heart failure[313-317]. Based on this, the Mayo Clinic established the first lipidomics-based test in clinical use to evaluate the risk of major adverse cardiovascular events in the following years[318-320].

However, only a few studies have focused on lipidomics, especially sphingolipidomics, in aortic aneurysm pathophysiology. One study showed alterations of lipidomic profile in the plasma of patients with aortic dissection compared to age-matched controls[321]. In particular, lysophosphatidylcholines (LPCs), such as LPC (20:0) showed diagnostic accuracy, whereas other sphingo- and phospholipids were reduced[321]. A similar alteration in LPC levels was identified in the plasma of patients with AAA[322]. A further study has demonstrated differences in the lipid profile in the plasma of patients with specific aortic dissection types, classified as Stanford A and Stanford B[323]. In addition to changes in the plasma, another study was able to detect lipidomic changes, including an increase in phosphatidylcholines, sphingomyelins, and triglycerides in the aneurysmatic aortic tissue[324]. Furthermore, the largest cohort study in the field of aortic pathologies, including 161 patients with AAA and 168 control patients with PAD, revealed an increase in diacylglycerides and triacylglycerides as significantly associated with AAA[325]. In addition, the authors detected significantly lower levels of S1P in patients with AAA compared to those with PAD, and S1P showed a negative correlation with C-reactive protein levels[325]. Overall, lipidomics analysis is a valuable tool for risk stratification, particularly in aortic diseases, as it offers the potential to identify novel molecular targets and patterns during aortic aneurysm disease progression.

1.5. Aim of the study

An aortic aneurysm and its potential progression to aortic dissection represent a life-threatening vascular condition characterized by progressive weakening and structural remodelling of the aortic wall. Its pathophysiology is highly complex and involves endothelial dysfunction, inflammation, ECM degradation and phenotypic switching of VSMCs. Despite extensive progress in vascular research, the molecular mechanisms driving aneurysm formation and rupture remain only partially understood. Moreover, there are currently no pharmacological interventions available that directly target the aneurysm itself to prevent disease progression or rupture.

The bioactive sphingolipid S1P has emerged as a regulator of vascular homeostasis, including vascular tone, VSMC phenotype or endothelial function. Furthermore, dysregulation in S1P levels have been associated with various cardiovascular conditions such as hypertension or atherosclerosis, both represent major risk factors contributing to aortic aneurysm development. However, the direct impact of S1P in the pathophysiology of aortic aneurysm formation and progression remains largely unknown. Therefore, the overall aim of this thesis was to elucidate the role of S1P in aortic aneurysm pathophysiology and to explore its potential as a diagnostic or therapeutic target.

To achieve this, the study first investigated whether S1P contributes to aneurysm formation, severity and rupture. For that the murine Ang II infusion model was used to induce aortic aneurysms and dissections. This model was combined with pharmacological inhibition of the S1P-degrading enzyme, S1P lyase, using DOP, enabling the assessment of how elevated S1P levels affect survival, incidence, and aneurysm severity. Transcriptomic and proteomic analyses were performed to elucidate molecular pathways involved in vascular remodelling driven by elevated S1P levels during aneurysm progression. Since previous studies have shown that S1P influences the phenotypic differentiation of VSMCs, a phenomenon of aneurysm pathophysiology, the present study further examined whether elevated S1P levels modulate this process during aneurysm progression.

Second, the project aimed to elucidate the role of S1PRs in the pathophysiology of aneurysms. As a first step changes in gene expression of S1PRs were analysed in aortic tissue to identify receptor subtypes potentially involved in aneurysm formation.

To further define their functional relevance, *in vitro* experiments using primary rat VSMCs were conducted to determine which S1PRs contribute to the phenotypic modulation of VSMCs, a key mechanism of vascular remodelling. For this purpose, receptor-specific agonists and antagonists were applied to dissect individual S1PR-mediated effects. Based on these findings, specific S1PR-deficient mice were crossbred with ApoE$^{-/-}$ mice and analysed in the Ang II infusion model to assess how receptor-specific modulation affects survival, aneurysm progression, and biomechanical vessel properties *in vivo* and *ex vivo*.

Third, considering that some S1PR modulators, such as FTY720 are clinically approved for the treatment of multiple sclerosis, this study also aimed to explore the therapeutic potential of this substance in aortic aneurysms. Given its established clinical use and its potential to act as a functional antagonist for multiple S1PRs, FTY720 was evaluated in the Ang II infusion model to determine whether pharmacological modulation of S1P signalling affects aneurysm progression,

Finally, the role of lipidomics analysis in cardiovascular diseases has gained increasing significance to predict disease outcomes and identify patients at risk. Building on these, this study aimed to characterize sphingolipid alterations in plasma and aortic tissue from patients with abdominal aortic aneurysms using LC-MS/MS analysis. The obtained lipid profiles may provide a basis for identifying novel molecular targets and for elucidating sphingolipid-driven mechanisms that contribute to aneurysm formation.

Taken together, the overall aim of the study was to elucidate the role of S1P in aortic aneurysm development, to dissect the underlying S1PR-mediated signaling pathways, and to identify potential diagnostic and therapeutic targets for potential aneurysm management.

2. Material

2.1. Devices and equipment

Table 1 List of devices

Device	Company
Anaesthesia workstation combi-vet®	Rothacher Medical GmbH, Heitenried, Switzerland
Blood Pressure Analysis System SC-1000	Hatteras Instruments, Grantsboro, USA
Centrifuge 5425	Eppendorf, Hamburg, Germany
Centrifuge 5430 R	Eppendorf, Hamburg, Germany
Centrifuge 5810 R	Eppendorf, Hamburg, Germany
Chemidoc, Universal Hood III	BioRad, Hercules, USA
CO2 Incubator HERAcell Vios 250i	Thermo Fisher Scientific, Waltham, USA
Column oven CTO-40C	Shimadzu, Kyoto, Japan
Degassing Unit DGU-405	Shimadzu, Kyoto, Japan
Eppendorf Water Bath 2763	Eppendorf, Hamburg, Germany
Fluorescence Microscope BZ-X810	Keyence, Osaka, Japan
Fluorescence Spectrophotometer Hitachi F-2500	Hitachi High-Tech Science Corporation, Tokio, Japan
GalliosTM 10/3 flow Cytometer	Beckmann Coulter, Brea, USA
Incubator 1000 Heidolph	Thermo Fisher Scientific, Waltham, USA
Leica EG 1150 C	Leica Biosystems, Nussloch, Germany
Mass spectrometer LCMS-8050	Shimadzu, Kyoto, Japan
Material Testing System EZ Test - SX	Shimadzu, Kyoto, Japan
Microscope Leica Wild M3C	Leica Biosystems, Nussloch, Germany
Microscope Nikon SMZ800	Nikon, Tokio, Japan
Microscope Olympus EP50	Olympus, Tokjio, Japan
Microplate reader, CLARIOstar Plus	BMG Labtech, Ortenberg, Germany

Nanodrop One	Thermo Fisher Scientific, Waltham, USA
Nitrogen-generator NGM 22-LC	CMC Instruments, Eschborn, Germany
Real-Time System CFX96™	BioRad, Hercules, USA
Rotary Pump E2M28	Shimadzu, Kyoto, Japan
Sliding Microtome Microm HM 430	Thermo Fisher Scientific, Waltham, USA
Solvent Delivery Unit LC-40D X3	Shimadzu, Kyoto, Japan
System controller SCL-40	Shimadzu, Kyoto, Japan
Thermal Cycler C100™	BioRad, Hercules, USA
Thermal Shake lite	VWR, Radnor, USA
Tissue Ruptor	Qiagen GmbH, Hilden, Germany
UHPLC Autoinjector SIL-40CX3	Shimadzu, Kyoto, Japan
Ultrasonic bath, Bandelin Sonorex, Super RK	BANDELIN electronic GmbH & Co. KG, Berlin, Germany
Vet abc Plus^{+} Scil	Antech Diagnostics Germany GmbH, Viernheim, Germany
Vortex Mixer Multitube, VXMTALB EU 1200 U/min - 2400 U/min	Ohaus Europe GmbH, Mänikon, Switzerland
Wire Myograph DMT620M	Danish Myo Technology A/S, Hinnerup, Denmark

2.2. Consumables

Table 2 List of consumables

Consumables	Company
0.5; 1.5; 2 mL Reaction Tube	Sarstedt, Nümbrecht, Germany
15 mL tube 120x17 mm	Sarstedt, Nümbrecht, Germany
50 mL tube 114x28 mm	Sarstedt, Nümbrecht, Germany
6 well cell culture plate	Sarstedt, Nümbrecht, Germany
Amersham™ Hybond™, PVDF Blotting Membrane, 0.2 µm	Cytiva, Marlborough, USA
Cover Glass	Engelbrecht, Edermünde, Germany

Epredia™SuperFrost Plus™Adhesion slides	Menzel, Braunschweig, Germany
Filter tip 10; 100; 200; 1000 µL	Sarstedt, Nümbrecht, Germany
High precision cover glasses	Paul Marienfeld, Lauda-Königshofen, Germany
Immobilon®-P Transfer Membrane, PVDF, 0.45 µm	Merck Millipore, Burlington, USA
Micro-inset G30s/6 mm	Ziemer Chromatographie, Langerwehe, Germany
Microlance 30G x ½“, 0.3 x 13 mm	BD Biosciences, Franklin Lakes, USA
Microlance 26G x ½“, 0.45 x 13 mm	BD Biosciences, Franklin Lakes, USA
Microlance 25G x 1“, 0.5 x 25 mm	BD Biosciences, Franklin Lakes, USA
Micro-osmotic pump Model 1004 Alzet®	DURECT Corporation, Cupertino, USA
Microscope slides Histo Bond	Paul Marienfeld, Lauda-Königshofen, Germany
Microseal® B seal Seals	BioRad, Hercules, USA
Microtome Blade - N35	Feather, Osaka, Japan
Multiply®-µStrip Pro 8-strip	Sarstedt, Nümbrecht, Germany
60 x 2.0 mm MultoHigh 100 RP18 column	CS Chromatography Service, Langerwehe, Germany
0.9% NaCl solution	Fresenius Kabi, Bad Homburg vor der Höhe, Germany
Omnifix-F Luer Solo Syringe - 1 mL	B. Braun, Melsungen, Germany
PCR – plate full skirt LP transparent	Sarstedt, Nümbrecht, Germany
Pestle, 1.5 mL	Bel-Art Inc., Wayne, USA
Screw cap, closed, PP, ND9	Carl Roth, Karlsruhe, Germany
Short-neck screw-thread bottle, G1- BF+FM	Ziemer Chromatographie, Langerwehe, Germany
T-75 & T-175 cell culture flask	Sarstedt, Nümbrecht, Germany
Tissue culture dish 30 x 15mm	Sarstedt, Nümbrecht, Germany
Tissue Ruptor® Disposable Probes	Qiagen GmbH, Hilden, Germany
QIAshredder	Qiagen GmbH, Hilden, Germany
Whatman 1 CHR	Cytiva, Marlborough, USA

2.3. Chemicals

2.3.1. Chemicals and reagents

Table 3 List of chemicals and reagents

Chemical/Reagent	Catalog No.	Company
4-Deoxy-pyridoxin hydrochlorid (DOP)	D0501	Sigma-Aldrich, St. Louis, USA
Acteylcholine chloride	A6625	Sigma-Aldrich, St. Louis, USA
Ammonium persulfate	A-3678	Sigma-Aldrich, St. Louis, USA
Angiotensin II	4006473	Bachem, Bubendorf, Switzerland
AUY954	Cay9000548	Cayman Chemical, Ann Abor, USA
Bovine Serum Albumin Fraction V (BSA)	11924	Serva, Heidelberg, Germany
Calcium chloride ($CaCl_2$)	141221	AppliChem, Darmstadt, Germany
Collagenase type II	C2-22	Sigma-Aldrich, St. Louis, USA
Cozy^{TM} Hi Prestained Protein Ladder	PRL0102	HighQu, Kraichtal, Germany
CYM 5520	Cay17638	Cayman Chemical, Ann Abor, USA
CYM 5541	Cay15190	Cayman Chemical, Ann Abor, USA
DAB-Substrate-Kit	34002	Thermo Fisher Scientific, Waltham, USA
Dimethylsulfoxide (DMSO)	D8418	Sigma-Aldrich, St. Louis, USA
Eosin	212954	Merck, Darmstadt, Germany
Ethanol, 100% (EtOH)	1HPH.1	Carl Roth, Karlsruhe, Germany
Ethylenediaminetetraacetic acid (EDTA)	4005-OP	Sigma-Aldrich, St. Louis, USA

Ethyleneglycol-bis(β-aminoethyl ether)-N,N,N',N'-tetraacetic acid (EGTA)	3054	Carl Roth, Karlsruhe, Germany
Ferric chlorid	372870	Merck, Darmstadt, Germany
Fluoromount G	00-4958-02	Thermo Fisher Scientific, Waltham, USA
Formic acid ROTIPURAN®	4724	Carl Roth, Karlsruhe, Germany
FTY720 (Fingolimod)	10008639	Cayman Chemical, Ann Abor, USA
Fura-2	F1221	Thermo Fisher Scientific, Waltham, USA
Glucose	G-7528	Sigma-Aldrich, St. Louis, USA
Glycine	G8898	Merck, Darmstadt, Germany
Halt™ Protease und Phosphatase Inhibitor Cocktail	78441	Thermo Fisher Scientific, Waltham, USA
Haematoxylin	2E-010	Waldeck GmbH & Co. KG, Münster, Germany
Hydrazine Hydrate	2255819	Sigma-Aldrich, St. Louis, USA
Indomethacin	405268	Merck, Darmstadt, Germany
Isoflurane (100%)	30372.00.00	Piramal Critical Care Deutschland GmbH, Hallbergmoos, Germany
JTE-013	Cay10009458	Cayman Chemical, Ann Abor, USA
Magnesium sulfate ($MgSO_4$)	M2773	Merck, Darmstadt, Germany
Mayer’s Haemalaun Solution	MHS32-1L	Merck, Darmstadt, Germany
Methanol (MeOH)	1A9L.1	Carl Roth, Karlsruhe, Germany

Methanol CHROMOSOLV™ LC-MS ≥ 99.9%	34966	Honeywell Riedel; Seelze, Germany
NIBR0213	Cay21513	Cayman Chemical, Ann Abor, USA
Nonfat dried milk powder	A0830	AppliChem, Darmstadt, Germany
Normal Serum Block	B927501	Biolegend, San Diego, USA
NP-40 (IGEPAL®)	I8896	Merck, Darmstadt, Germany
Oligo (dT) 18 Primer	10753741	Thermo Fisher Scientific, Waltham, USA
Paraffin	X880	Carl Roth, Karlsruhe, Germany
PBS Buffer (10x) Powder	A0965	AppliChem, Darmstadt, Germany
Pharm Lyse™	555899	BD Biosciences, Franklin Lakes, USA
Phenylephrine (Phe)	P6126	Sigma-Aldrich, St. Louis, USA
Pluronic™	P6866	Thermo Fisher Scientific, Waltham, USA
Potassium chloride (KCl)	A3582	AppliChem, Darmstadt, Germany
Potassium dihydrogen phosphate (KH_2PO_4)	104873	Merck, Darmstadt, Germany
Probenecid	P8761-25G	Merck, Darmstadt, Germany
Rimadyl (Carprofen)	QM01AE91	Zoetis, Parsippany, USA
Roti-Histofix 4.5%	2213.1	Carl Roth, Karlsruhe, Germany
ROTIPHORESE®Gel 30 (37,5:1)	3029.1	Carl Roth, Karlsruhe, Germany
S1PL-IN-1	HY-115566	MedChemExpress LLC, Monmouth Junction; USA

SDS Pellets	CN30.3	Carl Roth, Karlsruhe, Germany
Sodium azide (NaN_3)	S2002	Merck, Darmstadt, Germany
Sodium chloride (NaCl)	P029	Carl Roth, Karlsruhe, Germany
Sodium deoxycholate	D6750	Merck, Darmstadt, Germany
Sodium hydrogen carbonate ($NaHCO_3$)	6885	Carl Roth, Karlsruhe, Germany
Sphingosine 1-Phosphate, D-erythro (S1P)	BML-SL140	Enzo Life Sciences GmbH, Lörrach, Germany
Stable Peroxide-Substrate Buffer (10X)	34062	Thermo Fisher Scientific, Waltham, USA
Streptavidin-Protein, HRP	21124	Thermo Fisher Scientific, Waltham, USA
SYBR Powertrack	A46112	Thermo Fisher Scientific, Waltham, USA
Tetramethylethylenediamine (TEMED)	1.10732	Merck, Darmstadt, Germany
Tris Base	648311	Merck, Darmstadt, Germany
Tween-20®	11332465001	Merck, Darmstadt, Germany
TY-52156	Cay19119	Cayman Chemical, Ann Abor, USA
Van Gieson Solution	HT254	Merck, Darmstadt, Germany
Vitro-Clud® Embedding Medium	04-0001	Langenbrink, Emmendingen, Germany
Verhoeff's solution	10402.01000	Morphisto GmbH, Offenbach am Main, Germany
Western Blot HRP Substrate, Immobilon® Forte	WBLUF0500	Merck, Darmstadt, Germany

Xylene	2662.2	Carl Roth, Karlsruhe, Germany

2.3.2. Media, Buffer and Solutions

Table 4 List of media, solutions and supplements

Media/Supplement	Catalog No.	Company
0.05% Trypsin/EDTA	25300	Gibco Life Technologies, Carlsbad, USA
Accutase® solution	A6964	Sigma-Aldrich, St. Louis, USA
Antibiotic-Antimycotic (100 x) Solution	15240	Gibco Life Technologies, Carlsbad, USA
DMEM (1X) Dulbecco's Modified Eagle Medium	41965	Gibco Life Technologies, Carlsbad, USA
DPBS, without Calcium and Magnesium	14190	Gibco Life Technologies, Carlsbad, USA
Fetal bovine serum (FBS)	A5256801	Gibco Life Technologies, Carlsbad, USA
HBSS Hanks' Balanced Salt Solution	14175	Gibco Life Technologies, Carlsbad, USA
HBSS Hanks' Balanced Salt Solution, with $CaCl_2$, $MgCl_2$	14025	Gibco Life Technologies, Carlsbad, USA
HEPES Buffer solution (1M)	15630	Gibco Life Technologies, Carlsbad, USA
L-Glutamine 200 mM (100X)	25030	Gibco Life Technologies, Carlsbad, USA
Sodium pyruvate 100 mM	11360070	Gibco Life Technologies, Carlsbad, USA

Media composition

VSMC Growth Media	+ 1% Antibiotic-Antimycotic Solution + 10% FBS + 4 mM L- Glutamine + 1 mM Sodium pyruvate in DMEM (1X) Dulbecco's Modified Eagle Media
VSMC Starvation Media	+ 1% Antibiotic-Antimycotic Solution + 4 mM L- Glutamine + 1 mM Sodium pyruvate in DMEM (1X) Dulbecco's Modified Eagle media

Buffer & Solutions

FACS-Buffer	+ 1% BSA + 0.1% Sodium Azide in PBS
Krebs-Henseleit Buffer	+ 120 mM NaCl + 5 mM KCl + 1.5 mM $MgSO_4$ + 25 mM $NaHCO_3$ + 1.2 mM KH_2PO_4 + 10 mM Glucose + 3.5 mM $CaCl_2$ in ddH_2O

VSMC isolation enzyme mix	+ 1% Antibiotic-Antimycotic Solution + 2.5 % BSA + 0.2 % collagenase type II in HBSS Hanks' Balanced Salt Solution, with $CaCl_2$, $MgCl_2$
Wash buffer (Calcium Assay)	+ 1% BSA + 20 mM HEPES + 4.5 mM $NaHCO_3$ + 2.5 mM Probonecid in HBSS Hanks' Balanced Salt Solution, with $CaCl_2$, $MgCl_2$
Dye buffer	+ 1% BSA + 20 mM HEPES + 4.5 mM $NaHCO_3$ + 2.5 mM Probonecid in HBSS Hanks' Balanced Salt Solution, without $CaCl_2$, $MgCl_2$
RIPA buffer	+ 0.1% SDS + 1% NP-40 (IGEPAL®) + 0.5% Sodium deoxycholate + 1X Halt™ Protease & Phosphatase Inhibitor in PBS
Stacking gel buffer	+ 1 M Tris Base + 0.75% SDS in ddH_2O set pH to 6.8 with HCl

Resolving gel buffer	+ 1.5 M Tris Base + 0.386% SDS in ddH_2O set pH to 8.8 with HCl
Stacking gel	+ 17% Acrylamide (30%) + 14% Stacking gel buffer + 1% APS (10%) + 0.001% TEMED in H_2O
Resolving gel	+ 26% Separation gel buffer + *% Acrylamide (30%) + 1% APS (10%) + 0.001% TEMED *depending on gel percentage in ddH_2O
Running buffer	+ 192 mM Glycine + 25 mM Tris Base + 0.1% SDS in ddH_2O
Transfer buffer	+ 192 mM Glycine + 25 mM Tris Base + 20% MeOH in ddH_2O
Wash buffer (Western Blot)	+ 0.1% Tween-20 in PBS

2.3.3. Kits

Table 5 List of kits

Kit	Catalog No.	Company
Pierce™ BCA Protein Assay	23225	Thermo Fisher Scientific, Waltham, USA
innuPREP DNase I Digest Kit.	845-KS-5200010	IST innuscreen, Berlin, Germany
innuPREP RNA Mini Kit 2.0	845-KS-2040250	IST innuscreen, Berlin, Germany
RevertAid RT Kit	15255146	Thermo Fisher Scientific, Waltham, USA

2.4. Primer

2.4.1. Mouse primer

Table 6 List of mouse primer

Target gene	Sequence (5' → 3')	Company
Col1a1	Fw: GCTCCTCTTAGGGGCCACT Rv: CCACGTCTCACCATTGGGG	Eurofins Genomics, Ebersberg,Germany
Col3a1	Fw: CTGTAACATGGAAACTGGGGAAA Rv: CCATAGCTGAACTGAAAACCACC	Eurofins Genomics, Ebersberg,Germany
Eln	Fw: TGGTGCTACATGTTGGTGCT Rv: TCGAGGCTTCTGGTACTTGG	Eurofins Genomics, Ebersberg,Germany
Gapdh	Fw: AGGTCGGTGTGAACGGATTTG Rv: TGTAGACCATGTAGTTGAGGTCA	Eurofins Genomics, Ebersberg,Germany
S1pr1	Fw: ATGGTGTCCACTAGCATCCC Rv: TGCCTGTGTAGTTGTAATGCC	Eurofins Genomics, Ebersberg,Germany
S1pr2	Fw: ATGGGCGGCTTATACTCAGAG Rv: GCGCAGCACAAGATGATGAT	Eurofins Genomics, Ebersberg,Germany
S1pr3	Fw: ACTCTCCGGGAACATTACGAT Rv: CAAGACGATGAAGCTACAGGTG	Eurofins Genomics, Ebersberg,Germany
Tagln	Fw: CCGTGGAGATCCCAACTGGTTTA Rv: CATTTGAAGGCCAATGACGTGCT	Eurofins Genomics, Ebersberg,Germany
Acta2	Fw: ACGGCCGCCTCCTCTTCCTC Rv: GCCCAGCTTCGTCGTATTCC	Eurofins Genomics, Ebersberg,Germany
Mmp-2	Fw: TTCCCTAAGCTCATCGCAGACT Rv: CACGCTCTTGAGACTTTGGTTCT	Eurofins Genomics, Ebersberg,Germany
Mmp-9	Fw: CTGGACAGCCAGACACTAAAG Rv: CTCGCGGCAAGTCTTCAGAG	Eurofins Genomics, Ebersberg,Germany
Mmp-12	Fw: GGAGCTCACGGAGACTTCAACT Rv: CCTTGAATACCAGGTCCAGGATA	Eurofins Genomics, Ebersberg,Germany

Myh11	Fw: AACAAGGAACTCCGAAGCAA Rv: TTGTTCAATCTGCTCCTCCA	Eurofins Genomics, Ebersberg,Germany
Tgfb1	Fw: TACGCCTGAGTGGCTGTCTT Rv: GGTTCATGTCATGGATGGTG	BioTeZ GmbH, Berlin, Germany
Tgfb2	Fw: CTTCGACGTGACAGACGCT Rv: GCAGGGGCAGTGTAAACTTATT	BioTeZ GmbH, Berlin, Germany
Tgfbr2	Fw: CCGCTGCATATCGTCCTGTG Rv: AGTGGATGGATGGTCCTATTACA	BioTeZ GmbH, Berlin, Germany

2.4.2. Rat primer

Table 7 List of rat primer

Target gene	Sequence (5' → 3')	Company
Gapdh	Fw: AGGTCGGTGTGAACGGATTTG Rv: TGTAGACCATGTAGTTGAGGTCA	Eurofins Genomics, Ebersberg,Germany
S1pr1	Fw: TCGGACCTGTTAGCAGGAGT Rv: CGATAGCAAGGAGGCTGAAG	Eurofins Genomics, Ebersberg,Germany
S1pr2	Fw: ATGCCTACATCGCCAACATT Rv: CCTATGAGCCGTGGTCAGTT	Eurofins Genomics, Ebersberg,Germany
S1pr3	Fw: GCTTCATCGTCTTGGAGACC Rv: GAACGTCTTCCTACCGGACA	Eurofins Genomics, Ebersberg,Germany
Tagln	Fw: CCGTGGAGATCCCAACTGGTTTA Rv: CATTTGAAGGCCAATGACGTGCT	Eurofins Genomics, Ebersberg,Germany
Acta2	Fw: CCGAGATCTCACCGACTACC Rv: GTCCAGAGCGACATAGCACA	Eurofins Genomics, Ebersberg,Germany
Myh11	Fw: AACAAGGAACTCCGAAGCAA Rv: TTGTTCAATCTGCTCCTCCA	Eurofins Genomics, Ebersberg,Germany

2.5. Antibodies

2.5.1. Primary antibodies

Table 8 List of primary antibodies

Antibody	Host species	Dilution	Catalog No.	Application	Company
Glyceraldehyde-3-Phosphate Dehydrogenase (GAPDH)	mouse	1:1000	5G4cc	WB	HyTest Ltd, Turku, Finland
IgG2a	mouse	1:200	X 0943	IHC	Agilent, Santa Clara, USA

Myosin Light Chain 2	rabbit	1:100	8505S	WB	Cell Signaling Technology, Danvers, USA
Phospho-Myosin Light Chain 2 (Thr18/Ser19)	rabbit	1:100	95777	WB	Cell Signaling Technology, Danvers, USA
S1PR1	rabbit	1:500	ASR-011	WB	Alomone Labs, Jerusalem, Israel
S1PR2	rabbit	1:500	ASR-012	WB	Alomone Labs, Jerusalem, Israel
S1PR3	rabbit	1:500	ASR-013	WB	Alomone Labs, Jerusalem, Israel
Smooth Muscle Actin (ACTA2)	mouse	1:200	M0851	IHC	Agilent, Santa Clara, USA
Smooth Muscle Actin (ACTA2)	mouse	1:5000	A2547	WB	Sigma-Aldrich, St. Louis, USA
Tagln (TAGLN)	rabbit	1:1000	PA5-27463	WB	Invitrogen, Waltham, USA

2.5.2. Secondary antibodies

Table 9 List of secondary antibodies

Antibody	Host species	Dilution	Catalog No.	Application	Company
Biotin Mouse Anti-Mouse IgG2a	mouse	1:200	553504	IHC	BD Bioscience, Franklin Lakes, USA
Horse Anti-Mouse IgG Antibody (H+L), Peroxidase	horse	1:5000	PI-2000	WB	Vector Laboratories,Newark, USA
Goat Anti-Rabbit IgG Antibody (H+L), Peroxidase	goat	1:5000	PI-1000	WB	Vector Laboratories, Newark, USA

2.5.3. Antibodies for flow cytometry

Table 10 Antibodies for flow cytometry

Antibody	Host species	Conjugated	Catalog No.	Company
B220	rat	APC-eFluor 780	47-0452-82	Invitrogen, Waltham, USA
CD4	rat	APC	100412	Biolegend, San Diego, USA
CD44	rat	FITC	11-0441-85	Invitrogen, Waltham, USA
CD45.2	mouse	V500	562129	BD Biosciences, Franklin Lakes, USA
CD62L	mouse	PE-Cy7	25-0621-82	Invitrogen, Waltham, USA
CD8	rat	PE	15-2784-39	Invitrogen, Waltham, USA

2.6. Cells

Table 11 List of cells

Cell type	Species	Source
Vascular smooth muscle cells (VSMCs)	rat	Aorta

2.7. Mouse strains

Table 12 List of mouse strains

Mouse strain	International nomenclature	Origin
$ApoE^{-/-}$	B6.129P2-Apoetm1Unc/J	Charles River Laboratories, Wilmington, USA
$ApoE^{-/-}$ /$S1pr2^{-/-}$	B6.129-Apoetm1Unc/JS1pr2tm1Jch	Self-breeding, ZETT, Düsseldorf, Germany
$ApoE^{-/-}$ /$S1pr3^{-/-}$	B6.129-Apoetm1Unc/JS1pr3tm1Jch	Self-breeding, ZETT, Düsseldorf, Germany

2.8. Mouse diets

Table 13 List of diets

Diet	Ingredients	Special features	Company
Standard control diet	13% fat 19% protein 68% carbohydrates	20% casein	ssniff Spezialdiäten GmbH, Soest, Germany
Western Type diet I	43% fat; 28% protein 29% carbohydrates	21% milkfat 0.15% cholesterol 19.5% casein	Altromin Spezialfutter GmbH & Co. KG, Lage, Germany
Western Type diet II	43% fat 28% protein 29% carbohydrates	21% milkfat 0.15% cholesterol 19.5% casein without sodium cholate without vitamin B6	Altromin Spezialfutter GmbH & Co. KG, Lage, Germany

2.9. Software for analysis

Table 14 Software for data detection, presentation and analysis

Software	Company
BZ-X800 Analysis Software	Keyence, Osaka, Japan
Fiji (Fiji is just ImageJ)	National Institutes of Health, Bethesda, USA
FlowJo_v11	FlowJo, Ashland, USA
GraphPad Prism 10	GraphPad Software, Boston, USA
LabChart 7	ADInstruments, Sydney, Australia
LabChart Reader 8.1.25	ADInstruments, Sydney, Australia
NIS-Elements F2.30	Nikon, Tokio, Japan
SC1000 Comm	Hatteras Instruments, Grantsboro, USA
Scil vIP®	Scil animal care company GmbH, Viernheim, Germany

3. Methods

3.1. *In vivo* studies

3.1.1. Animal housing

All mouse strains were housed and bred in the animal facility at the University Hospital of Düsseldorf (Central Facility for Animal Research and Scientific Animal Welfare of the University Hospital Düsseldorf). Animals were maintained under controlled 12-hour light/dark cycles, between a temperature range of 20-24 °C and a humidity of 50-60%. Under housing conditions, mice received a standard control diet and water *ad libitum*. All mice were kept in groups with a size of two to five before experiments started. Cages were lined with absorbent bedding and pulp.

3.1.2. Experimental design

For all animal experiments only male mice with an age between 12-20 weeks were used. Animal experiments were done under permission of the Office for Nature, Environment and Consumer Protection of North Rhine-Westphalia (84-02.04.2017.A044; 81-02.04.2021.A012; 81-02.04.2022.A055). All animals received a Western Type diet (WTD) for a period of 5 weeks until the experimental endpoint. The group size for all experiments ranged from 14 to 25 animals. The Ang II infusion model was used to induce aortic aneurysms and dissections in mice. For this purpose, mini osmotic pumps filled with Ang II were implanted. Blood pressure was measured in a representative subset of the experimental cohorts via the tail cuff method before and after osmotic pump implantation. Depending on the hypothesis, the Ang II model was combined with a pharmacological treatment (FTY720 or DOP), which modulates the sphingolipid metabolism. The S1P lyase inhibitor, DOP was used to increase S1P levels in the mice. The S1PR modulator, FTY720 was used as a potential therapeutic option, as it acts on several S1PRs[326]. Apolipoprotein E knockout mice ($ApoE^{-/-}$) and $ApoE^{-/-}$ crossbred with S1PR2- or S1PR3-deficient mice (Table 12) were used within this experimental setup to evaluate the role of S1P signaling (Figure 6).

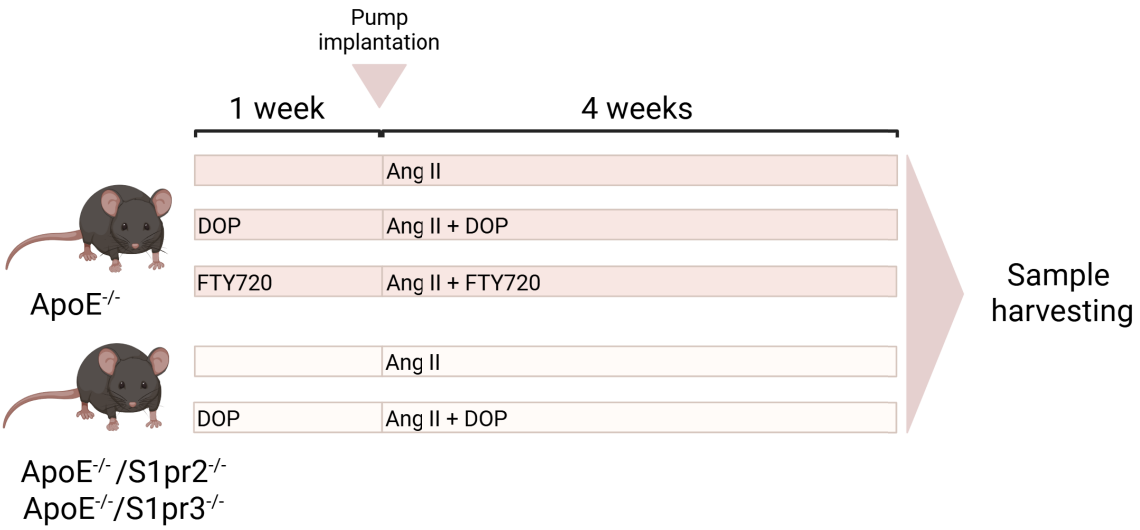

Figure 6: Experimental design. Apolipoprotein E knockout mice (ApoE$^{-/-}$) were fed a western type diet for 5 weeks. One week after feeding, mini osmotic pumps, filled with Angiotensin II (Ang II) were implanted into the mice. Four weeks after mini-osmotic pump implantation, mice were sacrificed and samples were taken. The Ang II model, was combined with a pharmacological inhibition of the S1P lyase by application of 4-deoxypyridoxine (DOP) or application of FTY720, as a S1PR modulator. Furthermore, ApoE$^{-/-}$ mice were crossed bred with S1PR2$^{-/-}$ and S1PR3$^{-/-}$ knockout mice. The created double knockout mice were infused with Ang II to investigate the impact of S1P signaling on aneurysm formation. Created with BioRender.com. Published under BioRender Publication Licence.

3.1.3. Ang II infusion model

The Ang II infusion model was employed to induce aneurysm formation and dissection in diverse strains of mice with ApoE$^{-/-}$ background. The mice were subjected to a high-calorie WTD one week before surgery, as well as for the next four weeks. Mouse weight was determined one day before surgery. Filling volume of Ang II was calculated based on the weight of each mouse (1,000 ng/kg/min in 0.9% NaCl), according to the manufacturer's guidelines[327]. Filled pumps were incubated overnight at 37 °C until surgery. Carprofen (5 mg/kg BW) was administered subcutaneously to the mice for analgesic purposes 30 min prior to the surgery. To induce anaesthesia, the mice were exposed to 2% isoflurane in an induction chamber. They were then placed onto a heated pad (37 °C) and anesthetized via a nose cone under an inflow of 1.5-2% isoflurane and 2 L/min oxygen as a carrier gas. After losing consciousness, the presence of pedal reflex was tested to ensure that mice did not experience any discomfort. Ointment was applied to prevent dryness of the eyes. The area, where the pump would be implanted was shaved using a razor to remove hair. A surgical scalpel was used to make a 1 cm incision into the skin behind the ear above the left shoulder blade. A small subcutaneous pocket was made using the haemostat. The filled pump was inserted and uniformly positioned into the pocket. By using resorbable silk, the

incision site was closed with two to three stitches. Over the next three days, the mice were administered Carprofen (5 mg/kg BW) to mitigate pain. Throughout the subsequent four weeks, the animals were monitored daily with regard to health status and survival. If animals died in between, the cause of death was examined to determine if it was due to rupture caused by an aneurysm. Finally, four weeks after pump implantation, mice were sacrificed under isoflurane anaesthesia, and *aortae* were examined for the evidence of aneurysms and dissections. Furthermore, blood and organ samples were collected for further analysis.

3.1.4. Pharmacological intervention

To investigate the extent to which sphingolipids, particularly S1P, influence the development of aortic aneurysms and dissections, pharmacological modulators of S1P signalling were combined with the Ang II infusion model (Figure 6). To inhibit S1P lyase, 4-deoxypyridoxine (DOP) was employed, while FTY720 was applied as a clinically approved S1PR modulator.

3.1.4.1. Pharmacological inhibition of the S1P lyase

S1P lyase inhibition was induced through administration of 4-deoxypyridoxine (DOP) at 30 mg/L in the drinking water, provided *ad libitum*. If combined with the Ang II infusion model, DOP was applied one week before pump implantation and for the following four weeks (Figure 6). To ensure the effect of DOP, which is also known as a vitamin B6 antagonist[328], a WTD without vitamin B6 supplementation was given over the experimental set-up. The supplemented DOP in the drinking water was replaced on a weekly basis.

3.1.4.2. Application of FTY720

The clinically approved S1PR modulator, FTY720 was applied to the mice at a dose of 10 µg/mL via the drinking water. In combination with the Ang II infusion model, FTY720 was applied one week prior to surgery to the animals and for the following four weeks. The supplemented FTY720 in the water was renewed weekly.

3.1.5. Blood pressure measurement

Systolic blood pressure (SBP) was measured non-invasively via tail cuff system (Hatteras Systems, SC1000 Blood Pressure Analysis System). The measuring principle is based on photoelectrically detected blood flow[329]. For this, the mouse was

placed under the specimen tray onto the measurement platform. The tail was threaded through the cuff and placed over a photosensor for detection. Blood flow in the tail produced oscillating waveforms, which were digitally detected. A measurement cycle consists of two phases. Once a stable pulse was registered in the initial phase, the cuff inflation was initiated. Following the system's detection of blood pressure, the cuff released during the second phase, the pressure and a new measurement cycle started. Each measurement took place under the same measurement conditions (Table 15), including at least 5-10 successively recorded cycles. The applied settings were chosen according to the manufacturer’s recommendations. A detailed definition of each measurement parameter was listed in the appendix (Table S 3). All mice were habituated to the measurement system for one week. During this week, all mice were placed daily under the specimen tray and baseline blood pressure was measured. Subsequently, blood pressure was measured regularly 2-5 days prior to osmotic pump implantation and 10-14 days after. All measurements took place at the same time of day and under the same external conditions. To prevent the mice from moving or pulling out their tail, the tail was lightly taped. All individual measurement cycles’ oscilliograms were manually reviewed and evaluated for their applicability to blood pressure assessment. Any measurement cycles in which a mouse moved were excluded from analysis.

Table 15 Settings for blood pressure measurement

Preliminary Cycles	5
Measurement Cycles	20
Movement Detection	No
Minimum Pulse Amplitude	5%
Number of Consecutive Peaks	70
Maximum Pressure	200 mmHg
Pulse Timeout	30 sec
Measurement Timeout	30 sec
Time between Measurements	2.5 sec
Systolic Threshold	20%
Diastolic Threshold	50%
Platform temperature	37 °C

3.1.6. Dissection and sample processing of mice

Animals were sacrificed and processed four weeks after osmotic pump implantation. Blood and the aorta were collected from all animals.

Mice were euthanized by isoflurane overdose following induction with 5% isoflurane. After verification and absence of righting and pedal reflex, mice were positioned on its back. Organs were exposed by a medial incision into the abdomen. The diaphragm was carefully disrupted and the thorax was opened upwards through a lateral incision.

Blood was harvested via heart puncture using syringes coated with 0.5 M EDTA solution to prevent coagulation. Total blood volume was determined. To investigate haematological parameters, 30 µL of whole blood were used for analysis with Scil VetABC Plus. Furthermore, 50 µL of the entire blood volume were used for flow cytometry analysis of immune cells. From the remaining blood, plasma was obtained by centrifugation (1,500 x g, 4 °C, 10 min). Samples were shock-frozen in liquid nitrogen and stored at -80 °C for later analysis.

Mice were perfused with PBS through the left ventricle of the heart to remove remaining blood from the aorta and other organs. Organs were removed and the aorta was exposed. Surrounding adipose tissue was cleaned off from the aorta. The aorta was dissected, extending from the aortic arch to the bifurcation. Depending on the subsequent experiments, the aorta was directly used, shock frozen and stored at -80 °C or alternatively fixed with 4.5% paraformaldehyde (PFA) at 4 °C for 24 h.

3.1.7. Vascular reactivity studies

The vasoactive properties of 2 mm abdominal aortic segments (proximal segment of the aortic bifurcation) were investigated. After sacrificing mice by isoflurane anaesthesia, the aortic segments were isolated from adjacent fat, mounted in a DMT 620M wire myograph (DMT, Denmark), and allowed to equilibrate for 60 min in Krebs-Henseleit buffer (Figure 7). During the equilibration phase, the *aortae* were slowly preloaded with 9.8 mN (as a simulation of the *in vivo* force), and the Krebs-Henseleit buffer was renewed every 15 min. After establishing the maximal contraction force by incubation with 80 mM KCl, the segments were washed by changing the buffer until they reached the baseline force of 9.8 mN. The segments were exposed to increasing doses of phenylephrine (Phe; 0.1 nM-3.5 µM) to determine vasoconstriction (Figure 8).

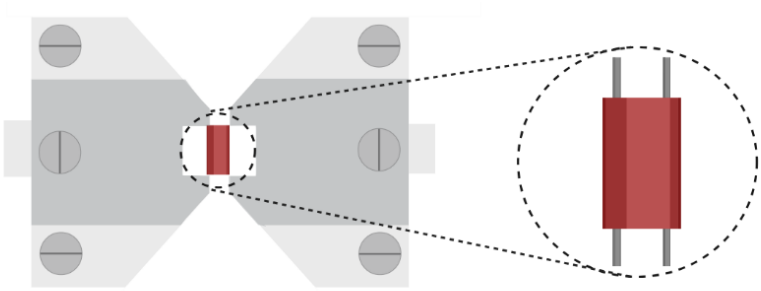

Figure 7: Schematic illustration of the wire myograph setup for vascular reactivity measurements. A 2 mm aortic segment is mounted on two parallel stainless steel wires and positioned between two jaws of the wire myograph system. The zoomed-in section shows the vessel segment positioned between the mounting wires. Created by BioRender.com. Published under BioRender Publication Licence.

Following this, the endothelial function was quantified by the dilation response to cumulative concentrations of acetylcholine (ACh; 0.1 nM-3.5 µM) in the presence of indomethacin (Indo; 10 µM). Indomethacin was used to inhibit cyclooxygenase-dependent prostaglandin synthesis and thereby eliminate prostanoid-mediated influences on vascular tone. Consequently, after additional washing steps with Krebs-Henseleit buffer, the vascular response to Ang II was assessed by cumulative doses (1 nM-1 µM) in the abdominal aortic segments. A representative tracing was shown in Figure 8.

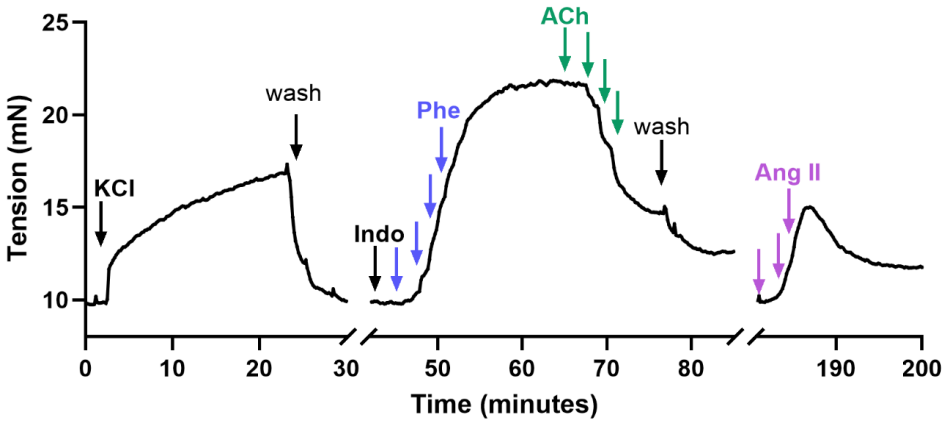

Figure 8: Representative tracing: Abdominal aortic segments (2 mm) were mounted into the wire myograph. The segments were pretensioned to 9.8 mN. Potassium chloride (KCl) was administrated for maximum contraction force. After washing steps Indomethacin (Indo) was administrated to the segments, followed by increasing doses of phenylephrine (Phe). After maximum response to Phe, cumulative doses of acetylcholine (ACh) were added to the segments. For abdominal segments, the contractile response to Ang II was then examined.

3.1.8. Macroscopic classification and assessment of aortic aneurysms

After pump implantation, the survival and condition of the mice were monitored daily. Since death-associated aortic rupture is known for the Ang II infusion model,[330,331] each dead mouse was subjected to a necropsy. The thorax and abdomen were opened and examined for haemorrhage, indicating aneurysm-related rupture. Survival analysis

comprised all animals, including those that died or had to be sacrificed due to rupture, and those that survived until study endpoint. All aneurysms were classified according to Daugherty's classification scheme based macroscopic phenotypical severity of the aortic aneurysms (Table 16)[332].

Table 16 Macroscopic classification of aortic aneurysms/ dissections

Severity scale	Criteria
None	No aneurysm
I	Dilated aortic lumen with no thrombus
II	Remodelled aortic tissue with thrombus
III	Distinct bulbous form of type II with thrombus
IV/Rupture	Multiple aneurysm/dissection or rupture

Table adapted from Daugherty et al.[332]

3.1.9. Histology of aortic aneurysm and dissections

Aortic tissue was fixed in 4.5% paraformaldehyde (PFA) for 24 h. Paraformaldehyde-fixed tissue was transferred to PBS (1X) containing 0.05% sodium azide and stored at 4 °C before proceeding with dehydration procedure. Dehydration of tissue samples was performed by the Central Facility for Animal Research and Scientific Animal Welfare of the University Hospital Düsseldorf. Afterwards, samples were embedded in paraffin and 5 µm thick transverse sections were prepared. Haematoxylin & Eosin, Verhoeff van Gieson, and immunohistological staining for smooth muscle actin (ACTA2) were performed to determine morphological alterations of the aorta.

3.1.9.1. Haematoxylin & Eosin (H&E) staining

Aortic sections were deparaffinised in xylene and gradually decreasing concentrations of ethanol (100% - 70%), then rehydrated and incubated in Mayer's haematoxylin. The sections were allowed to turn blue before being treated with 1% eosin solution and dehydrated again using gradually increasing concentrations of ethanol (70% - 100%). Finally, the sections were subjected to xylene immersion and permanently fixed. A detailed staining protocol with all steps and corresponding incubation times can be found in the appendix (Protocol 1).

3.1.9.2. Verhoeff van Gieson (VVG) staining

Verhoeff van Gieson staining was performed to visualize elastic fibres. Prior to incubation in Verhoeff's solution, aortic sections were deparaffinised in xylene followed

by rehydration in decreasing concentrations of ethanol (100%-70%). Destaining was initiated with 2% ferric chloride solution and completed with 5% sodium thiosulfate solution. Van Gieson's solution was used for collagen counterstaining. Finally, sections were rehydrated in increasing ethanol concentrations (70%-100%), immersed in xylene, and permanently fixed. A detailed staining protocol with all step and corresponding incubation times can be found in the appendix (Protocol 2).

3.1.9.3. Immunohistological staining for VSMCs

Since VSMCs are the major cell type in the media and involved in aortic aneurysm pathophysiology, immunohistochemistry for VSMCs was performed. An antibody against ACTA2, a well-established marker for VSMCs was used for detection. Aortic sections were deparaffinised in xylene followed by rehydration in decreasing concentrations of ethanol (100%-70%). Sections were washed in distilled water and blocked in 3% hydrogen peroxide for 10 min at room temperature. Afterwards, aortic sections were washed three times in PBS and stained with primary antibody for 1 h at room temperature. Primary antibody was diluted 1:200 in 3% rabbit serum. Wash steps were repeated and biotinylated secondary antibody, 1:200 in 3% rabbit serum, was added for 30 min to the aortic sections. Washing steps with PBS, followed by streptavidin-coupled peroxidase incubation for 45 min. Incubation for 5 min with the chromogen diaminobenzidine allowed visualization by the formation of insoluble coloured precipitates. Cell nuclei were counterstained with Haematoxylin. A detailed staining protocol with all steps and corresponding incubation times can be found in the appendix (Protocol 3).

3.1.10. Flow cytometry analysis of immune cells

Fluorescence Activated Cell Sorting (FACS) enables single cell analysis by detecting laser light scatter for size (FSC) and granularity (SSC), complemented by fluorescence-labelled antibodies to distinguish cell types and subsets. For flow cytometry analysis of immune cells, 50 µL of whole blood per staining were utilized. The whole blood samples underwent incubation with 2 mL BD Pharm Lyse™ Lysis Buffer (1:10 diluted in distilled water) to lyse RBCs. Incubation was carried out at room temperature for 7 min followed by a 7 min incubation step on ice. Subsequently, the samples underwent centrifugation at 450 x g for 5 min and supernatant was discarded. The remaining cells were washed with 2 mL of FACS buffer, centrifuged again under the same conditions, the supernatant discarded and 100 µL of FACS buffer added.

Fluorescent-labelled antibodies were applied to the cell suspension and incubated for 25 min at 4 °C. (Table 17) After incubation with antibody cocktail, samples were rinsed with 2 mL FACS buffer and centrifuged under the previous conditions. The supernatant was discarded, and samples were resuspended in 200 µL of FACS buffer before flow cytometry analysis on Gallios Flow Cytometer. At least 50,000 events were collected per sample. Gating strategy can be found in the appendix (Figure S 1).

Table 17 Overview of antibody cocktail for blood cells

Antibody	Main detected cell type	Conjugated	Concentration [µg/ml]
B220	B cells	APC-eFluor780	2
CD44	T cells, B cells	FITC	3.75
CD45.2	Leukocytes	V500	1.5
CD62L	Leukocytes	PE-Cy7	1.5
CD4	T cells	APC	1
CD8	T cells	PE	0.8

3.2. RNA Sequencing

All practical processes following RNA extraction that are part of the RNA sequencing procedure were carried out by Thorsten Wachtmeister from the Genomics & Transcriptomics laboratory under the direction of Dr. Jochen Hecht.

3.2.1. RNA Extraction and Quality Control

Total RNA was extracted from the thoracic aorta of mice treated with Ang II or Ang II and DOP for 10 days (n = 4 per group). RNA was isolated using the innuPREP Mini RNA Kit, which was combined with the innuPREP DNase I Digest Kit. All steps were performed according to the manufacturer's instructions. RNA concentration was quantified using a NanoDrop. A minimum concentration of 10 ng/µL of total RNA was submitted to the Genomics & Transcriptomics Laboratory (Heinrich-Heine-University, Düsseldorf) for all subsequent RNA sequencing procedures. First, total RNA samples were quantified fluorometrically using the Qubit fluorometer in combination with the RNA High Sensitivity Assay. RNA integrity was assessed by capillary electrophoresis using the Fragment Analyzer and the DNF-471 Total RNA High Sensitivity Assay. Samples with a RNA Quality Number (RQN) between 8 to 10 were used for further analysis.

3.2.2. Library Preparation and Sequencing

For library preparation, 50 ng of total RNA per sample were used following the manufacturer's instructions for the QuantSeq 3′ mRNA-Seq V2 Library Prep Kit with the UDI and UMI Second Strand Synthesis Module for QuantSeq FWD. After bead-based purification, libraries were normalized and sequenced on the NextSeq2000 system using single-end sequencing with a read length of 111 bp. The bclconvert tool was employed for base calling, conversion of bcl files to fastq format, adapter trimming, and demultiplexing.

3.2.3. Data analysis for RNA sequencing

Raw fastq files were processed using CLC Genomics Workbench (v24.0.1, QIAGEN, Venlo, NL). Unique Molecular Identifiers (UMIs) were removed from all reads and annotated, while reads lacking a UMI were discarded. Adapter and quality trimming was performed with default parameters, removing bases with a quality score below Q13 and allowing a maximum of two ambiguous nucleotides per read. High-quality reads obtained after trimming were mapped against the *Mus musculus* reference genome (GRCm39). Following sample grouping (four biological replicates per condition), differential expression analysis was conducted using the RNA-Seq analysis workflow implemented in CLC Genomics Workbench. Multigroup comparisons were performed, and statistical significance was assessed using false discovery rate (FDR) and Bonferroni correction. A p-value ≤ 0.05 was considered statistically significant. The final dataset provided by the RNA Sequencing Unit included $\log_2$ fold change values for group comparisons, along with read counts, counts per million (CPM), and transcripts per million (TPM) values for each gene. To explore the functional implications of the differentially expressed genes, enrichment analyses based on Gene Ontology (GO), Kyoto Encyclopaedia of Genes and Genomes (KEGG), and Gene Set Enrichment Analysis (GSEA) were carried out. These analyses were conducted to identify significantly enriched biological processes, molecular functions, cellular components, and relevant signaling pathways associated with the experimental conditions.

3.3. Proteomics analysis

For Proteomics analysis abdominal aorta of the same mice, which were provided to RNA sequencing, were used. Whole procedures including, sample preparation, protein

extraction, mass spectrometry analysis and quantification were provided by the Molecular Proteomics Laboratory of the Biomedical Research Centre under the direction of Dr. Anja Stefanski (BMFZ, Heinrich-Heine-University, Düsseldorf).

3.3.1. Sample preparation

Aortic tissue was homogenized in RIPA lysis buffer using a Tissue Lyser. Cell suspension was centrifuged for 15 min at 14,000 g and 4 °C. Protein concentration of supernatants was determined using Pierce™ 660 nm Protein Assay. A total of 10 µg protein from each sample was desalted by electrophoresis using a 4-12% Bis-Tris polyacrylamide gel run at 50 V for 10 min. After silver staining, protein bands were excised, followed by reduction, alkylation, and tryptic digestion. Peptides were then extracted using sonication, dissolved, and diluted in 0.1% (v/v) trifluoroacetic acid (TFA).

3.3.2. LC-MS analysis

For peptide analysis, 15 µL of peptide-TFA solution were subjected to nano-high-performance liquid chromatography electrospray ionization mass spectrometry system. The system consisted of an RSLCnano U3000 HPLC unit linked to an Orbitrap Elite mass spectrometer equipped with a nano-electrospray ion source. Initially, peptides were concentrated and desalted on a trapping column (Acclaim PepMap C18, 2 cm × 100 µm, 3 µm particle size, 100 Å pore size, Thermo Fisher Scientific) at a flow rate of 6 µL/min for 10 min, using 0.1% (v/v) TFA as the mobile phase. Separation was then performed on an analytical C18 column (25 cm × 75 µm, 2 µm particle size, 100 Å pore size) at 60 °C, applying a constant flow of 300 nL/min. The mobile phase consisted of solvent A (0.1% formic acid in water) and solvent B (0.1% formic acid, 84% acetonitrile in water), with a gradient from 4% to 40% B over 120 min. Peptides were eluted at 6 µL/min for 10 min using 0.1% TFA, ionized at 1,400 V, and introduced into the spectrometer operating in positive ion mode. Data were acquired in the m/z range of 350-1700 at a resolution of 60,000. Tandem mass spectra (MS/MS) were obtained in an ion trap using a data-dependent Top 20 method with a normalized collision energy of 35%. Dynamic exclusion was enabled with a repeat count of 1 and an exclusion duration of 45 seconds. Only precursor ions carrying charges of 2+ or 3+ were selected for fragmentation.

3.3.3. Computational mass spectrometric data analysis

Protein identification was carried out using Mascot as the search algorithm within Proteome Discoverer, employing the UniProt mouse database (Proteome ID: UP000000589). A peptide-level false discovery rate of 1% ($p \leq 0.01$) was applied as the cut-off criterion for reliable identification. Quantification of proteins was subsequently performed using Progenesis QI for Proteomics (Version 2.0, Nonlinear Dynamics, Waters Corporation).

3.3.4. Functional Analysis of proteomics data

A dataset containing the respective quantification values and log_2 fold change comparisons were provided for further analyses. To assess the biological significance of differentially expressed proteins, GO term enrichment analysis and KEGG pathway analysis were conducted.

3.4. Cell culture

3.4.1. Isolation of rat primary VSMCs

Primary VSMCs were isolated from Wistar rats kindly provided by local animal facility (Central Facility for Animal Research and Scientific Animal Welfare of the University Hospital Düsseldorf). All rats were sacrificed via CO_2 inhalation performed by qualified staff of the animal facility. The aorta was exposed as already described for mice above. The aorta was dissected from the aortic arch to the bifurcation after removing of surrounding adipose tissue. Then, the aorta was transferred into a tube filled with 1 mL of a prewarmed VSMC isolation enzyme mix and incubated 30 min at 37 °C. Subsequently, the aorta was transferred into a dish with prewarmed PBS and the adventitia was carefully removed by stripping it off. The remaining aorta was cut into small pieces (5-10 mm) and transferred into a new tube. After centrifugation (1,200 x g, 5 min, RT), the supernatant was removed and fresh 2 mL prewarmed enzyme mix was added to the small aorta pieces. The mixture was resuspended and incubated for 2 h. After half of the time, the mixture was gently inverted. The cell-enzyme mixture was centrifuged again (1,200 x g, 5 min, RT) and the pellet was resuspended in VSMC growth media. Finally, 10,000 cells were seeded into each well of a 6-well plate. Standard culture conditions (37 °C, 5% carbon dioxide, 95% humidity) were used. After 2-3 days VSMCs started spreading. For subsequent experiments, only VSMCs up to passage 5-10 were used.

3.4.2. Culture of primary rat VSMCs

Primary VSMCs isolated from *aortae* of rats were used for cell culture experiments. Cells were cultured in DMEM supplemented with 10% FBS, 2 mM glutamine, 1% antibiotic/antimycotic solution as well as 1 mM sodium pyruvate solution. Standard culture conditions were used (37 °C, 5% CO_2, 95% humidity). Cells were subcultured after reaching 90% confluency. For this, the medium was removed, cells were washed with 10 mL PBS and covered with 1 mL prewarmed Accutase®. After 2-5 min incubation time at 37 °C, when all cells were detached, the reaction of Accutase® was stopped with fresh DMEM. Then, cells were transferred to a new flask in ratio 1:10.

For experiments 100,000 cells were seeded per well into a 6-well plate. After reaching 80% confluency cells were starved overnight in DMEM culture medium without FBS. For subsequent experiments, fresh prewarmed starvation medium was used. No VSMCs cultured beyond passage 10 were used.

3.4.3. Cell stimulation

Rat VSMCs were used for all *in vitro* experiments. Cells were cultured in 6-well plates at a cell density of 100,000 cells/well for stimulation. Before stimulation, the cells were starved overnight by changing to cell culture media without FBS. Cells were treated with S1P, S1P analogues, and diverse S1PR agonists and antagonists (Table 18). Antagonists of S1PR signaling were administered 30 min before S1P treatment. Since it is known that Ang II is an essential inducer of VSMC remodelling, cells were additionally treated with Ang II alone or in combination with S1P. The cells were stimulated for 6 h and 24 h, respectively. In addition, the cells were stimulated with S1P over a period of 3 days. For this purpose, S1P was added twice a day, 10 h apart. Additionally, cells were treated for 5 days with the S1P lyase inhibitor S1PL-IN-1, which was administered once daily. To enhance the accumulation of S1P, Sph was administered concurrently.

Table 18 Overview of substances used for *in vitro* stimulation

Substance	Target	Solvent	Final concentration
Ang II	AT_1R; AT_2R	H_2O	100 nM
S1P	S1PR1-5	MeOH	1 µM
Sph	SphK1, 2	EtOH	1 µM
NIBR0213	S1PR1 antagonist	DMSO	100 nM

JTE-013	S1PR2 antagonist	DMSO	10 µM
TY52156	S1PR3 antagonist	DMSO	10 µM
AUY954	S1PR1 agonist	DMSO	10 µM
CYM5520	S1PR2 agonist	DMSO	10 µM
CYM5543	S1PR3 agonist	DMSO	10 µM
S1PL-IN-1	S1P lyase inhibitor	DMSO	1 µM

3.5. Intracellular calcium measurement

For examination of intracellular calcium release, VSMCs were seeded into a T175 flask. The media was discarded, cells were washed with PBS and 2 mL Accutase® was added to the cells. After 2-5 min incubation at 37 °C, the reaction of Accutase® was stopped by adding 10 mL culture medium. Then, cells were centrifuged for 5 min at 4 °C and 450 x g. The cell pellet was resuspended in 10 mL culture medium and cells were counted. Subsequently, VSMCs were centrifuged again under the previous conditions. Then, cells were resuspended in 10 mL Washing Buffer and centrifuged once again. Depending on the number of cells, VSMCs were resuspended in 0.5 mL Dye Buffer per one million cells. Dye Buffer contained 2.5 µL/mL Fura-2 and 1 µL/mL Pluronic. Fura-2 is a ratiometric fluorescent dye, which is excited at different wavelengths depending on whether the dye is bound to calcium or not. Pluronic is a non-ionic surfactant that supports Fura-2 entering the cells for loading. Subsequently, the cells were incubated in dye buffer at 37 °C for 30 min with gentle agitation every 10 min. Following incubation, the cells were centrifuged as previously described and washed once with wash buffer. Measurements were then performed at a concentration of 1×10^6 cells/mL. The released calcium, coupled to Fura-2, was excited at a wavelength of 340 nm, whereas the unbound Fura-2 was excited at 380 nm. The emission wavelength was 510 nm. The final calcium concentration was determined via the Grynkiewicz equation[333].

3.6. RNA Isolation

For RNA isolation from primary VSMCs and murine aorta, the innuPREP Mini RNA Kit 2.0 was used. The isolation procedure followed the manufacturer's protocol specific for cell and tissue specimens.

VSMCs, which were seeded on a 6-well plate were stimulated as intended. After the appropriate stimulation time, cells were washed with PBS. Then, PBS was removed and 400 µL RNA lysis buffer was added to the cells. VSMCs were scratched from the plate using a cell scraper. The cell lysate was loaded onto the Spin Filter D.

The abdominal part of the murine aorta was used for RNA isolation from tissue. First, the aortic tissue was transferred to a tube with 450 µL RNA lysis buffer and then mechanically homogenized by using a TissueRuptur II from Qiagen. Afterwards the mixture was loaded onto a QIAshredder spin column and centrifuged for 2 min at maximum speed. The flow-through was collected and loaded on Spin Filter D.

After this step, the same procedure was followed with the two sample types (VSMCs and aortic tissue) as described in the kit manual. Finally, RNA from aortic tissue and VSMCs was eluted in 50 µL by centrifugation at 6,000 x g for 1 min. RNA concentration was determined by NanoDrop. All RNA samples were stored at -80 °C.

3.7. Synthesis of complementary DNA (cDNA)

For cDNA synthesis the RevertAid First Strand cDNA Synthesis Kit was used. The synthesis was carried out according to the instructions of the kit manual. Per preparation 100-800 µL RNA were transcribed into cDNA. All cDNA samples were stored at -20 °C.

3.8. Real time quantitative PCR (RT qPCR)

The expression of all genes was detected by using SYBR® Green qPCR. Each reaction mix contains the following components:

Forward primer	0.5 µL
Reverse primer	0.5 µL
iQ SYBR® Green Supermix	10 µL
H_2O	8 µL
cDNA	1 µL
Total volume	20 µL

The following thermocycling protocol was performed by using CFX96 Real-Time System.

Step	Temperature (°C)	Time (min:s)	Cycles
Initialization	50	10:00	1
Denaturation	95	05:00	1
Denaturation	95	00:10	40
Annealing	60	00:30	
Elongation	72	00:30	
Denaturation	95	00:10	1
Extension	65	00:05	1

To evaluate the expression levels of each gene, the Ct value was normalized against GAPDH. Finally, relative changes in gene expressions were calculated by using the $2^{(-\Delta\Delta Ct)}$ method.

3.9. Western Blot analysis

3.9.1. Cell lysis and sample preparation

Treated VSMCs, cultured on 6-well plates, were washed with PBS after the appropriate stimulation time. PBS was removed from the plate and 60 µL RIPA lysis buffer supplemented with Halt™ protease and phosphatase inhibitor cocktail was added to the cells. Cells were detached using a scraper and the lysate was collected in tubes. The samples were incubated for 30 min on ice and shortly vortexed after 15 min. Following lysis, cell debris was removed by centrifugation at 12,000 x g for 5 min at 4 °C. Protein concentration was determined using Pierce™ BCA Protein Assay Kit. Prior to electrophoresis, samples were combined with 4x Laemmli buffer containing β-mercaptoethanol and heated at 90 °C for 2 min.

3.9.2. Sodium dodecyl sulfate polyacrylamide gel electrophoresis

Depending on the expected molecular weight of the target proteins, 10-15% gels were used. Gels were loaded with 10-20 µg protein. Electrophoresis was performed using running buffer. In order to ensure the consistent separation, the gel was left running 30 min at 70 V. Following separation in the stacking gel, the running voltage was adjusted to 130 V.

3.9.3. Western Blotting

To transfer the protein from the gel to the polyvinylidene difluoride (PVDF) membrane, the Mini Trans-Blot® Cell System was used. First, the PVDF membrane was activated for 10 s in methanol (MeOH). According to the instructions of the manual, the wet blot apparatus was assembled. Proteins were blotted for 960 min at 30 V under cooling conditions using transfer buffer. After the blotting process, the membrane was blocked for 1 h in 1x Roti®Block. Primary antibodies were diluted in 1x Roti®Block and added to the membrane. The membrane was incubated at 4 °C overnight. Subsequently, the membrane was washed three times for 10 min with washing buffer. The secondary antibodies were diluted in 1x Roti®Block and added to the membrane. The membrane was incubated for 2 h at room temperature with secondary antibody. After repeating the previous washing steps, proteins were detected. For that, the membrane was covered with enhanced chemiluminescence solution (ECL) and incubated for 30 s. The detection of the luminescent signal was detected via ChemiDoc™ XRS+ Imaging System.

3.10. Sphingolipid measurement by LC-MS/MS

Sphingolipid measurement was performed by using LC-MS/MS. All procedures on the mass spectrometer were carried out by Dr. Philipp Wollnitzke or Dr. Hannah Siera, while sample processing and final data analysis were completed by myself.

3.10.1. Sample preparation

Sphingolipids were analysed in murine and human plasma and aortic tissue samples. An internal standard was added to all samples during the preparation process to analyse the sphingolipid profile. The composition of the internal standard can be obtained from Table 19.

Plasma for LC-MS/MS analysis was prepared by addition of 250 µL MeOH to 50 µL plasma and 10 µL internal standard (Table 19). The samples were mixed for 5 min using a VX2500 Multi-Tube Vortexer and then incubated at -80 °C overnight. Afterwards, the samples were centrifuged for 10 min at 4 °C and 20,000 x g, and the supernatant was transferred into certified LC/MS glass vials for LC-MS/MS analysis.

Aortic tissue was weighted and shredded under liquid nitrogen with the assistance of a pestle. To the pulverized aortic tissue, 1 mL of MeOH and 10 µL of the internal

standard were added. Samples were incubated overnight at -80 °C and centrifuged under high-speed conditions (20,000 x g, 10 min, 4 °C). Supernatant was transferred to another tube and vacuum evaporated at 60 °C for 45 min. Finally, samples were resolved in 100 µL MeOH and transferred to a certified LC/MS vial for following analysis.

Table 19 Composition of internal standard

Lipid	Concentration (µM)
S1P (d18:1-d7)	0.1
Sph (d18:1-d7)	0.3
Cer (d18:1/15:0)	0.3
LPC (17:0)	0.3
PC (17:0/17:0)	0.3
SM (d18:1/17:0)	0.3
LPE (17:1)	5
PE (17:0/17:0)	5

3.10.2. Chromatographic separation and detection of lipid classes

For the analysis of different lipid classes (Table 20), including sphingolipids and phosphoglycerides, LC-MS/MS was performed using a LCMS-8050 triple quadrupole mass spectrometer. A Dual Ion Source combined with a Nexera X3 Front-End System ensured sensitive and specific identification of lipid species in plasma and aortic tissue. Different chromatographic columns, mobile phases, and gradient programs were used to ensure efficient separation of these lipid classes prior to mass spectrometric analysis.

Chromatographic separation of S1P, Sph, and ceramides, a MultiHigh-C18 reversed-phase (RP) column (2 × 60 mm, 3 µm particle size, 100 Å pore size) was employed, maintained at a constant temperature of 40 °C. Mobile phases included MeOH (solvent A) and 1% (v/v) aqueous formic acid (solvent B). A linear gradient increasing solvent A from 10% to 100% over a 3 min period (B-curve = -2) was applied to elute peptides. This was followed by re-equilibration to 10% solvent A for 2 min prior to the next injection. The flow rate was maintained at 0.4 mL/min, and an injection volume of 10 µL was applied for all runs.

Chromatographic separation was conducted using an Accucore Polar Premium column (3 × 150 mm, 2.6 µm particle size) for the targeted analysis of

phosphoglycerides and sphingomyelins. The mobile phases consisted of [A] 10 mM aqueous ammonium formate with 0.01% (v/v) formic acid and [B] acetonitrile with 0.01% (v/v) formic acid/isopropanol (1:1 mixture). Gradient elution was applied, beginning with 20% solvent B for 1 min, followed by a gradual increase to 40% solvent B within the next minute. The proportion of solvent B was then raised to 92.5% over 23 min, reaching 100% at 26 min, where it was held for an additional 9 min before re-equilibration to 20% solvent B from 35.1 to 38 min. The flow rate for this separation was maintained at 0.3 mL/min, and an injection volume of 1 µL was used for all samples.

Table 20 Lipid classes and metabolites measured with LC-MS/MS

Lipid class	Subclass	Members
Sphingolipids	Sphingoid base	Sph (d18:1)
	Phosphosphingolipid	S1P (d18:1)
	Ceramide (Cer)	(d18:1/14:0),(d18:1/16:0), (d18:1/18:0),(d18:1/20:0), (d18:1/22:0),(d18:1/24:0), (d18:1/24:1)
	Dihydroceramide (dhCer)	(d18:0/16:0),(d18:0/18:0), (d18:0/24:0),(d18:0/24:1)
	Sphingomyelin (SM)	(32:1), (32:2), (34:1), (34:2), (36:1), (36:2), (38:1), (38:2), (40:1), (40:2,) (40:7), (42:1), (42:2)
Glycerophospholipids	Phosphatidylcholine (PC)	(28:0), (30:0), (30:2), (32:0), (32:1), (32:2) (34:1), (34:2), (34:3), (34:4), (36:1), (36:2), (36:3), (36:4), (38:1), (38:3), (38:4), (38:5), (38:6), (40:4), (40:5), (40:6); (40:7), (40:8), (42:10)
	Phosphatidylethanolamine (PE)	(34:1), (34:2), (36:1), (36:2), (36:4), (38:4), (38:5), (38:6), (40:6)
	Lysophosphatidylcholine (LPC)	(14:0), (16:0), (18:0), (18:1), (18:2), (20:0), (20:1), (20:2), (20:3), (20:4)
	Lysophosphatidylethanolamine (LPE)	(16:0), (18:0), (18:1), (18:2), (20:4), (22:6)
Sterols	Cholesterols	Cholesterol

Mass spectrometric detection of S1P and Sph was performed using an electrospray ionization (ESI) source. In contrast, ceramides and steroids were analysed with an atmospheric pressure chemical ionization (APCI) source. The optimized MS settings for all lipid classes are listed in Table 21.

Table 21 Settings of LC-MS/MS

	Electrospray Ionization (ESI)	**Atmospheric Pressure Chemical Ionization (APCI)**
Nebulizing gas flow	3 L/min	2.4 L/min
Heating gas flow	10 L/min	3 L/min
Interface temperature	300 °C	300 °C
Desolvation temperature	526 °C	526 °C
Desolvation line temperature	250 °C	250 °C
Heat block temperature	400 °C	400 °C
Drying gas flow	10 L/min	3 L/min

Lipid quantification was conducted using multiple reaction monitoring (MRM) in positive ionization mode, allowing for the targeted detection of specific precursor and fragment ions. Standard curves for all sphingolipids except sphingomyelin were established by measuring increasing concentrations of the respective analytes in a concentration range of 10 nM to 5 µM. In contrast, standard curves for phosphoglycerides and sphingomyelin were created by measuring increasing concentrations of the target lipids in a range of 0.1 µM to 10 µM. Internal standards were used for the quantification (Table 19).

All mass spectrometric data were acquired using LabSolutions 5.114 (Shimadzu, Kyoto, Japan). Raw data files were processed using LabSolutions Insight, where MRM peak integration, background subtraction, and quantification were performed. For data analysis, calibration curves were generated, and linear regression analysis was conducted to determine the correlation coefficients of standard curves.

3.11. Human samples

3.11.1. Ethical compliance and sample collection

Abdominal aortic aneurysm tissue was obtained from patients undergoing open surgical or endovascular repair at the Clinic for Thoracic Surgery and Vascular Surgery (University Hospital Düsseldorf), the Clinic for Cardiovascular Surgery (University Hospital Düsseldorf) or the Section for Vascular and Endovascular Surgery (University Hospital Essen). Control aortic tissue was collected from donors undergoing liver transplantation, who had no clinical diagnosis or radiographic evidence of aortic aneurysm. For all cohorts, patients with hereditary disorders predisposing to aneurysm formation were excluded from the study. Additionally, it was ensured that only transmural tissue free of thrombotic material was collected.

Plasma samples were collected from the same cohorts as well as from an additional control group of healthy donors with comparable clinical conditions. The clinical characteristics of patients from whom plasma (Table S 4) and aortic tissue (Table S 5) were obtained are provided in the supplemental part.

All human plasma and tissue samples were used for sphingolipidomic analysis. The study was approved by the local ethics committee (Reference number: 18-8073-BO, Reference number: 5731R, Reference number: 2018-248_1, Reference number: 2018-298) and conducted in accordance with the principles of the Declaration of Helsinki.

3.11.2. Analysis of human sphingolipidomic data

Lipidomics data analysis was performed using MetaboAnalyst 5.0. Data were log_2-transformed and auto-scaled prior to statistical evaluation. Differential abundance was assessed by volcano plot analysis, and biomarker identification was conducted using random forest analysis. Principal component analysis (PCA) and Receiver operating characteristic curve (ROC) analysis was performed and visualized using GraphPad Prism 10. A comprehensive list of p-values for all tested lipids in plasma (Table S 6) and aortic tissue (Table S 7) compared with controls were provided in the supplemental part.

3.12. Statistical analysis

Statistical analyses were performed using GraphPad Prism 10 and MetaboAnalyst 5.0. The number of biological replicates (n) is indicated in the representative figure legend. In general, data are generally presented as mean ± standard error of mean (SEM).

Data was always assessed for normality using the Shapiro-Wilk for small sample sizes ($n \leq 8$), and the D'Agostino-Pearson test for larger cohorts ($n > 8$). Depending on data distribution and experimental design, either an unpaired t-test or Mann-Whitney test, a one-way ANOVA or a two-way ANOVA with repeated measures or multiple comparisons with Tukey's post hoc testing was performed. Fisher's exact test was used for group comparisons involving categorical variables and small sample sizes. For multiple testing correction in high-dimensional data, false discovery rate (FDR) adjustment was applied using the Benjamini-Hochberg method. Survival analyses were conducted using Kaplan–Meier estimation, with group differences evaluated via the log-rank (Mantel-Cox) test. Correlation analyses were performed using Pearson's or Spearman's correlation coefficients, depending on data characteristics. To quantify concentration-response relationships the area under the curve (AUC) was calculated and compared between groups. Random forest classification was used to identify discriminative lipid features, supported by receiver operating characteristic (ROC) curves to assess classification performance. A p-value ≤ 0.05 was considered statistically significant.

4. Results

4.1. Pharmacological inhibition of S1P lyase by DOP promotes aortic aneurysm formation and rupture in the Ang II model

Sphingosine-1-phosphate (S1P), a bioactive lipid, has been demonstrated to play a pivotal role in the regulation of vascular function and homeostasis[268]. Therefore, altered S1P levels and dysregulated S1P signaling have been implicated in the pathogenesis of various cardiovascular diseases[268]. Within this project, the primary objective was to investigate the potential involvement of S1P in the pathophysiology of aortic aneurysms and dissections.

To investigate whether S1P is involved in the development of aortic aneurysm formation and dissection, the Ang II infusion model was combined with a pharmacological inhibition of the S1P lyase, the only enzyme that can irreversibly degrade S1P, thereby increasing S1P levels (Figure 9).

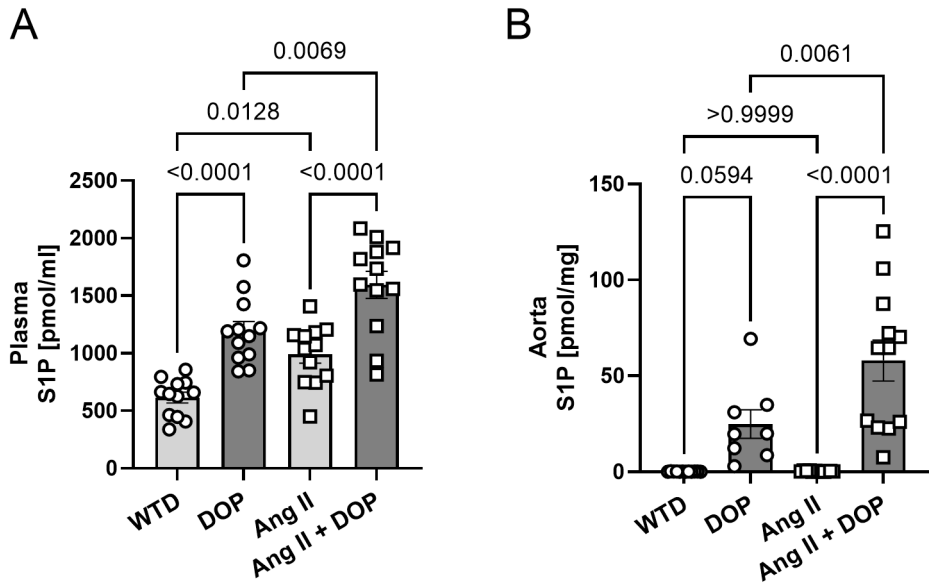

Figure 9: Elevation of S1P levels in plasma and aortic tissue following pharmacological inhibition of the S1P lyase. ApoE$^{-/-}$ mice were fed a western type diet (WTD) and infused with Ang II (1,000 ng/kg/min) for 28 days, with and without additional treatment using the S1P lyase inhibitor 4-deoxypyridoxine, DOP (30 mg/L; via drinking water). Control groups received WTD alone or WTD with DOP. Alterations in S1P levels were determined by LC-MS/MS (A) Plasma S1P levels (n = 12 per group) (B) S1P levels in aortic tissue (n = 12 per group). Data are represented as mean ± SEM. Statistical analysis was performed using one-way ANOVA with multiple comparisons.

For that purpose, ApoE$^{-/-}$ mice were fed a western type diet (WTD) and treated with DOP, the S1P lyase inhibitor, through their drinking water starting one week prior to mini osmotic pump implantation. As evidence of the efficiency of DOP, S1P levels in

plasma and aortic tissue were determined by LC-MS/MS (Figure 9). In the plasma of Ang II-infused mice with DOP, S1P levels were 2-fold increased, whereas aortic tissue indicated 175-fold higher S1P levels compared to mice that received only Ang II (Figure 9 A). In this context, other sphingolipids were also examined by LC-MS/MS. An increase in certain ceramide (Cer) species, namely Cer(d18:1/14:0), Cer(d18:1/16:0), Cer(d18:1/18:0), and Cer(d18:1/24:1) was observed in the plasma of Ang II-treated mice with DOP compared to those treated with Ang II alone (Table S 1). The S1P precursor Sph and Cer(d18:1/22:0) as well as Cer(d18:1/24:1) remain unchanged (Table S 1).

In aortic tissue of Ang II-treated mice with DOP, Sph and Cer(d18:1/16:0) levels were elevated compared to mice receiving Ang II alone. In contrast, the very long chain ceramides Cer(d18:1/22:0), Cer(d18:1/24:0) and Cer(d18:1/24:1) were reduced in Ang II-infused mice with DOP compared to mice treated with Ang II alone (Table S 2). No differences were observed in the levels of Cer(d18:1/14:0) and Cer(d18:1/18:0) between these two groups (Table S 2).

$ApoE^{-/-}$ mice not exposed to Ang II infusion were used as control groups. Mice receiving DOP showed increased S1P levels, with a 1.75-fold elevation in plasma and a 155-fold increase in aortic tissue relative to mice fed WTD alone (Figure 9 B). However, Ang II-infused animals treated with DOP exhibited a further significant increase in S1P levels in both plasma and aortic tissue when compared with animals receiving DOP alone (Figure 9 B).

Since administration of DOP leads to peripheral lymphopenia[334], the distribution of lymphocytes in the blood was measured by flow cytometry as biological proof of DOP effectiveness. Indeed, administration of DOP leads to a significant reduction in $CD4^+$ and $CD8^+$ T-cells as well as B-cells independent of Ang II infusion (Figure S 2). Ang II infusion alone had no effect on these lymphocytes subsets.

A characteristic feature of the Ang II infusion model is the occurrence of aortic ruptures leading to immediate death[335]. To address this, it was first examined whether DOP treatment contributed to alterations in survival under Ang II infusion. To investigate if Ang II-infused mice died based on aortic rupture, autopsy was performed of all mice dying within the 28-day period after mini osmotic pump implantation. During autopsy, chest and abdomen were examined for blood clots indicating aortic rupture as a cause of death. Only animals in which death could be clearly attributed to rupture, or those that survived until the end of the experiment, were included in the survival analysis.

Mice infused with Ang II+DOP showed a significant increase in mortality after 28 days (Figure 10 A).

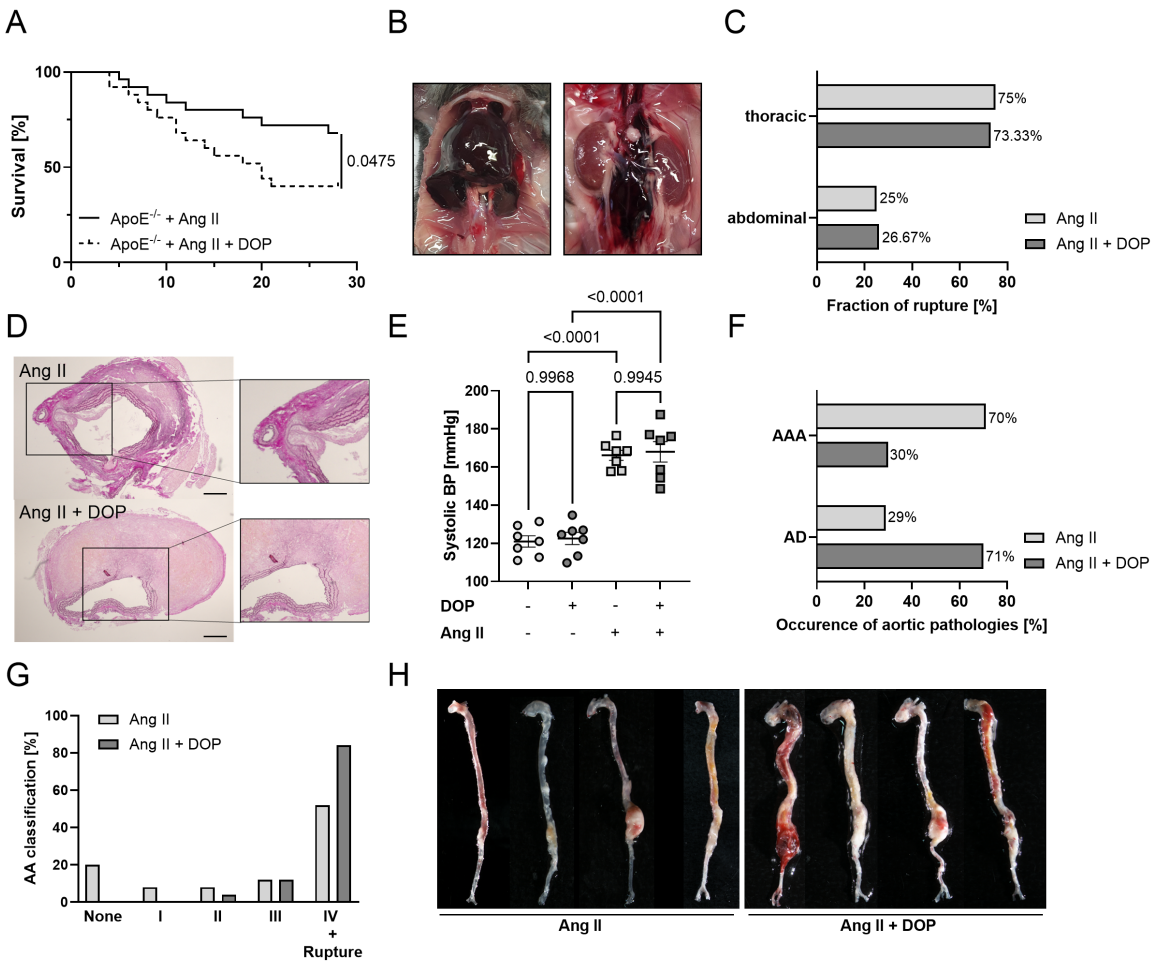

Figure 10: Pharmacological inhibition of the S1P lyase promotes aortic aneurysm formation and drives dissection and rupture. ApoE$^{-/-}$ mice were infused with Ang II (1,000 ng/kg/min) over 28 days or additionally treated with 4-deoxypyridoxine hydrochloride (DOP; 30 mg/L; via drinking water). (A) Kaplan Meier survival curve for 28 days of ApoE$^{-/-}$ mice treated with Ang II or Ang II+DOP; Log-rank (Mantel-Cox) test; P = 0.0475; (n = 25 per group) (B) Representative image of thoracic (left) and abdominal (right) rupture (C) Localization of ruptures in Ang II and Ang II+DOP treated mice (D) Representative image of dissection originating from the media; scale bar: 200 µm (E) Systolic blood pressure measured prior Ang II infusion and 10-14 days after Ang II infusion (n = 7-8 per group). Statistical analysis was performed using two-way ANOVA with repeated measurement. (F) Occurrence of aortic pathologies, categorized as abdominal aortic aneurysm (AAA) and aortic dissection (AD); Fishers' exact test; P = 0.0568 (G) Distribution of macroscopic aortic phenotypes categorized by the classification scheme of Daugherty; None - no aortic aneurysm; I - dilated lumen and no thrombus; II - remodelled tissue with thrombus; III - pronounced bulbous form containing thrombus; IV - dissection/multiple aneurysms with thrombus or rupture; Fisher's exact test; P = 0.0266 (H) Representative images of aortic aneurysms and dissections of ApoE$^{-/-}$ mice treated with Ang II or Ang II+DOP. Data are represented as mean ± SEM.

In the Ang II-treated group, 32% of the mice died from aortic aneurysm rupture, whereas 60% of the mice treated with Ang II+DOP died from aortic rupture (Figure 10 A). The localization of aortic ruptures was examined in all deceased animals (Figure 10 B). No significant differences were found between the two groups. The majority (more than 70%) of the animals exhibited ruptures predominantly in the thoracic aorta or aortic arch. The remaining aneurysms ruptured in the abdominal aorta in the region

of the renal arteries (Figure 10 C). In order to determine the origin of the rupturing aneurysms, H&E overview stainings were performed with these aortic aneurysms and dissections. For both cohorts, ruptures originated within the medial layer of the aortic wall (Figure 10 D).

Typically, aortic dissection constitutes a hallmark vascular pathology in the Ang II infusion model[336]. Accordingly, both the development of abdominal aortic aneurysms (AAA) and aortic dissections (AD) was evaluated macroscopically. Fisher's exact test showed a trend toward a higher incidence of ADs in the Ang II + DOP group than in the Ang II group. Although a trend was observed, the difference did not reach statistical significance ($P = 0.056$; Figure 10 F). The incidence of aneurysm formation including animals which died because of aortic rupture was 80% in the Ang II group. This rate is consistent with the known incidence of aortic aneurysms and dissections under hypercholesteremic conditions in this model[337]. In contrast, all Ang II-infused animals with DOP developed an aortic aneurysm. Aortic aneurysms and dissections of the surviving mice were phenotypically categorized according to a classification scheme defined by Alan Daugherty (Table 16)[338]. All Ang II-infused mice with DOP exhibited more progressive aneurysms of Type IV, with an incidence of 84% compared to 52% in the Ang II group. Fisher's exact test confirmed the phenotypic differences between both treatment groups ($P = 0.0266$; Figure 10 G). Control animals receiving either WTD or DOP alone were monitored for survival, aneurysm formation, and aortic dissections throughout the study. No abnormalities were observed in any of these parameters.

S1P levels have been shown to correlate positively with hypertension[288,339]. Therefore, to assess whether hypertension could contribute to the more progressive aneurysmal phenotypes, dissections and ruptures in Ang II+DOP mice, systolic blood pressure (SBP) was measured via tail cuff method. Mice which received DOP showed no differences in SBP under baseline conditions measured before Ang II administration (Figure 10 E). After implantation of Ang II-filled mini osmotic pumps, SBP raised but no difference was observed between both groups (Figure 10 E).

4.2. Ang II increases S1P levels, which associate with aneurysm severity

As Ang II infusion is a well-established model for inducing aortic aneurysms and dissections[336], the question arose whether aneurysm development under Ang II alone elevated S1P levels.

Ang II-treated mice showed significantly higher S1P levels in the plasma, with a 33% increase compared to mice receiving only WTD (Figure 11 A) . In aortic tissue of Ang II-infused mice, S1P levels were 50% higher than in the WTD group (Figure 11 B).

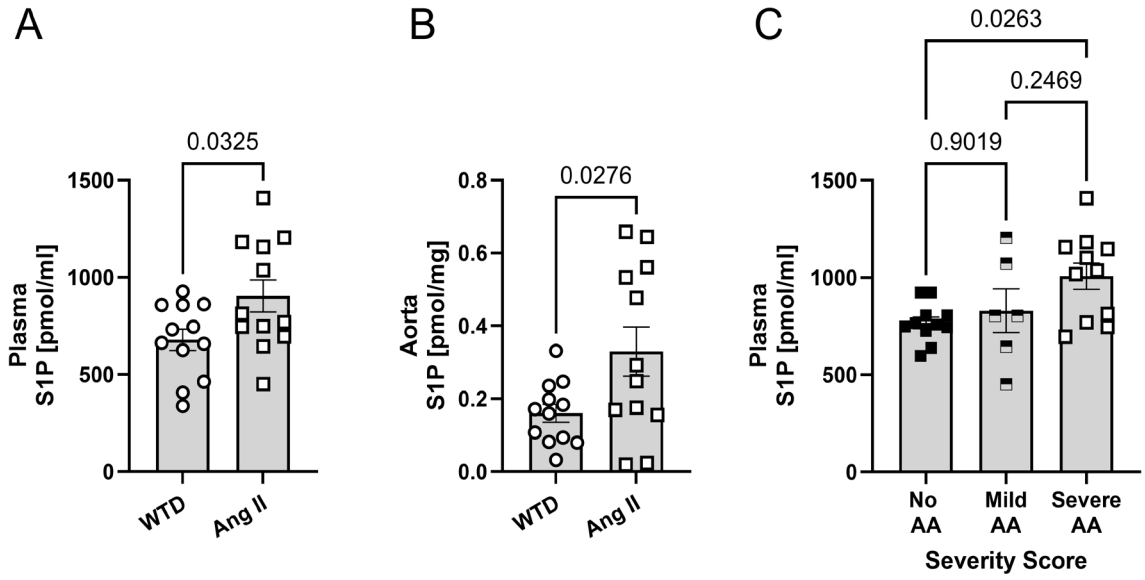

Figure 11: Elevated S1P levels upon Ang II infusion are associated with macroscopic aneurysm severity. S1P levels were measured by LC/MS-MS of ApoE$^{-/-}$ mice fed a western type diet (WTD) or additionally received Ang II (1,000 ng/kg min) for 28 days. (A) Plasma S1P levels (n = 12 per group) (B) S1P levels of aortic tissue (n = 12 per group) (C) Plasma S1P levels stratified by macroscopic aneurysm severity score (No AA, Mild AA, Severe AA) of Ang II infused ApoE$^{-/-}$ mice; No AA - no aortic aneurysm; Mild AA - Daugherty Score I + II; Severe AA - Daugherty Score III + IV; ($n_{No\ AA}$ = 13; $n_{Mild\ AA}$ = 7; $n_{Severe\ AA}$ = 11). For statistical analysis, unpaired T-Test, one-way ANOVA with multiple comparisons and Spearman correlation (P = 0.0134) was used. Data are represented as mean ± SEM.

In this study, DOP treatment was found to be associated with increased macroscopic aneurysm severity under Ang II infusion (Figure 10 G). To further assess whether S1P levels correlate with aneurysm severity as defined by the Daugherty classification, plasma S1P concentrations were analysed across the respective severity classes.

Indeed, plasma S1P levels increased with aneurysm severity (Figure 11 C), and a Spearman correlation confirmed that elevated plasma S1P levels were significantly associated with the macroscopic severity of an aneurysm (P = 0.0134). A separate graphical representation of the correlation was omitted, as the relationship is already

reflected in Figure 11 C. Mild aneurysms were defined as class I + II and severe aneurysms as class III and IV. No elevation in plasma S1P levels was detected in cases of mild aneurysms or in the absence of an aneurysm under Ang II infusion (Figure 11 C).

4.3. DOP-mediated S1P lyase inhibition promotes hyper-contractility and endothelial dysfunction in isolated aortic rings

Ang II infusion is known to induce vascular dysfunction through enhanced vasoconstriction and impaired vasodilation[340]. To investigate whether vascular function is altered under S1P lyase inhibition in animals, wire myograph studies with 2 mm aortic segments of the abdominal aorta, were performed.

Abdominal aortic rings from Ang II-infused mice exhibited a significantly enhanced contractile response to Phe compared to segments from WTD mice (§: $P < 0.0001$; Figure 12 A). Additionally, the maximum contraction to Phe was 4-fold higher in Ang II-infused *aortae* than in WTD controls (Figure 12 B). Ang II+DOP-treated mice exhibited an enhanced contractile response to Phe compared to *aortae* from Ang II-infused mice alone (#: $P < 0.0001$; Figure 12 A). Accordingly, maximal Phe-induced contraction was 1.3-fold higher in *aortae* from Ang II+DOP-treated mice than in those infused with Ang II (Figure 12 B). Furthermore, DOP treatment enhanced the contractile response to Phe even without Ang II infusion ($: $P < 0.0001$; Figure 12 A). Compared to WTD mice, Phe stimulation induced a 2.85-fold increase in maximal contraction under DOP alone (Figure 12 B). Additionally, the aortic segments of the Ang II+DOP group showed a significant increase in contractile response compared with those, which received only DOP (&: $P < 0.0001$; Figure 12 A).

To further evaluate whether *aortae* from Ang II-infused mice also exhibit a hypercontractile response to other vasoconstrictors, vascular reactivity was determined following stimulation with Ang II. A significantly enhanced contractile response was observed in the Ang II+DOP-treated group compared to Ang II alone (#: $P = 0.0004$; Figure 12 C). This resulted in a 1.7-fold increase in maximal contraction (Figure 12 D). A general increase in vasoconstriction was also detected in Ang II-infused mice relative to its WTD controls (§: $P = 0.0033$; Figure 12 C). In contrast, no differences were observed between mice, receiving only WTD compared to those treated with DOP alone.

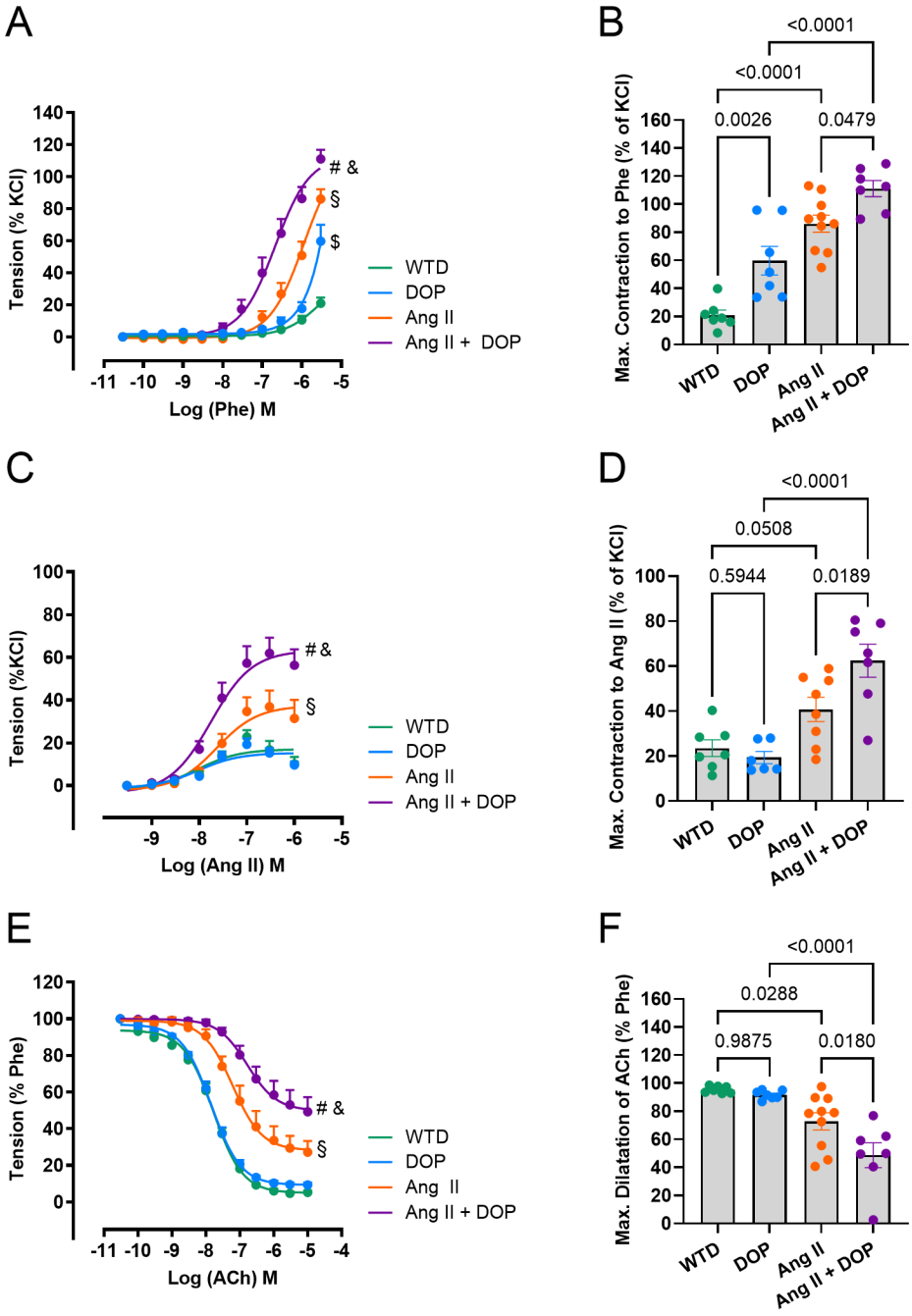

Figure 12: Vascular reactivity of abdominal aortic segments under Ang II infusion and S1P lyase inhibition, demonstrating enhanced hypercontractility and endothelial dysfunction. Abdominal aortic rings from mice treated with Ang II (1,000 ng/kg/min), Ang II in combination with the S1P lyase inhibitor DOP (30 mg/L, via drinking water), DOP alone, or Western-type diet (WTD) were mounted in a wire myograph to assess vascular function. (A) Phenylephrine (Phe) - induced contraction, expressed as percentage of maximal KCl response; § WTD vs Ang II: $P < 0.0001$; # Ang II vs Ang II+DOP: $P < 0.0001$; & DOP vs Ang II+DOP: $P < 0.0001$; $ WTD vs DOP: $P < 0.0001$ (B) Maximum contraction induced by Phe (C) Ang II - induced contraction; § WTD vs Ang II: $P = 0.0033$; # Ang II vs Ang II+DOP: $P = 0.0004$; & DOP vs Ang II+DOP: $P < 0.0001$. (D) Maximum contraction induced by Ang II. (E) Vasorelaxation in response to ACh; # Ang II vs Ang II+DOP: $P = 0.0010$; & DOP vs Ang II+DOP $P < 0.0001$; § WTD vs Ang II $P = 0.0017$. (F) Maximal ACh - induced dilation. Differences in vascular response were analysed using two-way ANOVA with multiple comparison (A, C, E). Significance was shown for the highest concentration of vasoactive substance. Differences in maximum vascular response were analysed using one-way ANOVA (B, D, F). Data are represented as mean ± SEM; (n = 7-10 per group).

To investigate potential alterations in endothelium-dependent vasodilation, aortic segments were exposed to increasing ACh concentrations after maximum Phe-induced contraction. No differences in ACh-induced vasodilation were observed between aortic rings from the WTD and DOP groups, with both groups reaching a maximum dilation of over 90%. Conversely to these findings, aortic segments from Ang II-treated mice displayed a significantly reduced relaxation response to ACh, indicative of endothelial dysfunction in this group (§: P = 0.0017; Figure 12 E). In line with this, the maximum ACh-induced relaxation in Ang II-infused *aortae* was 1.3-fold lower than in WTD *aortae*. Furthermore, the vasodilatory response differed significantly between Ang II and Ang II+DOP-treated aortic segments, with abdominal aortic rings from the Ang II+DOP group showing a 1.4-fold reduction in vasorelaxation compared to Ang II alone (Figure 12 F).

Taken together, the vascular reactivity studies demonstrated that S1P lyase inhibition in addition to Ang II infusion modulated vasoreactivity in aortic segments as evidenced by increased hypercontractility and endothelial dysfunction. Such S1P-induced hypercontractility may compromise proper aortic function and thereby contribute to the higher incidence of ruptures observed under these conditions.

4.4. Pharmacological inhibition of the S1P lyase alters gene expression and pathways related to vascular remodelling and the contractile apparatus in aortic aneurysms

Due to the more progressive aneurysmal phenotype and higher rupture rate observed in Ang II+DOP-treated mice, RNA sequencing was performed on isolated *aortae* to identify molecular mechanisms underlying these pathological changes. For this purpose, mice treated with Ang II were compared with mice receiving Ang II+DOP. Aortic samples were collected 10 days after Ang II-filled pump implantation, aiming to characterize the early molecular alterations in the aortic wall preceding aneurysm formation or rupture.

In *aortae* of Ang II+DOP-treated mice, a total of 1647 genes were downregulated and 2158 upregulated (Figure 13 A). KEGG pathway analysis on differentially expressed genes (DEGs) demonstrated downregulated pathways predominantly involved vascular smooth muscle contractility and ECM interactions including focal adhesion,

vascular smooth muscle contraction, and cytoskeleton in muscle cells (Figure 13 B). Among the upregulated pathways, notable enrichments were observed in immune signaling and cytoskeletal dynamics processes including chemokine signaling, cytokine-cytokine receptor interaction, and cytoskeleton regulation in muscle cells (Figure 13 C).

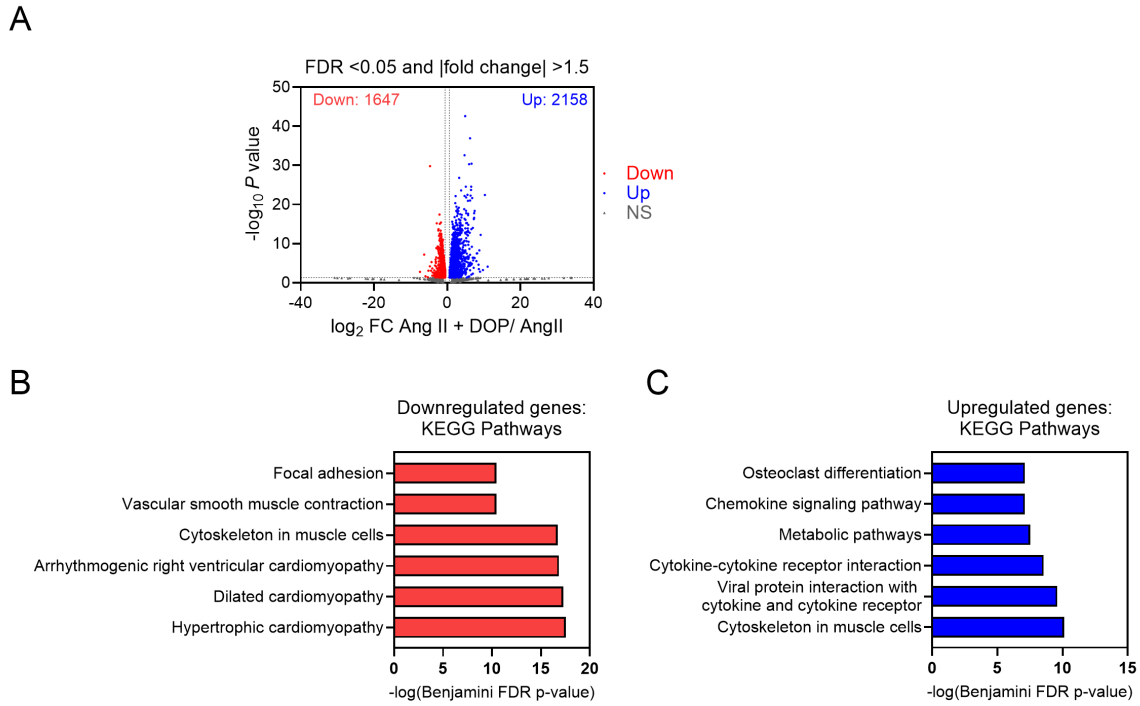

Figure 13: Transcriptomic analysis reveals altered gene expression and pathway regulation following S1P lyase inhibition in Ang II - infused mice. RNA sequencing was performed on aortic tissue from ApoE$^{-/-}$ mice, treated with Ang II or Ang II+DOP for 7 days (n = 4 per group) (A) Volcano plot showing differentially expressed genes in aortic tissue of Ang II+DOP - treated mice versus Ang II alone (FDR < 0.05 lfold changel > 1.5). Genes upregulated in the Ang II+DOP group are shown in blue (n = 2158); downregulated genes in red (n = 1647), and non-significant genes in gray. (B) KEGG pathway enrichment analysis of downregulated genes. (C) Enriched KEGG pathways including upregulated genes. Gene expression values are shown as -log (FDR-adjusted P value).

Next, Gene Ontology (GO) enrichment analysis of DEGs in aortic tissue from Ang II+DOP-treated mice revealed significant alterations in biological processes and cellular components (Figure 14). Notably, biological processes associated with smooth muscle contractility, including actomyosin structure organization, muscle contraction, and actin filament organization, were significantly enriched (Figure 14 A). Additionally, genes involved in calcium ion homeostasis and regulation of heart contraction were differentially expressed, suggesting altered excitation-contraction coupling in VSMCs.

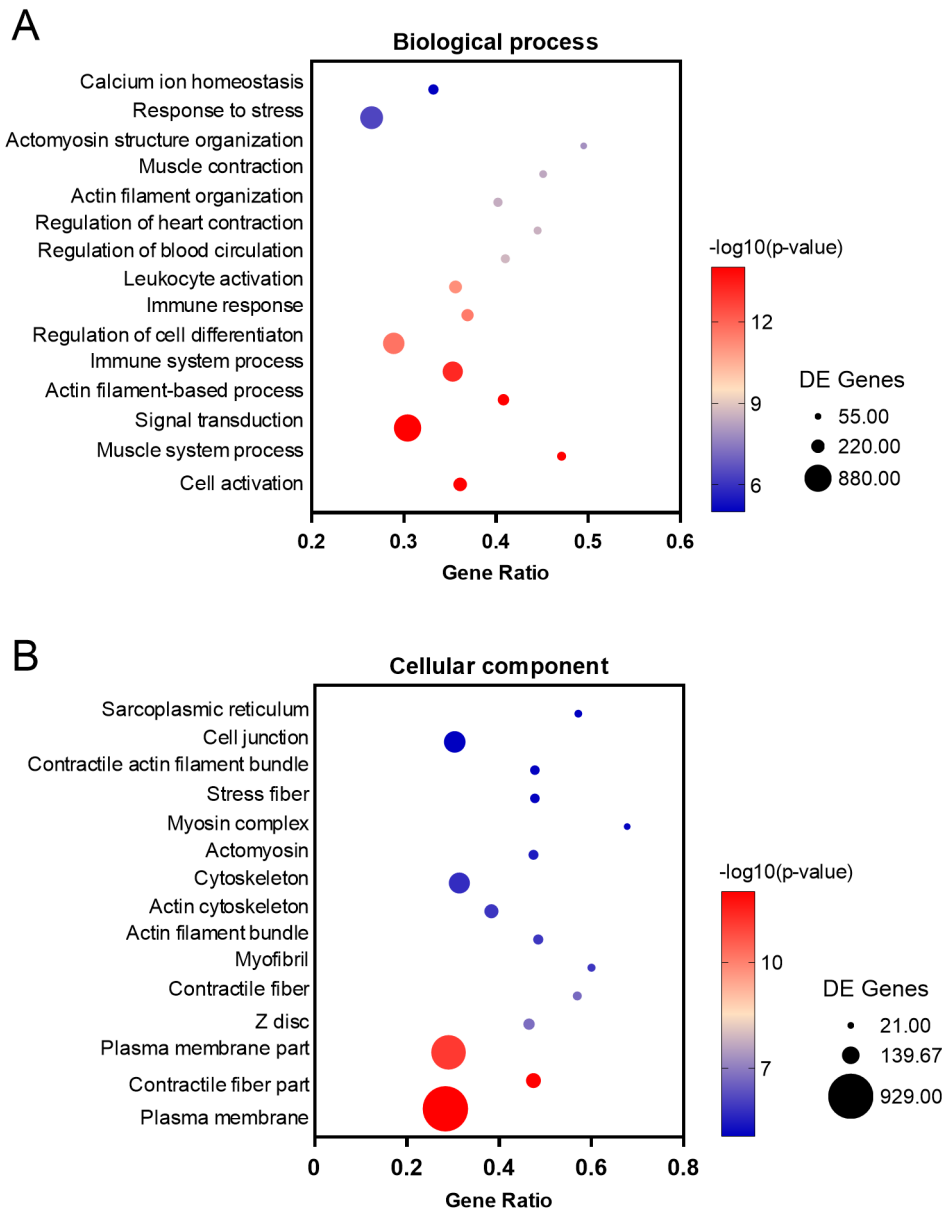

Figure 14: Biological processes altered by S1P lyase inhibition in Ang II-treated ApoE$^{-/-}$ mice (GO analysis). GO term enrichment analysis was performed on genes differentially expressed between Ang II+DOP and Ang II treated mice (n = 4 per group). (A) Differentially enriched biological processes. (B) Differentially enriched cellular components. Dot size reflects the number of differentially expressed (DE) genes; colour indicates statistical significance (-log$_{10}$ P value); gene ratio denotes the proportion of DE genes within the given GO terms.

Beyond contractile function, biological processes linked to immune activation, such as leukocyte activation, immune response, and regulation of cell differentiation, were also significantly enriched (Figure 14 A). To further delineate the structural consequences, differentially expressed genes (DEGs) identified in aortic tissue from Ang II+DOP-treated mice were analysed for enrichment in specific cellular components (Figure 14 B). The most enriched cellular components in Ang II+DOP-treated mice were contractile actin filament bundles, stress fibres, myofibrils and the actomyosin complex (Figure 14 B). All of these components are parts of the vascular contractile

apparatus[341]. Additional enrichment was also observed for cytoskeletal elements, such as actin filaments, as well as for plasma membrane-associated structures, including the Z-disc and parts of the contractile fibre (Figure 14 B). These results imply that the pharmacological increase of S1P levels through DOP modifies the expression of genes encoding for vascular contractility and integrity.

Several studies have suggested a genetic contribution to the progression of aortic aneurysms, including TAAs and AAAs as well as aortic dissections[37]. Gene families including TGF-β family members, ECM structural or remodelling genes as well as genes of the contractile apparatus have been demonstrated to be associated with aortic aneurysms[37]. To explore whether DOP treatment affected the expression of aneurysm-relevant gene families during Ang II infusion, selected gene sets from each of these families were analysed (Figure 15). Notably, gene sets related to smooth muscle contraction, cytoskeletal organization, and TGF-β signaling were downregulated in Ang II+DOP-treated mice (Figure 15 A). A corresponding heat map illustrates representative genes from the most significantly downregulated pathway, highlighting alterations in components of the vascular contractile apparatus (Figure 15 A).

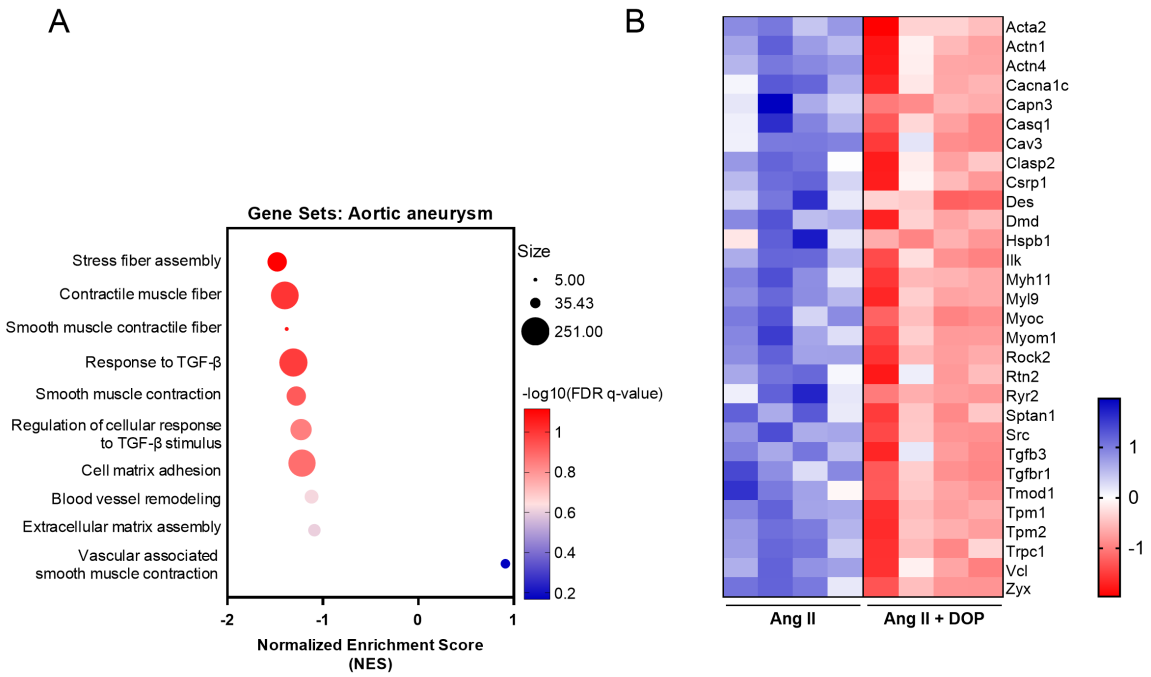

Figure 15: Downregulation of gene sets associated with aortic aneurysm in aortic tissue of Ang II+DOP treated ApoE$^{-/-}$ mice. (A) Gene Set Enrichment Analysis (GSEA) was performed using a curated gene set related to aortic aneurysms pathophysiology. RNA sequencing was conducted on aortic tissue from Ang II+DOP treated and Ang II-treated ApoE$^{-/-}$ mice (n = 4 per group). Dot size indicated number of genes per set, and colour represents statistical significance (-log$_{10}$ FDR adjusted q value); NES = normalized enrichment score. (B) Heat map showing Z-score normalized expression of selected representative genes derived from the top three downregulated gene sets identified in (A).

To complement transcriptomic data, proteomic analysis was performed using aortic tissue from the same animals. This analysis confirmed that Ang II+DOP treatment leads to the regulation of multiple pathways. Among the upregulated pathways were ROS-related processes, metabolic pathways, and pathways linked to neutrophil function (Figure 16 A). In contrast, downregulated pathways confirmed those previously identified at the transcriptomic level, including processes linked to vascular contractility, cytoskeletal organization, and smooth muscle function (Figure 16 B). The most abundant downregulated pathway was associated with vascular smooth muscle contraction. Representative genes from this pathway were selected and shown in a heat map, confirming reduced expression of several key players of contractile function under Ang II+DOP treatment (Figure 16 C).

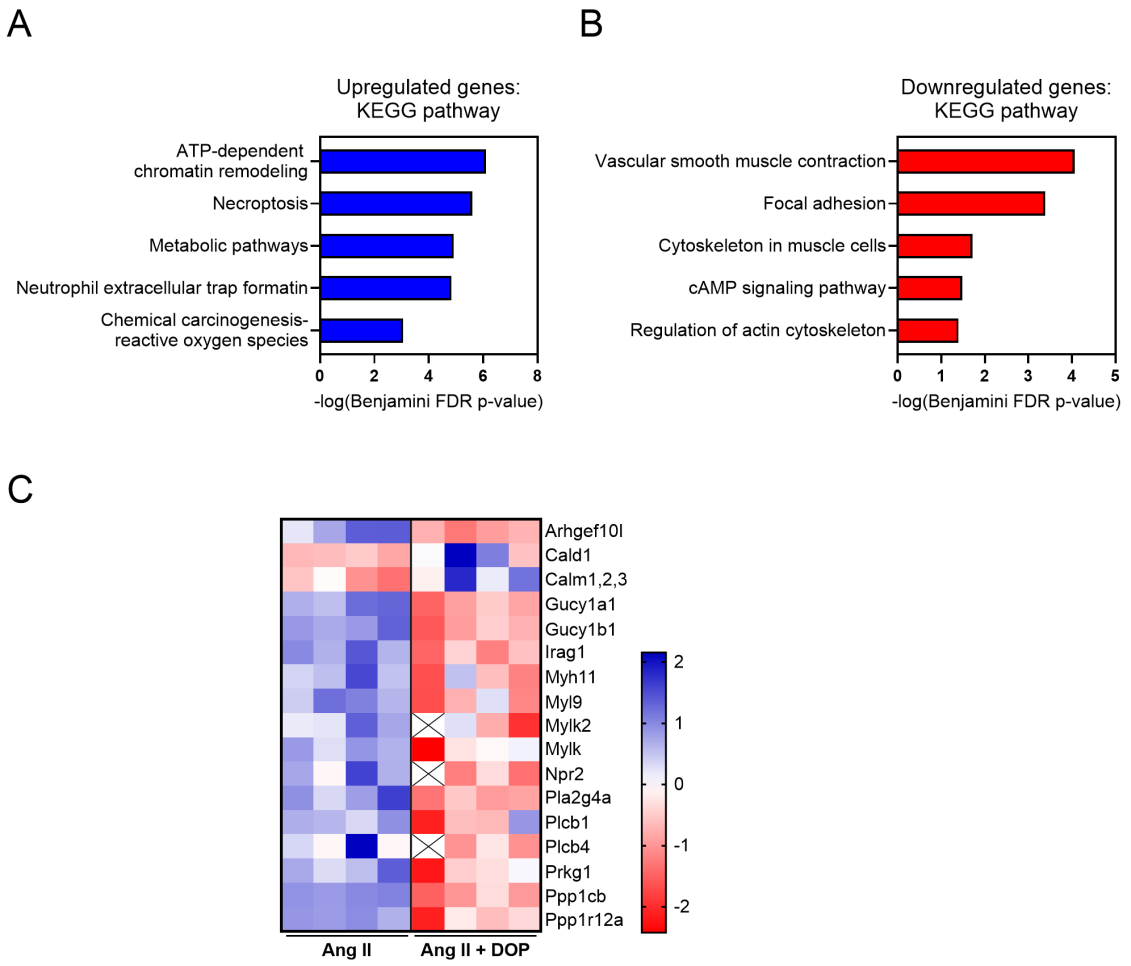

Figure 16: Proteomic alterations in the aortic tissue of Ang II+DOP treated ApoE$^{-/-}$ mice. ApoE$^{-/-}$ mice were infused with Ang II for 7 days and additionally treated with the S1P lyase inhibitor, DOP (30 mg/L). KEGG pathway enrichment analysis of significantly upregulated (A) and downregulated (B) proteins from aortic tissue (n = 4 per group). (C) Heat map of proteins associated with vascular smooth muscle contraction; $|\log_2$ fold change$| \leq 0.5$ and q-value < 0.05. Z-score-normalized protein expression values are shown for individual animals. X denotes missing values where no measurement could be determined.

Selected genes related to the contractile apparatus, the TGF-β signaling pathway, and the ECM were further validated by qPCR. In addition, *aortae* from control animals not infused with Ang II were analysed to assess the specific effects of DOP on gene expression independently of Ang II treatment. Gene expression analysis of contractile genes, including Acta2, Tagln and Myh11, revealed a more than 2-fold downregulation in aortic tissue of Ang II-infused mice compared to the WTD group (Figure 17 A). Interestingly, a remarkable downregulation of all three contractile genes was observed with DOP treatment alone compared to mice, which received only WTD (Figure 17 A). An additive effect was found in Ang II+DOP-treated mice, as gene expression of Acta2, Tagln and Myh11 was markedly reduced by more than 5-fold compared to mice receiving Ang II alone (Figure 17 A). Further analysis of TGF-β family members showed a significant downregulation of Tgfb2 and Tgfbr2, whereas expression of Tgfb1 remained unaltered under Ang II treatment (Figure 17 B). An additional reduction as observed for contractile genes under Ang II+DOP treatment compared to Ang II alone, could not be detected. Nevertheless, the administration of DOP led to a more than 2-fold reduction in the expression of Tgfb2 and Tgfbr2, a trend that was also evident under Ang II+DOP treatment (Figure 17 B).

Since degradation of the ECM and consequent loss of elastin and collagen content is known to occur in aneurysms, the expression of these structural genes was analysed[342-344]. Elastin (Eln) was significantly downregulated in aortic tissue of Ang II-infused mice with DOP treatment (Figure 17 C). Ang II alone did not induce any changes in Eln expression. Furthermore, a 2.2-fold downregulation of Eln was observed in *aortae* of animals which received DOP alone. Other ECM components, such as Col1a1 and Col3a1, remained unaltered under each treatment (Figure 17 C). Additionally, gene expression of MMPs (Mmp-2, Mmp-9, Mmp-12) was determined. Ang II infusion increased the expression of all MMPs. No difference was observed between the Ang II group and the Ang II+DOP group (Figure S 3).

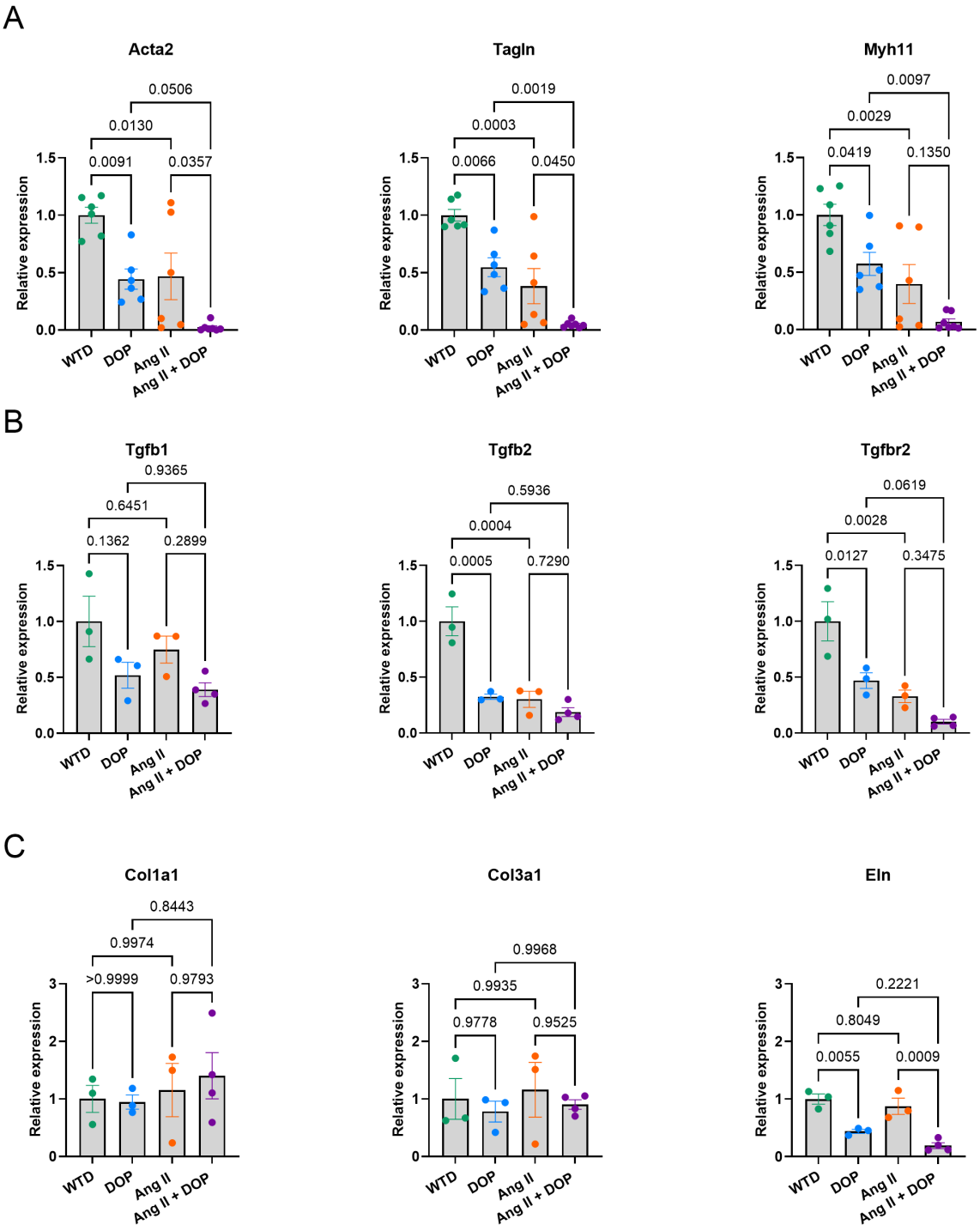

Figure 17: Expression levels of genes associated with vascular contractility, TGF-β signaling, and extracellular matrix organization. Relative expression of selected genes involved in (A) smooth muscle function (Acta2, Tagln, Myh11), (B) TGF- β signaling (Tgfb1, Tgfb2, Tgfbr2), and (C) extracellular matrix structure (Col1a1, Col3a1, Eln) were analysed in aortic tissue of mice infused with Ang II (1,000 ng/kg/min) or treated additionally with the S1P lyase inhibitor, DOP (30 mg/L, via drinking water) over 28 days. Control groups only received western type diet (WTD) or DOP alone. Data are represented as mean ± SEM (n = 3-6 per group). One-way ANOVA with multiple comparisons was used for statistical analysis.

Due to the observed downregulation of contractile genes and Eln expression at transcriptomic levels, histological stainings were performed to assess these changes in the aortic wall. Immuohistochemistry for ACTA2 revealed regional reduction of the expression in Ang II+DOP-treated *aortae* compared to Ang II alone (Figure 18 A). To evaluate structural integrity of elastic fibres, Elastica-van Gieson (EvG) staining was performed. Ang II + DOP-treated *aortae* exhibited pronounced elastic fibre disruptions (Figure 18 B). Quantification of elastin breaks confirmed a significant increase of approximately 55% in *aortae* of the Ang II+DOP group compared to those from Ang II-infused mice (Figure 18 C).

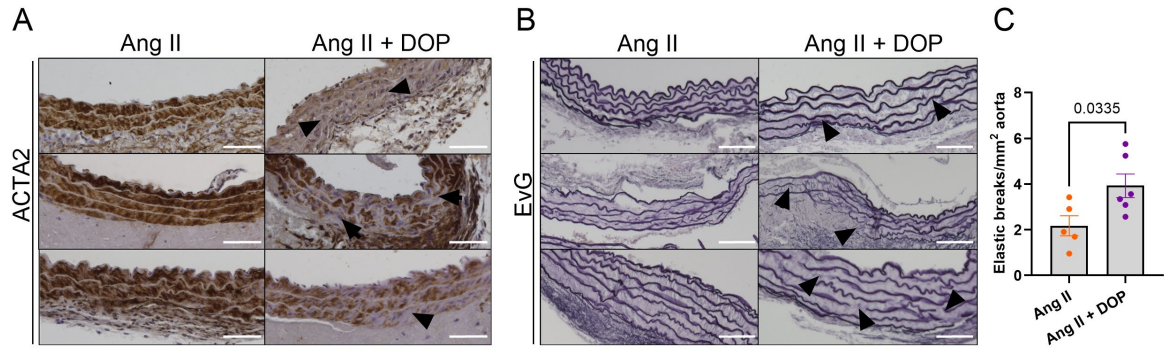

Figure 18: Loss of contractile marker and elastic fibre disruption in aortic tissue of Ang II-infused mice with pharmacological S1P lyase inhibition. (A) Representative images of immunohistochemical staining of ACTA2 in aortic section of Ang II and Ang II+DOP-treated ApoE$^{-/-}$ mice. Black arrows show areas of reduced ACTA2 (B) Representative Elastica van Gieson (EvG) staining showing structural disruption of elastic fibres. Black arrows indicate elastic fibre breaks. (C) Quantification of elastic fibre breaks per mm^2 of aortic sections. Data are shown as mean ± SEM (n = 5-6 per group). Unpaired T-test was used for statistical analysis. Scale bar = 100 µm

In summary, all these findings demonstrated that Ang II+DOP treatment disrupted the expression of genes and pathways critical for maintaining VSMC phenotype and aortic wall integrity. These changes were reflected across molecular and structural levels, suggesting that elevated S1P levels by DOP contributed to a destabilized vascular phenotype that may accelerate aneurysm progression.

4.5. Contractile gene expression is under control of S1PR signaling in cultured VSMCs

The phenotypic modulation of VSMCs marked by the loss of contractile gene expression, is a key event in the progression of aortic aneurysms[92,93]. S1P is known to control VSMC phenotype and behaviour[345]. Considering the role of S1P signaling in VSMC regulation, and given the *in vivo* evidence of VSMC involvement in aneurysm progression under Ang II+DOP treatment, S1PR signaling was investigated as a potential mechanism contributing to the downregulation of contractile gene expression. Therefore, primary rat VSMCs were exposed to S1P and Ang II for different time points. To elucidate the role of S1PRs, certain S1P analogues as well as S1PR antagonists and agonists were used.

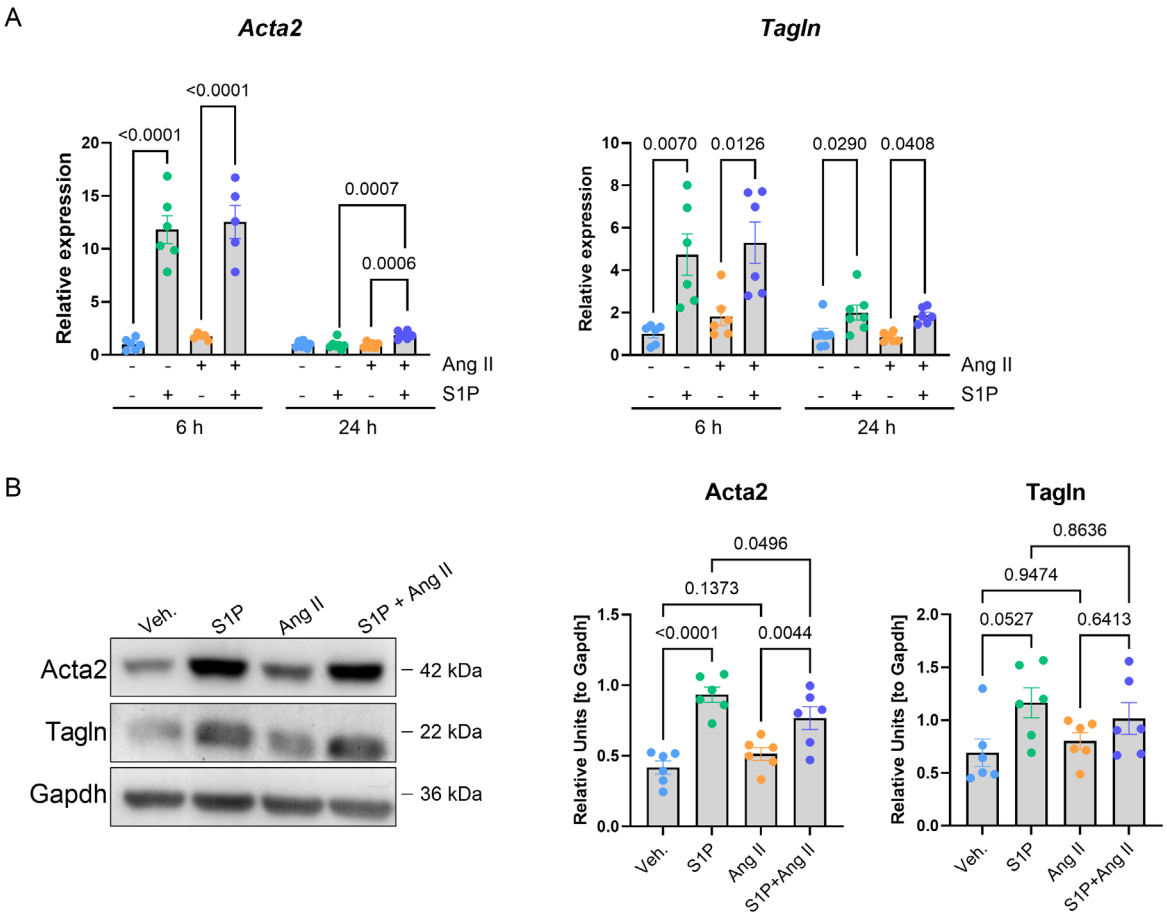

Figure 19: Upregulation of contractile markers upon acute S1P stimulation. VSMCs were treated for 6 h or 24 h with 1 µM S1P, 100 nM Ang II or both. (A) Relative gene expression for Acta2 and Tagln. (B) Western blot (left) and quantification (right) of Acta2 and Tagln after stimulation with S1P, Ang II or both after 24 h. Gapdh was used as loading control. Data are presented as mean ± SEM (n = 5-7 per group). Statistical analysis was performed using one-way ANOVA with multiple comparisons. For clarity, only statistically significant differences are displayed in A.

Stimulation with S1P showed a remarkable upregulation of Acta2 (11-fold) and Tagln (4-fold) in comparison to the vehicle control (Veh.) after 6 h (Figure 19 A), whereas Ang II treatment alone did not lead to an increase in contractile gene expression. A combined treatment with S1P and Ang II also did not show an additive effect (Figure 19 A). In comparison, the expression of Tagln but not Acta2 remained only slightly elevated after 24 h. This mild increase in Tagln expression was observed following stimulation with S1P alone as well as with the combination of S1P and Ang II (Figure 19 A). This observation was confirmed by Western blot analysis, which demonstrated increased protein levels of Acta2 and Tagln, 24 h after S1P treatment. In contrast, Ang II stimulation alone did not induce changes in the expression of contractile markers (Figure 19 B).

Since acute S1P stimulation induced rather than suppressed contractile gene expression, it was hypothesized that tonic/long-term stimulation, mimicking *in vivo* conditions, might exert the opposite effect. To address this, VSMCs were subjected to prolonged S1P stimulation over several days. As a result, tonic S1P stimulation promoted a significant downregulation of Acta2 (1.4-fold) and Tagln (1.2-fold) in VSMCs compared to the vehicle control (Figure 20 A). Additionally, VSMCs were treated with Sph, as a precursor of S1P in combination with the S1P lyase inhibitor, S1PL-IN-1 to elevate intracellular S1P levels. To confirm the effectiveness of S1P lyase inhibition, the elevation of S1P in VSMCs was determined by LC/MS-MS (Figure 20 B). Affirming the conclusion that tonic S1P has an effect on downregulating contractile genes, the expression of both Acta2 and Tagln was indeed significantly downregulated, with a reduction of more than 90% compared to vehicle-treated controls (Figure 20 C).

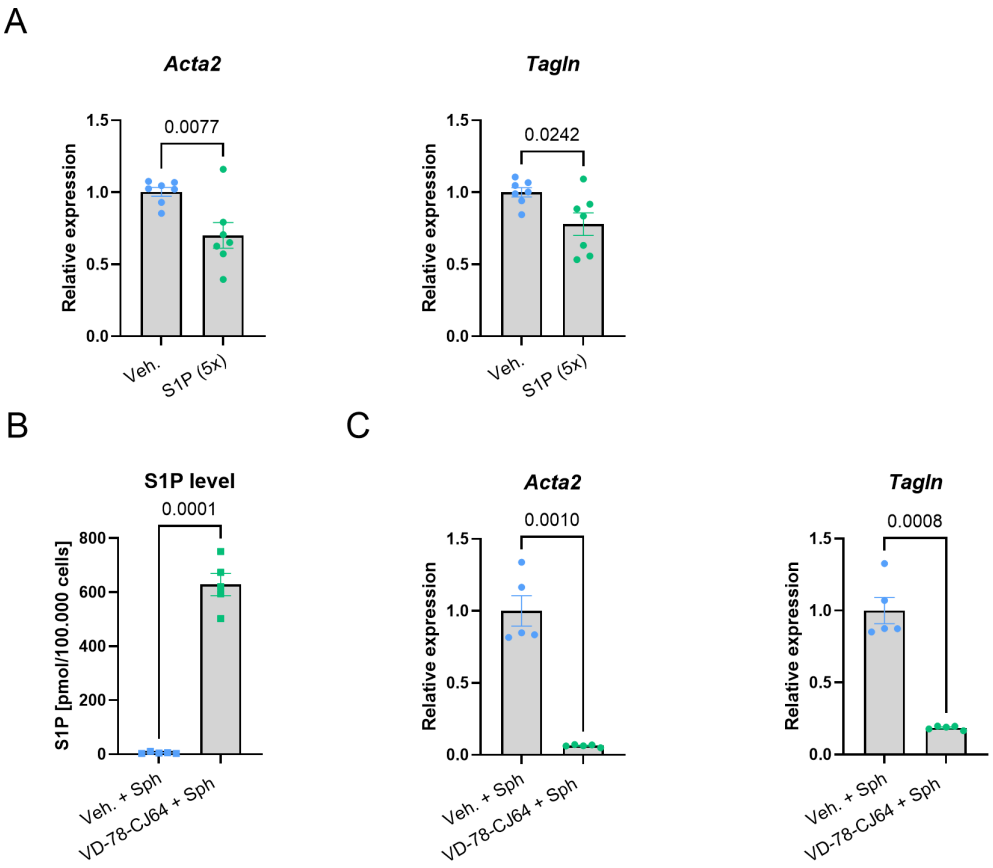

Figure 20: Reduced expression of contractile marker in VSMCs upon tonic S1P stimulation or S1P lyase inhibition. (A) Relative gene expression of Acta2 and Tagln of VSMCs stimulated with 1 µM S1P twice daily at 6 h intervals for two consecutive days, followed by a single stimulation on day 3. Cells were harvested 6 h after final stimulation; n = 7. VSMCs were stimulated with 1 µM sphingosine (Sph) in the presence or absence of the S1P lyase inhibitor, S1PL-IN-1 (1 µM) for 5 days. (B) S1P levels measured by LC/MS-MS and (C) relative gene expression of Acta2 and Tagln was determined; n = 5. Data are represented as mean ± SEM. Unpaired t- test was used for statistical analysis.

In summary, the results indicate that S1P mediates opposing effects on the expression of contractile genes via both acute and tonic signaling. To investigate which S1PR subtypes were responsible for these effects, cells were pretreated with specific receptor antagonists prior to S1P exposure. VSMCs were shown to express the S1P receptors S1PR1, S1PR2, and S1PR3, whereas under basal conditions S1PR2 is the highest expressed subtype (Figure 21 A). Strikingly, inhibition of S1PR2 using JTE-013 effectively blocked the S1P-induced upregulation of Acta2 and Tagln after 6 h, as shown by gene expression analysis (Figure 21 B). Treatment with JTE-013 alone had no effect on baseline expression levels of these genes. Furthermore, the antagonization of S1PR1, by NIBR0213 or S1PR3 by TY-52156, showed no inhibitory effect on contractile gene expression (Figure 21 B).

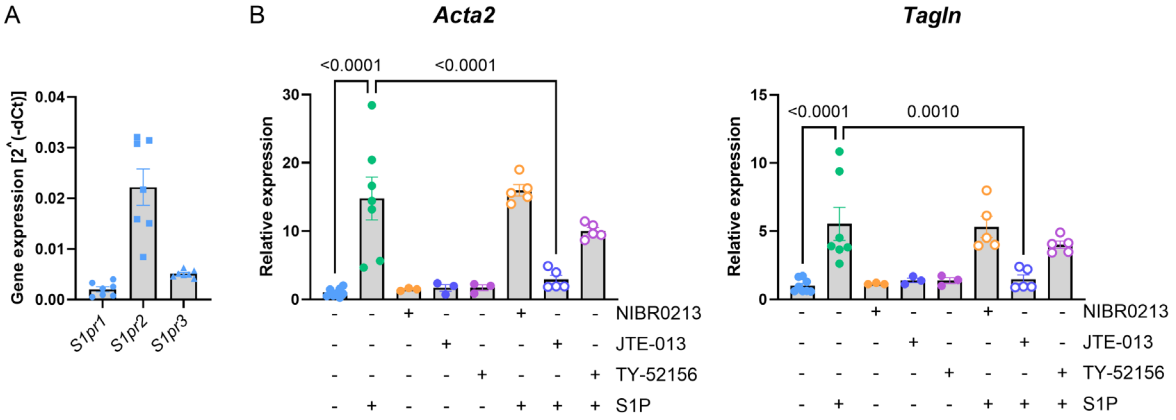

Figure 21: Acute activation of S1PR2 is responsible for upregulation of contractile marker in VSMCs after S1P stimulation. (A) S1P-receptor (S1pr1-3) expression in VSMCs determined by RT-qPCR. (B) Relative gene expression of Acta2 and Tagln of VSMCs treated with S1P (1 µM, 6 h) stimulation in the presence or absence of S1PR antagonists (NIBR0213: S1PR1 100 nM, JTE-013: S1PR2 10 µM, TY-52156: S1PR3 10 µM; 30 min pre-treatment). Only statistically relevant comparisons are shown for clarity. Data are represented as mean ± SEM (n = 3-7 per group). One-way ANOVA with multiple comparisons was used for statistical analysis.

In addition to S1PR antagonism, stimulation with the selective S1PR2 agonist CYM-5520 further confirmed that acute S1P signaling via S1PR2 promoted contractile gene expression (Figure 22). After 6 h of stimulation, a significant increase in Acta2 and Tagln gene expression was observed, indicating a transcriptional response mediated by S1PR2, whereas the selective stimulation of S1PR1 and S1PR3 had no effect.

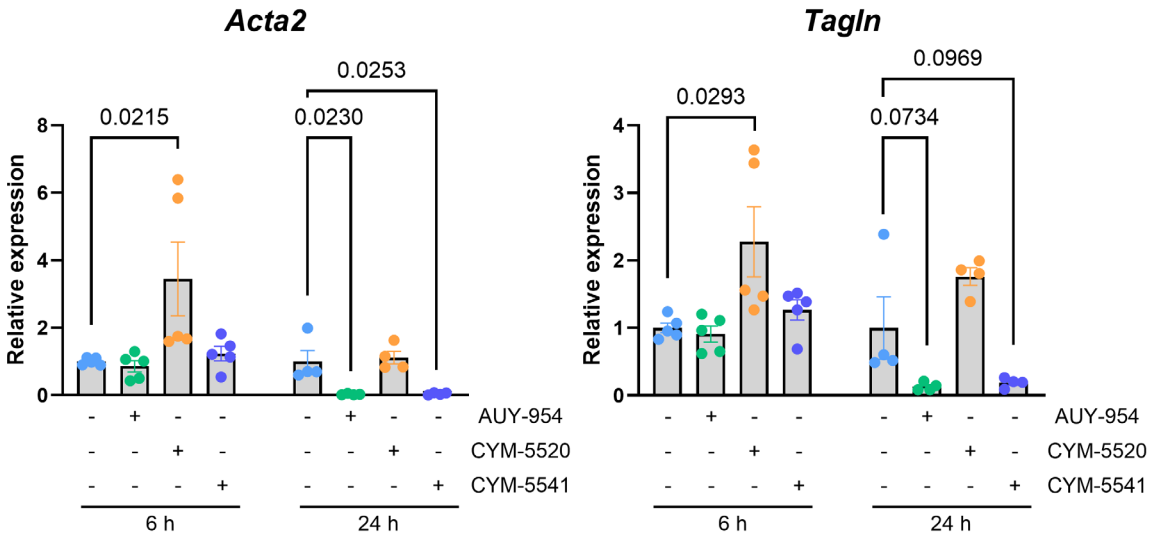

Figure 22: Acute and tonic S1PR signaling differentially modulate the expression of contractile genes in VSMCs. Relative gene expression of Acta2 and Tagln after stimulation with selective S1PR agonists (AUY-954: S1PR1 10 µM, CYM-5520: S1PR2 10 µM, CYM-5541: S1PR3 10 µM) for 6 h and 24 h. Data are presented as mean ± SEM (n = 4-5 per group). One-way analysis with multiple comparisons was used for statistical analysis. Only statistically relevant comparisons are displayed.

In contrast, prolonged stimulation of S1PR1 with AUY-954 and S1PR3 with CYM-5541 caused a strong downregulation of Acta2 expression, by approximately 7-fold and 5-fold, respectively (Figure 22). Although Tagln expression was not significantly affected, both treatments showed a clear trend toward decreased expression, indicating that S1PR1 and S1PR3 may contributed to the suppression of the contractile phenotype under tonic stimulation (Figure 22).

Together, these findings indicated that acute S1P signaling through S1PR2 enhanced the contractile phenotype of VSMCs, whereas prolonged stimulation of S1PR1 or S1PR3 induced a shift toward a less contractile state. Additionally, this is consistent with tonic S1P signaling contributing to phenotypic modulation involved in aneurysm formation.

4.6. S1PR gene expression is altered in the Ang II model of aortic aneurysms

Following these observations, the question was raised whether S1PR expression was altered under Ang II infusion. Since S1PR1-S1PR3 are the main S1PRs expressed in the vasculature the mRNA levels of each receptor were determined in three different parts of the aorta: the aortic arch, the thoracic and the abdominal aorta of ApoE$^{-/-}$ mice. The distribution of S1PR1-S1PR3 varied in each aortic part (Figure 23). In the aortic arch and in the thoracic aorta, the S1PR1 mRNA level was most frequently expressed. The S1PR2 and S1PR3 was less expressed compared to S1PR1.

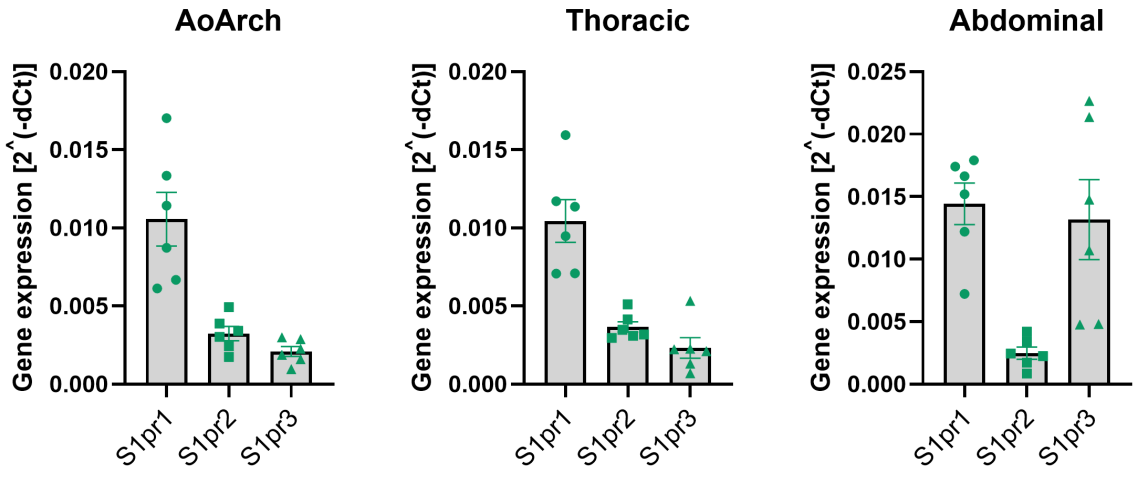

Figure 23: Differential expression of S1PR subtypes across regional segments of *aortae* of ApoE$^{-/-}$ mice. RT-qPCR analysis of S1pr1, S1pr2, and S1pr3 mRNA expression in distinct aortic regions of ApoE$^{-/-}$ mice: aortic arch (AoArch), thoracic aorta, and abdominal aorta of ApoE$^{-/-}$ mice. Gene expression is shown as 2^(-dCt), normalized to Gapdh as housekeeping gene. Data are presented as mean ± SEM (n = 6 each group).

Additionally, in these aortic parts, the S1PR3 was the lowest expressed subtype (Figure 23). In contrast S1PR3 was the most prominent S1PR expressed in the abdominal aortic part followed by S1PR1. Here, the lowest mRNA expression level was found for S1PR2 (Figure 23).

To clarify whether Ang II infusion promoted changes in S1PR expression during aneurysm progression, aortic segments from mice, which received only WTD and mice infused with Ang II were analysed. In all aortic parts, the expression of both S1PR1 and S1PR2 was significantly upregulated under Ang II infusion compared to the WTD group (Figure 24). S1PR3 expression was differentially regulated along the aorta, showing significant upregulation in the aortic arch and thoracic segments, but a marked downregulation in the abdominal aorta. Specifically, Ang II infusion led to a 2.3-fold decrease in S1PR3 expression in the abdominal region (Figure 24). Receptor expression was also assessed under Ang II+DOP treatment. Across all examined S1P receptors, expression patterns mirrored those observed with Ang II treatment alone (Figure S 4). The addition of DOP did not exert any further effect on S1PR expression in the different parts of the aorta (Figure S 4).

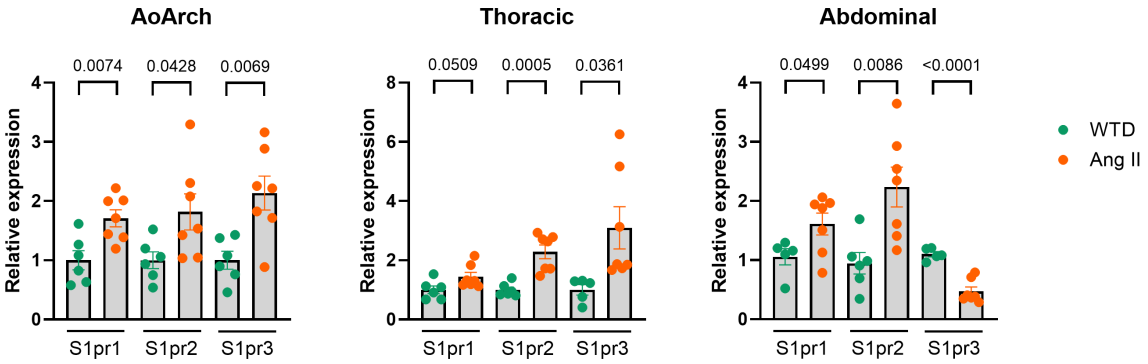

Figure 24: Angiotensin II infusion modulates regional S1PR expression along the murine aorta. Relative gene expression of S1pr1, S1pr2 and S1pr3 in different anatomical segments of the aorta (aortic arch, thoracic and abdominal aorta) from ApoE$^{-/-}$ mice receiving either a western type diet (WTD) or Ang II infusion for 14 days. Data are represented as mean ± SEM (n = 6-7 per each group). T-test was used for statistical analysis between both groups.

In summary, S1PRs displayed distinct regional distribution patterns within the aorta, suggesting segment-specific functions. Under aneurysmal conditions induced by Ang II infusion, expression of S1PR1-3 was generally increased in the aortic arch, thoracic aorta, and abdominal aorta, with the exception of S1PR3, which was downregulated in the abdominal region. These findings indicate enhanced S1P-S1PR signaling during aneurysm progression, along with region-specific differences across aortic segments.

4.7. S1PR2 deficiency has no effect on aortic aneurysm development *in vivo*

To investigate whether the absence of S1PR2 as stimulator of contractile gene expression *in vitro* alters aortic aneurysm formation under Ang II infusion, ApoE$^{-/-}$/S1pr2$^{-/-}$ mice were generated and analysed in the Ang II model.

Survival analysis over 28 days revealed no difference between Ang II-infused ApoE$^{-/-}$ and ApoE$^{-/-}$/S1pr2$^{-/-}$ mice (Figure 25 A).

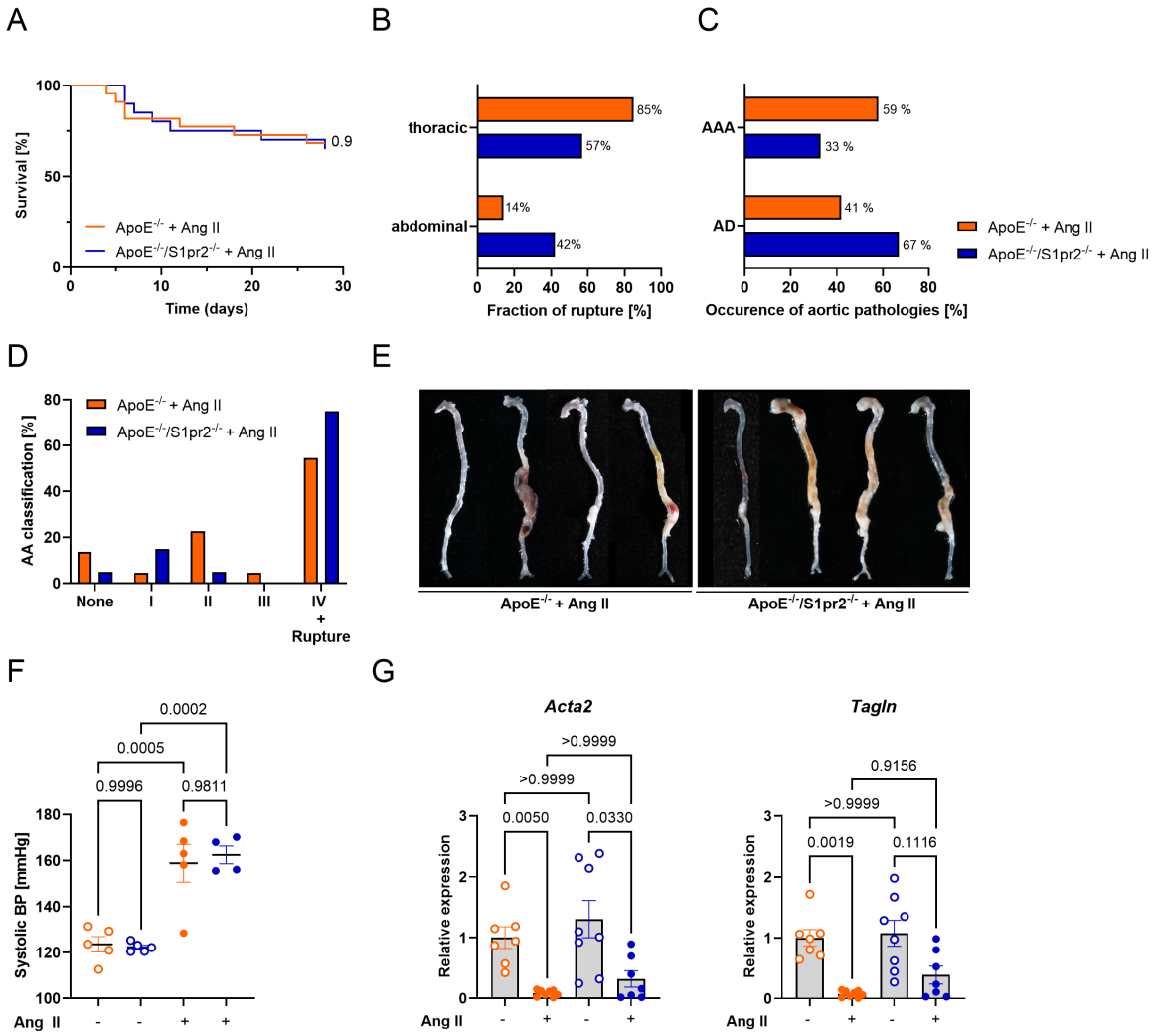

Figure 25: Loss of S1PR2 does not have an influence on aortic aneurysm pathophysiology. ApoE$^{-/-}$/S1pr2$^{-/-}$ received a western type diet and were infused with Ang II (1,000 ng/kg/min) over 28 days. (A) Kaplan-Meyer survival analysis of ApoE$^{-/-}$ and ApoE$^{-/-}$/S1pr2$^{-/-}$ mice infused with Ang II, $n_{ApoE^{-/-}}$ =22 $n_{ApoE^{-/-}/S1pr2^{-/-}}$ =20. (B) Distribution of aortic rupture site (thoracic or abdominal). (C) Incidence of abdominal aortic aneurysm (AAA) or aortic dissection (AD) in ApoE$^{-/-}$ and ApoE$^{-/-}$/S1pr2$^{-/-}$ mice following Ang II infusion. (D) Classification of aneurysm severity based on macroscopic assessment according to Daugherty. None – no aortic aneurysm; I - dilated lumen and no thrombus; II - remodelled tissue with thrombus; III - pronounced bulbous form containing thrombus; IV - dissection/multiple aneurysms with thrombus or rupture. (E) Representative images of aortic aneurysms and dissections. (F) Systolic blood pressure of ApoE$^{-/-}$ and ApoE$^{-/-}$/S1pr2$^{-/-}$ mice before and 10-14 days after Ang II infusion (n = 4-5 per group). (G) Relative gene expression of contractile markers Acta2 and Tagln in aortic tissue of ApoE$^{-/-}$ and ApoE$^{-/-}$/S1pr2$^{-/-}$ receiving western type diet or additionally Ang II infusion for 28 days. Data are presented as mean ± SEM (n = 7-8 per group). Statistical analysis was performed using Fisher's exact test (B-D), two-way ANOVA with repeated measurement or multiple comparisons (F-G).

Furthermore, the localization of aortic ruptures, whether thoracic or abdominal, did not differ between the two genotypes after Ang II infusion (Figure 25 B). When assessing the prevalence of aortic pathologies, including abdominal aortic aneurysms and aortic dissections, no major changes were observed (Figure 25 C). Additionally, aneurysm severity as classified by Daugherty's scoring system showed a comparable distribution between ApoE$^{-/-}$ and ApoE$^{-/-}$/S1pr2$^{-/-}$ mice (Figure 25 D & E). SBP was similarly raised by Ang II in both genotypes (Figure 25 F). Interestingly, analysis of the contractile markers, Acta2 and Tagln revealed a similar reduction in gene expression after Ang II infusion, contrary to their upregulation after acute S1P stimulation *in vitro* (Figure 25 G).

Since S1PR2 has been associated with vasoconstriction in various vascular beds[346], vasoreactivity studies were performed using aortic segments from Ang II-infused ApoE$^{-/-}$ and ApoE$^{-/-}$/S1pr2$^{-/-}$ mice, as well as from their non-infused controls. Wire myograph studies were performed to clarify whether the hypercontractile response induced by Ang II is mediated via S1PR2 and can be modulated by its genetic deletion. Both, ApoE$^{-/-}$ and ApoE$^{-/-}$/S1pr2$^{-/-}$ mice infused with Ang II, demonstrated an increased vasoconstrictive response to Phe compared to the WTD control groups (Figure 26 A). Analysis of the maximum contractile response to Phe revealed no significant difference between Ang II-infused ApoE$^{-/-}$ and ApoE$^{-/-}$/S1pr2$^{-/-}$ mice, indicating that S1PR2 deletion did not alter the maximum Phe-induced vasoconstriction (Figure 26 B).

A similar contractile pattern was observed following stimulation with Ang II. Both Ang II-infused genotypes exhibited an overall increase in vasoconstriction relative to their non-infused controls (Figure 26 C). Notably, the extent of this increase was comparable between ApoE$^{-/-}$ and ApoE$^{-/-}$/S1pr2$^{-/-}$ mice, indicating that the loss of S1PR2 did not alter the overall Ang II-induced vascular reactivity (Figure 26 C). Furthermore, no significant differences were detected in the maximum contractile response to Ang II, with both genotypes displaying an approximately 2-fold increase relative to WTD controls (Figure 26 D).

ApoE$^{-/-}$/S1pr2$^{-/-}$ mice showed impaired vasodilation after Ang II infusion in response to ACh, indicating that S1PR2 was not involved in endothelium-dependent relaxation in aortic segments of mice with or without Ang II infusion (Figure 26 E). Consistently, analysis of maximal vasodilation confirmed that the loss of the S1PR2 has no effect on endothelial function (Figure 26 F).

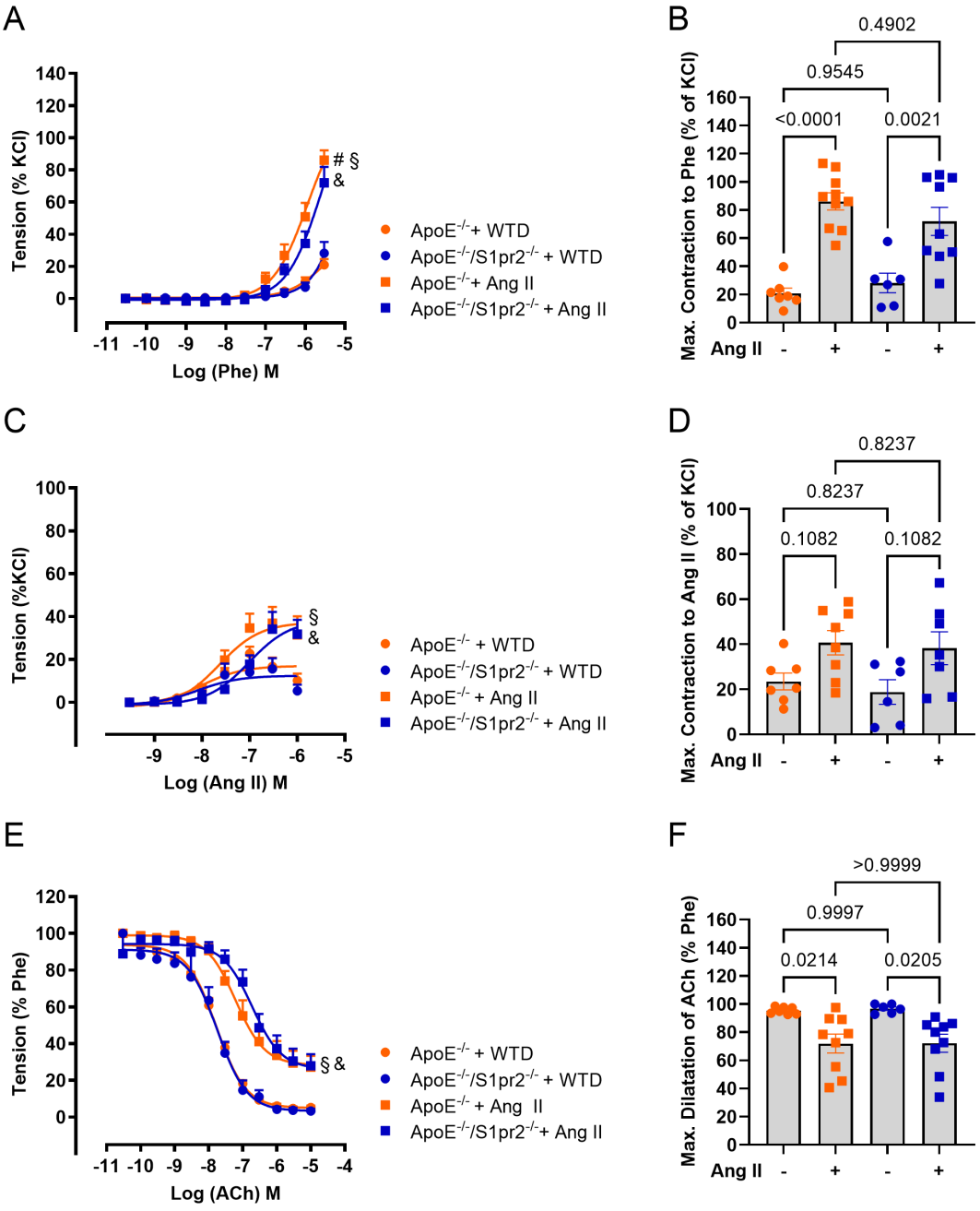

Figure 26: Vascular reactivity of ApoE$^{-/-}$/S1pr2$^{-/-}$ under Ang II infusion, showing no difference compared to ApoE$^{-/-}$ Ang II controls. Wire myography was used to assess vascular contractility and dilation of aortic rings from ApoE$^{-/-}$/S1pr2$^{-/-}$ compared to ApoE$^{-/-}$ maintained on a western type diet (WTD) with or without Ang II (1,000 ng/kg/min) infusion. (A) Contractile response to increasing phenylephrine (Phe) concentrations expressed as percentage of maximal KCl response; § ApoE$^{-/-}$ WTD vs ApoE$^{-/-}$ Ang II: P < 0.0001; # ApoE$^{-/-}$ Ang II vs ApoE$^{-/-}$/S1pr2$^{-/-}$ Ang II: P = 0.0129; & ApoE$^{-/-}$/S1pr2$^{-/-}$ WTD vs ApoE$^{-/-}$/S1pr2$^{-/-}$ Ang II: P < 0.0001 (B) Maximal contraction in response to Phe. (C) Vasoconstriction to increasing concentrations of Ang II expressed as percentage of maximal KCl response; § ApoE$^{-/-}$ WTD vs ApoE$^{-/-}$ Ang II: P = 0.0019; &: ApoE$^{-/-}$/S1pr2$^{-/-}$ WTD vs ApoE$^{-/-}$/S1pr2$^{-/-}$ Ang II: P = 0.0007 (D) Maximum contraction to Ang II. (E) Acetylcholine (ACh) - induced vasorelaxation in Phe induced pre-contracted aortic rings; § ApoE$^{-/-}$ WTD vs ApoE$^{-/-}$ Ang II: P = 0.0017; &: ApoE$^{-/-}$/S1pr2$^{-/-}$ WTD vs ApoE$^{-/-}$/S1pr2$^{-/-}$ Ang II: P = 0.0111 and (F) corresponding maximal dilation. Data are presented as mean ± SEM (n =6-10 per group). Statistical analysis was determined using two-way ANOVA with multiple comparisons (A-F).

Taken together, global loss of S1PR2 in Ang II-infused mice did not affect aneurysm formation, incidence, or severity, nor did it alter phenotypic switching or vascular reactivity.

4.8. Aortic aneurysm progression under DOP is not altered in ApoE$^{-/-}$/S1pr2$^{-/-}$ mice

Despite the dispensability of S1PR2 for aortic aneurysm formation under Ang II, the possibility remained that it may be responsible for the aggravating effect of DOP in the same model. To investigate this, ApoE$^{-/-}$ and ApoE$^{-/-}$/S1pr2$^{-/-}$ mice were infused with Ang II in combination with DOP.

Survival analysis over a period of 28 days showed no significant difference between both group (Figure 27 A). Moreover, the localization of rupture, as well as the frequency of aortic pathologies including abdominal aortic aneurysms and aortic dissections, did not differ between ApoE$^{-/-}$ and ApoE$^{-/-}$/S1pr2$^{-/-}$ animals treated with Ang II+DOP (Figure 27 B & C).

Aneurysm severity according to the macroscopic classification scheme of Daugherty indicated a similar distribution in both analysed genotypes. As previously observed in Ang II+DOP-treated ApoE$^{-/-}$ mice, the majority of aneurysms in ApoE$^{-/-}$/S1pr2$^{-/-}$ mice receiving the same treatment were also classified as type IV (Figure 27 D & E). Ang II+DOP treatment caused a similar increase in SBP in both genotypes (Figure 27 F). Interestingly, expression of the contractile genes Acta2 and Tagln was 3-fold higher in ApoE$^{-/-}$/S1pr2$^{-/-}$ mice compared to ApoE$^{-/-}$ mice under Ang II+DOP treatment (Figure 27 G). This indicates that the downregulation of contractile genes was absent in ApoE$^{-/-}$/S1pr2$^{-/-}$ mice under Ang II+DOP treatment, supporting that S1PR2 is required for the suppression of contractile gene expression under tonic S1P levels caused by DOP (Figure 27 G).

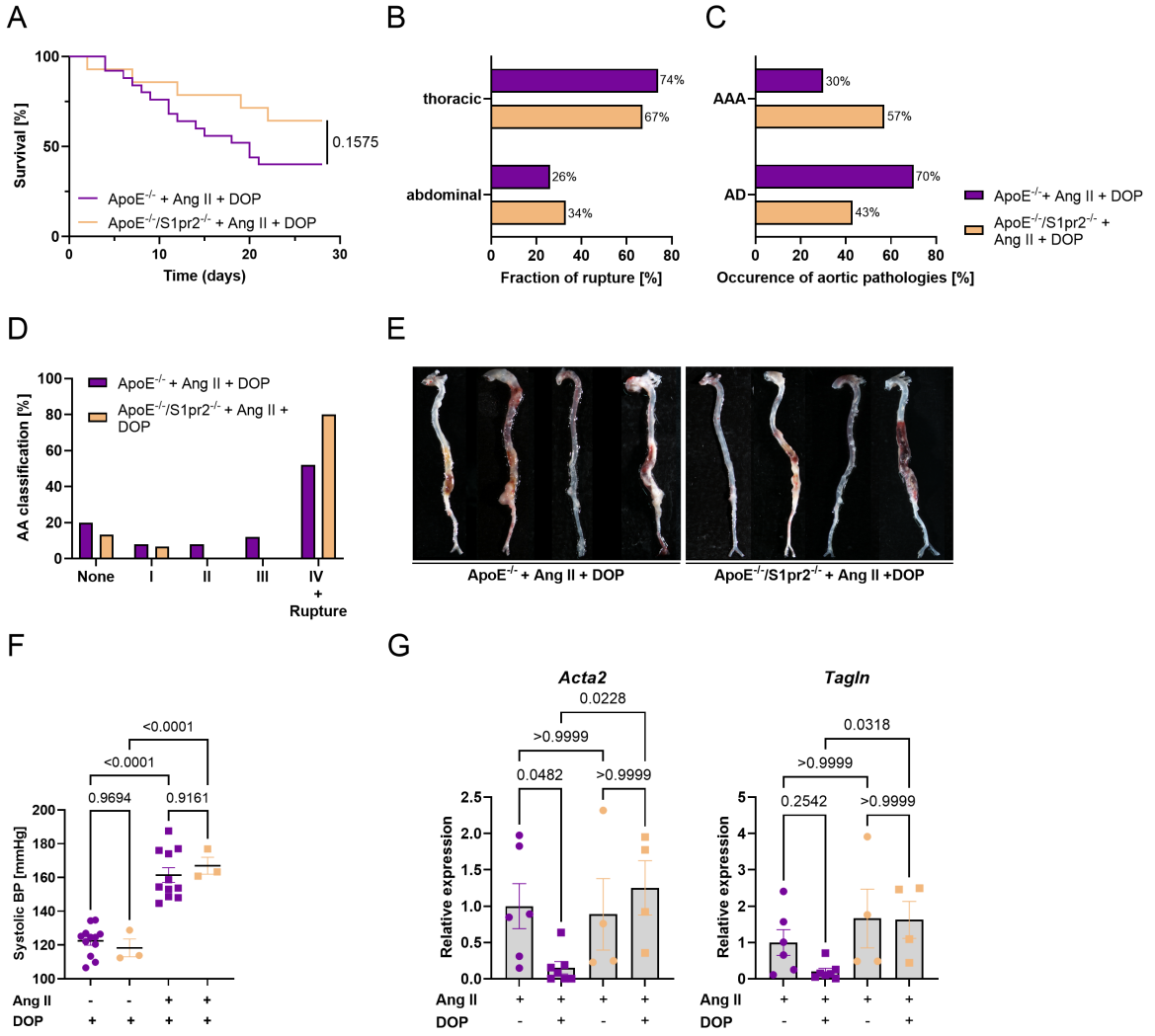

Figure 27: S1PR2 deletion does not have an influence on aortic aneurysm pathophysiology in the presence of pharmacologically induced S1P lyase inhibition. ApoE$^{-/-}$ and ApoE$^{-/-}$/S1pr2$^{-/-}$ received a western type diet with DOP (30 mg/L via drinking water) and were infused with Ang II (1,000 ng/kg/min; 28 days). (A) Kaplan-Meyer survival curve; $n_{ApoE^{-/-}}$ = 25 $n_{ApoE^{-/-}/S1pr2^{-/-}}$ = 14. (B) Distribution of aortic rupture site (thoracic or abdominal). (C) Incidence of abdominal aortic aneurysm (AAA) or aortic dissection (AD) in ApoE$^{-/-}$ and ApoE$^{-/-}$/S1pr2$^{-/-}$ mice following S1P lyase inhibition via DOP and Ang II infusion. (D) Classification of aneurysm severity based on macroscopic assessment according to Daugherty. None – no aortic aneurysm; I - dilated lumen and no thrombus; II - remodelled tissue with thrombus; III - pronounced bulbous form containing thrombus; IV - dissection/multiple aneurysms with thrombus or rupture. (E) Representative images of aortic aneurysms and dissections. (F) Systolic blood pressure of ApoE$^{-/-}$ and ApoE$^{-/-}$/S1pr2$^{-/-}$ mice treated with DOP before and 10-14 days after Ang II infusion; $n_{ApoE^{-/-}}$ = 11-12 $n_{ApoE^{-/-}/S1pr2^{-/-}}$ = 3 (G) Relative gene expression of contractile markers Acta2 and Tagln in aortic tissue of ApoE$^{-/-}$ and ApoE$^{-/-}$/S1pr2$^{-/-}$ receiving western type diet with DOP or additionally Ang II infusion for 28 days (n= 4-7 per group). Data are presented as mean ± SEM. Statistical analysis was performed using Fisher's exact test (B-D), two-way ANOVA with repeated measures or multiple comparison (F-G).

Since contractile genes were not downregulated by DOP in Ang II-treated ApoE$^{-/-}$/S1pr2$^{-/-}$ mice, vasoreactivity studies of aortic segments were performed to identify possible alterations in vasoconstriction and -dilation. Hereby, aortic segments from ApoE$^{-/-}$ and ApoE$^{-/-}$/S1pr2$^{-/-}$ mice treated with DOP and with or without Ang II infusion were analysed. ApoE$^{-/-}$/S1pr2$^{-/-}$ mice treated with Ang II+DOP, showed a reduced vasoconstrictive response to Phe compared to ApoE$^{-/-}$ mice with the same treatment (Figure 28 A). However, maximum vasoconstrictive response to Phe revealed no difference between both genotypes under Ang II+DOP treatment (Figure 28 B). Furthermore, no differences in the vasoconstrictive response to Phe were found between ApoE$^{-/-}$ and ApoE$^{-/-}$/S1pr2$^{-/-}$ mice with DOP treatment alone.

Similar observations were detected after using Ang II as a second vasoconstrictor. ApoE$^{-/-}$/S1pr2$^{-/-}$ mice treated with Ang II+DOP did not show an enhanced vasoconstrictive response compared to ApoE$^{-/-}$ mice with the same treatment (Figure 28 B). Additionally, the vasoconstrictive response in ApoE$^{-/-}$/S1pr2$^{-/-}$ treated with Ang II+DOP was similar to that of ApoE$^{-/-}$/S1pr2$^{-/-}$ mice, receiving DOP alone (Figure 28 C). Between ApoE$^{-/-}$ and ApoE$^{-/-}$/S1pr2$^{-/-}$ mice with DOP treatment, no alterations in vasoconstrictive response to Ang II were identified (Figure 28 D).

To evaluate the endothelial-dependent vasodilation, the response to ACh was assessed after Phe-induced contraction. Interestingly, ApoE$^{-/-}$/S1pr2$^{-/-}$ mice treated with Ang II+DOP exhibited a more pronounced impairment in endothelium-dependent vasodilation compared to ApoE$^{-/-}$/S1pr2$^{-/-}$ mice receiving DOP alone. Specifically, the maximal vasodilatory response to ACh was reduced by approximately 2-fold in ApoE$^{-/-}$/S1pr2$^{-/-}$ treated with Ang II+DOP compared to those with DOP treatment (Figure 28 E). Under DOP treatment alone, the vasodilatory response between ApoE$^{-/-}$ and ApoE$^{-/-}$/S1pr2$^{-/-}$ mice was not altered (Figure 28 F).

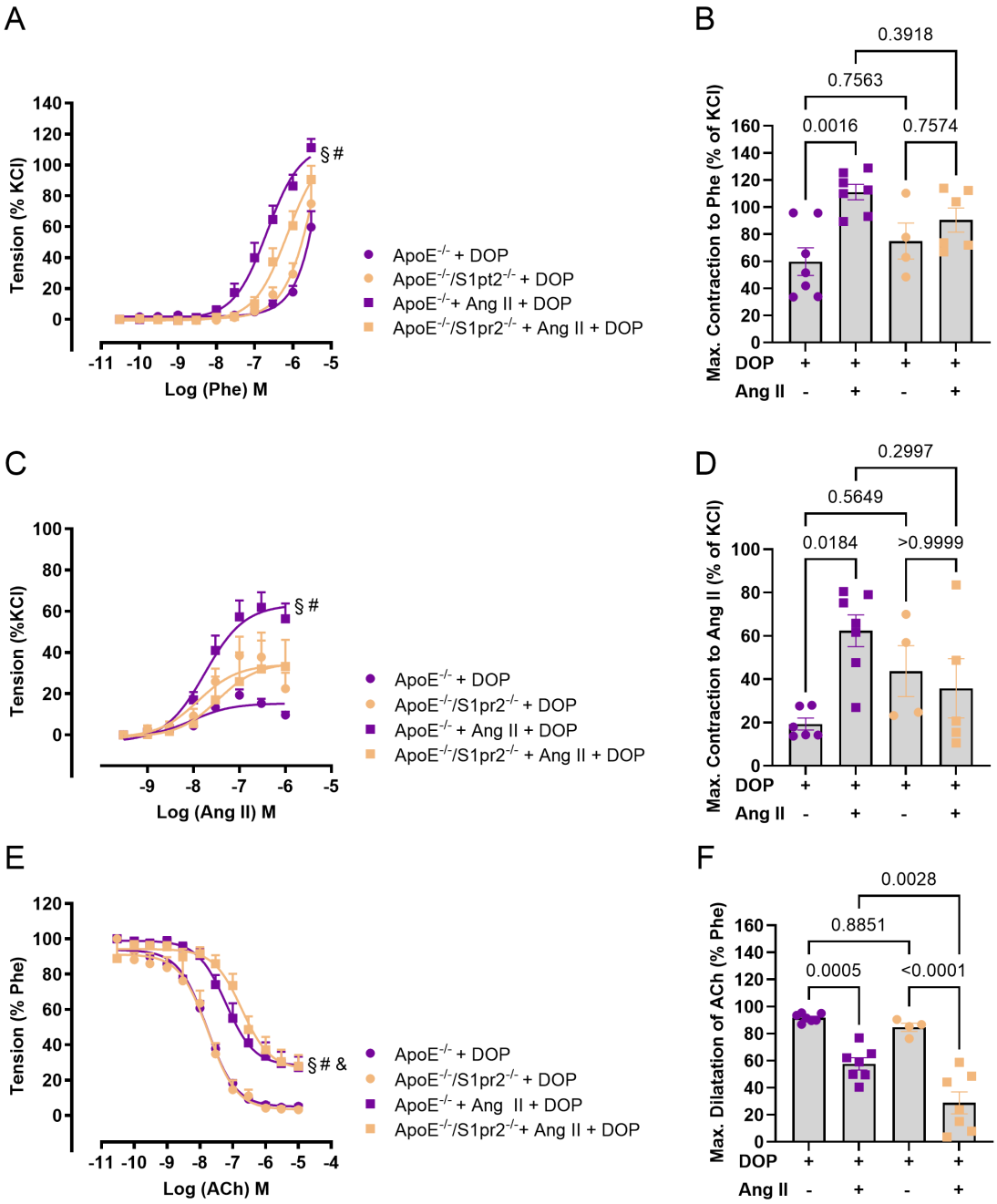

Figure 28: Endothelial dysfunction in ApoE$^{-/-}$/S1pr2$^{-/-}$ mice under Ang II infusion and pharmacologically induced S1P lyase inhibition. Wire myography was used to assess vascular contractility and dilation of aortic rings from ApoE$^{-/-}$/S1pr2$^{-/-}$ compared to ApoE$^{-/-}$ maintained on a western type diet (WTD) and DOP (30 mg/L in drinking water) with or without Ang II infusion. (A) Contractile response curve to Phe; § ApoE$^{-/-}$ + DOP vs ApoE$^{-/-}$ Ang II+DOP: P < 0.0001; # ApoE$^{-/-}$ Ang II+DOP vs ApoE$^{-/-}$/S1pr2$^{-/-}$ Ang II+DOP: P = 0.0085 (B) maximal contraction to Phe. (C) Vasoconstriction to increasing concentrations of Ang II; § ApoE$^{-/-}$ DOP vs ApoE$^{-/-}$ Ang II+DOP: P < 0.0001; # ApoE$^{-/-}$ Ang II+DOP vs ApoE$^{-/-}$/S1pr2$^{-/-}$ Ang II+DOP: P = 0.0298 (D) maximum contraction to Ang II (E) Acetylcholine (ACh) - induced vasorelaxation in Phe induced pre-contracted aortic rings; § ApoE$^{-/-}$ + DOP vs ApoE$^{-/-}$ Ang II+DOP: P < 0.0001; # ApoE$^{-/-}$ Ang II+DOP vs ApoE$^{-/-}$/S1pr2$^{-/-}$: P = 0.0011; & ApoE$^{-/-}$/S1pr2$^{-/-}$ + DOP vs ApoE$^{-/-}$/S1pr2$^{-/-}$ Ang II+DOP: P < 0.0001(F) Maximal dilation values to ACh. Data are presented as mean ± SEM (n = 4-7 per group). Statistical analysis was determined using two-way ANOVA with multiple comparisons (A-F).

In summary, ApoE$^{-/-}$/S1pr2$^{-/-}$ mice treated with Ang II+DOP showed no benefit in survival, aneurysm formation, nor severity. While the prevention of Ang II+DOP-induced downregulation of contractile markers indicates that S1PR2 contributes to the

phenotypic switch under elevated S1P conditions, endothelial dysfunction was even more pronounced in S1PR2-deficient mice. This finding suggests that the absence of S1PR2, although beneficial for VSMC contractility, is detrimental to endothelial function, effects that may counteract *in vivo*, resulting in no net effect on aortic aneurysm formation.

4.9. S1PR3 knockout mice are protected against aneurysm rupture

Based on prior evidence that tonic S1P signaling induces S1PR3-mediated downregulation of contractile genes *in vitro*, and thereby potentially contributes to aneurysm formation and rupture, the functional role of S1PR3 was further investigated *in vivo*. To address this, ApoE$^{-/-}$/S1pr3$^{-/-}$ mice were generated and infused with Ang II over a period of 28 days. In comparison to Ang II- infused ApoE$^{-/-}$ mice, ApoE$^{-/-}$/S1pr3$^{-/-}$ mice show a remarkable improvement in survival. In detail, only 8% of the S1pr3-deficient mice died because of rupture (Figure 29 A). No differences were observed in localization of rupture or in the incidence of abdominal aortic aneurysms or dissections (Figure 29 B & C). Furthermore, while overall survival was enhanced, aneurysm severity by macroscopic analysis using the classification scheme of Daugherty revealed no differences between both Ang II-infused genotypes (Figure 29 D & E). Ang II infusion led to an increase in SBP in both genotypes, with no significant differences between ApoE$^{-/-}$ and ApoE$^{-/-}$/S1pr3$^{-/-}$ animals (Figure 29 F). In order to identify the impact of S1PR3 deficiency on VSMC phenotype, the expression levels of contractile genes were determined in aortic tissue of Ang II-infused ApoE$^{-/-}$ and ApoE$^{-/-}$/S1pr3$^{-/-}$ mice and the respective non-infused controls. Loss of S1PR3 resulted in higher expression of contractile genes in Ang II-infused ApoE$^{-/-}$/S1pr3$^{-/-}$ compared to ApoE$^{-/-}$ mice with the same treatment, with Acta2 showing a 4.2-fold and Tagln a 4.85-fold increase in expression (Figure 29 G). Without Ang II infusion, no alteration in contractile gene expression was observed between both genotypes.

In summary, these findings indicated that tonic S1P signaling via S1PR3 promoted phenotypic switching of VSMCs, which could have contributed to structural weakening of the aortic wall and the progression of aneurysm and rupture.

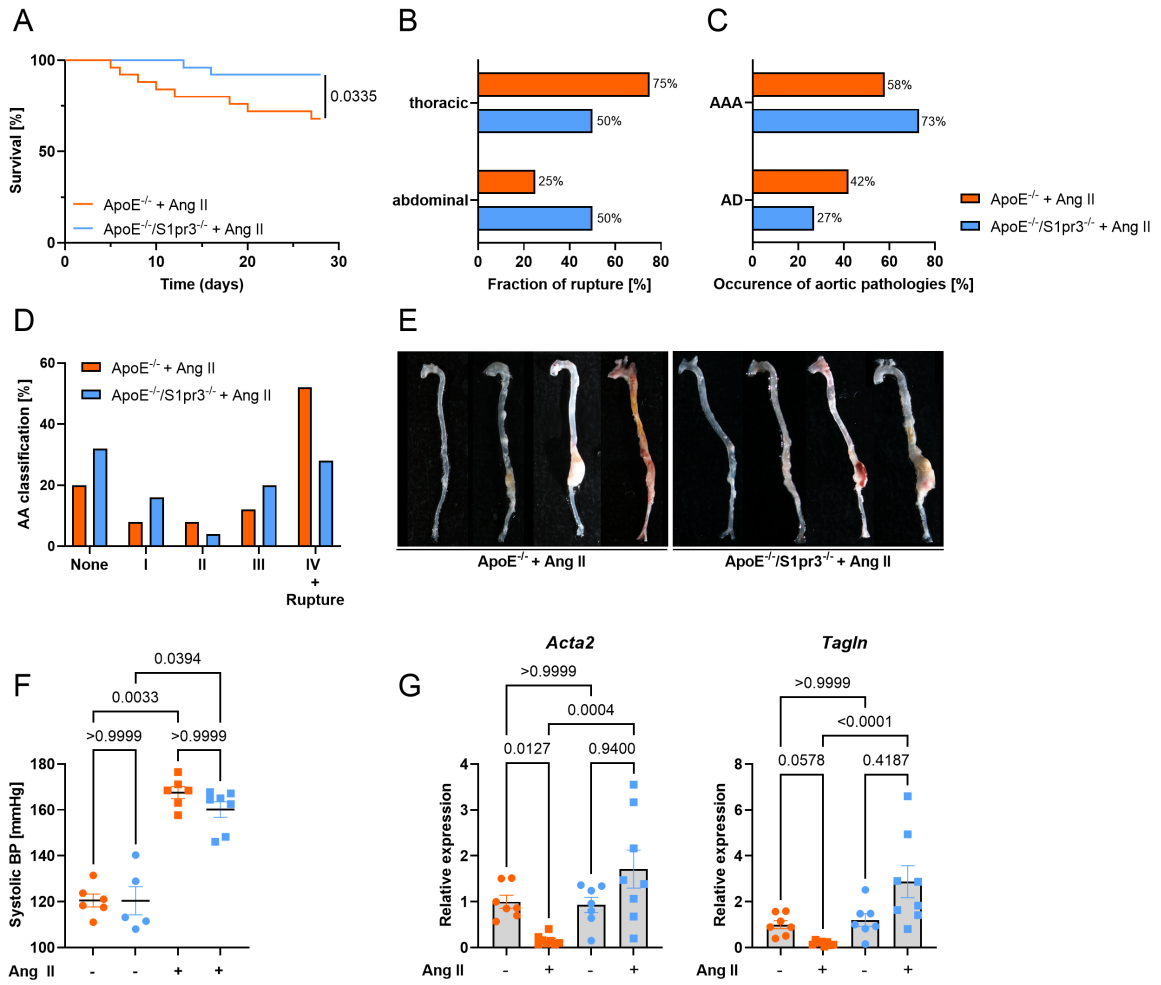

Figure 29: Loss of S1PR3 reduced the incidence of aortic aneurysm rupture and maintains contractile integrity in Ang II-infused mice. ApoE$^{-/-}$ and ApoE$^{-/-}$/S1pr3$^{-/-}$ mice were fed a western type diet and received Ang II infusion (1,000 ng/kg/min; 28 days). (A) Kaplan Meier survival curve (n= 25 per group). (B) Localization of aortic rupture (thoracic and abdominal). (C) Incidence of aortic pathologies divided into abdominal aortic aneurysms (AAA) and aortic dissections (AD) based on macroscopic evaluation. (D) Assessment of aneurysm severity based on Daugherty's classification system: none = no aneurysm; I = dilated lumen without thrombus; II = remodelled vessel wall with thrombus; III = pronounced bulbous form with thrombus; IV = multiple aneurysms or rupture. (E) Representative images of *aortae* with aneurysmal and dissecting lesions. (F) Systolic blood pressure (SBP) before and 10-14 days after Ang II infusion (n = 5-7 per group). (G) Relative gene expression of contractile markers Acta2 and Tagln in the aortic tissue of both genotypes after 28 days of Ang II infusion (n =7-8 per group). Data are represented as mean ± SEM. Statistical analysis was performed using Fisher's exact test (B-D) and two-way ANOVA with repeated measures or multiple comparisons (F-G).

Next, the vascular reactivity was analysed by wire myography using aortic segments from ApoE$^{-/-}$ and ApoE$^{-/-}$/S1pr3$^{-/-}$ mice with or without Ang II infusion. As previously observed, Ang II-infused ApoE$^{-/-}$ mice exhibited a pronounced hypercontractile response to Phe compared to their non-infused controls. This effect did not occur in ApoE$^{-/-}$/S1pr3$^{-/-}$ mice with Ang II (Figure 30 A). In contrast, the vasoconstrictive response to Phe was not enhanced in Ang II-infused ApoE$^{-/-}$/S1pr3$^{-/-}$ mice compared to their non-infused controls (Figure 30 A).

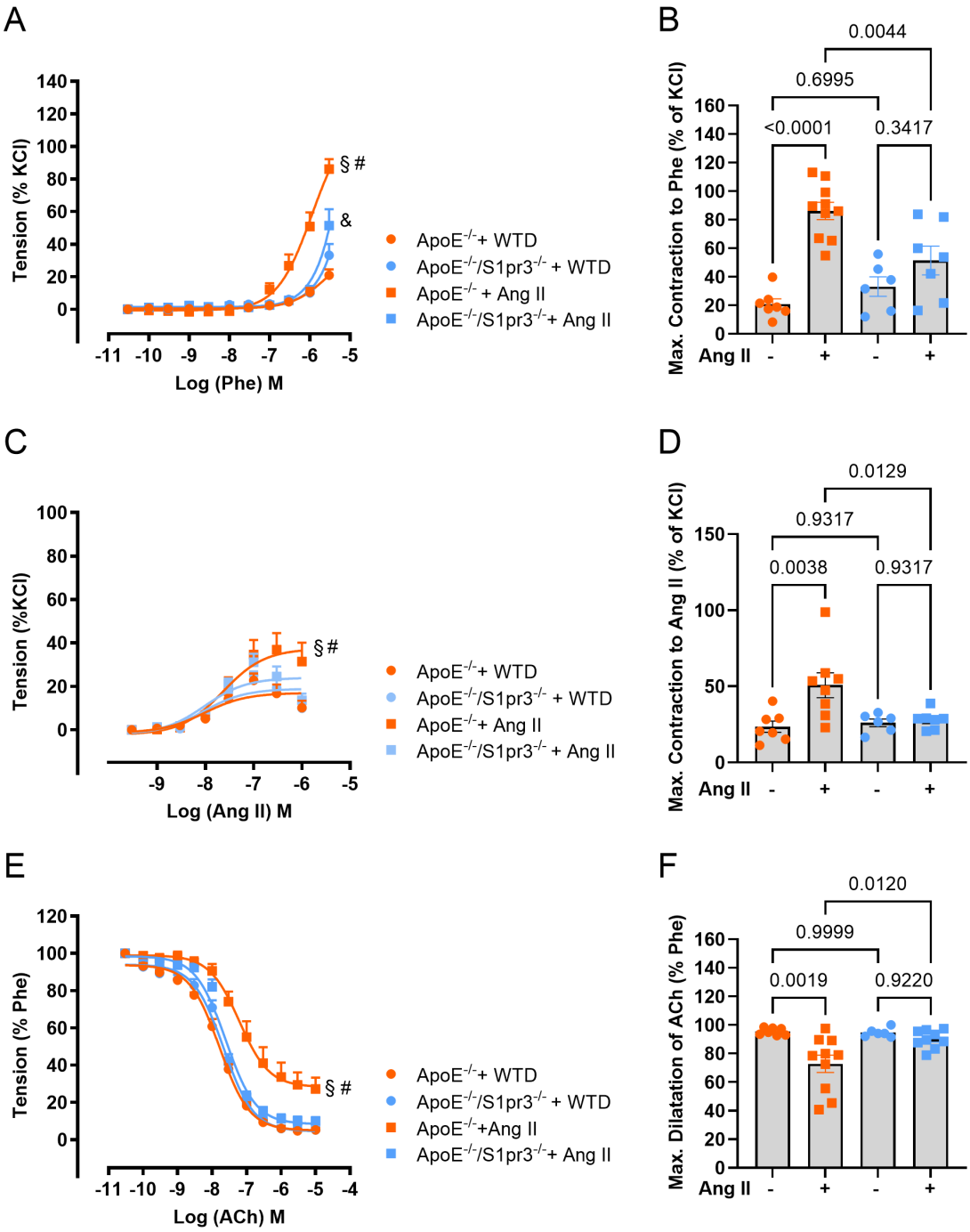

Figure 30: Loss of S1PR3 maintains vascular reactivity in response to Ang II- induced vascular dysfunction. Abdominal aortic rings from ApoE$^{-/-}$ and ApoE$^{-/-}$/S1pr3$^{-/-}$, fed a western type diet (WTD) with or without additional Ang II infusion were mounted in a wire myograph for functional analysis. (A) Vasoconstriction in response to increasing concentrations of phenylephrine (Phe) expressed as percentage of maximal KCl response. § ApoE$^{-/-}$ + WTD vs ApoE$^{-/-}$ + Ang II: P < 0.0001; # ApoE$^{-/-}$ + Ang II vs ApoE$^{-/-}$/S1pr3$^{-/-}$ + Ang II: P < 0.0001; & ApoE$^{-/-}$/S1pr3$^{-/-}$ + WTD vs ApoE$^{-/-}$/S1pr3$^{-/-}$ + Ang II: P = 0.0020 (B) Maximum constriction to Phe. (C) Vasoconstriction in response to increasing concentrations of Ang II expressed as a percentage of the maximal KCl response; § ApoE$^{-/-}$ + WTD vs ApoE$^{-/-}$ + Ang II: P = 0.0006; # ApoE$^{-/-}$ + Ang II vs ApoE$^{-/-}$/S1pr3$^{-/-}$ + Ang II: P = 0.0039 (D) Maximum constriction to Ang II. (E) Vascular relaxation induced by acetylcholine (ACh) relative to preceding Phe-induced vasoconstriction. § ApoE$^{-/-}$ + WTD vs ApoE$^{-/-}$ + Ang II: P = 0.0004; # ApoE$^{-/-}$ + Ang II vs ApoE$^{-/-}$/S1pr3$^{-/-}$ + Ang II: P = 0.0039 (F) Maximum vasodilation in response to ACh. Data are presented as mean ± SEM (n = 6-10 per group). Statistical analysis was determined using two-way ANOVA with multiple comparisons (A, C, E) and two-way ANOVA with multiple comparisons (B, D, F).

In line with this, the maximum contraction to Phe demonstrated an 4.12-fold increase in ApoE$^{-/-}$ following Ang II infusion, which was absent in S1pr3-deficient mice with the same treatment (Figure 30 B). Without Ang II infusion, no alteration in vasoconstrictive response was observed between both genotypes.

S1pr3-deficient mice infused with Ang II showed a lower vasoconstrictive response to Ang II compared to Ang II-infused ApoE$^{-/-}$ (Figure 30 C). The maximal vasoconstrictive response to Ang II was reduced 1.8-fold in Ang II-infused ApoE$^{-/-}$/S1pr3$^{-/-}$ mice compared to Ang II-infused ApoE$^{-/-}$ mice, reaching levels comparable to those observed in ApoE$^{-/-}$/S1pr3$^{-/-}$ mice on WTD alone (Figure 30 D).

In contrast to the pronounced endothelial dysfunction to ACh in Ang II-infused ApoE$^{-/-}$ mice, the endothelial response was completely preserved in ApoE$^{-/-}$/S1pr3$^{-/-}$ mice, independent of Ang II infusion (Figure 30 E). This observation was further supported after the quantification of maximal dilation. In detail, Ang II-infused ApoE$^{-/-}$/S1pr3$^{-/-}$ mice exhibited a maximal ACh-induced dilation of 90% whereas ApoE$^{-/-}$ mice under the same treatment showed a significantly reduced response around 73% (Figure 30 F). Notably, the dilation capacity of Ang II-infused ApoE$^{-/-}$/S1pr3$^{-/-}$ mice did not differ from that of ApoE$^{-/-}$/S1pr3$^{-/-}$ mice receiving WTD alone, in clear contrast to ApoE$^{-/-}$ control groups (Figure 30 F).

Taken together, these findings highlight that S1PR3 is a critical mediator of Ang II-induced phenotypic switch, vascular hypercontractility, endothelial dysfunction and aortic rupture during aneurysm development.

4.10. S1PR3 deficiency attenuates aneurysm formation/rupture in the Ang II model and prevents hypercontractility

To investigate whether the beneficial effect of S1PR3 deficiency persists under tonic S1P stimulation *in vivo*, ApoE$^{-/-}$/S1pr3$^{-/-}$ mice were treated with DOP in the Ang II model.

Kaplan-Meier survival analysis revealed a significantly improved outcome for Ang II-infused ApoE$^{-/-}$/S1pr3$^{-/-}$ mice with DOP compared to ApoE$^{-/-}$ controls with the same treatment (Figure 31 A). Interestingly, analysis of rupture location and incidence of abdominal aortic aneurysms or aortic dissections showed no significant difference between both groups (Figure 31 B & C). However, the macroscopic evaluation according to Daugherty's classification scheme revealed a significant difference

(Fisher's exact test; P = 0.0075) in aortic aneurysm phenotype, defined by a reduced association of *aortae* from ApoE$^{-/-}$/S1pr3$^{-/-}$ mice with severe types (Figure 31 D & E).

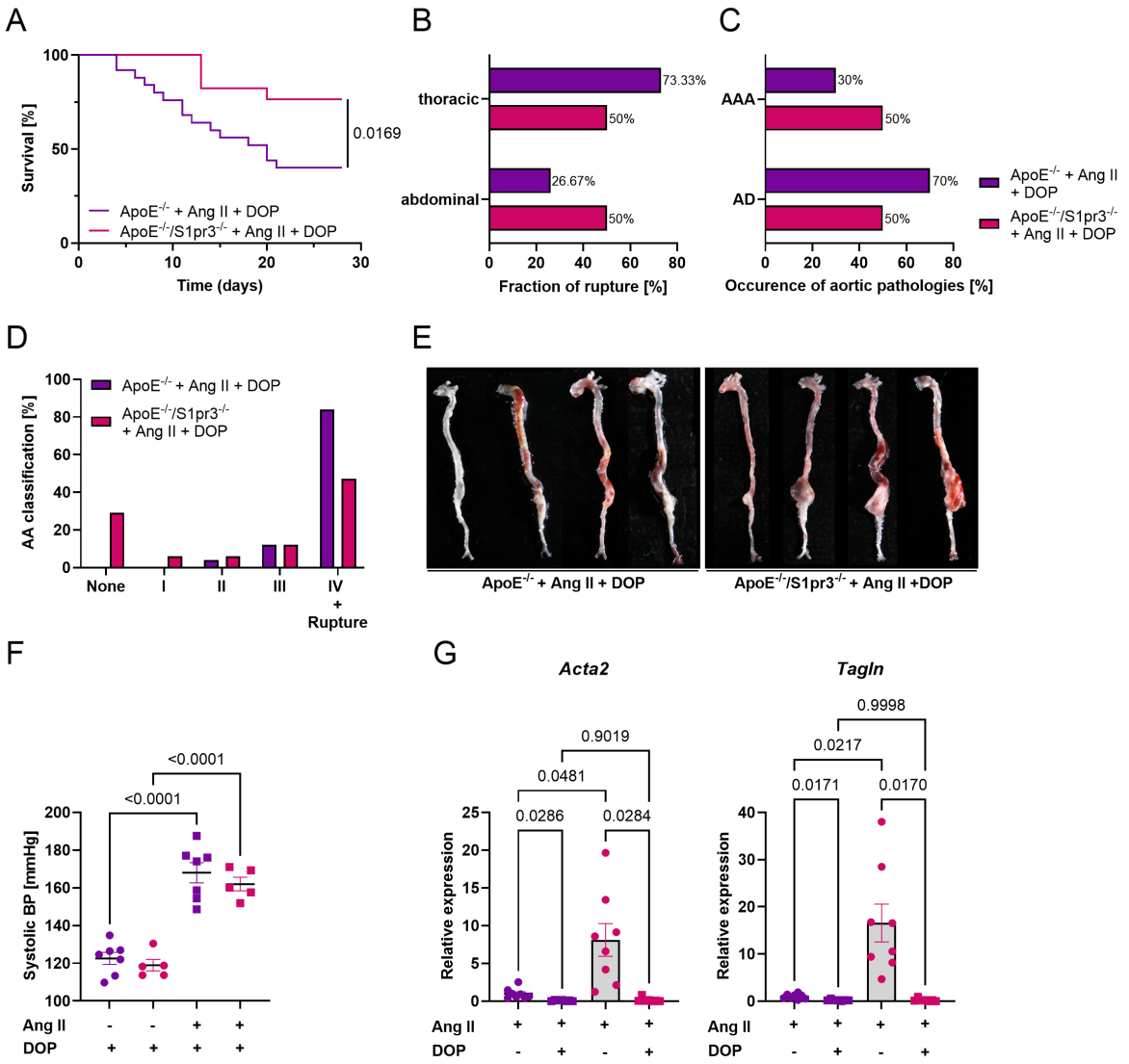

Figure 31: Deletion of S1PR3 improves survival in Ang II-infused mice under pharmacological inhibition of S1P lyase. ApoE$^{-/-}$ and ApoE$^{-/-}$/S1pr3$^{-/-}$ were fed a western type diet and received the S1P lyase inhibitor DOP (30 mg/L, via drinking water, in combination with Ang II infusion (1,000 ng/kg/min) for a duration of 28 days (A) Kaplan-Meier survival curve; $n_{ApoE^{-/-}}$ = 25; $n_{ApoE^{-/-}/S1p3^{-/-}}$ = 17 (B) Localization of rupture sites (thoracic and abdominal). (C) Incidence of abdominal aortic aneurysms (AAA) and aortic dissections (AD) determined by macroscopic examination. (D) Aneurysm severity categorized according to the modified Daugherty classification: None = no aneurysm; I = dilated lumen without thrombus; II = remodelled wall with thrombus; III = pronounced bulbous with thrombus; IV = dissecting or ruptured aneurysm. (E) Representative images of aneurysmal and dissecting *aortae*. (F) Systolic blood pressure measured via tail-cuff method in both genotypes treated with DOP before and 10-14 days after Ang II infusion (n = 5-7). (G) Relative gene expression of contractile marker Acta2 and Tagln in aortic tissue of both genotypes infused with Ang II or additional DOP treatment (n = 7-8). Data are presented as mean ± SEM. Statistical significance was tested by Fisher's exact test (B-D) and two-way ANOVA with multiple comparisons (F-G).

SBP was similarly elevated in both genotypes upon Ang II+DOP treatment. Under DOP alone, no alterations in SBP were observed (Figure 31 F). Since Ang II+DOP leads to a massive downregulation of contractile markers in ApoE$^{-/-}$ mice, contractile gene

expression of Acta2 and Tagln was analysed in Ang II-infused ApoE$^{-/-}$/S1pr3$^{-/-}$ + DOP treatment. Gene expression analysis revealed that contractile markers Acta2 and Tagln were similarly suppressed in ApoE$^{-/-}$/S1pr3$^{-/-}$ mice with Ang II+DOP as in their ApoE$^{-/-}$ Ang II+DOP controls (Figure 31 G). Confirming the results from the previous chapter, ApoE$^{-/-}$/S1pr3$^{-/-}$ mice with Ang II exhibited a significantly higher expression of Acta2 (8.12-fold) and Tagln (16.58-fold) in the absence of DOP (Figure 31 G).

To examine how DOP modulates the vasoreactivity of Ang II-infused ApoE$^{-/-}$/S1pr3$^{-/-}$ vessels, aortic segments were analysed for their vasoconstrictive and vasodilatory response.

Aortae from Ang II+DOP-treated ApoE$^{-/-}$/S1pr3$^{-/-}$ mice exhibited a significantly enhanced vasoconstrictive response to increasing doses of Phe compared to ApoE$^{-/-}$ mice receiving the same treatment (Figure 32 A). The maximum contraction was 2.63-fold reduced in ApoE$^{-/-}$/S1pr3$^{-/-}$ mice treated with Ang II+DOP compared to ApoE$^{-/-}$ under Ang II+DOP treatment (Figure 32 A). These findings suggest that S1PR3 deficiency abolished the hypercontractile phenotype caused by Ang II+DOP treatment. Specifically, no differences in vasoconstrictive responses were observed between Ang II-infused ApoE$^{-/-}$/S1pr3$^{-/-}$ mice compared to ApoE$^{-/-}$/S1pr3$^{-/-}$, receiving Ang II+DOP, indicating that tonic S1P levels do not augment vascular contractility in the absence of S1PR3 (Figure 32 A & B).

Ang II+DOP-treated ApoE$^{-/-}$/S1pr3$^{-/-}$ mice showed a reduced vasoconstrictive response to Ang II, further confirmed by 3.32-fold reduction of maximum contraction compared to ApoE$^{-/-}$ mice with Ang II+DOP (Figure 32 C & D). Furthermore, between both genotypes treated with DOP alone, no difference in vasoconstrictive response was observed (Figure 32 D). In summary, this data confirms that loss of S1PR3 protects against Ang II-mediated enhancement of vasoconstriction.

ApoE$^{-/-}$/S1pr3$^{-/-}$ mice treated with Ang II+DOP showed a preserved dilation capacity compared to ApoE$^{-/-}$ with Ang II+DOP (Figure 32 E & F). Under DOP treatment alone, no difference was observed between both genotypes. Taken together, the loss of S1PR3 also exerted a protective effect on endothelial function.

In summary, the findings suggest that S1PR3 contributes to the adverse vascular effects of tonic S1P signalling during Ang II+DOP treatment, while its loss may protect against endothelial dysfunction and excessive vascular reactivity.

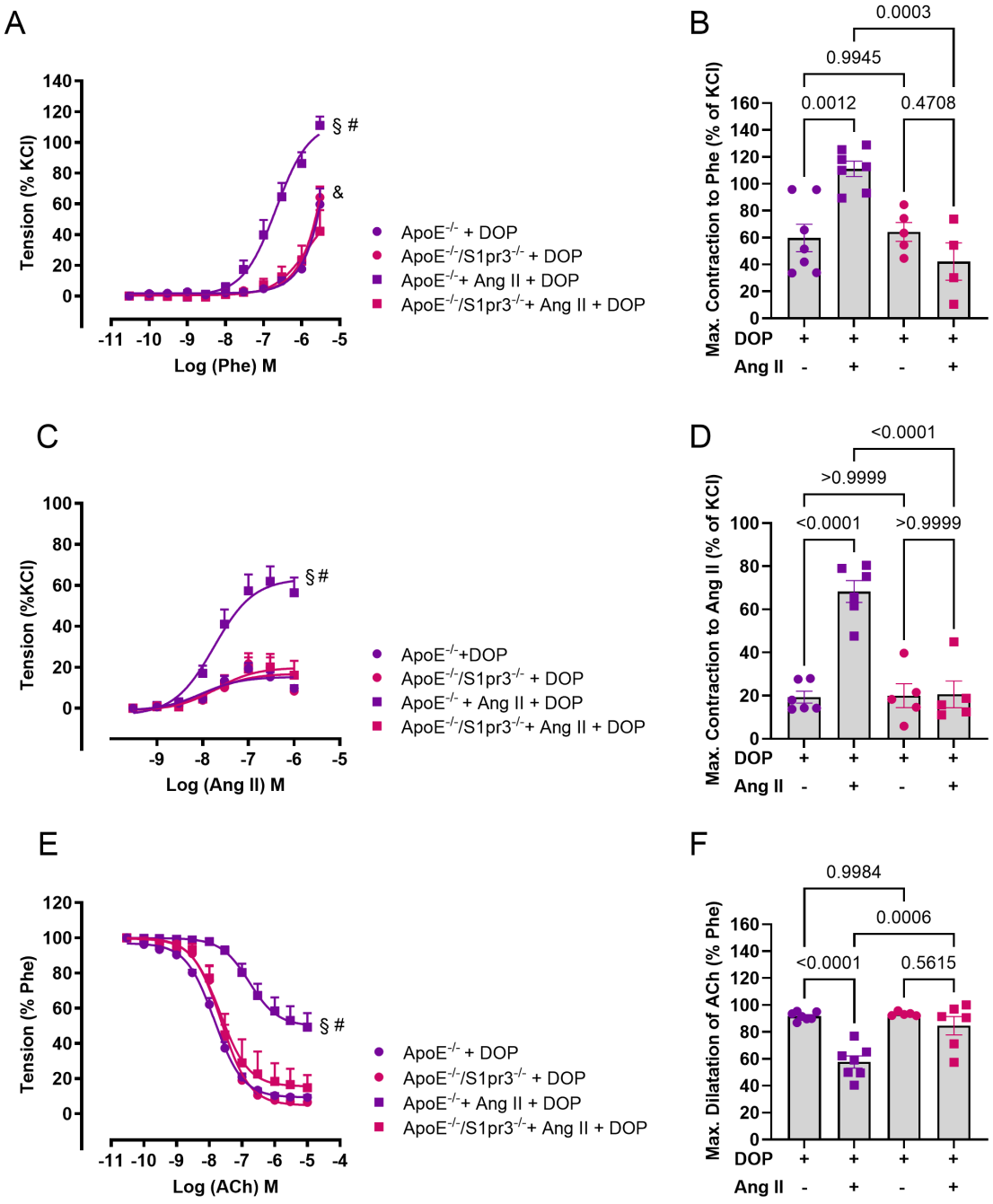

Figure 32: Loss of S1PR3 maintains vascular functionality in Ang II-infused mice with additional pharmacological inhibition of S1P lyase. ApoE$^{-/-}$ and ApoE$^{-/-}$/S1pr3$^{-/-}$ were treated with S1P lyase inhibitor DOP (30 mg/L in drinking water) and additionally infused with Ang II (1,000 ng/kg/min). Abdominal aortic rings were mounted in a wire myograph to assess vascular function. (A) Contractile response to phenylephrine (Phe) normalized to maximal vasoconstriction to KCl. § ApoE$^{-/-}$ + DOP vs ApoE$^{-/-}$ + Ang II+DOP: P < 0.0001; # ApoE$^{-/-}$ + Ang II+DOP vs ApoE$^{-/-}$/S1pr3$^{-/-}$ + Ang II+DOP: P < 0.0001; & ApoE$^{-/-}$/S1pr3$^{-/-}$ + DOP vs ApoE$^{-/-}$/S1pr3$^{-/-}$ + Ang II+DOP: P = 0.0126 (B) Maximal vasoconstriction to Phe. (C) Contractile response to Ang II normalized to maximal vasoconstriction to KCl. § ApoE$^{-/-}$ + DOP vs ApoE$^{-/-}$ + Ang II+DOP: P < 0.0001; # ApoE$^{-/-}$ + Ang II+DOP vs ApoE$^{-/-}$/S1pr3$^{-/-}$ + Ang II+DOP: P < 0.0001 (D) Maximal vasoconstriction in response to Ang II. (E) Acetylcholine (ACh) - induced vasodilation after pre-constriction with Phe. § ApoE$^{-/-}$ + DOP vs ApoE$^{-/-}$ + Ang II+DOP: P < 0.0001; # ApoE$^{-/-}$ + Ang II+DOP vs ApoE$^{-/-}$/S1pr3$^{-/-}$ + Ang II+DOP: P < 0.0001 (F) Maximal vasodilatation in response to ACh. Data are represented as mean ± SEM (n = 4-7 per group). Statistical analysis was performed using two-way ANOVA with multiple comparisons (A-F).

4.11. S1P/S1PR3 signaling promotes calcium-dependent MLC phosphorylation in VSMCs

S1P signaling is associated with the mobilization of intracellular calcium, a key mechanism that is essential in VSMC contractility[232,281]. Since *aortae* from Ang II-infused mice with pharmacologically elevated S1P levels exhibited hypercontractility, the role of S1P in VSMC calcium homeostasis was analysed. To assess the involvement of specific S1PRs in Ca^{2+} release in VSMCs, cells were loaded with the ratiometric calcium indicator Fura-2 and pretreated with selective antagonists for S1PR1-3 prior to S1P stimulation. Stimulation with S1P induced an increase in intracellular Ca^{2+} levels (Figure 33 A).

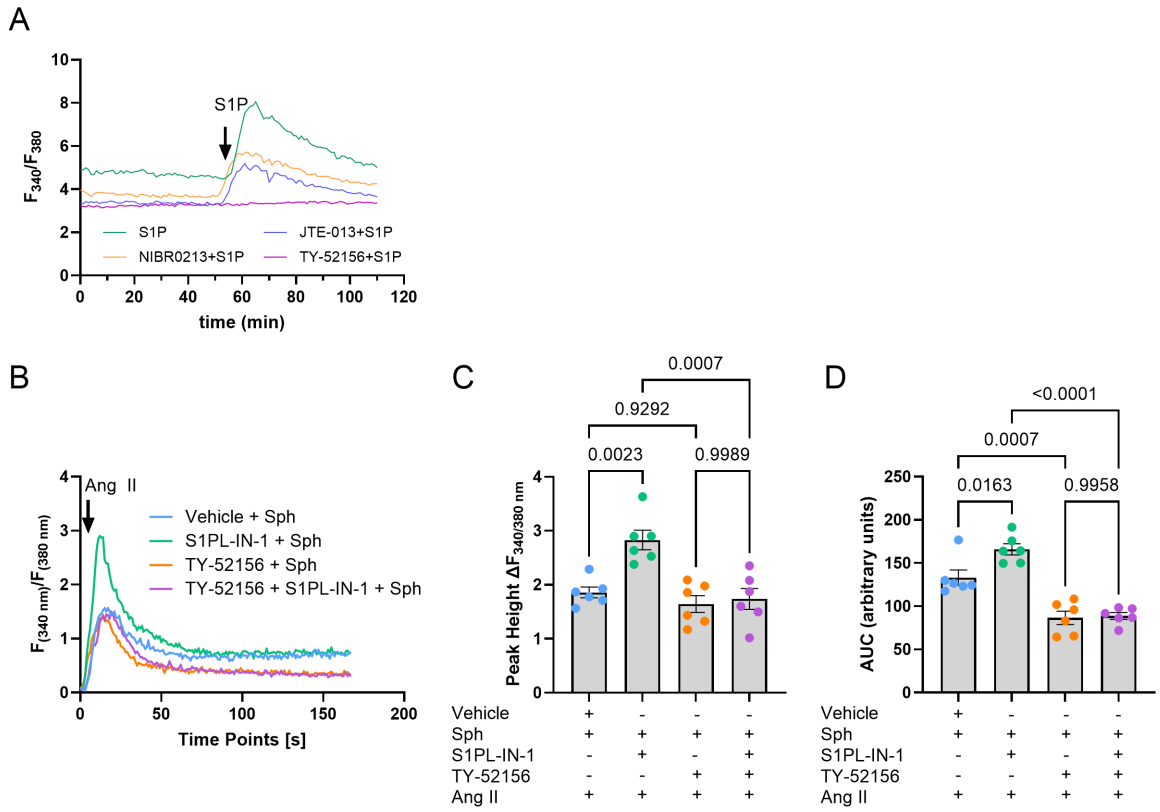

Figure 33: Intracellular accumulation of S1P enhances the calcium response to Ang II stimulation in VSMCs in an S1PR3-dependent manner. For calcium imaging, VSMCs were loaded with the ratiometric dye Fura-2, and intracellular Ca^{2+} release was monitored following stimulation with S1P (1 µM) and Ang II (100 nM). (A) Representative tracing of intracellular Ca^{2+} of Fura-2 loaded VSMCs, which received 15 min prior S1P stimulation, S1PR antagonists (S1PR1: NIBR0213 (10 µM), S1PR2: JTE-013 (10 µM), S1PR3: TY-52156 (10 µM). (B) Representative tracing of intracellular Ca^{2+} of Fura-2 loaded VSMCs. VSMCs were treated daily with S1PL-IN-1 (1 µM) and Sph (1 µM) for 5 days, or with additional antagonization of S1PR3 via TY-521561 (10 µM) 1 h prior S1PL-IN-1 and Sph stimulation. Intracellular calcium was measured after Ang II (100 nM) injection and (C) Peak Height and (D) AUC was shown. Data are presented as F_{340}/F_{380} ratios (A-B) or as mean ± SEM (C-D; n = 6 per group). Statistical analysis was performed using one-way ANOVA with multiple comparisons.

Notably, this response was completely abolished by inhibition of S1PR3 using TY-52156, indicating that S1P-dependent calcium mobilization is mediated predominantly through S1PR3. In contrast, blocking of S1PR1 or S1PR2 had no measureable effect on Ca^{2+} release (Figure 33 A). Preincubation with S1PR antagonists led to a slight reduction in the basal Ca^{2+} response (Figure 33 A). Then an *in vitro* model using VSMCs was established to investigate whether tonic S1P stimulation influenced Ca^{2+} release and whether S1PR3 is specifically involved in this process. Therefore, Ca^{2+} flux was measured after daily treatment for five days with the S1P lyase inhibitor S1PL-IN-1 in combination with the S1P precursor Sph. This treatment led to an intracellular increase in S1P in VSMCs (Figure 20 B). VSMCs were additionally pre-treated with S1PR3 inhibitor, TY-521561. Subsequently, the Ca^{2+} release after Ang II stimulation of these cells, was measured using Fura-2. Interestingly, an increase in intracellular Ca^{2+} was observed in VSMCs pre-treated with the S1P lyase inhibitor and Sph, indicating that tonic S1P levels induced an elevation in mobilized Ca^{2+} (Figure 33 B & C). Quantitative analysis of the Ca^{2+} peak following Ang II stimulation revealed a 1.5-fold increase in VSMCs with tonic S1P levels compared to the respective control, without S1P lyase inhibitor. This effect was abolished by pre-treatment with TY-52156 (Figure 33 B). However, the pre-treatment with TY-52156 did not alter the Ca^{2+} peak in VSMCs in the absence of tonic S1P stimulation (Figure 33 B). Further analysis of total calcium release, assessed by calculating the area under the curve (AUC) after Ang II stimulation, showed an increase in Ca^{2+} in VSMCs treated with S1PL-IN-1 and Sph compared to cells without S1P lyase inhibition (Figure 33 C). In line with previous results, pre-treatment with TY-52156 led to a 1.87-fold reduction in total Ca^{2+} release under conditions of tonic S1P levels (Figure 33 C). Interestingly, a comparable reduction in Ca^{2+} mobilization was also observed in VSMCs without S1P lyase inhibition following Ang II stimulation (Figure 33 C). In this setting, the total Ca^{2+} release was approximately 35% lower in VSMCs pre-treated with TY-52156 compared to those treated with Sph alone (Figure 33 C). These findings suggest that intracellularly accumulated S1P led to calcium mobilisation in VSMCs. Furthermore, the data indicate that Ang II-induced calcium signalling is partly mediated through S1PR3 activation.

Given the finding that S1PR3 in mediating intracellular Ca^{2+} mobilization, the phosphorylation of myosin light chain (p-MLC) as key event in mediating VSMC contraction was analysed. The phosphorylation of MLC is a critical part of VSMC contractility[347,348].

Following Ang II stimulation for 30 min, cells primed with Sph exhibited an increase in p-MLC (Figure 34 A). This phosphorylation was even more enhanced under tonic S1P levels (Figure 34 A). Interestingly, the addition of the S1PR3 antagonist TY-52156 completely prevented the phosphorylation of MLC in the presence or absence of S1PL-IN-1 demonstrating that S1PR3 is involved in Ang II induced MLC phosphorylation. Total MLC and GAPDH levels remained stable across experimental groups, confirming consistent protein loading (Figure 34 A).

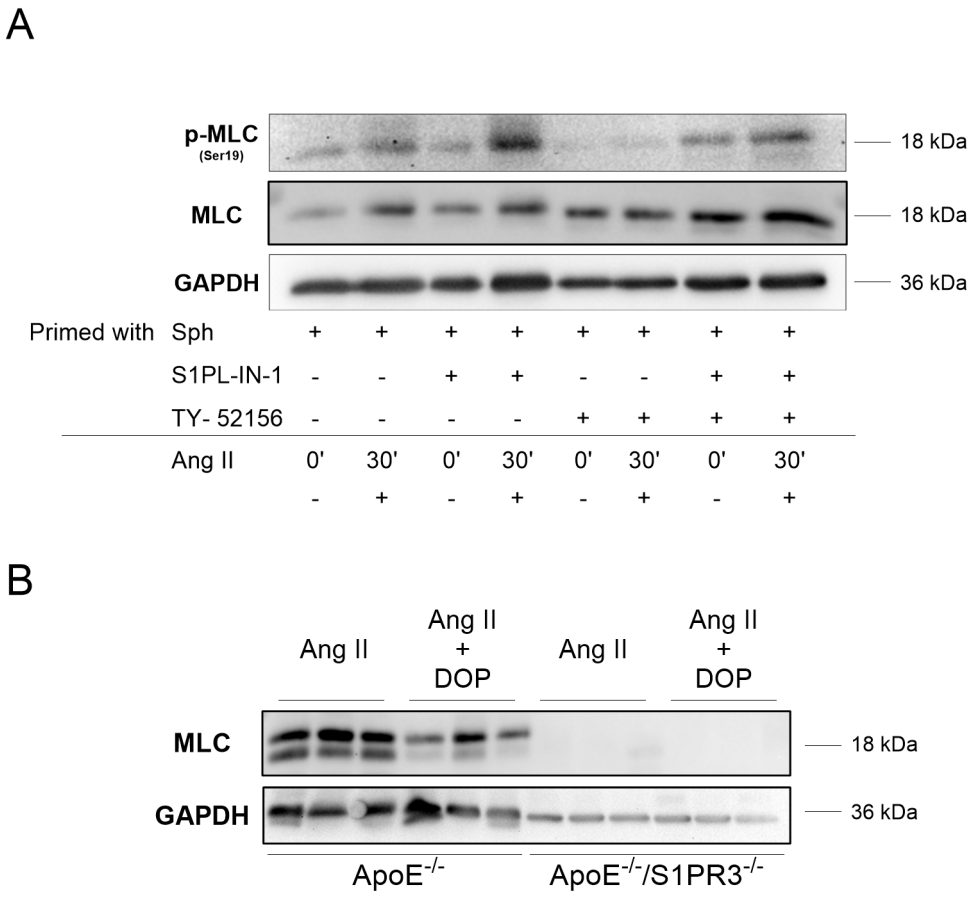

Figure 34: Intracellular S1P promotes Ang II-induced phosphorylation of myosin light chain (p-MLC) in an S1PR3-dependent manner. (A) Representative western blot of phosphorylated myosin light chain (p-MLC, Ser19), total MLC and GAPDH as loading control in VSMCs pre-treated daily over 5 days with S1P lyase inhibitor (S1PL-IN-1, 1 µM), sphingosine (Sph, 1 µM) or both. Pre-treated with S1PR3 antagonist TY-52156 (10 µM) 30 min prior stimulation. After 5 days, VSMCs were stimulated with Ang II (100 nM) for 30 min. The blot is representative of three independent experiments. (B) Western blot analysis of MLC expression in *aortae* of ApoE$^{-/-}$ and ApoE$^{-/-}$/S1pr3$^{-/-}$infused with Ang II (1,000 ng/kg/min) or additionally treated with DOP (30 mg/L via drinking water). GAPDH served as loading control.

To further validate whether S1PR3 contributed to the hypercontractile state of the aorta under tonic S1P levels and Ang II infusion, MLC expression was assessed in aortic tissue of Ang II-infused ApoE$^{-/-}$ and ApoE$^{-/-}$/S1pr3$^{-/-}$ mice treated with or without DOP. Western blot analysis revealed a remarkable reduction in total MLC in ApoE$^{-/-}$/S1pr3$^{-/-}$

mice regardless of S1P lyase inhibition. This finding indicated that S1PR3 may also contribute to the maintenance of MLC protein expression (Figure 34 B). Interestingly, total MLC expression was slightly reduced in *aortae* from Ang II-infused ApoE$^{-/-}$ mice treated with the S1P lyase inhibitor DOP, compared to ApoE$^{-/-}$ mice receiving Ang II alone (Figure 34 B). Off note, since the aortic tissue was not acutely stimulated with Ang II prior to protein isolation, p-MLC could not be reliably assessed. Therefore, the analysis was restricted to total MLC expression.

4.12. FTY720 treatment does not affect aortic aneurysm formation and outcome in the Ang II infusion model

As S1PR modulator FTY720 is clinically approved and targets S1PR1, S1PR3, S1PR4 and S1PR5, its potential influence on the development of aortic aneurysms was analysed in the Ang II model.

Survival analysis over 28 days revealed no difference between Ang II-infused ApoE$^{-/-}$ mice and those additionally treated with FTY720 (Figure 35 A). Furthermore, the localization of rupture and the incidence of aortic pathologies, including abdominal aortic aneurysms and aortic dissections, did also not differ between both groups (Figure 35 B & C). Macroscopic classification according to Daugherty revealed no alterations in aortic aneurysm phenotype (Figure 35 D & E). Since some studies have linked FTY720 administration to alterations in blood pressure[349,350], systolic blood pressure was analysed in Ang II-infused ApoE$^{-/-}$ receiving FTY720. No alterations were observed between both groups regardless of FTY720 administration (Figure 35 F).

The contractile gene expression showed a 5.95-fold reduction for Acta2 and a 4.65-fold reduction for Tagln in Ang II-infused ApoE$^{-/-}$ mice compared to the respective non-infused controls (Figure 35 G). Simultaneously, Ang II-infused ApoE$^{-/-}$ mice treated with FTY720 showed the same reduction in contractile marker expression. Furthermore, no alterations in contractile marker expression were observed between ApoE$^{-/-}$ mice receiving FTY720 and untreated controls (Figure 35 G).

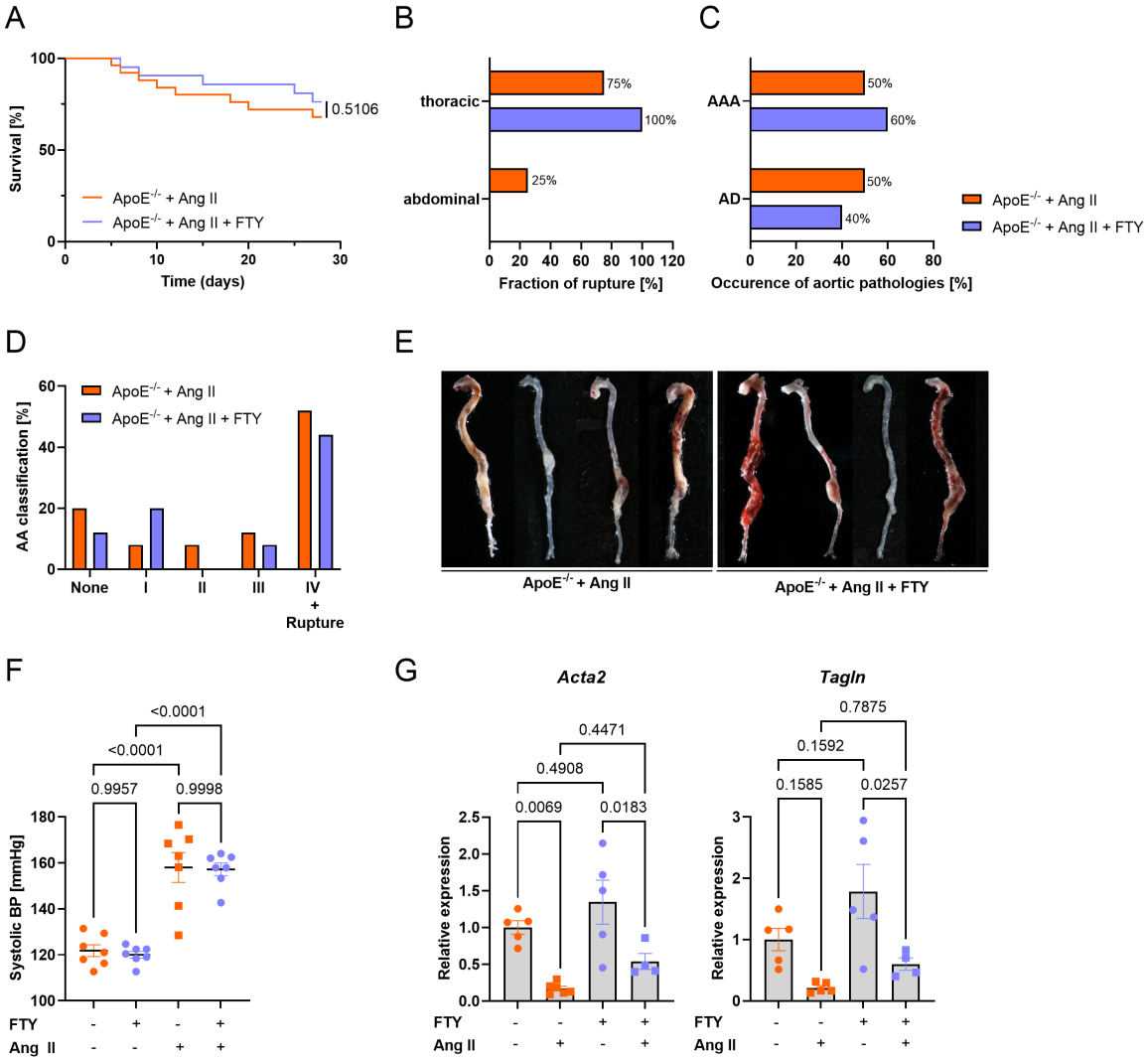

Figure 35: Functional S1P receptor modulation by FTY720 (FTY) does not prevent aneurysm formation or rupture in Ang II-infused ApoE$^{-/-}$ mice. ApoE$^{-/-}$ mice were infused with Ang II or received additionally the S1PR modulator FTY720 (FTY, 10 µg/mL via drinking water) over a period of 28 days. (A) Kaplan-Meier survival curve. $n_{Ang\ II} = 25$; $n_{Ang\ II + FTY} = 21$ (B) Distribution of aortic rupture sites (thoracic or abdominal). (C) Incidence of abdominal aortic aneurysm (AAA) or aortic dissection (AD) based on macroscopic assessment. (D) Aneurysm severity grading according to Daugherty's classification. None = no aneurysm; I = dilated lumen without thrombus; II = remodelled wall with thrombus; III = pronounced bulbous with thrombus; IV = dissecting or ruptured aneurysm. (E) Representative images of aneurysmal and dissecting *aortae*. (F) Systolic blood pressure in ApoE$^{-/-}$ mice treated with FTY before and 10-14 days after Ang II infusion (n = 7 per group). (G) Relative gene expression of contractile marker Acta2 and Tagln in aortic tissue of ApoE$^{-/-}$ treated with or without FTY and received additional Ang II infusion (n = 4-6 per group). Data are presented as mean ± SEM. Statistical significance was tested by Fisher's exact test (B-D) and two-way ANOVA with repeated measures or multiple comparisons (F-G).

Different studies have showed that FTY720 induces vasodilation in different vascular beds[295]. Therefore, vasoreactivity studies were performed with aortic segments from ApoE$^{-/-}$ mice receiving FTY720 for 28 days and with or without additional Ang II infusion.

Phe-induced vasoconstriction was similarly increased in *aortae* from Ang II- and Ang II + FTY720-treated ApoE$^{-/-}$ mice (Figure 36 A&B). Similarly, FTY720 alone had no effect on basal Phe-induced vasoconstriction compared to ApoE$^{-/-}$ controls (Figure 36 B).

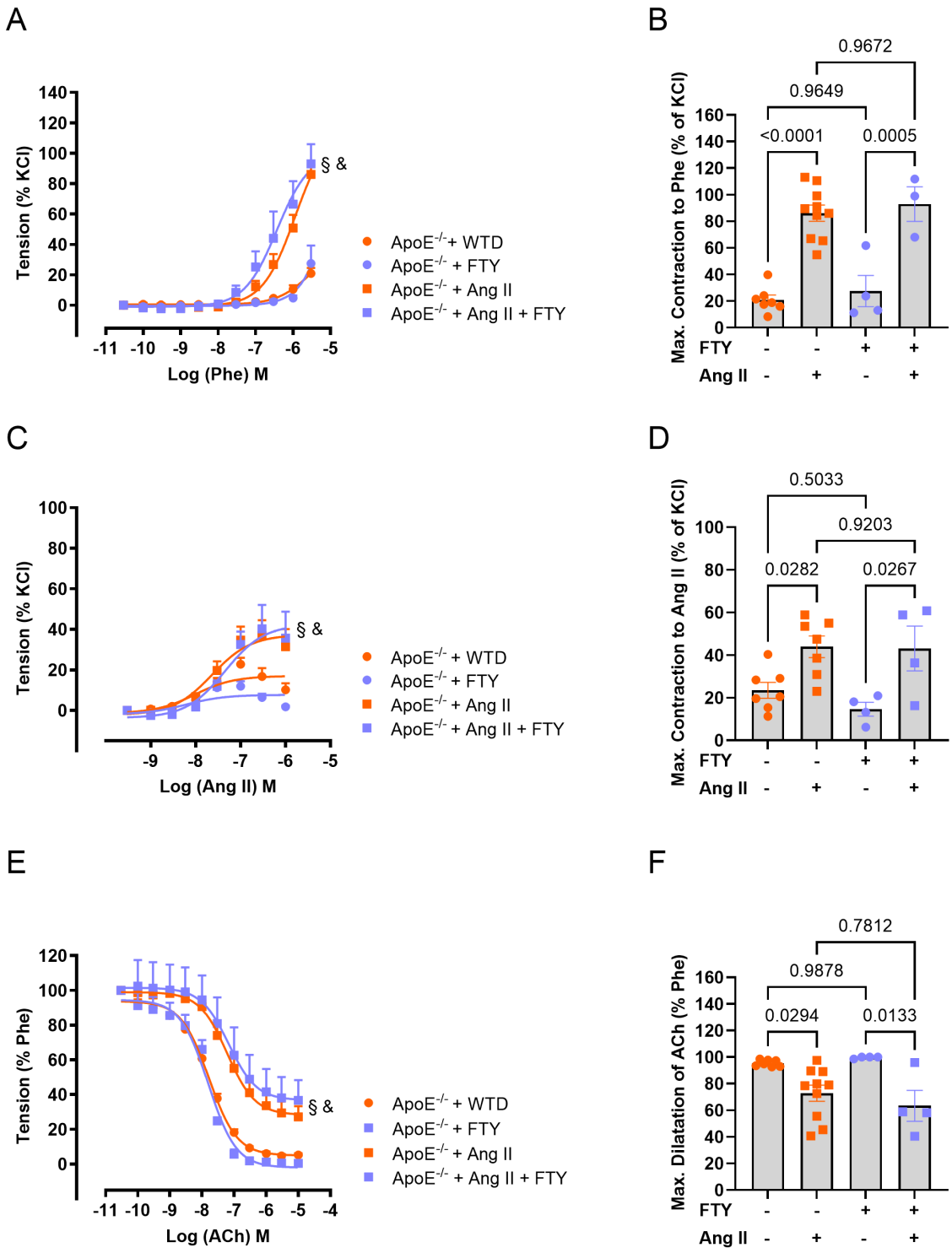

Figure 36: Vascular reactivity remains unaltered by S1PR modulation by FTY720 in Ang II-treated mice. ApoE$^{-/-}$ were treated with or without FTY720 (FTY; 10 µg/mL in drinking water) and additionally infused with Ang II (1,000 ng/kg/min) under a western type diet (WTD). Abdominal aortic rings were mounted in a wire myograph to assess vascular function. (A) Contractile response to phenylephrine (Phe) normalized to maximal vasoconstriction to KCl. § WTD vs Ang II: $P < 0.0001$; & FTY vs FTY + Ang II: $P < 0.0001$ (B) Maximal vasoconstriction to Phe. (C) Contractile response to Ang II normalized to maximal vasoconstriction to KCl. (D) Maximal vasoconstriction in response to Ang II. § WTD vs Ang II: $P = 0.0037$; & FTY vs FTY + Ang II: $P = 0.0013$ (E) Acetylcholine (ACh) - induced vasodilation after pre-constriction with Phe. (F) Maximal vasodilatation in response to ACh. § WTD vs Ang II: $P = 0.0252$; & FTY vs FTY + Ang II: $P = 0.0069$ Data are represented as mean ± SEM (n=3-10 per group). Statistical analysis was performed using two-way ANOVA (A-F).

Consistent with these findings, the increased vasoconstriction observed in *aortae* from Ang II and Ang II+FTY720-treated ApoE$^{-/-}$ mice was not altered using Ang II as vasoconstrictor (Figure 36 C&D). No differences were found between animals with WTD and additional FTY720 treatment without Ang II infusion (Figure 36 D).
The Ang II+FTY720 group showed a similar extent in reduced vasorelaxation as the Ang II-infused ApoE$^{-/-}$ cohort (Figure 36 E&F). Similarly, FTY720 alone did not alter baseline vasorelaxation (Figure 36 F).

Taken together, Ang II-infused animals treated with the S1PR modulator, FTY720, showed no benefit in survival, aneurysm incidence, phenotypic switch or hypercontractility compared to mice which received on Ang II infusion.

4.13. S1P alterations in the sphingolipidome of AAA patients highlight its role in pathogenesis of aortic disease

To gain insights into the potential role of sphingolipids and particularly S1P in the pathogenesis of abdominal aortic aneurysms (AAA), plasma and aortic tissue samples of patients suffering from AAA were analysed by targeted sphingolipidomic profiling using LC/MS-MS. The clinical characteristics of patients from whom plasma (Table S 4) and aortic tissue (Table S 5) were obtained are provided in the supplemental part. The analysis included around 50 lipid species, such as ceramides, sphingomyelins, lysophospholipids and phospholipids. Plasma and aortic tissue samples were obtained from patients undergoing surgical repair for AAA. Non-aneurysmal organ and plasma donors served as control samples. To minimize with confounding factors, individuals with known hereditary aortic syndromes were excluded from the study.

In plasma, targeted sphingolipididomic analysis revealed specific differences across the lipid species, with prominent changes in sphingolipids. Notably, S1P was remarkably elevated in AAA plasma compared to control samples (Figure 37 A). Precursors of S1P, sphinganine (Spha) and Sph, were reduced in plasma of patients with AAA. A similar pattern was observed for different sphingomyelin (SM) species, which were also reduced in AAA plasma samples compared to the respective controls. Additional changes were observed in lysophosphatidylethanolamines (LPE), where an increase in plasma of AAA patients was detected (Figure 37 A). This highlights that a broad spectrum of lipids is altered in plasma of AAA patients. Furthermore, sphingolipipidomic analysis revealed a distinct separation between AAA patients (red)

and controls (blue) in principal component analysis (PCA) with the first two components accounting for 32.57% (PC1) and 13.37% (PC2) of the total variance (Figure 37 B).

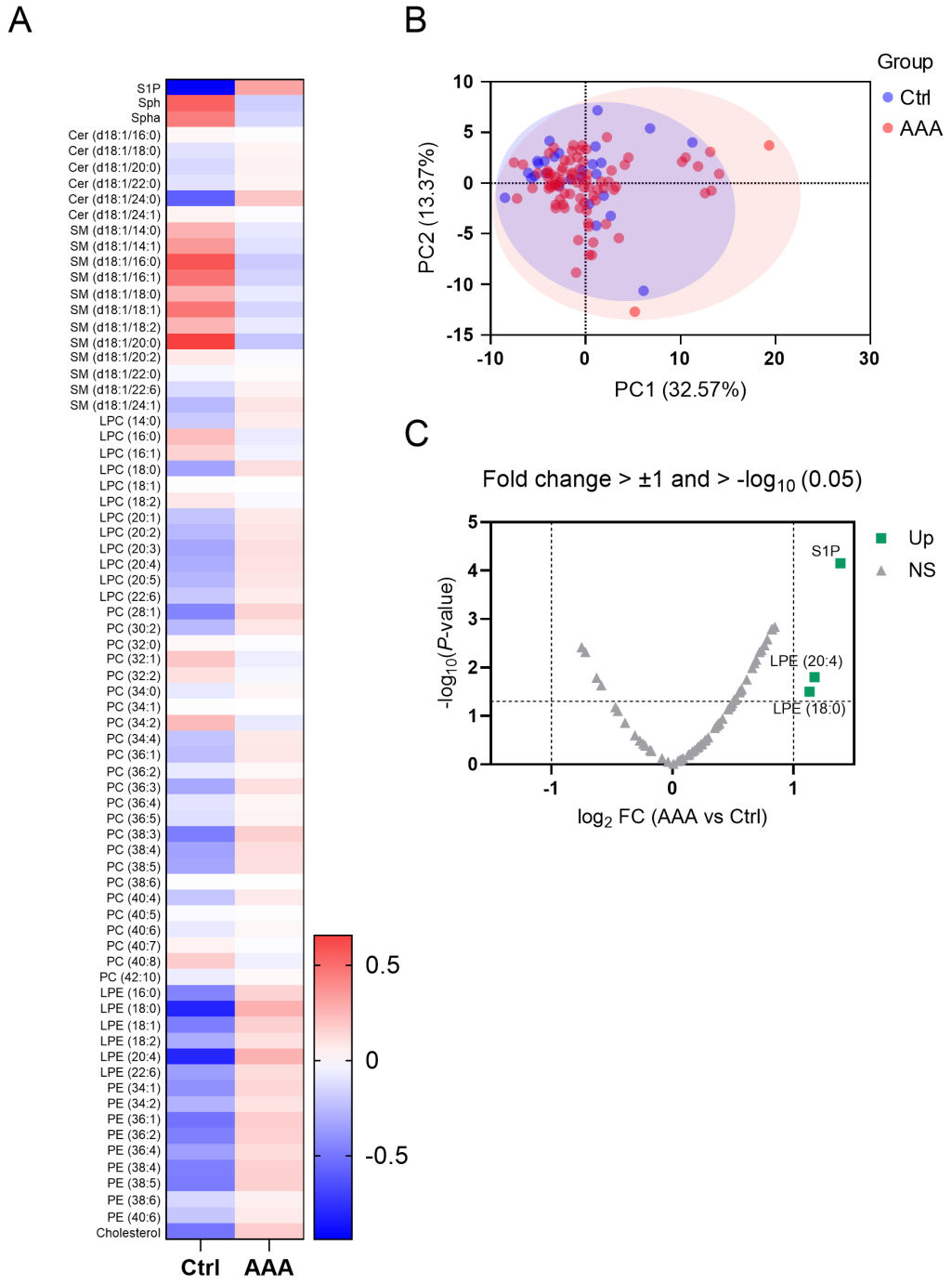

Figure 37: Distinct plasma sphingolipidomic profile in patients with abdominal aortic aneurysms. Plasma lipid composition was assessed in patients with AAA (n = 82) and non-aneurysmal controls (Ctrl, n = 27) using LC/MS-MS. (A) Heat map showing z-score normalized intensities of selected sphingolipids, lysophosphatidylcholines (LPC), phosphatidylcholines (PC) and lysophosphatidylethanolamine (LPE) or phosphatidylethanonolamines (PE), and cholesterol. Each column represents the average of all patients per group. (B) Principal component analysis (PCA) of all quantified lipid species between AAA and Ctrl samples. (C) Volcano plot comparing lipid species between AAA and Ctrl. Log_2 fold changes (AAA vs. Ctrl) are plotted against log_{10} (P values). Lipids with a fold change > |1| and $p < 0.05$ are considered significantly altered (green).

This revealed a partial separation between AAA patients and controls, indicating distinct alterations in specific lipid species, although a considerable overlap between the groups remained (Figure 37 B). Volcano plot analysis was used to further assess alterations in the plasma sphingolipidome of AAA patients, using a log_2 fold-change cutoff of >1 in combination with a statistical significance ($P < 0.05$). Interestingly, S1P was identified as the most significantly upregulated sphingolipid, followed by LPE species LPE (20:4) and LPE (18:0) (Figure 37 C). A comprehensive quantitative comparison of all plasma lipid species between control and AAA patients is provided in the supplementary part (Table S 6).

To investigate whether sphingolipid alterations are also present in the aneurysmal tissue, the same sphingolipidomic analysis was performed. Profiling revealed marked differences in lipid species between aortic tissue of AAA patients and controls. A heat map shows a consistent upregulation of diverse sphingolipid species, including S1P, Sph and ceramides (Figure 38 A).

In line with this, PCA analysis revealed a clear group separation between AAA and control samples with PC1 and PC2 explaining 34.0% and 26.4% of the variance (Figure 38 B). While AAA samples displayed a broader distribution, suggesting higher variability, they nevertheless clustered distinctly from controls, underscoring a common underlying lipidomic signature in aneurysmal tissue (Figure 38 B). Furthermore, volcano plot analysis was used to assess differential lipid expression between both groups. Multiple lipid species were significantly elevated in AAA samples, surpassing both fold-change (>1) and statistical thresholds ($P = 0.05$). Notably, S1P was among the most strongly upregulated sphingolipids, followed by LPC (20:0) and Cer(d18:1/24:1) (Figure 38 C). A comprehensive quantitative comparison of all plasma lipid species between control and AAA patients is provided in the supplementary part (Table S 7).

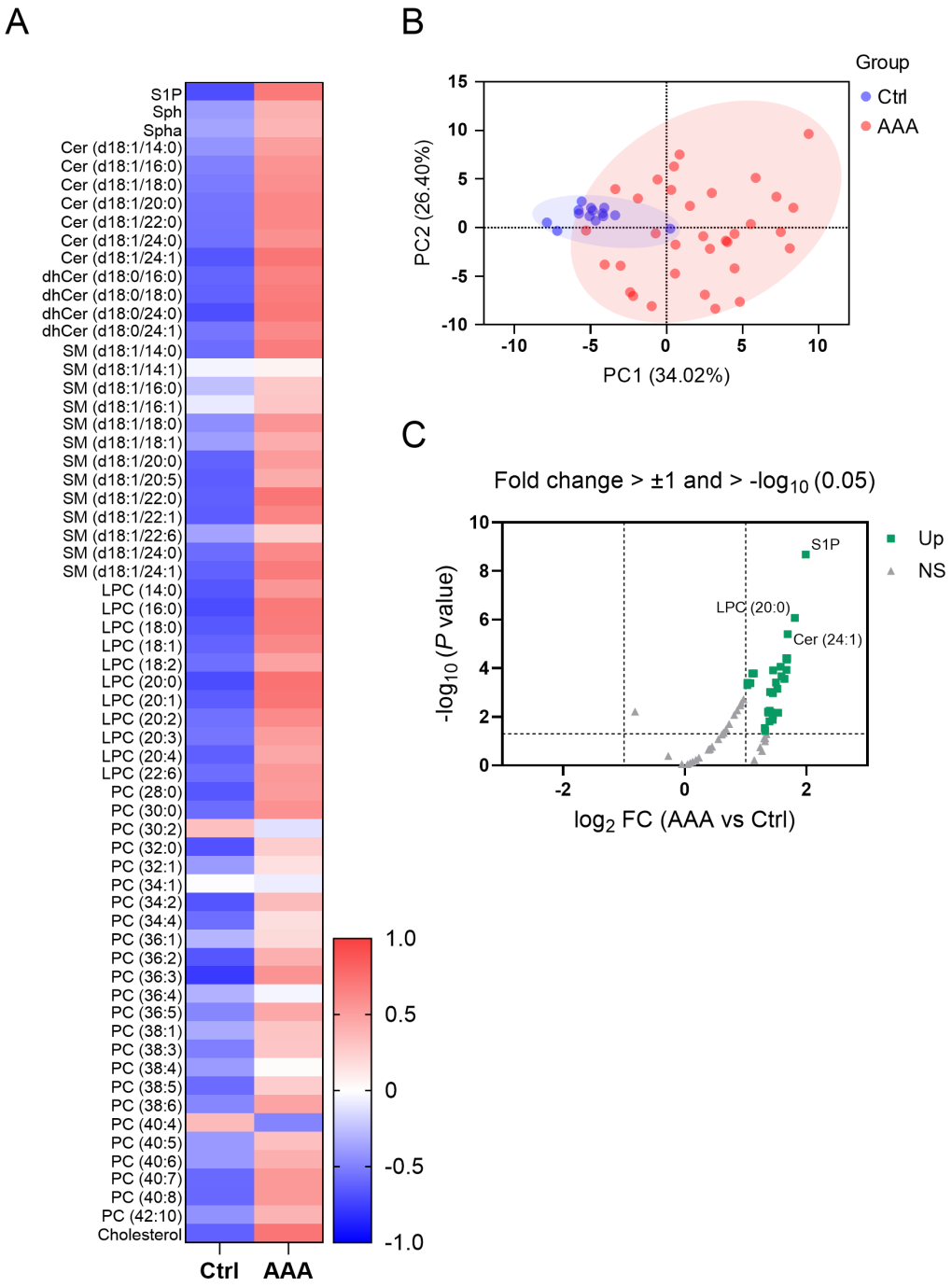

Figure 38: Distinct sphingolipidomic profile in aortic tissue of patients with abdominal aortic aneurysms. Lipid composition was assessed in aortic tissue of patients with AAA (n = 33) and non-aneurysmal controls (Ctrl, n = 14) using LC/MS-MS. (A) Heat map showing z-score normalized intensities of selected sphingolipids, lysophosphatidylcholines (LPC), phosphatidylcholines (PC) and lysophosphatidylethanolamines (LPE) or phosphatidylethanonolamines (PE), and cholesterol. Each column represents the average of all patients per group. (B) Principal component analysis (PCA) of all quantified lipid species between AAA and Ctrl samples. (C) Volcano plot comparing lipid species between AAA and Ctrl. Log_2 fold changes (AAA vs. Ctrl) are plotted against log_{10} (P values). Lipids with a fold change > |1| and $p < 0.05$ are considered significantly altered (green).

Since S1P was identified as the most differentially expressed lipid species in both plasma and aortic tissue of AAA patients compared to controls, it was selected as a molecule of interest for subsequent quantitative analysis. S1P levels were found to be significantly elevated in both biological compartments (Figure 39 A & B). Specifically,

S1P concentrations were increased by 2.14-fold in plasma and by 1.67-fold in aortic tissue of AAA patients relative to non-aneurysmal controls (Figure 39 A & B). To assess the diagnostic potential of S1P, receiver operating characteristic (ROC) curve analysis was performed (Figure 39 C). The resulting AUC of 0.89 (95% CI: 0.84-0.95; P < 0.0001) highlights the high sensitivity and specificity of S1P as a discriminative marker between AAA and control samples (Figure 39 C).

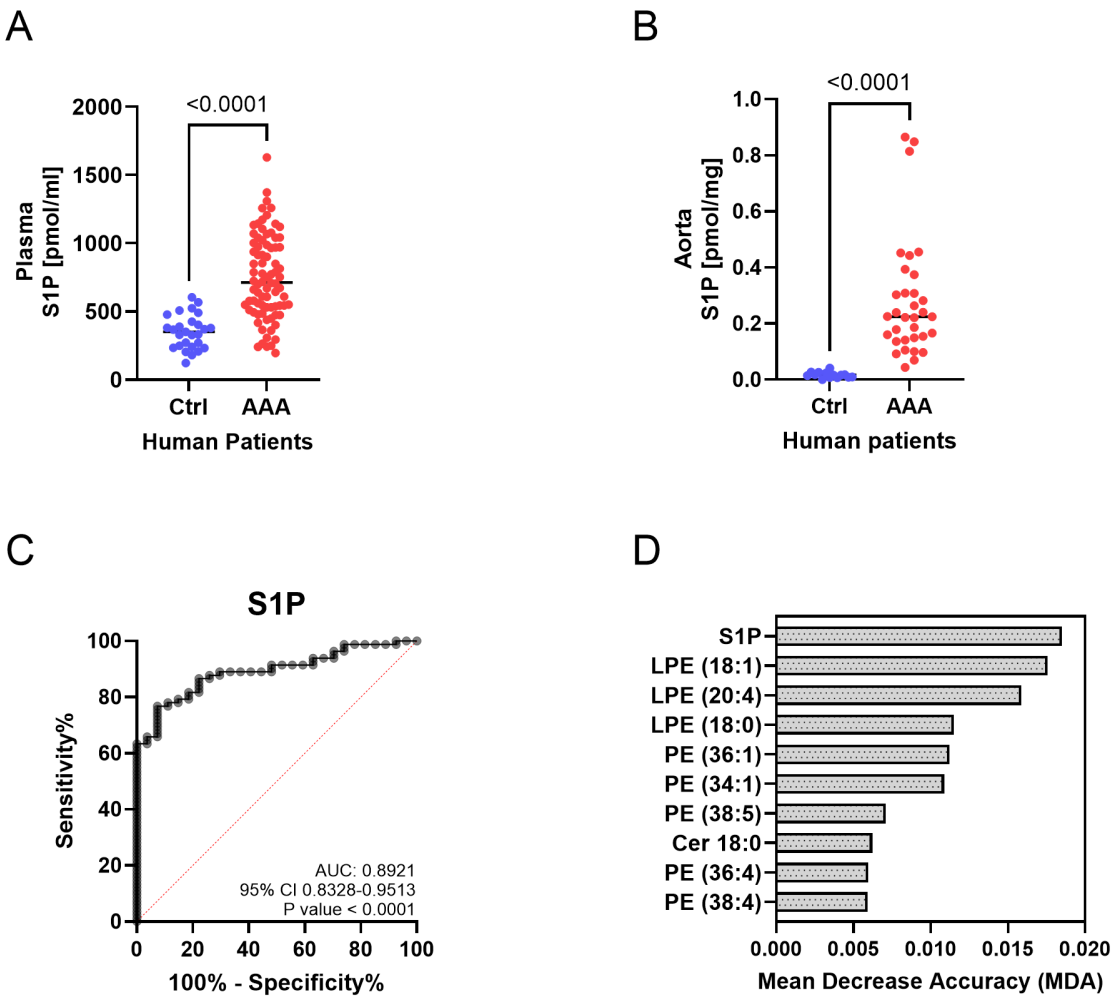

Figure 39: Increased S1P levels in AAA patients identify S1P as a molecular target in human AAA pathophysiology. S1P levels were measured by LC/MS-MS in plasma (A) and aortic tissue (B) of AAA patients compared to Ctrl. (Plasma: n_{Ctrl} =27; n_{AAA} = 82; Aorta: n_{Ctrl} = 14; n_{AAA} = 33 (C) Receiver operating characteristic (ROC) curve of plasma S1P levels for the discrimination between AAA and control subjects. Area under the curve (AUC) = 0.8921; 95% CI: 0.8328–0.9513; P < 0.0001. (D) Variable importance plot based on mean decrease in accuracy (MDA) illustrating the top lipid species relevant for differentiating AAA from control samples.

In detail, ROC curve analysis identified an optimal plasma S1P cut-off of 527.6 pmol/mL, which discriminated patients with AAA from controls with a sensitivity of 76.8% and a specificity of 92.6% (Youden Index = 0.694). Thus, plasma S1P levels above this threshold are strongly indicative of AAA presence. In addition, Random Forest classification analysis of the entire lipidomic dataset identified S1P as the most

interesting feature for distinguishing AAA patients from controls, as reflected by its highest mean decrease in accuracy (MDA) score.

Additional lipids contributing to group separation included several LPEs and phosphatidylethanolamines (PEs) (Figure 39 D). This classification model was further validated by out-of-bag (OOB) error estimation (Figure S 5). The overall classification error was 16.7%, with a low misclassification rate for AAA patients (6.1%; 77 out of 82 correctly classified). In contrast, the higher error rate for controls (50%) likely reflected greater heterogeneity within the non-aneurysmal group (Figure S 5).

To further elucidate the involvement of S1P signaling in AAA pathogenesis, the expression of the major vascular S1P receptors (S1PR1–S1PR3) and the contractile marker ACTA2 was analysed in aortic tissue samples from AAA patients and non-aneurysmal controls. ACTA2 was included in this analysis as a marker of the contractile phenotype, which is downregulated during the phenotypic switch of vascular smooth muscle cells commonly observed in AAA (Figure 40 A)[351].

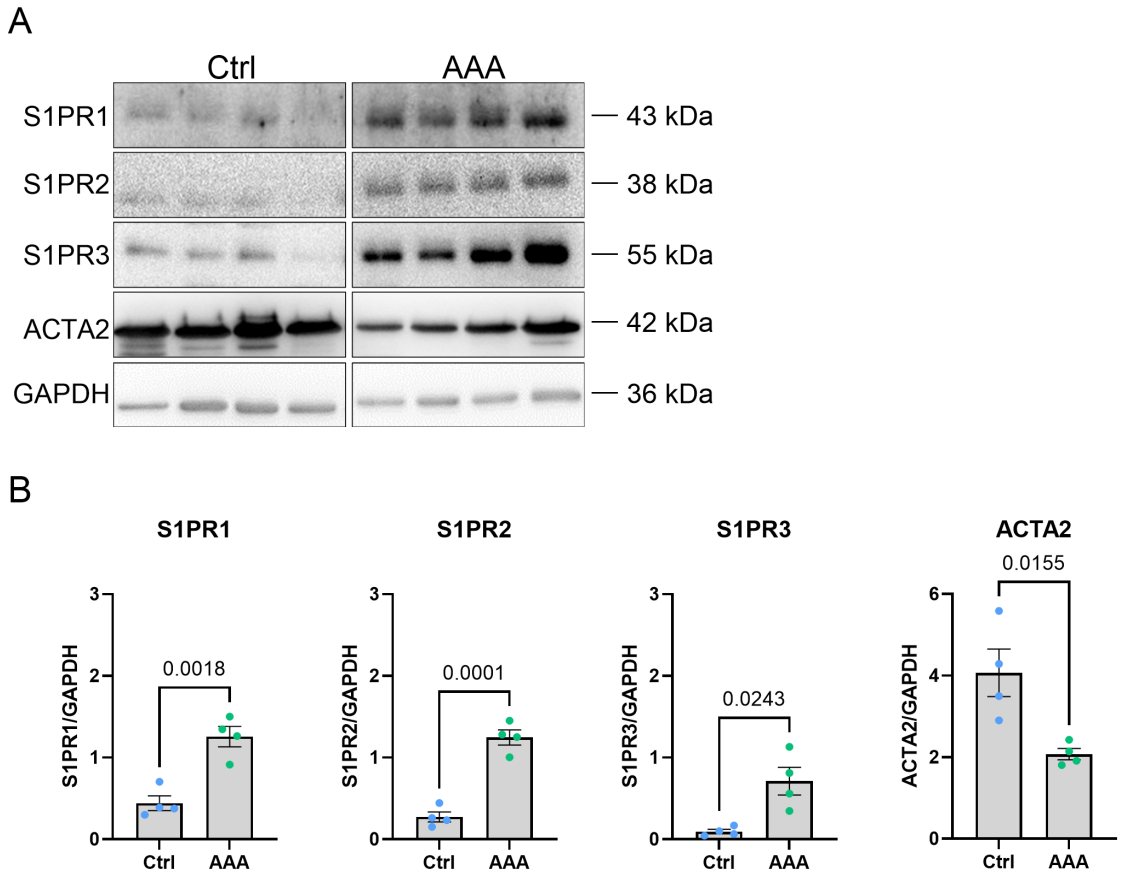

Figure 40: Differential expression of S1P receptors in aortic tissue of AAA patients. (A) Representative Western blot analysis of S1P receptors (S1PR1-S1PR3) and the contractile marker ACTA2 in aortic tissue from patients suffering from AAA and control patients (Ctrl). GAPDH was used as loading control. (B) Quantification of protein expression normalized to GAPDH. Data are presented as mean ± SEM (n = 4 per group). Statistical analysis was performed using t-test.

As shown in the representative Western blot, AAA tissue exhibited markedly increased expression levels of all three S1PRs (Figure 40 A). Quantification confirmed that protein levels of S1PR1, S1PR2, and S1PR3 were significantly elevated in AAA samples by 2.85-fold, 4.56-fold, and 7.63-fold, respectively, compared to controls (Figure 40 B). Notably, this upregulation of S1P receptors was accompanied by a significant reduction in ACTA2 expression (1.96-fold decrease), indicating a loss of the contractile phenotype.

In summary, sphingolipidomic analysis revealed unique alterations of different lipid species in the plasma and in the aortic tissue of patients with AAA. Among all detected sphingolipid species, S1P showed the most pronounced and statistically significant increase in both plasma and tissue samples. Furthermore, S1P in the plasma showed the highest discriminatory and predictive value among all analysed sphingolipids, consistently distinguishing between AAA patients and controls. Additionally, elevated expression of S1PRs, highlighting the S1P/S1PR signaling axis as the most prominently altered sphingolipid pathway and a potential target for therapeutic intervention.

5. Discussion

S1P is a bioactive sphingolipid primarily generated by erythrocytes, endothelial cells and platelets[188,198,199]. Its metabolic and cardiovascular functions are tightly regulated through signaling via distinct S1PRs (S1PR1-5)[352,353]. Alterations in S1P levels and its role in the pathophysiology of diverse cardiovascular diseases have been identified, highlighting the critical role of S1P/S1PR signaling in preserving vascular health[354-356]. Nevertheless, the impact of S1P signaling on abdominal aortic aneurysm progression remains unclear. The pathophysiology of aortic aneurysms is highly complex and involves inflammation, ECM degradation, endothelial dysfunction and changes in VSMCs[5,44]. S1P/S1PR signaling has been implicated in each of these processes, highlighting its potential relevance in aortic aneurysm development and progression.

Therefore, S1P has been examined in these study in greater detail regarding aneurysm development and progression. To investigate this experimentally, the Ang II infusion model was used, a well-described model that induces abdominal aortic aneurysms and dissections[327,357]. This experimental model was complemented by pharmacological modulation of S1P metabolism and receptor signaling, as well as by studies in the respective S1PR knockout mice.

To provide a framework for the following discussion, the key findings of this dissertation are outlined below before being interpreted in the context of aneurysm pathophysiology.

This study provides the first evidence that increased S1P levels, achieved by pharmacological inhibition of the S1P lyase, promote aortic aneurysm formation and rupture in a murine model. In addition, S1P levels were found to be consistently elevated under Ang II infusion, further linking S1P metabolism to aneurysm development.

Furthermore, this study also demonstrated, that S1P activated two distinct pathways, which regulated contractile VSMC phenotype. Acute activation of S1PR2 induced expression of contractile genes, whereas tonic signaling via S1PR1 and S1PR3 suppressed their expression.

It was also observed that aneurysm development is associated with vascular hypercontractility and endothelial dysfunction. These two processes are both exacerbated by elevated S1P levels.

By linking the phenotypic changes observed in VSMCs with alterations in aortic vascular reactivity, this study demonstrated for the first time that tonic S1P/S1PR3 signaling represented a key regulatory mechanism under elevated S1P levels. Mechanistically, tonic activation of S1P/S1PR3 axis compromised aortic wall stability by driving a phenotypic switch in VSMCs and promoting a hypercontractile state, thereby accelerating aneurysm progression and rupture. Strikingly, loss of S1PR3 preserved the contractile phenotype, attenuated vasoconstriction and prevented aortic rupture in mice (Figure 41).

Additionally, within this study, the S1PR modulator FTY720 was evaluated as a potential pharmacological strategy to prevent or treat aortic aneurysm formation, due to its reported association with reduced atherosclerotic lesion development in murine models and its broad-spectrum inhibition of several S1PRs[358]. Here, it was observed that application of FTY720 under Ang II infusion did not result in any attenuation of aortic aneurysm formation and rupture.

Finally, in a translational approach, sphingolipid profiles were analysed in plasma and aortic tissue from patients with abdominal aortic aneurysms and compared to those without the disease. Remarkably, S1P levels were elevated in both plasma and aortic tissue of aneurysm patients. Comprehensive sphingolipidomic analysis revealed distinct alterations in lipid composition, indicating broader dysregulation of sphingolipid metabolism. Notably, plasma S1P emerged as a particularly promising marker distinguishing patients with abdominal aortic aneurysms from controls, underscoring its potential as a molecular target for future therapeutic strategies.

Together, these findings address the central aim of this dissertation, namely to elucidate the role of S1P/S1PR signalling in the pathophysiology of aortic aneurysm formation. The data demonstrate that increased S1P not only promotes aneurysm development and rupture *in vivo*, but also modulates key cellular and vascular mechanisms and its plasma concentrations discriminate patients with AAA from controls. Thus, the study establishes S1P as a critical player in aneurysm disease and highlights its potential as a therapeutic target for potential pharmacological treatment of aortic aneurysms.

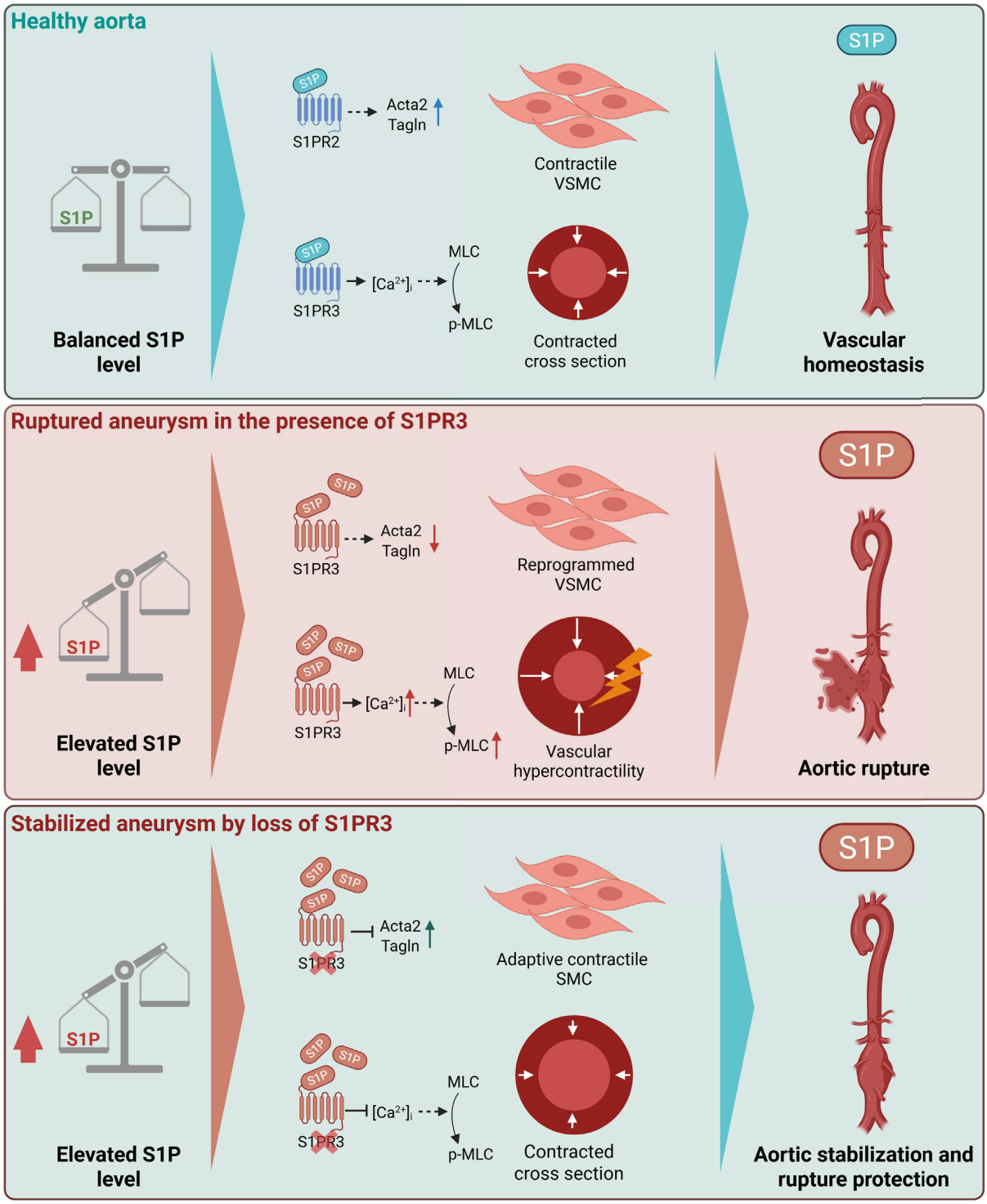

Figure 41: Schematic overview of the role of S1P/S1PR3 signaling under aortic aneurysm progression. Under basal vascular conditions activation, balanced S1P levels and S1PR signaling maintain vascular homeostasis. Activation of S1PR2 promotes an upregulation of contractile markers (Acta2, Tagln). S1P/S1PR3 signaling contributes to vascular contraction by release of intracellular calcium, which ends up in phosphorylation of myosin light chain (MLC). Under pathophysiological conditions, elevated tonic S1P levels activate S1PR3 which drives phenotypic switch including downregulation of contractile markers and hypercontractility through increasing intracellular calcium levels $[Ca^{2+}]_i$. This tonic S1P/S1PR3 signaling promotes aneurysm formation and rupture. S1PR3 deficiency leads to aortic stabilization and protects from rupture caused by a reduced vascular contractility and adaptive contractile VSMC phenotype. Created with BioRender.com. Published under BioRender Publication License.

5.1. S1P/S1PR signaling plays a causal role in aneurysm pathophysiology by modulating VSMC phenotype and vascular contractility

5.1.1. S1P as a pathophysiological target in aortic aneurysm formation

In the current study, S1P was identified for the first time as a causal player in aortic aneurysm progression. The most striking observation was that mice with pharmacologically elevated systemic S1P levels were associated with a substantially aggravated aneurysm phenotype and increased rupture-associated mortality. These findings further support the link between S1P signaling and vascular remodelling processes, and extend it to aortic aneurysm disease in addition to already demonstrated links to hypertension and atherosclerosis in mice and humans[288,292,303,354,359,360].

Elevated S1P levels observed in this study are in line with previous reports in hypertensive patients and Ang II-infused mice [288,359,361]. Among other findings, studies in Ang II-infused mice have demonstrated that genetic deficiency of SphK1, a key enzyme responsible for S1P synthesis, attenuates the Ang II-induced increase in blood pressure[361]. In general, SphK1 knockout mice did not display reduced blood pressure under basal conditions[361]. These findings suggest that the impact of S1P produced by SphK1 on systemic blood pressure regulation is predominantly evident under hypertensive conditions, such as chronic Ang II infusion, driving vascular remodelling. In the present study, the increase in blood pressure known to occur under Ang II infusion was confirmed [292]. Notably, pharmacological inhibition of the S1P lyase, which further elevated systemic S1P levels, did not result in an additional rise in blood pressure. The rupture-related mortality in the Ang II model may therefore be partially attributed to the blood pressure-raising effects of S1P. To fully exclude this confounding factor, the Ang II infusion model should be performed in SphK1-deficient mice. This approach would allow distinguishing whether the contribution of S1P to aneurysm formation is independent of its hypertensive effects. However, as additional elevation of S1P levels through DOP treatment further aggravated the Ang II-induced phenotype, S1P is likely to exert effects beyond those related to blood pressure regulation. Alternatively, S1P production following Ang II infusion alone may not be sufficient to elicit the full biological response of S1P signaling, or, finally, other metabolites accumulating upon S1P lyase inhibition may additionally contribute to the

observed aggravation. In line with this, Cassis *et al*. demonstrated, that aneurysm formation under Ang II infusion occurs independently of hypertension[362], further supporting the notion that additional S1P-medaited mechanisms may contribute to aneurysm pathogenesis.

Next to the association of S1P with hypertension, it has also been extensively studied in the context of atherosclerosis which could be a risk factor for aortic aneurysm development[303,358,360,363]. Here, its role is highly dependent on the involved vascular and immune cell types, the downstream signaling pathways activated by distinct S1PRs, and its concentration[360].

For instance, HDL-associated S1P exerts vasoprotective functions by promoting vasorelaxation through S1PR1- and S1PR3-mediated eNOS activation and by maintaining endothelial barrier intgrity[279,364]. These vasoprotective effects contribute to the anti-atherogenic properties of S1P, though it also exhibits pro-atherogenic properties. In this context, S1P promotes the infiltration of inflammatory cells, such as monocytes, macrophages or lymphocytes [297,365]. Notably, bone marrow transplantation experiments in a murine model for atherosclerosis have demonstrated that these pro-atherogenic effects are not exclusively mediated by immune cells[297]. In these studies, replacement of the bone marrow of ApoE$^{-/-}$ mice with S1PR3-deficient mice bone marrow and vice versa revealed that both hematopoietic and non-hematopoietic cells contribute to macrophage accumulation within atherosclerotic lesions[297]. These findings indicate that S1PR signaling within the vascular wall, in addition to its role in immune cells, plays an essential part in promoting vascular inflammation and remodelling. In the present study contribution of leukocytes to the DOP-mediated aggravation remained uncertain, as leukocytes are known to play important roles in aneurysm formation and DOP treatment induces peripheral lymphopenia[5,366,367]. Therefore, further studies should be conducted to examine the S1P-driven effects on inflammatory cells within this model in more detail. However, since FTY720 treatment also induces peripheral lymphopenia[368], but did not led to differences in aneurysm severity or increased mortality, lymphopenia can likely be excluded as a driving factor for the progressive aneurysm development and the elevated rupture-associated mortality observed under DOP treatment. Moreover, as S1PR3-deficient mice were protected from Ang II-induced aneurysm formation without exhibiting lymphopenia or other haematological abnormalities, these findings further support the notion that

VSMC-mediated mechanisms, rather than immune cell-dependent effects, predominantly account for the observed phenotype.

A hallmark of aortic aneurysm development is structural remodelling of the vascular wall. An increase in MMP activity leads to the fragmentation of collagen and elastic fibres, which promotes ECM degradation[50,51,53]. Infiltration of immune cells further amplifies these processes[369,370]. Multiple studies have linked S1P signaling to several of these mechanisms. Regarding MMP regulation, some studies show conflicting results. In certain cancer cells, S1P has been shown to activate MMP-2 and MMP-9, thereby facilitating tumour invasion[235,371]. In contrast, in VSMCs it was observed that S1P inhibits TNF-α-induced MMP-9 activation, suggesting a possible protective effect against ECM degradtion[372]. In the present study, MMP expression was found to be increased in Ang II-treated *aortae*, confirming enhanced matrix remodelling in this model and consistent with previous studies[373,374]. However, pharmacological S1P lyase inhibition did not further affect MMP expression levels.

In the present study, sustained tonic S1P levels during aneurysm formation were associated with an increased number of elastin breaks within the aortic wall, a structural hallmark of aortic aneurysms[375]. In addition, elastin gene expression was significantly downregulated under tonic S1P conditions. Conversely, collagen gene expression remained unaltered at this stage. These findings suggest that tonic S1P levels influence ECM regulation. In addition to the transcriptomic changes observed in Ang II-infused mice with elevated tonic S1P, animals with tonic S1P alone, independent of Ang II infusion, also exhibited reduced elastin expression. Further studies will be required to determine whether these effects are mediated by increased MMP activity caused by S1P.

Moreover, this study showed for the first time a link between tonic S1P levels and various gene families that have been associated with hereditary aortic aneurysms[129]. Next to genes encoding for the contractile machinery, such as MYH11 or ACTA2, and components of the ECM, members of the TGF-β signaling pathway are known to be differentially expressed in patients suffering from hereditary aneurysms[129]. In the context of TGF-β signaling, numerous studies have shown contrasting findings in aortic aneurysms. For instance, patients with Marfan syndrome or other familial aortic syndromes were associated with an increase in TGF-β signaling[376,377]. Conversely, using TGF-β-neutralising antibodies ended up in the formation of fatal aortic dissections, indicating a protective role of TGF-β[135]. In the same study it was further

demonstrated that TGF-β blockade increased MMP-12 activity and macrophage infiltration, leading to enhanced ECM degradation and a higher risk of rupture[135]. In contrast, loss of TGFBR2 promoted aortic dissection, impaired the contractile apparatus of VSMCs, induced endothelial dysfunction and aortic hypercontractility[139,378]. With respect to this, S1P signaling was also capable altering TGF-β signaling. S1P has been reported to co-activate the TGF-β signaling pathway via SMAD phosphorylation[379]. Furthermore, S1P has been implicated in potentiating TGF-β-driven fibrotic responses[380,381]. In addition, the current study demonstrated also a link between tonic S1P levels and alterations in TGF-β signaling. In the Ang II+DOP model, RNA sequencing revealed a marked downregulation of the TGF-β signaling pathway compared to Ang II-infused mice. Detailed gene expression analysis revealed a significant suppression of TGFB2 and TGFBR2 expression. This finding was particularly noteworthy, as mice under Ang II infusion with pharmacological inhibition of S1P lyase, and the resulting elevation in tonic S1P levels, developed a vascular phenotype closely resembling that observed in TGFBR2-deficient mice[146,382]. Specifically, these animals showed a higher incidence of dissections, marked changes in the contractile apparatus, and altered vascular reactivity, including endothelial dysfunction and hypercontractility[146].

Overall, the present findings highlighted the multifaceted role of S1P signaling in the pathogenesis of aortic aneurysms. This role affected extracellular matrix homeostasis, vascular signaling pathways, and the structural integrity of the aortic wall. The broad spectrum of molecular mechanisms influenced by S1P highlights its central position in vascular remodelling and emphasised the need for further research to unravel its detailed contribution to aneurysm-associated processes. This study has concentrated on the multiple pronounced alterations of VSMC phenotype and function by S1P and S1P lyase inhibition that may be responsible for their effects on aortic aneurysm pathophysiology. This is discussed in detail in the next chapters.

5.1.2. Differential roles of S1P/S1PR signaling in VSMC contractile gene regulation during aneurysm development

A characteristic feature of aortic aneurysms is the phenotypic switch of VSMCs[92,93,95]. The phenotypic switch is defined by decreased expression of contractile genes, including ACTA2, MYH11, and TAGLN, which drives the transition of VSMCs from a contractile toward a synthetic and proliferative state[93,95]. In the present study, it was

demonstrated for the first time that tonic S1P levels, induced by pharmacological inhibition of the S1P lyase, during aneurysm development were associated with an enhanced phenotypic switch of VSMCs during aortic aneurysm progression. These findings are in line with the transcriptomic and proteomic analyses of the present study, which predominantly revealed a downregulation of processes linked to VSMCs, including contractility, focal adhesion, cytoskeletal organisation, and maintenance of the vascular integrity. This is of particular interest, as previous studies have implicated an important role of S1P in the regulation of key VSMC functions, including migration, proliferation, and phenotypic differentiation[383,384]. Regarding the regulation of contractile genes, Lockman *et al*. demonstrated that stimulation of VSMCs with S1P increased the expression of Acta2[383]. The findings of the current study, were in line with those of Lockman *et al.*, since an upregulation of contractile markers such as ACTA2 and TAGLN at both the mRNA level and protein level were observed after S1P treatment in VSMCs *in vitro*. However, in the current study it was further demonstrated that the effect of S1P on the regulation of contractile gene expression was dependent on both activated receptor subtype and the type of exposure. *In vitro*, acute stimulation of VSMCs with S1P led to an upregulation of contractile markers via S1PR2 activation, whereas after 24 hours, expression levels returned to baseline. In contrast, selective activation of S1PR1 and S1PR3 over 24 hours resulted in a pronounced downregulation of contractile genes. Together, these results provide the first evidence that VSMCs engage in two distinct modes of S1P signaling, in which an acute, receptor-driven active pathway and a sustained tonic pathway differentially influence contractile gene expression and phenotypic state. These findings suggest that the *in vivo* effect observed in Ang II-infused mice with DOP may be mediated predominantly through S1PR1 and S1PR3 activation. Consistent with this, *in vitro* experiments mimicking tonic S1P exposure in VSMCs reproduced the marked downregulation of contractile markers observed *in vivo*, thereby supporting the concept that tonic S1P signaling affected phenotypic modulation of VSMCs. These observations were consistent with previous findings by Wamhoff *et al*., who demonstrated also opposing effects of S1PR activation on VSMC phenotype[345]. In a rat carotid artery injury model, blockade of S1PR1 and S1PR3 inhibited S1P-induced proliferation, whereas S1PR2 inhibition reduced contractile gene expression[345]. In addition further studies have also demonstrated that the contractile phenotype of VSMCs was mediated through S1PR2 signaling, thereby confirming the *in vitro* findings of the current study[385,386].

Consistent with the S1PR-specific effects *in vitro*, the functional impact of S1P signaling on VSMC phenotype *in vivo* may be influenced by the distribution and abundance of S1PRs within the aorta, as different receptor subtypes exerted distinct and partly opposing effects. In the present study, the expression of S1PRs was systematically analysed across distinct aortic segments, both under basal conditions and following Ang II infusion. This approach was implemented because VSMCs arise from different embryological origins, depending on the distinct parts of the aorta[387]. VSMCs of the aortic arch are predominantly derived from neural crest-originating cell populations, whereas VSMCs of the thoracic aorta primarily originate from the somites[387]. In comparison, VSMCs of the abdominal aorta are mainly derived from the mesoderm[387]. Under basal conditions, S1PR expression displayed a distinct distribution pattern depending on the aortic region. However, it must be noted that, in addition to VSMCs, endothelial cells also express S1PRs in the aorta. Upon Ang II infusion, further region-specific changes in S1PR expression were observed. In all three segments an upregulation of all S1PRs was observed. The only exception was S1PR3, which was downregulated in the abdominal aorta under Ang II infusion. This heterogeneity in S1PR expression may influence not only the molecular and cellular mechanisms underlying aortic aneurysm progression but also the susceptibility to aneurysm formation and rupture in general. This would align with aortic homograft transplantation studies, which indicated that regional differences in disease susceptibility are largely determined by intrinsic properties of aortic cells rather than by local hemodynamic forces[388,389]. In these experiments, atherosclerosis-prone abdominal aortic segments consistently developed severe lesions even when transplanted into normally disease-resistant regions, such as the thoracic aorta, whereas thoracic segments maintained their resistance when placed in the abdominal position[388]. Taken together, these segment-specific differences observed in the current study are novel and crucial for the understanding of the progression of aneurysm formation but further targeted analyses will be required to define how these receptor distributions functionally influence aneurysm initiation, progression and rupture risk in specific aortic regions.

To further elucidate the functional role of individual S1PRs in regulating VSMC phenotypic modulation under aneurysm progression, the Ang II infusion model was applied in S1PR2- and S1PR3-deficient mice. In addition, both knockout strains were analysed under tonic S1P levels. Of note, as global S1PR1-deficiency results in

embryonic lethality due to endothelial leakage, knockout analyses were restricted to S1PR2- and S1PR3-deficient mice[390]. These two receptor subtypes were of particular interest, as previous *in vitro* data indicated opposing effects on VSMC phenotype regulation, with S1PR2 generally promoting the maintenance of the contractile state, whereas S1PR3 downregulating contractile markers (Figure 21).

In S1PR2-deficient mice infused with Ang II, aneurysm incidence and mortality were comparable to controls. Moreover, contractile marker expression was reduced to a similar extent as under Ang II infusion alone, indicating that the absence of S1PR2 did not further aggravate the phenotypic switch of VSMCs. This suggests that, under aneurysmal conditions without tonic elevation of S1P, S1PR2-mediated acute upregulation of contractile markers does not play a decisive role in the progression of aortic aneurysms or in modulating the VSMC phenotype. Interestingly, these findings are not fully consistent with previous reports from Wamhoff *et al*. and Yang *et al.*, in which S1PR2 signaling exerted a protective effect on the maintenance of the contractile VSMC phenotype in vascular injury models. In those settings, S1PR2 expression was associated with enhanced expression of contractile markers following acute injury[345,386]. This discrepancy may reflect fundamental differences between acute vascular injury models and chronic aneurysm-promoting conditions, as well as the complex remodelling processes involved. Tonic S1P levels did not confer better survival in Ang II-infused S1PR2-deficient mice, suggesting that the presence of elevated S1P alone, without functional S1PR2 signaling, is insufficient to prevent disease progression under these conditions. However, the significant downregulation of contractile marker genes that was typically observed under tonic S1P exposure was absent in the S1PR2-deficient animals. This finding strongly suggested that S1PR2 signaling plays a pivotal role in the accelerated phenotypic switch of VSMCs induced by tonic S1P elevation. Taken together these findings indicated that the reduction or attenuation of phenotypic switching alone is not sufficient to prevent aneurysm development. At this stage, other pathophysiological processes such as enhanced ECM degradation or persistent inflammation may act as additional dominant drivers of disease progression.

In the context of aortic pathologies Pan *et al*. observed in a model of thoracic aortic dissection that pharmacological S1PR2 inhibition, using JTE-013 led to a reduced rupture-based mortality associated with a marked reduction in VSMC apoptosis and infiltration of inflammatory cells[391]. On the one hand, this study indicated that S1PR2

signaling promotes vascular inflammation during aneurysm progression resulting in adverse vascular remodelling[391]. However, on the other hand there was a discrepancy to the current study, where no benefit in survival and aneurysm formation was observed in global S1PR2-deficient mice. These differences were likely attributable, at least in part, to fundamental variations in the experimental design. Specifically, Pan *et al*. employed the Ang II infusion model in combination with β-aminopropionitrile (BAPN), a lysyl oxidase inhibitor that further destabilizes the aortic wall, in C57BL/6 mice[391]. This model used by Pan *et al.* is another aortic aneurysm or dissection model[391]. In this study, the combination induced a distinct pathophysiological state, characterized by pronounced extracellular matrix weakening, which may increase the relative contribution of inflammatory mechanisms targeted by S1PR2 inhibition[392]. Furthermore, Pan *et al.* reported no increase in blood pressure following Ang II infusion, which raised methodological concerns, given that elevated blood pressure is a well-established feature of this model. In addition, the pharmacological inhibitor JTE-013 used in their study exhibited limited receptor selectivity, as several reports have shown that it also interfered with S1PR4 and other targets[393,394]. This lack of specificity may have contributed to the protective effects observed in their model. The protective outcome reported by Pan et al. may therefore be model-specific, reflecting both the unique mechanisms engaged under BAPN-induced matrix destabilization and potential off-target actions of JTE-013.

Interestingly, while the present data suggested that S1PR2 participated in the downregulation of contractile markers under tonic S1P conditions, S1PR3 activation appeared to exert an even stronger effect on the loss of the contractile phenotype. In accordance with this observation, Wamhoff *et al.* reported that the initial upregulation of S1PR3 following vascular injury was associated with phenotypic modulation of VSMCs[345], characterized by reduced expression of contractile genes. These similarities prompted a more detailed investigation of S1PR3-deficient mice in the context of aneurysm progression. The present study highlighted, that S1PR3-deficient mice are less prone to aortic rupture although animals still developed aortic aneurysms. Interestingly, a marked preservation of contractile gene expression was observed in the *aortae* of S1PR3-deficient mice following Ang II infusion. This finding suggested that the phenotypic switch mediated by S1PR3 activation is prevented in the absence of this receptor during aortic aneurysm development. However, the development of aortic aneurysms could not be prevented, which is likely attributable to the involvement

of numerous additional pathomechanisms associated with aneurysm formation, such as extracellular matrix degradation or chronic inflammation. Nevertheless, the findings align with previous reports demonstrating that S1PR3 deficiency is associated with reduced VSMCs proliferation and diminished intimal hyperplasia[345,395]. This finding suggests that S1PR3 plays a role in early vascular remodelling processes[345,395]. Consistent with these results, Wamhoff et al. showed that S1PR3 and S1PR1 were preferentially upregulated during early vascular remodelling, whereas S1PR2 expression increased only at later disease stages[345]. This temporal pattern may explain why S1PR3 deficiency primarily affected early remodelling and rupture susceptibility, but not the overall development of aneurysms. However, as with S1PR2 inhibiting the phenotypic switch alone appeared to be insufficient for preventing the development or progression of aortic aneurysms. Interestingly, the current data implied the existence of an additional protective mechanism under tonic S1P conditions. S1PR3-deficient mice still displayed a markedly reduced susceptibility and lethality to rupture, and their *aortae* appeared more stable and less progressed. These findings underscored the pivotal contribution of S1PR3 signaling to aneurysm destabilization and rupture, suggesting that its absence confered significant protection to the aortic wall.

In summary, the present work demonstrated that S1P can influence the contractile phenotype of VSMCs in a receptor- and state-dependent manner. Acute S1PR2 activation transiently preserved the contractile state, whereas tonic S1P signaling drove its downregulation. Conversely, S1PR3 activation can induce a reduction in contractile marker expression. Therefore, the role of S1P/S1PR signaling during vascular remodelling in aneurysm progression is highly complex and is likely influenced by multiple factors, including altered S1P levels under diseased conditions. Support for this notion was provided by Meissner *et al*., who demonstrated that S1P levels increase with prolonged Ang II infusion[288]. Additionally, the differential expression of S1PR subtypes across aortic regions and disease stages must be considered. The study did not assess temporal changes in S1PR expression in aortic tissue, but it is possible that during early vascular remodelling, S1PR3 predominantly mediates the downregulation of contractile genes. Such effects appear to be more pronounced under conditions where S1PR3 signaling is dominant. In later disease stages and under tonic S1P conditions, this role could be assumed by S1PR2. Consistently, Wamhoff *et al.* showed that S1PR3 and S1PR1 are preferentially

upregulated during early vascular remodelling, while S1PR2 expression only rises at later stages[345]. This pattern further illustrates how the balance between S1PR subtypes may change over time, influencing the phenotypic stability of VSMCs during disease progression.

5.1.3. Contribution of S1PR3 signaling in hypercontractile vascular response

The ability of VSMCs to contract is crucial in the regulation of vascular tone.[84] Contraction of VSMCs is primarily driven by an increase in intracellular Ca^{2+} [84]. This increase in cytosolic Ca^{2+}, promotes the formation of a Ca^{2+}-calmodulin complex, which activates MLCK. This leads to the phosphorylation of MLC and finally drives the formation of actin-myosin cross-bridges, which are necessary for filament contraction[84,90,396]. In addition to this Ca^{2+} dependent pathway, Ca^{2+} independent signaling could also contribute to sustained contraction[92]. Here, the activation of the RhoA/Rho-associated kinase (ROCK) pathway, inhibits the myosin light chain phosphatase (MLCP)[92,397]. This maintains the phosphorylated state of MLC and leads to prolonged contraction[92,398].

During aneurysm progression, the contractile function of the aorta is altered dependent on disease progression[399]. Under hypertensive conditions hypercontractile response to vasoconstrictors was observed[361,400,401]. Consistent with this concept, the present study demonstrated that abdominal aortic segments from $ApoE^{-/-}$ mice infused with Ang II, but without macroscopic aneurysmal dilation, exhibited a hypercontractile response to both Phe and Ang II stimulation. This hypercontractile state may represent a compensatory response of VSMCs to stabilize the vessel wall in the presence of Ang II-induced remodelling. In line with this Rodrigues-Diez *et al*. observed in an Ang II infusion model under high fat diet, that highly diseased aortic segments show a low response to vasoconstrictive agents, whereas low severity aortic segments show a remarkable increase in vasoconstriction[402]. Interestingly, the observed hypercontractile response appeared independent of the VSMC phenotype[402]. A consistent downregulation of the contractile marker ACTA2 was detected across different vascular segments, irrespective of disease severity[402]. The present study revealed similar findings, showing that a hypercontractile state of the aortic segment persisted despite phenotypic switching of VSMCs and concomitant loss of contractile marker expression. This apparent discrepancy may indicate that the downregulation of contractile genes does not necessarily reflect a loss of contractile capacity, but rather

represents a compensatory response to sustained or excessive contractile activation. Such a feedback mechanism may serve to limit excessive wall tension and prevent additional mechanical stress during aortic aneurysm progression.

In addition, it should be taken into account, that the hypercontractile response was observed for Ang II and Phe, which activate contraction through distinct upstream mechanisms. Phe predominantly induced vasoconstriction via α_1-adrenergic receptors coupled to G_q, leading to phospholipase C (PLC) activation and subsequent IP_3 - mediated Ca^{2+} mobilization[403-405]. In contrast, Ang II mediates vascular contraction through activation of Ang II type 1 receptor (AT_1), which could activate the G_q/PLC/Ca^{2+} pathway and the RhoA/ROCK pathway, thereby increasing intracellular Ca^{2+} [406,407]. With respect to this, S1P is also able to modulate vascular tone and contraction, predominantly through activation of S1PR2 and S1PR3[268,408-410]. Both receptors are coupled to $G_{12/13}$, triggering the RhoA/ROCK-mediated Ca^{2+} release, and G_q, which leads to activation of PLC/IP_3/Ca^{2+} pathway[268,408]. Dependent on different vascular beds, acute S1P stimulation was observed to induce vasoconstriction[286]. The current study revealed a new aspect in S1P-mediated vasoconstriction, since aortic segments of Ang II-infused mice under tonic S1P levels, achieved by pharmacological inhibition, induced a further increased hypercontractile response compared to the respective controls. This tonic S1P-driven hypercontractility represented a new uncharacterized mechanism within aortic aneurysm progression. Such an augmented contraction state under tonic S1P conditions may contribute substantially to the increased rupture rate and higher aneurysm incidence observed in this setting. Mechanistically, excessive vasoconstriction may impose additional wall stress on an already structurally weakened extracellular matrix, thereby accelerating pathological remodelling and promoting mechanical failure of the vessel wall.

Importantly, vascular tone is not only determined by VSMC-mediated contraction but also modulated by endothelial function[411]. Under physiological conditions the endothelium exerts a vasodilatory influence through the release of mediators such as nitric oxide (NO), which counteract vasoconstrictive stimuli[412]. Endothelial dysfunction, frequently observed under Ang II-induced vascular remodelling disrupts this balance by impairing NO bioavailability[413]. In line with this, the current study observed also under Ang II infusion an impaired response to ACh, which indicated endothelial dysfunction. This effect was even more pronounced in aortic segments from Ang II-infused mice with tonic S1P levels, where endothelium-dependent relaxation was

further impaired. This observation suggests the possibility that tonic S1P levels could also influence endothelial function via S1PR-dependent pathways. Evidence for this could be that S1P stabilizes the endothelial barrier under physiological conditions[197,364,414,415]. However, high S1P levels have been shown to disrupt the endothelial barrier[416,417], which could also occur within the Ang II infusion model with tonic S1P. Therefore, such effects could contribute, alongside VSMC-driven mechanisms, to enhanced vascular hypercontractility and aneurysm progression. Further studies are necessary, which will focus more on endothelial alterations in this disease model. In particular, endothelial cell-specific S1PR knockout models would be of great importance to elucidate the precise role of individual S1PRs in the regulation of vasodilation and vascular tone. Such approaches could help to determine whether endothelial S1PR signaling contributes to vascular dysfunction during aneurysm progression.

Due to the role of S1P in modulating vascular tone through S1PR2 and S1PR3, the observed hypercontractility under tonic S1P conditions required further investigation of the contribution of possibly involved S1PRs. Therefore, vascular reactivity was also assessed in S1PR2- and S1PR3- deficient mice under Ang II infusion alone, or in combination with tonic S1P levels, caused by S1P lyase inhibition.

S1PR2-deficient mice did not exhibit any significant alterations in vascular function, indicating that both the Ang II-induced hypercontractile state and the accompanying endothelial dysfunction remained unchanged in the absence of S1PR2. These absence of changes in vascular reactivity align with the finding that S1PR2 deficiency did not affect survival or aortic aneurysm formation under Ang II infusion.

Under tonic S1P conditions, S1PR2-deficient mice displayed an unchanged maximal contractile response, while the overall vasoconstrictive activity over time was slightly reduced. Despite this minor difference, the hypercontractile phenotype remained evident. Endothelium-dependent relaxation to ACh was further impaired, suggesting that endothelial dysfunction is exacerbated. Endothelial dysfunction, reflected by the impaired ACh-mediated vasodilation observed under tonic S1P conditions, may promote pathological wall remodelling through sustained inflammatory activation. However, the unchanged aneurysm incidence and survival of S1PR2-deficient mice indicate that these functional alterations alone are not decisive for disease progression or outcome. Taken together, these findings suggest that S1PR2 contributes to the

regulation of vascular reactivity under tonic S1P conditions but has no major impact on aneurysm development or survival.

In contrast this study highlights a remarkable influence of S1PR3 in vascular reactivity during Ang II infusion and aneurysm formation. Interestingly, S1PR3-deficient mice were protected from Ang II-induced hypercontractility, exhibiting normal vasoconstriction and preserved endothelial function under both Ang II and tonic S1P conditions. Notably, this preserved vasoreactivity was accompanied by a lower rupture rate in the absence or presence of tonic S1P levels, although aneurysms continued to develop. This finding suggests that reduced vascular tone in the absence of S1PR3 may decrease wall stress and provide protection against rupture. However, S1PR3 is also known to exert endothelial-protective effects by inducing eNOS-dependent NO production under physiological conditions[418,419]. In the context of Ang II infusion, however, this vasodilatory function appeared to be outweighed by endothelial dysfunction, conditions that favour S1PR3 signaling in VSMCs and thereby promote vasoconstrictive responses. Furthermore, S1PR3 activation is known to promote vasoconstriction via both G_q- and $G_{12/13}$-coupled pathways, leading to increased intracellular Ca^{2+} mobilization[420]. In line with this, the current study provided additional mechanistic evidence that S1PR3 contributes to hypercontractility under tonic S1P conditions. *In vitro* experiments demonstrated that tonic S1P levels in Ang II-treated VSMCs induced a pronounced increase in intracellular Ca^{2+} release and enhanced phosphorylation of MLC, both of which were substantially attenuated or abolished upon pharmacological S1PR3 inhibition.

Taken together, the absence of S1PR3 not only prevented vascular hypercontractility but was also associated with a marked improvement in survival, suggesting that targeting S1PR3 signaling may represent a promising strategy to stabilise aortic aneurysms by reducing rupture risk. These effects highlight S1PR3 as a mechanistically relevant and therapeutically attractive target in the context of aneurysm progression. Future studies employing cell type-specific S1PR3 deletions, particularly in endothelial cells and VSMCs, will be essential to dissect the individual contributions of S1PR3 signaling within the vascular wall and to further refine its influence on aortic aneurysm progression.

5.2. The potential of S1PR modulators for the treatment of aortic aneurysms

In the current study, the effects of the S1PR modulator and S1P analogue, FTY720 were examined in the murine Ang II infusion model to determine its effects on aneurysm formation and pathophysiology. FTY720, which is clinically approved since 2011 for the treatment of multiple sclerosis, acts primarily through functional antagonism of S1PR1, while it binds also to all S1PRs except S1PR2[421,422]. Upon phosphorylation *in vivo* by sphingosine kinase 2, FTY720 induces prolonged internalization of S1PR1, thereby impairing the reappearance of the receptor to the membrane surface[423-425]. This functional downregulation results in the retention of lymphocytes within secondary lymphoid organs, due to the suppression of S1PR1-dependent egress[426]. Importantly, Daugherty *et al*., investigated that total lymphocyte deficiency did not alter aortic aneurysm formation or diameter[427]. In detail, although lymphocyte infiltration has been detected in aneurysmal tissue of Ang II-infused mice, Rag-1-deficient mice show still aneurysm formation in the absence of lymphocytes, even though Ang II-induced atherosclerosis was reduced[335,427]. This suggests that inflammation, possibly driven by lymphocytes, is not essential for aneurysm formation in this model. Therefore, any potential effects of FTY720 are unlikely to be mediated by lymphopenia alone. Instead, the focus of this study was on alternative FTY720 mediated effects.

In the present study, chronic administration of FTY720 during Ang II infusion failed to exert any protective effects on aortic aneurysm progression. Endothelial dysfunction persisted, with markedly reduced ACh-induced vasorelaxation, and neither systolic blood pressure nor aneurysm incidence or rupture rates were affected.

Thus, despite the reported vasodilatory and atheroprotective properties of FTY720[358,428], no beneficial outcome was observed under Ang II-induced aneurysm conditions.

Furthermore, the results of this study contrast with Cantalupo *et al*., who demonstrated that chronic infusion of FTY720 under hypertensive conditions, led to an even higher systolic blood pressure and an impaired vasorelaxation in mesenteric arteries[350]. In the current study, however, blood pressure or vascular dysfunction did not further aggravate. While Cantalupo *et al.* used mesenteric arteries for their analysis, the current study focused on abdominal aortic segments. The variability is consistent with previous studies that demonstrated that the vascular effects of FTY720 or S1P, on

vascular tone, including vasodilation and also vasoconstriction, are dependent on the vascular bed and the S1PR receptor signaling, which is involved[429]. Furthermore, the formation of aortic aneurysms and dissections in these ApoE-deficient mice have to be noted. Because even though vascular reactivity studies were performed always with distal infrarenal abdominal aorta, which did not show macroscopic signs of aneurysmal dilation, the presence of an upstream aneurysm could still influence vascular tone. This is supported by evidence that Ang II-induced aneurysm formation has been associated with early morphological changes, which can affect vascular reactivity even in regions without visible dilation[430]. With regard to the absence of even higher blood pressure under chronic FTY720 administration in mice, which were already hypertensive, it must be taken into account that in this study, the increase in blood pressure was measured 10-14 days after the start of Ang II infusion. Cantalupo *et al*., on the other hand, only showed a significant increase in blood pressure with chronic FTY720 administration after more than 30 days[350]. After a time frame comparable to the observation period of the present study, no differences in blood pressure were detected in their experiments either. Even if FTY720 causes changes in blood pressure at later time points, such delayed effects are likely to be of minor relevance in the Ang II-induced aneurysm model used in this study, given that the observation period is limited to 28 days. Therefore, any blood pressure changes occurring after this period would not affect aneurysm formation or rupture within the observation period.

Furthermore, in the context of aortic aneurysm formation, the present study showed no beneficial effects caused by FTY720 treatment on aneurysm incidence or rupture. These findings contrast with a previously published study, which reported, that FTY720 has a protective effect in the same model[431]. However, the focus of that study was not on the modulatory effects of FTY720 on S1P/S1PR signaling or its previously described impact on lymphocytes and vascular tone, but rather on its function as a TRPM channel blocker[431]. Nevertheless, the study has notable methodological limitations. Both FTY720 and its phosphorylated metabolite (FTY720-P) were tested in the same aneurysm model. Interestingly, FTY720-P failed to demonstrate any protective effect, such as rupture and aneurysm incidence were similar to those observed with Ang II treatment alone[431]. These findings are consistent with those of the present study. This discrepancy is relevant, as FTY720 is known to be rapidly phosphorylated *in vivo* by sphingosine kinase 2, resulting in FTY720-P being the primary bioactive form[258,432]. Consequently, it is expected that the phosphorylated

metabolite will mirror or even enhance the efficacy of FTY720 *in vivo*. However, the lack of effect observed with FTY720-P, combined with the reported benefit of unphosphorylated FTY720, raises questions regarding the interpretation of the results. The authors do not provide a mechanistic explanation for this inconsistency, which limits the reliability of the proposed protective role of FTY720 in this model.

Additionally, previous studies showed that FTY720-P induced prolonged internalization and functional antagonism of S1PR1[424,433]. In this study, it was identified that tonic activation of S1PR1 led to a reduced expression of contractile markers in VSMCs. Thus, internalization of S1PR1 by FTY720 may actually favour the maintenance of a contractile VSMC phenotype. However, other studies reported that FTY720 did not induce the internalisation of S1PR3[433,434]. This implies that under tonic conditions, S1PR3 signaling remains active, thereby counterbalancing or even outweighing the functional loss of S1PR1. Consequently, persistent S1PR3 activation may promote the downregulation of contractile markers and contribute to hypercontractility during aortic aneurysm progression.

Although FTY720 has shown beneficial effects on atherosclerosis progression and vascular reactivity in some mouse models, no protective effects were observed for aortic aneurysms. Nevertheless, next-generation S1P analogues such as siponimod, ponesimod, or ozanimod have been developed, which are considerably more selective and target individual S1P receptor subtypes[435]. Testing their efficacy in the context of aortic aneurysm pathology represents a promising future direction to dissect receptor-specific mechanisms. Moreover, as several of these agents are already clinically approved, successful preclinical findings could be rapidly translated into patient-oriented therapeutic strategies. Building on this concept, the availability of highly specific agonists and antagonists for S1PR2 and S1PR3 will be essential to pharmacologically define their individual roles in aneurysm formation and progression. Ultimately, combinations of receptor-specific agonists and antagonists may prove to be the most effective therapeutic approach, simultaneously addressing endothelial cell- and VSMC- specific mechanisms in aortic aneurysm development.

5.3. Sphingolipid profiling in human abdominal aortic aneurysms

In the present study, sphingolipid profiles in both plasma and aortic tissue were shown to be altered in patients suffering from abdominal aortic aneurysms in comparison to healthy controls. These findings support the growing recognition of bioactive lipids

involved in aortic aneurysms and dissections[321,322,436]. The majority of these descriptive studies highlight that several lipid classes, including phospholipids (PCs), sphingolipids and lysophospholipids are significantly altered in the plasma or in aortic tissue[321,322,436]. Such lipidomic shifts in both compartments probably reflect local and metabolic alterations due to aneurysm formation. Phospholipid species have been associated with increasing vascular inflammation in the aortic wall[437,438]. In addition, lysophospholipids have been associated with development of atherosclerosis, especially atheroma formation[439,440]. An increase in sphingolipid species, including ceramides was associated with vascular damage, hypertension and atherosclerosis[441]. Numerous studies have also been conducted on S1P, highlighting its dual nature in atherosclerosis[442]. In the context of vascular inflammation, locally elevated S1P concentrations function as chemoattractant, promoting the recruitment of inflammatory cells to the vascular wall[443,444]. Furthermore dependent on the S1P levels and the associated S1PR signaling, S1P enhances or disrupts endothelial barrier[445-447]. Additionally, HDL-bound S1P is associated with anti-atherosclerotic properties, whereas albumin-bound S1P drives atherosclerotic mechanisms[299,448]. With respect to alterations in S1P levels, lower levels were measured in the plasma of patients with atherosclerosis or coronary artery disease[354,355]. A recent study identified also lower S1P levels as a marker for endothelial damage in preeclampsia[356]. On the other site, higher levels of S1P in plasma were associated with hypertension[288]. These numerous studies collectively underscore the complexity of lipid mediated processes in vascular diseases. The functional impact of individual lipid species appears to be highly variable dependent on local and systemic concentrations, involved cell types, receptor signaling, the specific pathophysiological state and the presence of comorbidities. These dynamic and diverse behaviour complicates the interpretation of lipidomic data sets. Nevertheless, the identification of disease associated lipid patterns, may provide important insights into disease mechanisms and support the identification of potential future molecular targets for disease prediction, stratification or treatment.

In the context of aortic aneurysms and dissections, lipidomic analysis remains largely descriptive, and functional interpretations are lacking. For instance, sphingomyelin (SM) species were increased in the aortic tissue of patients with ascending thoracic aortic aneurysms[449]. Furthermore, altered serum levels of sphinganine and specific ceramide species were observed in patients with aortic dissection, and these reductions were found to differ between Stanford type A and type B dissections,

suggesting their potential utility for subtype differentiation[436]. A separate study highlights that lipid composition varies across distinct regions of the aortic media, including normal, transitional, and aneurysmal zones, in patients with thoracic aortic aneurysms of both atherosclerotic and non-atherosclerotic origin, as well as in those with abdominal atherosclerotic aneurysms[324]. While all of these studies reported altered lipid signatures in patients with aortic aneurysms or dissections, most of them focus on either circulating or tissue-specific changes, but rarely address both simultaneously. The present study, provides the first combined analysis of plasma and aneurysmal tissue samples, allowing direct comparison between systemic and local lipid changes. Of particular interest in this investigation was S1P, which exhibited the most significant difference in both compartments, plasma and aortic tissue of patients with abdominal aortic aneurysms. This finding indicates that S1P is a potential disease biomarker that in addition, is causally involved in the pathophysiology of human abdominal aortic aneurysms.

In line with this, it was observed that S1PRs are highly upregulated in aortic tissue of patients with abdominal aortic aneurysms. Qu *et al*. observed in aortic tissue of patients with abdominal aortic aneurysms a downregulation of S1PR2, an upregulation of S1PR3, whereas S1PR1 remained undetectable[450]. However, the current study was able to show an increased protein expression of all three S1PRs in aortic tissue of aneurysm patients. This discrepancy may be attributed to several factors, including variations in tissue sampling, disease stage or cellular composition. In contrast to Qu *et al.*, who performed immunohistochemical analyses on end-stage human aneurysm specimens, the present study used quantitative Western blotting of carefully dissected aortic wall tissue excluding intraluminal thrombus, thereby reducing tissue heterogeneity and improving the accuracy of protein quantification. Furthermore, technical limitations, such as the limited antibody specificity available at the time of the earlier study from Qu *et al.*, may also have affected the accuracy of receptor detection. Consequently, the observed upregulation of all three S1PR subtypes may more robustly reflect the total receptor abundance in the diseased aortic wall rather than regional expression differences detectable by histological staining. Taken together, the concurrent increase in aortic tissue S1P levels and S1PR expression points toward an enhanced activation of S1P/S1PR signaling pathways, which may contribute to vascular remodelling and aneurysm progression.

Building on these tissue-level findings, subsequent analyses focused on circulating lipid species to determine whether the observed changes in S1P signaling translate into measurable systemic alterations with potential diagnostic relevance. Quantitative and ROC curve analysis of plasma S1P levels, demonstrated its potential prognostic value in disease stratification. Moreover, random forest analysis identified S1P as the highest-ranking variable based on mean decrease in accuracy (MDA), outperforming other lipid species including several lysophosphatidylethanolamines, phosphatidylethanolamines, and Cer(d18:1/18:0). These results further support the potential of S1P as a key lipid marker in aortic aneurysm pathophysiology.

Finally, these findings align with current approaches in cardiovascular research, such as the CERT2 score, which combine defined lipid species to predict cardiovascular risk[307]. In detail, the CERT2 score combined specific ceramide ratios including Cer(d18:1/16:0), Cer(d18:1/18:0) and Cer(d18:1/24:1), as well as selected phosphatidylcholines[307]. The CERT2 score has already been successfully applied to many cardiovascular diseases, such as coronary heart disease and heart failure[307,451]. The current study suggests that the development of a lipid-based score may also be possible for aortic aneurysms, as an altered lipid profile was observed. Combining key sphingolipid markers, such as S1P, which was clearly associated with aneurysm pathophysiology, together with already established clinical parameters, could present a promising approach for the future to improve risk classification, patient monitoring or disease diagnosis in aortic aneurysms.

6. Outlook

The pathophysiology of abdominal aortic aneurysms and dissections is highly complex, and not all mechanisms have been fully elucidated to date. Since many aneurysms remain unnoticed, there is a high risk of rupture with increasing growth and without monitoring. Furthermore, as no pharmacological approaches have yet developed, that specifically target aortic aneurysms, it is essential to identify new molecular targets that are suitable for early diagnosis, monitoring or pharmacological therapy.

Given the current lack of targeted pharmacological therapies for aortic aneurysms, the identification of molecular pathways that can be therapeutically modulated is of high translational relevance. Since S1P/S1PR signaling has emerged as a central regulator of vascular integrity and remodelling, dissecting its cell type-specific functions represents an important next step. In this regard, single-cell RNA sequencing would provide an essential first step to identify the distinct vascular and immune cell populations that contribute to aneurysm initiation and progression. However, the generation and analysis of S1PR-deficient mouse models with VSMC- or endothelium-specific deletions will help to clarify receptor-specific contributions to aneurysm development. Especially, VSMC-specific knockout mice lacking S1PR3 could provide a deeper insight and understanding of the role of S1PR3 during aneurysm progression. A detailed investigation of S1PR3-mediated Ca^{2+} mobilization could be also of particular interest, since hypertension alters the activity of key calcium channels and transporters, which disrupts the calcium homeostasis and contributes to vascular dysfunction[92,452]. In this context, it will be crucial to determine whether S1PR3 signaling interacts with various calcium-handling mechanisms in VSMCs, including L-type Ca^{2+} channels, store-operated calcium entry, and intracellular release pathways. Despite its potential relevance, the role of disturbed calcium signaling in the pathogenesis of aortic aneurysm formation remains poorly understood and therefore a profound investigation would be necessary.

Once a more detailed understanding of the contribution of S1P/S1PR3 signaling to aortic aneurysm development has been established, pharmacological modulation of this pathway may represent a promising therapeutic approach to stabilize aneurysm progression and preserve vascular integrity. Rather than targeting the receptor system unspecifically, the development of S1PR-selective agonists and antagonists offers the possibility of achieving precise modulation of S1P signaling in defined vascular cell

types, thereby minimizing off-target effects. Recent advances in the generation of second-generation S1P receptor modulators, such as ozanimod or siponimod, demonstrate that receptor-selective compounds with improved pharmacokinetic profiles and safety characteristics are clinically feasible. Translating these concepts to aneurysm therapy could offer an innovative approach to counteract maladaptive S1P/S1PR-driven vascular remodelling in aortic aneurysm development and progression.

Furthermore, the role of S1P in Ang II-induced disease should be further investigated, as increased S1P levels were observed in this model. The S1P-producing enzymes SphK1 and SphK2 therefore represent interesting research targets. Studying Sphk1- and Sphk2 deficient mice in the Ang II-induced aneurysm model would help to clarify whether the rise in S1P levels directly contributes to aneurysm formation or is merely a secondary, confounding effect of Ang II infusion. Regarding this, especially SphK1 has already been linked to Ang II-induced vascular dysfunction[292]. Siedlinski *et al.* reported that Ang II infusion induces SphK1 upregulation, while Sphk1-deficient mice displayed reduced blood pressure compared to wild type controls under the same conditions[292]. Therefore, SphK1-deficient mice should first be examined under Ang II infusion, to analyse aortic aneurysm development and ruptures. A further approach to reduce S1P levels during aortic aneurysm development would be the direct pharmacological inhibition of SphKs. In murine models, the selective SphK1 inhibitor PF-543 has already been successfully used to reduce Ang II-induced cardiac hypertrophy[453]. Furthermore, inhibition of SphK2 by Opaganib (ABC294640), which has already progressed into clinical trials for cancer therapy, may represent an additional promising strategy to lower S1P levels[454,455]. Therefore, the reduction of S1P could be an additional future therapeutic approach to prevent or attenuate aortic aneurysm formation and progression.

Furthermore, the mechanism underlying the increase in S1P levels during aneurysm progression remains incompletely understood. Although S1P can be produced by various cell types, the main sources are red blood cells, endothelial cells, platelets, and immune cells[188,198,199,456]. All of these cell types are involved the pathophysiology of aortic aneurysms[457]. In order to determine a possible link between these cell types and the higher S1P levels under aneurysm progression, their respective role should be systematically investigated. This could include the quantification of intracellular S1P levels in these cell types under Ang II infusion in mice or in patients with aortic

aneurysms. A closer examination of S1P-producing enzymes (SphK1 and SphK2) and degrading enzymes, such as S1P lyase, in these cell types could provide further important insights. Such analyses may clarify how dysregulated S1P metabolism drives vascular remodelling and aneurysm progression.

Importantly, the role of S1P transporters should also be addressed to identify the cellular sources of extracellular S1P. The transporter MFSD2B is almost exclusively expressed in erythrocytes and platelets, whereas SPNS2 is mainly expressed in endothelial cells and to a lesser extent, in VSMC. Characterizing the activity and regulation of these transporters may therefore provide critical information on S1P release dynamics during aneurysm development.

Finally, as HDL is the predominant S1P carrier in plasma, and recent large-scale cohort data demonstrated that low HDL-C levels are strongly associated with an increased risk of abdominal aortic aneurysm formation[458], the investigation of HDL-associated S1P transport represents a promising translational direction.

In line with the observed endothelial dysfunction, endothelial cells represent a relevant target for further investigation using endothelial-specific knockout models. S1P is a key regulator of endothelial barrier integrity, and altered S1P signaling has been associated with endothelial dysfunction[194,447]. In this context, elevated S1P levels could be both a cause and a consequence of endothelial damage, since S1P signaling via S1PR2 and S1PR3 has been shown to impair endothelial function, thereby exacerbating vascular pathology[414,416,447]. Endothelial integrity is crucial for vascular homeostasis, and its dysfunction is implicated in the onset of aneurysm development. So finally, more research is needed to understand how changes in S1P signaling affect endothelial function, including barrier integrity, NO bioavailability, or vasorelaxation, during aneurysm progression.

Extensive sphingolipidome analysis revealed further sphingolipids to be altered during aneurysm progression. In recent years, lipid alterations in cardiovascular disease have gained attention as disease drivers or potential biomarkers. Therefore, the development of lipid-based risk stratification tools, such as the CERT2 score, is a promising approach in clinical use. The CERT2 score, which combines a set of ceramides and phospholipid species, has shown prognostic value for major adverse cardiovascular events, particularly in coronary artery disease[311,312]. Due to the complexity of aortic aneurysms, a lipidomic risk score adjusted for aneurysms could be a useful tool for disease detection and monitoring. Regarding this, it would also be

of particular interest to determine whether alterations in lipid profiles, or specific lipid species, correlate with parameters of aneurysm pathology such as aneurysm size, growth rate, or rupture risk. However, stratification between different cardiovascular diseases would be required, since lipid species and their pathophysiological roles vary between different cardiovascular diseases[441,459]. Therefore, further studies are needed to identify aortic aneurysm-specific lipid patterns and evaluate their predictive value in clearly characterized patients. Within this context, the investigation of other lipid species altered during aortic aneurysm progression would be helpful to identify novel molecular targets.

Among these, ceramides have gained increasing attention due to their involvement in key pathological mechanisms such as vascular inflammation, oxidative stress or apoptosis[460-463]. Within this study, elevated levels of specific ceramide species, including Cer(d18:1/16:0) and Cer(d18:1/24:1), were identified in plasma and aneurysmal tissue. Therefore, studying the contribution of ceramides in experimental aortic aneurysm models could provide further important insights into disease pathophysiology.

The results presented in this study were generated in mice and within one of several established models of abdominal aortic aneurysms and dissections. To ensure inter-model and inter-species reproducibility and to identify the most relevant and conserved S1P-driven mechanisms of aneurysm disease, further validation across complementary models is required. First, the porcine pancreatic elastase model induces a true infrarenal aortic aneurysm through enzymatic degradation of elastin and better isolates elastolysis as a principal driver of aneurysm formation[464]. Second, the BAPN model, via inhibition of LOX and impaired collagen/elastin cross-linking, induces matrix instability and can be combined with elastase to yield more severe, progressive aneurysms[464]. This is well suited to interrogate S1P effects on extracellular-matrix integrity and wall mechanics. Finally, large-animal abdominal aortic aneurysm models, particularly in the pig, provide valuable translational insight, as they closely resemble the human vascular anatomy, hemodynamics, and wall structure[465]. Porcine models induced by perivascular elastase application, chemical injury, or combined BAPN treatment have been shown to reproduce chronic aneurysm expansion and thrombus formation[465], thereby offering a valuable model for preclinical evaluation of therapeutic strategies. Future investigations employing these complementary models will be essential to define model-specific and conserved mechanisms of S1P/S1PR signaling

in aneurysm pathogenesis. Such comparative approaches will help determine whether S1P-mediated effects on vascular remodelling, inflammation, and thrombosis are universally relevant or context-dependent, thereby refining the translational potential of S1P-targeted therapeutic strategies.

In summary, the current study highlights especially the role of S1P but also of other sphingolipids as important molecules in the understanding of aortic aneurysm pathophysiology, due to its effects on key pathophysiological processes. Determining precisely how S1P and its metabolic sphingolipid network is involved in these processes remain essential goals for future research. In this context, the development of S1P-based drugs targeting specific cell types and receptor subtypes may offer novel and more precise therapeutic approaches for this devastating disease.

7. References

1 Czerny, M. *et al.* EACTS/STS Guidelines for Diagnosing and Treating Acute and Chronic Syndromes of the Aortic Organ. *The Annals of Thoracic Surgery* 118, 5-115 (2024). https://doi.org/10.1016/j.athoracsur.2024.01.021

2 Pfaltzgraff, E. R. *et al.* Embryonic domains of the aorta derived from diverse origins exhibit distinct properties that converge into a common phenotype in the adult. *J Mol Cell Cardiol* 69, 88-96 (2014). https://doi.org/10.1016/j.yjmcc.2014.01.016

3 Xie, M. *et al.* The crosstalks between vascular endothelial cells, vascular smooth muscle cells, and adventitial fibroblasts in vascular remodeling. *Life Sciences* 361, 123319 (2025). https://doi.org/https://doi.org/10.1016/j.lfs.2024.123319

4 Paruchuri, V. *et al.* Aortic Size Distribution in the General Population: Explaining the Size Paradox in Aortic Dissection. *Cardiology* 131, 265-272 (2015). https://doi.org/10.1159/000381281

5 Cho, M. J., Lee, M.-R. & Park, J.-G. Aortic aneurysms: current pathogenesis and therapeutic targets. *Experimental & Molecular Medicine* 55, 2519-2530 (2023). https://doi.org/10.1038/s12276-023-01130-w

6 Sakalihasan, N. *et al.* Abdominal aortic aneurysms. *Nature Reviews Disease Primers* 4, 34 (2018). https://doi.org/10.1038/s41572-018-0030-7

7 Nienaber, C. A. & Clough, R. E. Management of acute aortic dissection. *The Lancet* 385, 800-811 (2015). https://doi.org/https://doi.org/10.1016/S0140-6736(14)61005-9

8 De Bakey, M. E. *et al.* SURGICAL MANAGEMENT OF DISSECTING ANEURYSMS OF THE AORTA. *The Journal of Thoracic and Cardiovascular Surgery* 49, 130-149 (1965). https://doi.org/https://doi.org/10.1016/S0022-5223(19)33323-9

9 von Segesser, L. K. *et al.* Dissection of the descending thoracic aorta extending into the ascending aorta: A therapeutic challenge. *The Journal of Thoracic and Cardiovascular Surgery* 108, 755-761 (1994). https://doi.org/https://doi.org/10.1016/S0022-5223(94)70304-3

10 Daily, P. O., Trueblood, H. W., Stinson, E. B., Wuerflein, R. D. & Shumway, N. E. Management of acute aortic dissections. *Ann Thorac Surg* 10, 237-247 (1970). https://doi.org/10.1016/s0003-4975(10)65594-4

11 Sievers, H. H. *et al.* Aortic dissection reconsidered: type, entry site, malperfusion classification adding clarity and enabling outcome prediction. *Interact Cardiovasc Thorac Surg* 30, 451-457 (2020). https://doi.org/10.1093/icvts/ivz281

12 Bobadilla, J. L. & Kent, K. C. Screening for abdominal aortic aneurysms. *Adv Surg* 46, 101-109 (2012). https://doi.org/10.1016/j.yasu.2012.03.006

13 Writing Group, M. *et al.* 2010 ACCF/AHA/AATS/ACR/ASA/SCA/SCAI/SIR/STS/SVM Guidelines for the Diagnosis and Management of Patients With Thoracic Aortic Disease. *Circulation* 121, e266-e369 (2010). https://doi.org/10.1161/CIR.0b013e3181d4739e

14 Landenhed, M. *et al.* Risk profiles for aortic dissection and ruptured or surgically treated aneurysms: a prospective cohort study. *J Am Heart Assoc* 4, e001513 (2015). https://doi.org/10.1161/jaha.114.001513

15 Yamaguchi, T. *et al.* Population-based incidence and outcomes of acute aortic dissection in Japan. *Eur Heart J Acute Cardiovasc Care* 10, 701-709 (2021). https://doi.org/10.1093/ehjacc/zuab031
16 Song, P. *et al.* The Global and Regional Prevalence of Abdominal Aortic Aneurysms: A Systematic Review and Modeling Analysis. *Ann Surg* 277, 912-919 (2023). https://doi.org/10.1097/sla.0000000000005716
17 Sidloff, D. *et al.* Aneurysm Global Epidemiology Study. *Circulation* 129, 747-753 (2014). https://doi.org/10.1161/CIRCULATIONAHA.113.005457
18 Svensjö, S., Björck, M. & Wanhainen, A. Current prevalence of abdominal aortic aneurysm in 70-year-old women. *Br J Surg* 100, 367-372 (2013). https://doi.org/10.1002/bjs.8984
19 A comparative study of the prevalence of abdominal aortic aneurysms in the United Kingdom, Denmark, and Australia. *J Med Screen* 8, 46-50 (2001). https://doi.org/10.1136/jms.8.1.46
20 Sandiford, P., Mosquera, D. & Bramley, D. Trends in incidence and mortality from abdominal aortic aneurysm in New Zealand. *Br J Surg* 98, 645-651 (2011). https://doi.org/10.1002/bjs.7461
21 Powell, J. T. *et al.* Long-term outcomes of immediate repair compared with surveillance of small abdominal aortic aneurysms. *N Engl J Med* 346, 1445-1452 (2002). https://doi.org/10.1056/NEJMoa013527
22 Mofidi, R. *et al.* Influence of sex on expansion rate of abdominal aortic aneurysms. *Br J Surg* 94, 310-314 (2007). https://doi.org/10.1002/bjs.5573
23 Lo, R. C. *et al.* Relative importance of aneurysm diameter and body size for predicting abdominal aortic aneurysm rupture in men and women. *J Vasc Surg* 59, 1209-1216 (2014). https://doi.org/10.1016/j.jvs.2013.10.104
24 Solberg, S., Singh, K., Wilsgaard, T. & Jacobsen, B. K. Increased growth rate of abdominal aortic aneurysms in women. The Tromsø study. *Eur J Vasc Endovasc Surg* 29, 145-149 (2005). https://doi.org/10.1016/j.ejvs.2004.11.015
25 Trenner, M. *et al.* Effect Modification of Sex and Age for the Hospital Volume-Outcome Relationship in Abdominal Aortic Aneurysm Treatment: Secondary Data Analysis of the Nationwide German Diagnosis Related Groups Statistics From 2005 to 2014. *J Am Heart Assoc* 9, e014534 (2020). https://doi.org/10.1161/jaha.119.014534
26 Egorova, N. N. *et al.* Effect of gender on long-term survival after abdominal aortic aneurysm repair based on results from the Medicare national database. *J Vasc Surg* 54, 1-12.e16; discussion 11-12 (2011). https://doi.org/10.1016/j.jvs.2010.12.049
27 Abedi, N. N. *et al.* Gender and 30-day outcome in patients undergoing endovascular aneurysm repair (EVAR): An analysis using the ACS NSQIP dataset. *Journal of Vascular Surgery* 50, 486-491.e484 (2009). https://doi.org/https://doi.org/10.1016/j.jvs.2009.04.047
28 Fuentes Pérez, A., Lozano González, R., Lee, P. C., Vouyouka, A. & Erben, Y. Mortality After Ruptured Abdominal Aortic Aneurysm Repair in Women (Open and Endovascular Approaches): A Literature Review and Meta-Analysis. *J Surg Res* 305, 258-264 (2025). https://doi.org/10.1016/j.jss.2024.11.037
29 Marcaccio, C. L. *et al.* Disparities in reporting and representation by sex, race, and ethnicity in endovascular aortic device trials. *J Vasc Surg* 76, 1244-1252.e1242 (2022). https://doi.org/10.1016/j.jvs.2022.05.003
30 Isselbacher, E. M., Lino Cardenas, C. L. & Lindsay, M. E. Hereditary Influence in Thoracic Aortic Aneurysm and Dissection. *Circulation* 133, 2516-2528 (2016). https://doi.org/doi:10.1161/CIRCULATIONAHA.116.009762

31 Albornoz, G. *et al.* Familial Thoracic Aortic Aneurysms and Dissections—Incidence, Modes of Inheritance, and Phenotypic Patterns. *The Annals of Thoracic Surgery* 82, 1400-1405 (2006). https://doi.org/https://doi.org/10.1016/j.athoracsur.2006.04.098

32 Guo, D. C. *et al.* Mutations in smooth muscle alpha-actin (ACTA2) lead to thoracic aortic aneurysms and dissections. *Nat Genet* 39, 1488-1493 (2007). https://doi.org/10.1038/ng.2007.6

33 Hoffjan, S. *et al.* Three novel mutations in the ACTA2 gene in German patients with thoracic aortic aneurysms and dissections. *Eur J Hum Genet* 19, 520-524 (2011). https://doi.org/10.1038/ejhg.2010.239

34 Zhu, L. *et al.* Mutations in myosin heavy chain 11 cause a syndrome associating thoracic aortic aneurysm/aortic dissection and patent ductus arteriosus. *Nat Genet* 38, 343-349 (2006). https://doi.org/10.1038/ng1721

35 Wang, L. *et al.* Mutations in myosin light chain kinase cause familial aortic dissections. *Am J Hum Genet* 87, 701-707 (2010). https://doi.org/10.1016/j.ajhg.2010.10.006

36 Guo, D. C. *et al.* LOX Mutations Predispose to Thoracic Aortic Aneurysms and Dissections. *Circ Res* 118, 928-934 (2016). https://doi.org/10.1161/circresaha.115.307130

37 Gyftopoulos, A., Ziganshin, B. A., Elefteriades, J. A. & Ochoa Chaar, C. I. Comparison of Genes Associated with Thoracic and Abdominal Aortic Aneurysms. *Aorta (Stamford)* 11, 125-134 (2023). https://doi.org/10.1055/s-0043-57266

38 Aggarwal, S., Qamar, A., Sharma, V. & Sharma, A. Abdominal aortic aneurysm: A comprehensive review. *Exp Clin Cardiol* 16, 11-15 (2011).

39 Asmundo, L. *et al.* Incidental diagnosis and reporting rate of abdominal aortic aneurysms on lumbar spine magnetic resonance imaging. *Quantitative Imaging in Medicine and Surgery* 15, 3543-3550 (2025).

40 Kent, K. C. Abdominal Aortic Aneurysms. *New England Journal of Medicine* 371, 2101-2108 (2014). https://doi.org/doi:10.1056/NEJMcp1401430

41 von Allmen, R. S., Camm, A. J., Lüscher, T. F., Maurer, G. & Serruys, P. W. in *The ESC Textbook of Cardiovascular Medicine* (ed Raimund Erbel) 0 (Oxford University Press, 2018).

42 Schmitz-Rixen, T., Böckler, D., Vogl, T. J. & Grundmann, R. T. Endovascular and Open Repair of Abdominal Aortic Aneurysm. *Dtsch Arztebl Int* 117, 813-819 (2020). https://doi.org/10.3238/arztebl.2020.0813

43 Isselbacher, E. M. *et al.* 2022 ACC/AHA Guideline for the Diagnosis and Management of Aortic Disease. *JACC* 80, e223-e393 (2022). https://doi.org/doi:10.1016/j.jacc.2022.08.004

44 Gao, J. *et al.* The mechanism and therapy of aortic aneurysms. *Signal Transduction and Targeted Therapy* 8, 55 (2023). https://doi.org/10.1038/s41392-023-01325-7

45 DeRoo, E. *et al.* Endothelial Dysfunction in the Pathogenesis of Abdominal Aortic Aneurysm. *Biomolecules* 12 (2022). https://doi.org/10.3390/biom12040509

46 Thayaparan, D. *et al.* Endothelial dysfunction drives atherosclerotic plaque macrophage-dependent abdominal aortic aneurysm formation. *Nature Immunology* 26, 706-721 (2025). https://doi.org/10.1038/s41590-025-02132-8

47 Hasan, M. *et al.* Disturbed hemodynamics and oxidative stress interaction in endothelial dysfunction and AAA progression: Focus on Nrf2 pathway. *Int J Cardiol* 389, 131238 (2023). https://doi.org/10.1016/j.ijcard.2023.131238

48 Yang, X. *et al.* Targeting endothelial tight junctions to predict and protect thoracic aortic aneurysm and dissection. *Eur Heart J* 44, 1248-1261 (2023). https://doi.org/10.1093/eurheartj/ehac823
49 Kadoglou, N. P. & and Liapis, C. D. Matrix metalloproteinases: contribution to pathogenesis, diagnosis, surveillance and treatment of abdominal aortic aneurysms. *Current Medical Research and Opinion* 20, 419-432 (2004). https://doi.org/10.1185/030079904125003143
50 Sakalihasan, N., Limet, R. & Defawe, O. D. Abdominal aortic aneurysm. *The Lancet* 365, 1577-1589 (2005). https://doi.org/https://doi.org/10.1016/S0140-6736(05)66459-8
51 Longo, G. M. *et al.* Matrix metalloproteinases 2 and 9 work in concert to produce aortic aneurysms. *J Clin Invest* 110, 625-632 (2002). https://doi.org/10.1172/jci15334
52 Koole, D. *et al.* Intraluminal abdominal aortic aneurysm thrombus is associated with disruption of wall integrity. *Journal of Vascular Surgery* 57, 77-83 (2013). https://doi.org/https://doi.org/10.1016/j.jvs.2012.07.003
53 Tanios, F. *et al.* Interaction of biomechanics with extracellular matrix components in abdominal aortic aneurysm wall. *Eur J Vasc Endovasc Surg* 50, 167-174 (2015). https://doi.org/10.1016/j.ejvs.2015.03.021
54 Raaz, U. *et al.* Segmental aortic stiffening contributes to experimental abdominal aortic aneurysm development. *Circulation* 131, 1783-1795 (2015). https://doi.org/10.1161/circulationaha.114.012377
55 Wang, X. *et al.* Increased Collagen Deposition and Elevated Expression of Connective Tissue Growth Factor in Human Thoracic Aortic Dissection. *Circulation* 114, I-200-I-205 (2006). https://doi.org/10.1161/CIRCULATIONAHA.105.000240
56 Bobryshev, Y. V. & Lord, R. S. A. Vascular-associated lymphoid tissue (VALT) involvement in aortic aneurysm. *Atherosclerosis* 154, 15-21 (2001). https://doi.org/https://doi.org/10.1016/S0021-9150(00)00441-X
57 Chan, W. L. *et al.* Atherosclerotic Abdominal Aortic Aneurysm and the Interaction Between Autologous Human Plaque-Derived Vascular Smooth Muscle Cells, Type 1 NKT, and Helper T Cells. *Circulation Research* 96, 675-683 (2005). https://doi.org/10.1161/01.RES.0000160543.84254.f1
58 Takagi, H., Watanabe, T., Mizuno, Y., Kawai, N. & Umemoto, T. Circulating Interleukin-6 Levels Are Associated with Abdominal Aortic Aneurysm Presence: A Meta-analysis and Meta-regression of Case–Control Studies. *Annals of Vascular Surgery* 28, 1913-1922 (2014). https://doi.org/https://doi.org/10.1016/j.avsg.2014.06.058
59 Johnston, W. F. *et al.* Inhibition of Interleukin-1β Decreases Aneurysm Formation and Progression in a Novel Model of Thoracic Aortic Aneurysms. *Circulation* 130, S51-S59 (2014). https://doi.org/10.1161/CIRCULATIONAHA.113.006800
60 Guzik, B. *et al.* Mechanisms of oxidative stress in human aortic aneurysms — Association with clinical risk factors for atherosclerosis and disease severity. *International Journal of Cardiology* 168, 2389-2396 (2013). https://doi.org/https://doi.org/10.1016/j.ijcard.2013.01.278
61 Miller, F. J. *et al.* Oxidative Stress in Human Abdominal Aortic Aneurysms. *Arteriosclerosis, Thrombosis, and Vascular Biology* 22, 560-565 (2002). https://doi.org/10.1161/01.ATV.0000013778.72404.30
62 Siu, K. L., Miao, X. N. & Cai, H. Recoupling of eNOS with folic acid prevents abdominal aortic aneurysm formation in angiotensin II-infused apolipoprotein E

null mice. *PLoS One* 9, e88899 (2014). https://doi.org/10.1371/journal.pone.0088899

63 Chalupsky, K. & Cai, H. Endothelial dihydrofolate reductase: Critical for nitric oxide bioavailability and role in angiotensin II uncoupling of endothelial nitric oxide synthase. *Proceedings of the National Academy of Sciences* 102, 9056-9061 (2005). https://doi.org/doi:10.1073/pnas.0409594102

64 Owens, G. K. Regulation of differentiation of vascular smooth muscle cells. *Physiological Reviews* 75, 487-517 (1995). https://doi.org/10.1152/physrev.1995.75.3.487

65 Quintana, R. A. & Taylor, W. R. Cellular Mechanisms of Aortic Aneurysm Formation. *Circulation Research* 124, 607-618 (2019). https://doi.org/10.1161/CIRCRESAHA.118.313187

66 di Gioia, C. R. T., Ascione, A., Carletti, R. & Giordano, C. Thoracic Aorta: Anatomy and Pathology. *Diagnostics (Basel)* 13 (2023). https://doi.org/10.3390/diagnostics13132166

67 Yu, Y. *et al.* Vascular smooth muscle cell phenotypic switching in atherosclerosis. *Heliyon* 10, e37727 (2024). https://doi.org/10.1016/j.heliyon.2024.e37727

68 Bayliss, W. M. On the local reactions of the arterial wall to changes of internal pressure. *The Journal of Physiology* 28, 220-231 (1902). https://doi.org/https://doi.org/10.1113/jphysiol.1902.sp000911

69 Narayanan, A. S., Sandberg, L. B., Ross, R. & Layman, D. L. The smooth muscle cell. III. Elastin synthesis in arterial smooth muscle cell culture. *J Cell Biol* 68, 411-419 (1976). https://doi.org/10.1083/jcb.68.3.411

70 Tukaj, C. Enhanced proliferation of aortal smooth muscle cells treated by 1,25(OH)2D3 in vitro coincides with impaired formation of elastic fibres. *Int J Exp Pathol* 89, 117-124 (2008). https://doi.org/10.1111/j.1365-2613.2008.00578.x

71 Saphirstein, R. J. & Morgan, K. G. The contribution of vascular smooth muscle to aortic stiffness across length scales. *Microcirculation* 21, 201-207 (2014). https://doi.org/10.1111/micc.12101

72 Ross, R. The smooth muscle cell. II. Growth of smooth muscle in culture and formation of elastic fibers. *J Cell Biol* 50, 172-186 (1971). https://doi.org/10.1083/jcb.50.1.172

73 Bennett, M. R., Sinha, S. & Owens, G. K. Vascular Smooth Muscle Cells in Atherosclerosis. *Circulation Research* 118, 692-702 (2016). https://doi.org/10.1161/CIRCRESAHA.115.306361

74 Sorokin, V. *et al.* Role of Vascular Smooth Muscle Cell Plasticity and Interactions in Vessel Wall Inflammation. *Frontiers in Immunology* Volume 11 - 2020 (2020). https://doi.org/10.3389/fimmu.2020.599415

75 Lièvre, C. S. L. & Douarin, N. M. L. Mesenchymal derivatives of the neural crest: analysis of chimaeric quail and chick embryos. *Development* 34, 125-154 (1975). https://doi.org/10.1242/dev.34.1.125

76 Groot, A. C. G.-d., DeRuiter, M. C., Bergwerff, M. & Poelmann, R. E. Smooth Muscle Cell Origin and Its Relation to Heterogeneity in Development and Disease. *Arteriosclerosis, Thrombosis, and Vascular Biology* 19, 1589-1594 (1999). https://doi.org/10.1161/01.ATV.19.7.1589

77 Elmarasi, M. *et al.* Phenotypic switching of vascular smooth muscle cells in atherosclerosis, hypertension, and aortic dissection. *Journal of Cellular Physiology* 239, e31200 (2024). https://doi.org/https://doi.org/10.1002/jcp.31200

78 Chamley-Campbell, J., Campbell, G. R. & Ross, R. The smooth muscle cell in culture. *Physiological Reviews* 59, 1-61 (1979). https://doi.org/10.1152/physrev.1979.59.1.1
79 Nagai, R., Kuro-o, M., Babij, P. & Periasamy, M. Identification of two types of smooth muscle myosin heavy chain isoforms by cDNA cloning and immunoblot analysis. *J Biol Chem* 264, 9734-9737 (1989).
80 Lees-Miller, J. P., Heeley, D. H., Smillie, L. B. & Kay, C. M. Isolation and characterization of an abundant and novel 22-kDa protein (SM22) from chicken gizzard smooth muscle. *Journal of Biological Chemistry* 262, 2988-2993 (1987). https://doi.org/https://doi.org/10.1016/S0021-9258(18)61457-7
81 Miano, J. M., Long, X. & Fujiwara, K. Serum response factor: master regulator of the actin cytoskeleton and contractile apparatus. *Am J Physiol Cell Physiol* 292, C70-81 (2007). https://doi.org/10.1152/ajpcell.00386.2006
82 Salmon, M., Gomez, D., Greene, E., Shankman, L. & Owens, G. K. Cooperative binding of KLF4, pELK-1, and HDAC2 to a G/C repressor element in the SM22α promoter mediates transcriptional silencing during SMC phenotypic switching in vivo. *Circ Res* 111, 685-696 (2012). https://doi.org/10.1161/circresaha.112.269811
83 Wang, Z., Wang, D.-Z., Pipes, G. C. T. & Olson, E. N. Myocardin is a master regulator of smooth muscle gene expression. *Proceedings of the National Academy of Sciences* 100, 7129-7134 (2003). https://doi.org/doi:10.1073/pnas.1232341100
84 Horowitz, A., Menice, C. B., Laporte, R. & Morgan, K. G. Mechanisms of smooth muscle contraction. *Physiol Rev* 76, 967-1003 (1996). https://doi.org/10.1152/physrev.1996.76.4.967
85 Chadwick, C. C., Saito, A. & Fleischer, S. Isolation and characterization of the inositol trisphosphate receptor from smooth muscle. *Proc Natl Acad Sci U S A* 87, 2132-2136 (1990). https://doi.org/10.1073/pnas.87.6.2132
86 Amberg, G. C. & Navedo, M. F. Calcium dynamics in vascular smooth muscle. *Microcirculation* 20, 281-289 (2013). https://doi.org/10.1111/micc.12046
87 Moosmang, S. *et al.* Dominant role of smooth muscle L-type calcium channel Cav1.2 for blood pressure regulation. *Embo j* 22, 6027-6034 (2003). https://doi.org/10.1093/emboj/cdg583
88 Guo, R.-w. *et al.* Stim1- and Orai1-mediated store-operated calcium entry is critical for angiotensin II-induced vascular smooth muscle cell proliferation. *Cardiovascular Research* 93, 360-370 (2012). https://doi.org/10.1093/cvr/cvr307
89 Xu, S. Z. & Beech, D. J. TrpC1 is a membrane-spanning subunit of store-operated Ca(2+) channels in native vascular smooth muscle cells. *Circ Res* 88, 84-87 (2001). https://doi.org/10.1161/01.res.88.1.84
90 Van Lierop, J. E. *et al.* Activation of smooth muscle myosin light chain kinase by calmodulin. Role of LYS(30) and GLY(40). *J Biol Chem* 277, 6550-6558 (2002). https://doi.org/10.1074/jbc.M111404200
91 Rombouts, K. B. *et al.* The role of vascular smooth muscle cells in the development of aortic aneurysms and dissections. *Eur J Clin Invest* 52, e13697 (2022). https://doi.org/10.1111/eci.13697
92 Touyz, R. M. *et al.* Vascular smooth muscle contraction in hypertension. *Cardiovascular Research* 114, 529-539 (2018). https://doi.org/10.1093/cvr/cvy023

93 Tang, H. Y. *et al.* Vascular Smooth Muscle Cells Phenotypic Switching in Cardiovascular Diseases. *Cells* 11 (2022). https://doi.org/10.3390/cells11244060
94 Kawai-Kowase, K. & Owens, G. K. Multiple repressor pathways contribute to phenotypic switching of vascular smooth muscle cells. *American Journal of Physiology-Cell Physiology* 292, C59-C69 (2007). https://doi.org/10.1152/ajpcell.00394.2006
95 Ailawadi, G. *et al.* Smooth muscle phenotypic modulation is an early event in aortic aneurysms. *J Thorac Cardiovasc Surg* 138, 1392-1399 (2009). https://doi.org/10.1016/j.jtcvs.2009.07.075
96 Chen, R., McVey, D. G., Shen, D., Huang, X. & Ye, S. Phenotypic Switching of Vascular Smooth Muscle Cells in Atherosclerosis. *Journal of the American Heart Association* 12, e031121 (2023). https://doi.org/10.1161/JAHA.123.031121
97 Shankman, L. S. *et al.* KLF4-dependent phenotypic modulation of smooth muscle cells has a key role in atherosclerotic plaque pathogenesis. *Nature Medicine* 21, 628-637 (2015). https://doi.org/10.1038/nm.3866
98 Yap, C., Mieremet, A., de Vries, C. J. M., Micha, D. & de Waard, V. Six Shades of Vascular Smooth Muscle Cells Illuminated by KLF4 (Krüppel-Like Factor 4). *Arterioscler Thromb Vasc Biol* 41, 2693-2707 (2021). https://doi.org/10.1161/atvbaha.121.316600
99 Chen, P. Y. *et al.* Smooth Muscle Cell Reprogramming in Aortic Aneurysms. *Cell Stem Cell* 26, 542-557.e511 (2020). https://doi.org/10.1016/j.stem.2020.02.013
100 Steitz, S. A. *et al.* Smooth Muscle Cell Phenotypic Transition Associated With Calcification. *Circulation Research* 89, 1147-1154 (2001). https://doi.org/10.1161/hh2401.101070
101 Durham, A. L., Speer, M. Y., Scatena, M., Giachelli, C. M. & Shanahan, C. M. Role of smooth muscle cells in vascular calcification: implications in atherosclerosis and arterial stiffness. *Cardiovasc Res* 114, 590-600 (2018). https://doi.org/10.1093/cvr/cvy010
102 Sun, Y. *et al.* Smooth muscle cell-specific runx2 deficiency inhibits vascular calcification. *Circ Res* 111, 543-552 (2012). https://doi.org/10.1161/circresaha.112.267237
103 Wirka, R. C. *et al.* Atheroprotective roles of smooth muscle cell phenotypic modulation and the TCF21 disease gene as revealed by single-cell analysis. *Nat Med* 25, 1280-1289 (2019). https://doi.org/10.1038/s41591-019-0512-5
104 Hao, H. *et al.* Phenotypic modulation of intima and media smooth muscle cells in fatal cases of coronary artery lesion. *Arterioscler Thromb Vasc Biol* 26, 326-332 (2006). https://doi.org/10.1161/01.ATV.0000199393.74656.4c
105 Faggiotto, A., Ross, R. & Harker, L. Studies of hypercholesterolemia in the nonhuman primate. I. Changes that lead to fatty streak formation. *Arteriosclerosis* 4, 323-340 (1984). https://doi.org/10.1161/01.atv.4.4.323
106 Rong, J. X., Shapiro, M., Trogan, E. & Fisher, E. A. Transdifferentiation of mouse aortic smooth muscle cells to a macrophage-like state after cholesterol loading. *Proc Natl Acad Sci U S A* 100, 13531-13536 (2003). https://doi.org/10.1073/pnas.1735526100
107 Allahverdian, S., Chehroudi, A. C., McManus, B. M., Abraham, T. & Francis, G. A. Contribution of intimal smooth muscle cells to cholesterol accumulation and macrophage-like cells in human atherosclerosis. *Circulation* 129, 1551-1559 (2014). https://doi.org/10.1161/circulationaha.113.005015

108 Vengrenyuk, Y. *et al.* Cholesterol loading reprograms the microRNA-143/145-myocardin axis to convert aortic smooth muscle cells to a dysfunctional macrophage-like phenotype. *Arterioscler Thromb Vasc Biol* 35, 535-546 (2015). https://doi.org/10.1161/atvbaha.114.304029

109 Davies, J. D. *et al.* Adipocytic differentiation and liver x receptor pathways regulate the accumulation of triacylglycerols in human vascular smooth muscle cells. *J Biol Chem* 280, 3911-3919 (2005). https://doi.org/10.1074/jbc.M410075200

110 López-Candales, A. *et al.* Decreased vascular smooth muscle cell density in medial degeneration of human abdominal aortic aneurysms. *Am J Pathol* 150, 993-1007 (1997).

111 Zhang, J., Schmidt, J., Ryschich, E., Schumacher, H. & Allenberg, J. R. Increased apoptosis and decreased density of medial smooth muscle cells in human abdominal aortic aneurysms. *Chin Med J (Engl)* 116, 1549-1552 (2003).

112 Rowe, V. L. *et al.* Vascular smooth muscle cell apoptosis in aneurysmal, occlusive, and normal human aortas. *J Vasc Surg* 31, 567-576 (2000).

113 Henderson, E. L. *et al.* Death of smooth muscle cells and expression of mediators of apoptosis by T lymphocytes in human abdominal aortic aneurysms. *Circulation* 99, 96-104 (1999). https://doi.org/10.1161/01.cir.99.1.96

114 Wang, Q., Shu, C., Su, J. & Li, X. A crosstalk triggered by hypoxia and maintained by MCP-1/miR-98/IL-6/p38 regulatory loop between human aortic smooth muscle cells and macrophages leads to aortic smooth muscle cells apoptosis via Stat1 activation. *Int J Clin Exp Pathol* 8, 2670-2679 (2015).

115 Acilan, C. *et al.* Smooth muscle cells isolated from thoracic aortic aneurysms exhibit increased genomic damage, but similar tendency for apoptosis. *DNA Cell Biol* 31, 1523-1534 (2012). https://doi.org/10.1089/dna.2012.1644

116 Adiguzel, Z. *et al.* Evaluation of apoptotic molecular pathways for smooth muscle cells isolated from thoracic aortic aneurysms in response to oxidized sterols. *Mol Biol Rep* 41, 7875-7884 (2014). https://doi.org/10.1007/s11033-014-3681-9

117 Lu, H. *et al.* Vascular Smooth Muscle Cells in Aortic Aneurysm: From Genetics to Mechanisms. *Journal of the American Heart Association* 10, e023601 (2021). https://doi.org/10.1161/JAHA.121.023601

118 Zeng, T. *et al.* Cytokines in aortic dissection. *Clinica Chimica Acta* 486, 177-182 (2018). https://doi.org/https://doi.org/10.1016/j.cca.2018.08.005

119 Airhart, N. *et al.* Smooth muscle cells from abdominal aortic aneurysms are unique and can independently and synergistically degrade insoluble elastin. *J Vasc Surg* 60, 1033-1041; discussion 1041-1032 (2014). https://doi.org/10.1016/j.jvs.2013.07.097

120 Patel, M. I., Melrose, J., Ghosh, P. & Appleberg, M. Increased synthesis of matrix metalloproteinases by aortic smooth muscle cells is implicated in the etiopathogenesis of abdominal aortic aneurysms. *J Vasc Surg* 24, 82-92 (1996). https://doi.org/10.1016/s0741-5214(96)70148-9

121 Bou-Gharios, G., Ponticos, M., Rajkumar, V. & Abraham, D. Extra-cellular matrix in vascular networks. *Cell Prolif* 37, 207-220 (2004). https://doi.org/10.1111/j.1365-2184.2004.00306.x

122 Sukhova, G. K., Shi, G. P., Simon, D. I., Chapman, H. A. & Libby, P. Expression of the elastolytic cathepsins S and K in human atheroma and

regulation of their production in smooth muscle cells. *J Clin Invest* 102, 576-583 (1998). https://doi.org/10.1172/jci181

123 Lipp, C. *et al.* Expression of a disintegrin and metalloprotease in human abdominal aortic aneurysms. *J Vasc Res* 49, 198-206 (2012). https://doi.org/10.1159/000332959

124 Shen, M., Hu, M., Fedak, P. W. M., Oudit, G. Y. & Kassiri, Z. Cell-Specific Functions of ADAM17 Regulate the Progression of Thoracic Aortic Aneurysm. *Circ Res* 123, 372-388 (2018). https://doi.org/10.1161/circresaha.118.313181

125 Guo, X. & Chen, S. Y. Transforming growth factor-β and smooth muscle differentiation. *World J Biol Chem* 3, 41-52 (2012). https://doi.org/10.4331/wjbc.v3.i3.41

126 Shi, Y. & Massagué, J. Mechanisms of TGF-β Signaling from Cell Membrane to the Nucleus. *Cell* 113, 685-700 (2003). https://doi.org/https://doi.org/10.1016/S0092-8674(03)00432-X

127 Takeda, N. *et al.* TGF-β Signaling-Related Genes and Thoracic Aortic Aneurysms and Dissections. *Int J Mol Sci* 19 (2018). https://doi.org/10.3390/ijms19072125

128 Huang, C. & Zhang, W. Abdominal aortic aneurysm complicated by descending thoracic aortic dissection in a patient with TGFBR1 mutation. *Egyptian Journal of Medical Human Genetics* 25, 85 (2024). https://doi.org/10.1186/s43042-024-00556-9

129 Isselbacher, E. M., Cardenas, C. L. L. & Lindsay, M. E. Hereditary Influence in Thoracic Aortic Aneurysm and Dissection. *Circulation* 133, 2516-2528 (2016). https://doi.org/doi:10.1161/CIRCULATIONAHA.116.009762

130 Mizuguchi, T. *et al.* Heterozygous TGFBR2 mutations in Marfan syndrome. *Nat Genet* 36, 855-860 (2004). https://doi.org/10.1038/ng1392

131 Tran-Fadulu, V. *et al.* Analysis of multigenerational families with thoracic aortic aneurysms and dissections due to TGFBR1 or TGFBR2 mutations. *Journal of Medical Genetics* 46, 607 (2009). https://doi.org/10.1136/jmg.2008.062844

132 Schepers, D. *et al.* A mutation update on the LDS-associated genes TGFB2/3 and SMAD2/3. *Hum Mutat* 39, 621-634 (2018). https://doi.org/10.1002/humu.23407

133 Angelov, S. N. *et al.* TGF-β (Transforming Growth Factor-β) Signaling Protects the Thoracic and Abdominal Aorta From Angiotensin II-Induced Pathology by Distinct Mechanisms. *Arterioscler Thromb Vasc Biol* 37, 2102-2113 (2017). https://doi.org/10.1161/atvbaha.117.309401

134 Gallo, E. M. *et al.* Angiotensin II-dependent TGF-β signaling contributes to Loeys-Dietz syndrome vascular pathogenesis. *J Clin Invest* 124, 448-460 (2014). https://doi.org/10.1172/jci69666

135 Wang, Y. *et al.* TGF-beta activity protects against inflammatory aortic aneurysm progression and complications in angiotensin II-infused mice. *J Clin Invest* 120, 422-432 (2010). https://doi.org/10.1172/jci38136

136 Chen, X. *et al.* TGF-β Neutralization Enhances AngII-Induced Aortic Rupture and Aneurysm in Both Thoracic and Abdominal Regions. *PLoS One* 11, e0153811 (2016). https://doi.org/10.1371/journal.pone.0153811

137 Yang, P. *et al.* Smooth muscle cell-specific Tgfbr1 deficiency promotes aortic aneurysm formation by stimulating multiple signaling events. *Scientific Reports* 6, 35444 (2016). https://doi.org/10.1038/srep35444

138 Chen, P.-Y. *et al.* Smooth Muscle Cell Reprogramming in Aortic Aneurysms. *Cell Stem Cell* 26, 542-557.e511 (2020). https://doi.org/10.1016/j.stem.2020.02.013
139 Zhu, J. *et al.* Loss of Transforming Growth Factor Beta Signaling in Aortic Smooth Muscle Cells Causes Endothelial Dysfunction and Aortic Hypercontractility. *Arteriosclerosis, Thrombosis, and Vascular Biology* 41, 1956-1971 (2021). https://doi.org/doi:10.1161/ATVBAHA.121.315878
140 Dimopoulos, G. J., Semba, S., Kitazawa, K., Eto, M. & Kitazawa, T. Ca2+-Dependent Rapid Ca2+ Sensitization of Contraction in Arterial Smooth Muscle. *Circulation Research* 100, 121-129 (2007). https://doi.org/10.1161/01.RES.0000253902.90489.df
141 Matsuda, K., Lozinskaya, I. & Cox, R. H. Augmented contributions of voltage-gated Ca2+ channels to contractile responses in spontaneously hypertensive rat mesenteric arteries. *Am J Hypertens* 10, 1231-1239 (1997). https://doi.org/10.1016/s0895-7061(97)00225-2
142 Gao, Y. J. & Lee, R. M. Hydrogen peroxide induces a greater contraction in mesenteric arteries of spontaneously hypertensive rats through thromboxane A(2) production. *Br J Pharmacol* 134, 1639-1646 (2001). https://doi.org/10.1038/sj.bjp.0704420
143 Kitazawa, T., Eto, M., Woodsome, T. P. & Brautigan, D. L. Agonists Trigger G Protein-mediated Activation of the CPI-17 Inhibitor Phosphoprotein of Myosin Light Chain Phosphatase to Enhance Vascular Smooth Muscle Contractility*. *Journal of Biological Chemistry* 275, 9897-9900 (2000). https://doi.org/https://doi.org/10.1074/jbc.275.14.9897
144 Wilson, J. L. *et al.* Unraveling endothelin-1 induced hypercontractility of human pulmonary artery smooth muscle cells from patients with pulmonary arterial hypertension. *PLoS One* 13, e0195780 (2018). https://doi.org/10.1371/journal.pone.0195780
145 Tajima, H. *et al.* Enhanced vascular contraction induced by exposure to angiotensin II mediated by endothelin-1 biosynthesis following PKCβ activation. *American Journal of Physiology-Heart and Circulatory Physiology* 328, H484-H495 (2025). https://doi.org/10.1152/ajpheart.00541.2024
146 Zhu, J. *et al.* Loss of Transforming Growth Factor Beta Signaling in Aortic Smooth Muscle Cells Causes Endothelial Dysfunction and Aortic Hypercontractility. *Arterioscler Thromb Vasc Biol* 41, 1956-1971 (2021). https://doi.org/10.1161/atvbaha.121.315878
147 Fatehi-Hassanabad, Z., Fatehi, M. & Shahidi, M. I. Endothelial dysfunction in aortic rings and mesenteric beds isolated from deoxycorticosterone acetate hypertensive rats: possible involvement of protein kinase C. *European Journal of Pharmacology* 494, 199-204 (2004). https://doi.org/https://doi.org/10.1016/j.ejphar.2004.05.012
148 Huveneers, S., Daemen, M. J. A. P. & Hordijk, P. L. Between Rho(k) and a Hard Place. *Circulation Research* 116, 895-908 (2015). https://doi.org/10.1161/CIRCRESAHA.116.305720
149 Hannun, Y. A. & Obeid, L. M. Sphingolipids and their metabolism in physiology and disease. *Nature Reviews Molecular Cell Biology* 19, 175-191 (2018). https://doi.org/10.1038/nrm.2017.107
150 Thudichum, J. A Treatise on the chemical constitution of the brain: based throughout upon original researches. London: Bailliere, Tindall, and Cox. *Biomed. J. Digit. Proj* (1884).

151 Quinville, B. M., Deschenes, N. M., Ryckman, A. E. & Walia, J. S. A Comprehensive Review: Sphingolipid Metabolism and Implications of Disruption in Sphingolipid Homeostasis. *International Journal of Molecular Sciences* 22, 5793 (2021).
152 Futerman, A. H. & Hannun, Y. A. The complex life of simple sphingolipids. *EMBO Rep* 5, 777-782 (2004). https://doi.org/10.1038/sj.embor.7400208
153 Merrill, A. H. & Wang, E. Biosynthesis of long-chain (sphingoid) bases from serine by LM cells. Evidence for introduction of the 4-trans-double bond after de novo biosynthesis of N-acylsphinganine(s). *Journal of Biological Chemistry* 261, 3764-3769 (1986). https://doi.org/https://doi.org/10.1016/S0021-9258(17)35713-7
154 Merrill, A. H. Characterization of serine palmitoyltransferase activity in Chinese hamster ovary cells. *Biochimica et Biophysica Acta (BBA) - Lipids and Lipid Metabolism* 754, 284-291 (1983). https://doi.org/https://doi.org/10.1016/0005-2760(83)90144-3
155 Beeler, T. *et al.* The Saccharomyces cerevisiae TSC10/YBR265w gene encoding 3-ketosphinganine reductase is identified in a screen for temperature-sensitive suppressors of the Ca2+-sensitive csg2Delta mutant. *J Biol Chem* 273, 30688-30694 (1998). https://doi.org/10.1074/jbc.273.46.30688
156 Mandon, E. C., Ehses, I., Rother, J., van Echten, G. & Sandhoff, K. Subcellular localization and membrane topology of serine palmitoyltransferase, 3-dehydrosphinganine reductase, and sphinganine N-acyltransferase in mouse liver. *J Biol Chem* 267, 11144-11148 (1992).
157 Stoffel, W., LeKim, D. & Sticht, G. Biosynthesis of dihydrosphingosine in vitro. *Hoppe Seylers Z Physiol Chem* 349, 664-670 (1968). https://doi.org/10.1515/bchm2.1968.349.1.664
158 Kuo, A. & Hla, T. Regulation of cellular and systemic sphingolipid homeostasis. *Nature Reviews Molecular Cell Biology* 25, 802-821 (2024). https://doi.org/10.1038/s41580-024-00742-y
159 Fukasawa, M., Nishijima, M. & Hanada, K. Genetic Evidence for ATP-dependent Endoplasmic Reticulum-to-Golgi Apparatus Trafficking of Ceramide for Sphingomyelin Synthesis in Chinese Hamster Ovary Cells. *Journal of Cell Biology* 144, 673-685 (1999). https://doi.org/10.1083/jcb.144.4.673
160 Hanada, K. *et al.* Molecular machinery for non-vesicular trafficking of ceramide. *Nature* 426, 803-809 (2003). https://doi.org/10.1038/nature02188
161 Kolesnick, R. Signal transduction through the sphingomyelin pathway. *Mol Chem Neuropathol* 21, 287-297 (1994). https://doi.org/10.1007/bf02815356
162 Spence, M. W., Clarke, J. T. & Cook, H. W. Pathways of sphingomyelin metabolism in cultured fibroblasts from normal and sphingomyelin lipidosis subjects. *J Biol Chem* 258, 8595-8600 (1983).
163 Sugiura, M. *et al.* Ceramide Kinase, a Novel Lipid Kinase: MOLECULAR CLONING AND FUNCTIONAL CHARACTERIZATION *. *Journal of Biological Chemistry* 277, 23294-23300 (2002). https://doi.org/10.1074/jbc.M201535200
164 Dressler, K. A. & Kolesnick, R. N. Ceramide 1-phosphate, a novel phospholipid in human leukemia (HL-60) cells. Synthesis via ceramide from sphingomyelin. *J Biol Chem* 265, 14917-14921 (1990).
165 Parveen, F. *et al.* Role of Ceramidases in Sphingolipid Metabolism and Human Diseases. *Cells* 8 (2019). https://doi.org/10.3390/cells8121573
166 Schulze, H., Schepers, U. & Sandhoff, K. Overexpression and mass spectrometry analysis of mature human acid ceramidase. *Biol Chem* 388, 1333-1343 (2007). https://doi.org/10.1515/bc.2007.152

167 El Bawab, S. *et al.* Molecular cloning and characterization of a human mitochondrial ceramidase. *J Biol Chem* 275, 21508-21513 (2000). https://doi.org/10.1074/jbc.M002522200

168 Hwang, Y. H., Tani, M., Nakagawa, T., Okino, N. & Ito, M. Subcellular localization of human neutral ceramidase expressed in HEK293 cells. *Biochem Biophys Res Commun* 331, 37-42 (2005). https://doi.org/10.1016/j.bbrc.2005.03.134

169 Sakamoto, W., Coant, N., Canals, D., Obeid, L. M. & Hannun, Y. A. Functions of neutral ceramidase in the Golgi apparatus. *J Lipid Res* 59, 2116-2125 (2018). https://doi.org/10.1194/jlr.M088187

170 Gault, C. R., Obeid, L. M. & Hannun, Y. A. An overview of sphingolipid metabolism: from synthesis to breakdown. *Adv Exp Med Biol* 688, 1-23 (2010). https://doi.org/10.1007/978-1-4419-6741-1_1

171 Mao, C. *et al.* Cloning and characterization of a mouse endoplasmic reticulum alkaline ceramidase: an enzyme that preferentially regulates metabolism of very long chain ceramides. *J Biol Chem* 278, 31184-31191 (2003). https://doi.org/10.1074/jbc.M303875200

172 Xu, R., Antwi Boasiako, P. & Mao, C. Alkaline ceramidase family: The first two decades. *Cellular Signalling* 78, 109860 (2021). https://doi.org/https://doi.org/10.1016/j.cellsig.2020.109860

173 Kohama, T. *et al.* Molecular Cloning and Functional Characterization of Murine Sphingosine Kinase *. *Journal of Biological Chemistry* 273, 23722-23728 (1998). https://doi.org/10.1074/jbc.273.37.23722

174 Liu, H. *et al.* Molecular Cloning and Functional Characterization of a Novel Mammalian Sphingosine Kinase Type 2 Isoform *. *Journal of Biological Chemistry* 275, 19513-19520 (2000). https://doi.org/10.1074/jbc.M002759200

175 Maceyka, M. *et al.* SphK1 and SphK2, sphingosine kinase isoenzymes with opposing functions in sphingolipid metabolism. *J Biol Chem* 280, 37118-37129 (2005). https://doi.org/10.1074/jbc.M502207200

176 Johnson, K. R., Becker, K. P., Facchinetti, M. M., Hannun, Y. A. & Obeid, L. M. PKC-dependent activation of sphingosine kinase 1 and translocation to the plasma membrane. Extracellular release of sphingosine-1-phosphate induced by phorbol 12-myristate 13-acetate (PMA). *J Biol Chem* 277, 35257-35262 (2002). https://doi.org/10.1074/jbc.M203033200

177 Maceyka, M. *et al.* SphK1 and SphK2, Sphingosine Kinase Isoenzymes with Opposing Functions in Sphingolipid Metabolism*. *Journal of Biological Chemistry* 280, 37118-37129 (2005). https://doi.org/https://doi.org/10.1074/jbc.M502207200

178 Pyne, S., Long, J. S., Ktistakis, N. T. & Pyne, N. J. Lipid phosphate phosphatases and lipid phosphate signalling. *Biochem Soc Trans* 33, 1370-1374 (2005). https://doi.org/10.1042/bst0331370

179 Mandala, S. M. *et al.* Molecular cloning and characterization of a lipid phosphohydrolase that degrades sphingosine-1- phosphate and induces cell death. *Proc Natl Acad Sci U S A* 97, 7859-7864 (2000). https://doi.org/10.1073/pnas.120146897

180 Ogawa, C., Kihara, A., Gokoh, M. & Igarashi, Y. Identification and characterization of a novel human sphingosine-1-phosphate phosphohydrolase, hSPP2. *J Biol Chem* 278, 1268-1272 (2003). https://doi.org/10.1074/jbc.M209514200

181 Jasinska, R. *et al.* Lipid phosphate phosphohydrolase-1 degrades exogenous glycerolipid and sphingolipid phosphate esters. *Biochem J* 340 (Pt 3), 677-686 (1999).
182 Ogawa, C., Kihara, A., Gokoh, M. & Igarashi, Y. Identification and Characterization of a Novel Human Sphingosine-1-phosphate Phosphohydrolase, hSPP2*. *Journal of Biological Chemistry* 278, 1268-1272 (2003). https://doi.org/https://doi.org/10.1074/jbc.M209514200
183 Le Stunff, H., Galve-Roperh, I., Peterson, C., Milstien, S. & Spiegel, S. Sphingosine-1-phosphate phosphohydrolase in regulation of sphingolipid metabolism and apoptosis. *J Cell Biol* 158, 1039-1049 (2002). https://doi.org/10.1083/jcb.200203123
184 Zhou, J. & Saba, J. D. Identification of the first mammalian sphingosine phosphate lyase gene and its functional expression in yeast. *Biochem Biophys Res Commun* 242, 502-507 (1998). https://doi.org/10.1006/bbrc.1997.7993
185 Wakashima, T., Abe, K. & Kihara, A. Dual functions of the trans-2-enoyl-CoA reductase TER in the sphingosine 1-phosphate metabolic pathway and in fatty acid elongation. *J Biol Chem* 289, 24736-24748 (2014). https://doi.org/10.1074/jbc.M114.571869
186 Lee, M., Lee, S. Y. & Bae, Y.-S. Functional roles of sphingolipids in immunity and their implication in disease. *Experimental & Molecular Medicine* 55, 1110-1130 (2023). https://doi.org/10.1038/s12276-023-01018-9
187 Cartier, A. & Hla, T. Sphingosine 1-phosphate: Lipid signaling in pathology and therapy. *Science* 366, eaar5551 (2019). https://doi.org/doi:10.1126/science.aar5551
188 Venkataraman, K. *et al.* Vascular endothelium as a contributor of plasma sphingosine 1-phosphate. *Circ Res* 102, 669-676 (2008). https://doi.org/10.1161/circresaha.107.165845
189 Książek, M., Chacińska, M., Chabowski, A. & Baranowski, M. Sources, metabolism, and regulation of circulating sphingosine-1-phosphate. *J Lipid Res* 56, 1271-1281 (2015). https://doi.org/10.1194/jlr.R059543
190 Christoffersen, C. *et al.* Endothelium-protective sphingosine-1-phosphate provided by HDL-associated apolipoprotein M. *Proc Natl Acad Sci U S A* 108, 9613-9618 (2011). https://doi.org/10.1073/pnas.1103187108
191 Fleming, J. K. & Wojciak, J. M. Measuring Sphingosine-1-Phosphate/Protein Interactions with the Kinetic Exclusion Assay. *Methods Mol Biol* 1697, 1-8 (2018). https://doi.org/10.1007/7651_2017_5
192 Zhang, X. Y. *et al.* Specific tissue expression and cellular localization of human apolipoprotein M as determined by in situ hybridization. *Acta Histochem* 105, 67-72 (2003). https://doi.org/10.1078/0065-1281-00687
193 Christoffersen, C. *et al.* Endothelium-protective sphingosine-1-phosphate provided by HDL-associated apolipoprotein M. *Proceedings of the National Academy of Sciences* 108, 9613-9618 (2011). https://doi.org/doi:10.1073/pnas.1103187108
194 Christensen, P. M. *et al.* Impaired endothelial barrier function in apolipoprotein M-deficient mice is dependent on sphingosine-1-phosphate receptor 1. *Faseb j* 30, 2351-2359 (2016). https://doi.org/10.1096/fj.201500064
195 Lin, Y.-C. *et al.* Designer high-density lipoprotein particles enhance endothelial barrier function and suppress inflammation. *Science Signaling* 17, eadg9256 (2024). https://doi.org/doi:10.1126/scisignal.adg9256

196 Blaho, V. A. *et al.* HDL-bound sphingosine-1-phosphate restrains lymphopoiesis and neuroinflammation. *Nature* 523, 342-346 (2015). https://doi.org/10.1038/nature14462
197 Wilkerson, B. A., Grass, G. D., Wing, S. B., Argraves, W. S. & Argraves, K. M. Sphingosine 1-phosphate (S1P) carrier-dependent regulation of endothelial barrier: high density lipoprotein (HDL)-S1P prolongs endothelial barrier enhancement as compared with albumin-S1P via effects on levels, trafficking, and signaling of S1P1. *J Biol Chem* 287, 44645-44653 (2012). https://doi.org/10.1074/jbc.M112.423426
198 Hänel, P., Andréani, P. & Gräler, M. H. Erythrocytes store and release sphingosine 1-phosphate in blood. *Faseb j* 21, 1202-1209 (2007). https://doi.org/10.1096/fj.06-7433com
199 Yatomi, Y., Ruan, F., Hakomori, S. & Igarashi, Y. Sphingosine-1-phosphate: a platelet-activating sphingolipid released from agonist-stimulated human platelets. *Blood* 86, 193-202 (1995).
200 Kawahara, A. *et al.* The sphingolipid transporter spns2 functions in migration of zebrafish myocardial precursors. *Science* 323, 524-527 (2009). https://doi.org/10.1126/science.1167449
201 Kupperman, E., An, S., Osborne, N., Waldron, S. & Stainier, D. Y. R. A sphingosine-1-phosphate receptor regulates cell migration during vertebrate heart development. *Nature* 406, 192-195 (2000). https://doi.org/10.1038/35018092
202 Fukuhara, S. *et al.* The sphingosine-1-phosphate transporter Spns2 expressed on endothelial cells regulates lymphocyte trafficking in mice. *J Clin Invest* 122, 1416-1426 (2012). https://doi.org/10.1172/jci60746
203 Mendoza, A. *et al.* The transporter Spns2 is required for secretion of lymph but not plasma sphingosine-1-phosphate. *Cell Rep* 2, 1104-1110 (2012). https://doi.org/10.1016/j.celrep.2012.09.021
204 Schwab, S. R. *et al.* Lymphocyte sequestration through S1P lyase inhibition and disruption of S1P gradients. *Science* 309, 1735-1739 (2005). https://doi.org/10.1126/science.1113640
205 Matloubian, M. *et al.* Lymphocyte egress from thymus and peripheral lymphoid organs is dependent on S1P receptor 1. *Nature* 427, 355-360 (2004). https://doi.org/10.1038/nature02284
206 Schwab, S. R. *et al.* Lymphocyte Sequestration Through S1P Lyase Inhibition and Disruption of S1P Gradients. *Science* 309, 1735-1739 (2005). https://doi.org/doi:10.1126/science.1113640
207 Niazi, H. *et al.* Murine platelet production is suppressed by S1P release in the hematopoietic niche, not facilitated by blood S1P sensing. *Blood Advances* 3, 1702-1713 (2019). https://doi.org/https://doi.org/10.1182/bloodadvances.2019031948
208 Nguyen, T. Q. *et al.* Erythrocytes efficiently utilize exogenous sphingosines for S1P synthesis and export via Mfsd2b. *Journal of Biological Chemistry* 296, 100201 (2021). https://doi.org/https://doi.org/10.1074/jbc.RA120.012941
209 Vu, T. M. *et al.* Mfsd2b is essential for the sphingosine-1-phosphate export in erythrocytes and platelets. *Nature* 550, 524-528 (2017). https://doi.org/10.1038/nature24053
210 Hisano, Y., Kobayashi, N., Yamaguchi, A. & Nishi, T. Mouse SPNS2 Functions as a Sphingosine-1-Phosphate Transporter in Vascular Endothelial Cells. *PLOS ONE* 7, e38941 (2012). https://doi.org/10.1371/journal.pone.0038941

211 Le, T. N. U. *et al.* Mfsd2b and Spns2 are essential for maintenance of blood vessels during development and in anaphylactic shock. *Cell Reports* 40, 111208 (2022). https://doi.org/https://doi.org/10.1016/j.celrep.2022.111208
212 Zhao, P. *et al.* Efficacy of AAV9-mediated SGPL1 gene transfer in a mouse model of S1P lyase insufficiency syndrome. *JCI Insight* 6 (2021). https://doi.org/10.1172/jci.insight.145936
213 Martelletti, E., Ingham, N. J. & Steel, K. P. Reversal of an existing hearing loss by gene activation in Spns2 mutant mice. *Proceedings of the National Academy of Sciences* 120, e2307355120 (2023). https://doi.org/doi:10.1073/pnas.2307355120
214 Kharel, Y. *et al.* Mechanism of sphingosine 1-phosphate clearance from blood. *Biochemical Journal* 477, 925-935 (2020). https://doi.org/10.1042/bcj20190730
215 Strub, G. M., Maceyka, M., Hait, N. C., Milstien, S. & Spiegel, S. Extracellular and intracellular actions of sphingosine-1-phosphate. *Adv Exp Med Biol* 688, 141-155 (2010). https://doi.org/10.1007/978-1-4419-6741-1_10
216 Alvarez, S. E., Milstien, S. & Spiegel, S. Autocrine and paracrine roles of sphingosine-1-phosphate. *Trends Endocrinol Metab* 18, 300-307 (2007). https://doi.org/10.1016/j.tem.2007.07.005
217 Sukocheva, O. *et al.* Estrogen transactivates EGFR via the sphingosine 1-phosphate receptor Edg-3: the role of sphingosine kinase-1. *J Cell Biol* 173, 301-310 (2006). https://doi.org/10.1083/jcb.200506033
218 Mattie, M., Brooker, G. & Spiegel, S. Sphingosine-1-phosphate, a putative second messenger, mobilizes calcium from internal stores via an inositol trisphosphate-independent pathway. *J Biol Chem* 269, 3181-3188 (1994).
219 Wang, W., Graeler, M. H. & Goetzl, E. J. Type 4 sphingosine 1-phosphate G protein-coupled receptor (S1P4) transduces S1P effects on T cell proliferation and cytokine secretion without signaling migration. *Faseb j* 19, 1731-1733 (2005). https://doi.org/10.1096/fj.05-3730fje
220 Hobson, J. P. *et al.* Role of the Sphingosine-1-Phosphate Receptor EDG-1 in PDGF-Induced Cell Motility. *Science* 291, 1800-1803 (2001). https://doi.org/doi:10.1126/science.1057559
221 Massberg, S. *et al.* Immunosurveillance by hematopoietic progenitor cells trafficking through blood, lymph, and peripheral tissues. *Cell* 131, 994-1008 (2007). https://doi.org/10.1016/j.cell.2007.09.047
222 Hobson, J. P. *et al.* Role of the sphingosine-1-phosphate receptor EDG-1 in PDGF-induced cell motility. *Science* 291, 1800-1803 (2001). https://doi.org/10.1126/science.1057559
223 Rutherford, C. *et al.* Regulation of cell survival by sphingosine-1-phosphate receptor S1P1 via reciprocal ERK-dependent suppression of Bim and PI-3-kinase/protein kinase C-mediated upregulation of Mcl-1. *Cell Death Dis* 4, e927 (2013). https://doi.org/10.1038/cddis.2013.455
224 Lee, M.-J. *et al.* Sphingosine-1-Phosphate as a Ligand for the G Protein-Coupled Receptor EDG-1. *Science* 279, 1552-1555 (1998). https://doi.org/doi:10.1126/science.279.5356.1552
225 Xiao, S., Peng, K., Li, C., Long, Y. & Yu, Q. The role of sphingosine-1-phosphate in autophagy and related disorders. *Cell Death Discovery* 9, 380 (2023). https://doi.org/10.1038/s41420-023-01681-x
226 Lee, M. J. *et al.* Akt-mediated phosphorylation of the G protein-coupled receptor EDG-1 is required for endothelial cell chemotaxis. *Mol Cell* 8, 693-704 (2001). https://doi.org/10.1016/s1097-2765(01)00324-0

227 Ryu, Y. *et al.* Sphingosine-1-phosphate, a platelet-derived lysophospholipid mediator, negatively regulates cellular Rac activity and cell migration in vascular smooth muscle cells. *Circ Res* 90, 325-332 (2002). https://doi.org/10.1161/hh0302.104455

228 Li, M. H. *et al.* S1P/S1P1 signaling stimulates cell migration and invasion in Wilms tumor. *Cancer Lett* 276, 171-179 (2009). https://doi.org/10.1016/j.canlet.2008.11.025

229 Lee, M.-J., Evans, M. & Hla, T. The Inducible G Protein-coupled Receptor edg-1 Signals via the Gi/Mitogen-activated Protein Kinase Pathway (∗). *Journal of Biological Chemistry* 271, 11272-11279 (1996). https://doi.org/https://doi.org/10.1074/jbc.271.19.11272

230 Windh, R. T. *et al.* Differential coupling of the sphingosine 1-phosphate receptors Edg-1, Edg-3, and H218/Edg-5 to the G(i), G(q), and G(12) families of heterotrimeric G proteins. *J Biol Chem* 274, 27351-27358 (1999). https://doi.org/10.1074/jbc.274.39.27351

231 Sugimoto, N., Takuwa, N., Okamoto, H., Sakurada, S. & Takuwa, Y. Inhibitory and stimulatory regulation of Rac and cell motility by the G12/13-Rho and Gi pathways integrated downstream of a single G protein-coupled sphingosine-1-phosphate receptor isoform. *Mol Cell Biol* 23, 1534-1545 (2003). https://doi.org/10.1128/mcb.23.5.1534-1545.2003

232 Ghosh, T. K., Bian, J. & Gill, D. L. Sphingosine 1-phosphate generated in the endoplasmic reticulum membrane activates release of stored calcium. *Journal of Biological Chemistry* 269, 22628-22635 (1994). https://doi.org/https://doi.org/10.1016/S0021-9258(17)31692-7

233 Zhang, Q., Peyruchaud, O., French, K. J., Magnusson, M. K. & Mosher, D. F. Sphingosine 1-Phosphate Stimulates Fibronectin Matrix Assembly Through a Rho-Dependent Signal Pathway. *Blood* 93, 2984-2990 (1999). https://doi.org/https://doi.org/10.1182/blood.V93.9.2984

234 Yamazaki, Y. *et al.* Edg-6 as a putative sphingosine 1-phosphate receptor coupling to Ca(2+) signaling pathway. *Biochem Biophys Res Commun* 268, 583-589 (2000). https://doi.org/10.1006/bbrc.2000.2162

235 Kim, E.-S. *et al.* Sphingosine 1-phosphate regulates matrix metalloproteinase-9 expression and breast cell invasion through S1P3–Gαq coupling. *Journal of Cell Science* 124, 2220-2230 (2011). https://doi.org/10.1242/jcs.076794

236 Sanchez, T. *et al.* PTEN as an effector in the signaling of antimigratory G protein-coupled receptor. *Proc Natl Acad Sci U S A* 102, 4312-4317 (2005). https://doi.org/10.1073/pnas.0409784102

237 Gräler, M. H., Bernhardt, G. & Lipp, M. EDG6, a novel G-protein-coupled receptor related to receptors for bioactive lysophospholipids, is specifically expressed in lymphoid tissue. *Genomics* 53, 164-169 (1998). https://doi.org/10.1006/geno.1998.5491

238 Im, D. S. *et al.* Characterization of a novel sphingosine 1-phosphate receptor, Edg-8. *J Biol Chem* 275, 14281-14286 (2000). https://doi.org/10.1074/jbc.275.19.14281

239 Walzer, T. *et al.* Natural killer cell trafficking in vivo requires a dedicated sphingosine 1-phosphate receptor. *Nat Immunol* 8, 1337-1344 (2007). https://doi.org/10.1038/ni1523

240 Gräler, M. H. *et al.* The sphingosine 1-phosphate receptor S1P4 regulates cell shape and motility via coupling to Gi and G12/13. *J Cell Biochem* 89, 507-519 (2003). https://doi.org/10.1002/jcb.10537

241 Martínez-Morales, J. C., Romero-Ávila, M. T., Reyes-Cruz, G. & García-Sáinz, J. A. S1P(1) receptor phosphorylation, internalization, and interaction with Rab proteins: effects of sphingosine 1-phosphate, FTY720-P, phorbol esters, and paroxetine. *Biosci Rep* 38 (2018). https://doi.org/10.1042/bsr20181612

242 Reeves, P. M., Kang, Y. L. & Kirchhausen, T. Endocytosis of Ligand-Activated Sphingosine 1-Phosphate Receptor 1 Mediated by the Clathrin-Pathway. *Traffic* 17, 40-52 (2016). https://doi.org/10.1111/tra.12343

243 Thangada, S. *et al.* Cell-surface residence of sphingosine 1-phosphate receptor 1 on lymphocytes determines lymphocyte egress kinetics. *J Exp Med* 207, 1475-1483 (2010). https://doi.org/10.1084/jem.20091343

244 Rutherford, C. *et al.* Phosphorylation-independent internalisation and desensitisation of the human sphingosine-1-phosphate receptor S1P3. *Cell Signal* 17, 997-1009 (2005). https://doi.org/10.1016/j.cellsig.2004.11.018

245 Limbu, K. R. *et al.* Targeting sphingosine 1-phosphate and sphingosine kinases in pancreatic cancer: mechanisms and therapeutic potential. *Cancer Cell International* 24, 353 (2024). https://doi.org/10.1186/s12935-024-03535-7

246 Seol, G. H. *et al.* Sphingosine-1-Phosphate–Induced Intracellular Ca2+ Mobilization in Human Endothelial Cells. *Endothelium* 12, 263-269 (2005). https://doi.org/10.1080/10623320500476716

247 Itagaki, K. *et al.* Sphingosine 1-phosphate has dual functions in the regulation of endothelial cell permeability and Ca2+ metabolism. *J Pharmacol Exp Ther* 323, 186-191 (2007). https://doi.org/10.1124/jpet.107.121210

248 Hopson, K. P., Truelove, J., Chun, J., Wang, Y. & Waeber, C. S1P activates store-operated calcium entry via receptor- and non-receptor-mediated pathways in vascular smooth muscle cells. *Am J Physiol Cell Physiol* 300, C919-926 (2011). https://doi.org/10.1152/ajpcell.00350.2010

249 Bootman, M. D., Berridge, M. J. & Roderick, H. L. Calcium Signalling: More Messengers, More Channels, More Complexity. *Current Biology* 12, R563-R565 (2002). https://doi.org/https://doi.org/10.1016/S0960-9822(02)01055-2

250 Xu, S. Z. *et al.* A sphingosine-1-phosphate-activated calcium channel controlling vascular smooth muscle cell motility. *Circ Res* 98, 1381-1389 (2006). https://doi.org/10.1161/01.RES.0000225284.36490.a2

251 Strub, G. M. *et al.* Sphingosine-1-phosphate produced by sphingosine kinase 2 in mitochondria interacts with prohibitin 2 to regulate complex IV assembly and respiration. *Faseb j* 25, 600-612 (2011). https://doi.org/10.1096/fj.10-167502

252 Hait, N. C. *et al.* Regulation of histone acetylation in the nucleus by sphingosine-1-phosphate. *Science* 325, 1254-1257 (2009). https://doi.org/10.1126/science.1176709

253 Shen, Z., Liu, C., Liu, P., Zhao, J. & Xu, W. Sphingosine 1-phosphate (S1P) promotes mitochondrial biogenesis in Hep G2 cells by activating Peroxisome proliferator-activated receptor γ coactivator 1α (PGC-1α). *Cell Stress Chaperones* 19, 541-548 (2014). https://doi.org/10.1007/s12192-013-0480-5

254 Hong, S.-W. *et al.* Deficiency of Sphingosine-1-Phosphate Reduces the Expression of Prohibitin and Causes β-Cell Impairment via Mitochondrial Dysregulation. *Endocrinol Metab* 33, 403-412 (2018). https://doi.org/10.3803/EnM.2018.33.3.403

255 Coyle, P. K., Freedman, M. S., Cohen, B. A., Cree, B. A. C. & Markowitz, C. E. Sphingosine 1-phosphate receptor modulators in multiple sclerosis treatment: A practical review. *Ann Clin Transl Neurol* 11, 842-855 (2024). https://doi.org/10.1002/acn3.52017

256 Brinkmann, V. *et al.* The immune modulator FTY720 targets sphingosine 1-phosphate receptors. *J Biol Chem* 277, 21453-21457 (2002). https://doi.org/10.1074/jbc.C200176200
257 Brinkmann, V. *et al.* Fingolimod (FTY720): discovery and development of an oral drug to treat multiple sclerosis. *Nature Reviews Drug Discovery* 9, 883-897 (2010). https://doi.org/10.1038/nrd3248
258 Mandala, S. *et al.* Alteration of Lymphocyte Trafficking by Sphingosine-1-Phosphate Receptor Agonists. *Science* 296, 346-349 (2002). https://doi.org/doi:10.1126/science.1070238
259 Brinkmann, V. FTY720 (fingolimod) in Multiple Sclerosis: therapeutic effects in the immune and the central nervous system. *Br J Pharmacol* 158, 1173-1182 (2009). https://doi.org/10.1111/j.1476-5381.2009.00451.x
260 Kappos, L. *et al.* Oral Fingolimod (FTY720) for Relapsing Multiple Sclerosis. *New England Journal of Medicine* 355, 1124-1140 (2006). https://doi.org/doi:10.1056/NEJMoa052643
261 Gold, R. *et al.* Assessment of cardiac safety during fingolimod treatment initiation in a real-world relapsing multiple sclerosis population: a phase 3b, open-label study. *J Neurol* 261, 267-276 (2014). https://doi.org/10.1007/s00415-013-7115-8
262 Bravo, G. Á., Cedeño, R. R., Casadevall, M. P. & Ramió-Torrentà, L. Sphingosine-1-Phosphate (S1P) and S1P Signaling Pathway Modulators, from Current Insights to Future Perspectives. *Cells* 11, 2058 (2022).
263 Sandborn, W. J. *et al.* Etrasimod as induction and maintenance therapy for ulcerative colitis (ELEVATE): two randomised, double-blind, placebo-controlled, phase 3 studies. *Lancet* 401, 1159-1171 (2023). https://doi.org/10.1016/s0140-6736(23)00061-2
264 Scott, F. L. *et al.* Ozanimod (RPC1063) is a potent sphingosine-1-phosphate receptor-1 (S1P1) and receptor-5 (S1P5) agonist with autoimmune disease-modifying activity. *British Journal of Pharmacology* 173, 1778-1792 (2016). https://doi.org/https://doi.org/10.1111/bph.13476
265 Gergely, P. *et al.* The selective sphingosine 1-phosphate receptor modulator BAF312 redirects lymphocyte distribution and has species-specific effects on heart rate. *British Journal of Pharmacology* 167, 1035-1047 (2012). https://doi.org/https://doi.org/10.1111/j.1476-5381.2012.02061.x
266 Zhao, Z., Lv, Y., Gu, Z. C., Ma, C. L. & Zhong, M. K. Risk for Cardiovascular Adverse Events Associated With Sphingosine-1-Phosphate Receptor Modulators in Patients With Multiple Sclerosis: Insights From a Pooled Analysis of 15 Randomised Controlled Trials. *Front Immunol* 12, 795574 (2021). https://doi.org/10.3389/fimmu.2021.795574
267 Sandborn, W. J. *et al.* Ozanimod as Induction and Maintenance Therapy for Ulcerative Colitis. *New England Journal of Medicine* 385, 1280-1291 (2021). https://doi.org/doi:10.1056/NEJMoa2033617
268 Jozefczuk, E., Guzik, T. J. & Siedlinski, M. Significance of sphingosine-1-phosphate in cardiovascular physiology and pathology. *Pharmacological Research* 156, 104793 (2020). https://doi.org/https://doi.org/10.1016/j.phrs.2020.104793
269 Liu, Y. *et al.* Edg-1, the G protein-coupled receptor for sphingosine-1-phosphate, is essential for vascular maturation. *J Clin Invest* 106, 951-961 (2000). https://doi.org/10.1172/jci10905

270 Argraves, K. M. *et al.* Sphingosine-1-phosphate signaling promotes critical migratory events in vasculogenesis. *J Biol Chem* 279, 50580-50590 (2004). https://doi.org/10.1074/jbc.M404432200
271 Xiong, Y., Yang, P., Proia, R. L. & Hla, T. Erythrocyte-derived sphingosine 1-phosphate is essential for vascular development. *J Clin Invest* 124, 4823-4828 (2014). https://doi.org/10.1172/jci77685
272 Gaengel, K. *et al.* The sphingosine-1-phosphate receptor S1PR1 restricts sprouting angiogenesis by regulating the interplay between VE-cadherin and VEGFR2. *Dev Cell* 23, 587-599 (2012). https://doi.org/10.1016/j.devcel.2012.08.005
273 Jung, B. *et al.* Flow-regulated endothelial S1P receptor-1 signaling sustains vascular development. *Dev Cell* 23, 600-610 (2012). https://doi.org/10.1016/j.devcel.2012.07.015
274 Sanchez, T. *et al.* Induction of vascular permeability by the sphingosine-1-phosphate receptor-2 (S1P2R) and its downstream effectors ROCK and PTEN. *Arterioscler Thromb Vasc Biol* 27, 1312-1318 (2007). https://doi.org/10.1161/atvbaha.107.143735
275 Singleton, P. A., Dudek, S. M., Ma, S.-F. & Garcia, J. G. N. Transactivation of Sphingosine 1-Phosphate Receptors Is Essential for Vascular Barrier Regulation: NOVEL ROLE FOR HYALURONAN AND CD44 RECEPTOR FAMILY*. *Journal of Biological Chemistry* 281, 34381-34393 (2006). https://doi.org/https://doi.org/10.1074/jbc.M603680200
276 Wu, J. *et al.* Sphingosine-1-Phosphate Receptor 3 Induces Endothelial Barrier Loss via ADAM10-Mediated Vascular Endothelial-Cadherin Cleavage. *Int J Mol Sci* 24 (2023). https://doi.org/10.3390/ijms242216083
277 Sammani, S. *et al.* Differential effects of sphingosine 1-phosphate receptors on airway and vascular barrier function in the murine lung. *Am J Respir Cell Mol Biol* 43, 394-402 (2010). https://doi.org/10.1165/rcmb.2009-0223OC
278 Igarashi, J. & Michel, T. Sphingosine-1-phosphate and modulation of vascular tone. *Cardiovasc Res* 82, 212-220 (2009). https://doi.org/10.1093/cvr/cvp064
279 Nofer, J. R. *et al.* HDL induces NO-dependent vasorelaxation via the lysophospholipid receptor S1P3. *J Clin Invest* 113, 569-581 (2004). https://doi.org/10.1172/jci18004
280 Katunaric, B., SenthilKumar, G., Schulz, M. E., De Oliveira, N. & Freed, J. K. S1P (Sphingosine-1-Phosphate)-Induced Vasodilation in Human Resistance Arterioles During Health and Disease. *Hypertension* 79, 2250-2261 (2022). https://doi.org/10.1161/hypertensionaha.122.19862
281 Coussin, F., Scott, R. H., Wise, A. & Nixon, G. F. Comparison of Sphingosine 1-Phosphate–Induced Intracellular Signaling Pathways in Vascular Smooth Muscles. *Circulation Research* 91, 151-157 (2002). https://doi.org/10.1161/01.RES.0000028150.51130.36
282 Dantas, A. P., Igarashi, J. & Michel, T. Sphingosine 1-phosphate and control of vascular tone. *Am J Physiol Heart Circ Physiol* 284, H2045-2052 (2003). https://doi.org/10.1152/ajpheart.01089.2002
283 Morales-Ruiz, M. *et al.* Sphingosine 1-phosphate activates Akt, nitric oxide production, and chemotaxis through a Gi protein/phosphoinositide 3-kinase pathway in endothelial cells. *J Biol Chem* 276, 19672-19677 (2001). https://doi.org/10.1074/jbc.M009993200
284 Coussin, F., Scott, R. H., Wise, A. & Nixon, G. F. Comparison of sphingosine 1-phosphate-induced intracellular signaling pathways in vascular smooth

muscles: differential role in vasoconstriction. *Circ Res* 91, 151-157 (2002). https://doi.org/10.1161/01.res.0000028150.51130.36

285 Ohmori, T. *et al.* Sphingosine 1-phosphate induces contraction of coronary artery smooth muscle cells via S1P2. *Cardiovasc Res* 58, 170-177 (2003). https://doi.org/10.1016/s0008-6363(03)00260-8

286 Levkau, B. Sphingosine-1-Phosphate in the Regulation of Vascular Tone. *Circulation Research* 103, 231-233 (2008). https://doi.org/doi:10.1161/CIRCRESAHA.108.181610

287 Kerage, D., Gombos, R. B., Wang, S., Brown, M. & Hemmings, D. G. Sphingosine 1-phosphate-induced nitric oxide production simultaneously controls endothelial barrier function and vascular tone in resistance arteries. *Vascular Pharmacology* 140, 106874 (2021). https://doi.org/https://doi.org/10.1016/j.vph.2021.106874

288 Jujic, A. *et al.* Plasma S1P (Sphingosine-1-Phosphate) Links to Hypertension and Biomarkers of Inflammation and Cardiovascular Disease: Findings From a Translational Investigation. *Hypertension* 78, 195-209 (2021). https://doi.org/10.1161/hypertensionaha.120.17379

289 Forrest, M. *et al.* Immune cell regulation and cardiovascular effects of sphingosine 1-phosphate receptor agonists in rodents are mediated via distinct receptor subtypes. *J Pharmacol Exp Ther* 309, 758-768 (2004). https://doi.org/10.1124/jpet.103.062828

290 Greig, F. H. *et al.* Requirement for sphingosine kinase 1 in mediating phase 1 of the hypotensive response to anandamide in the anaesthetised mouse. *Eur J Pharmacol* 842, 1-9 (2019). https://doi.org/10.1016/j.ejphar.2018.10.027

291 Wilson, P. C. *et al.* Inhibition of Sphingosine Kinase 1 Ameliorates Angiotensin II-Induced Hypertension and Inhibits Transmembrane Calcium Entry via Store-Operated Calcium Channel. *Mol Endocrinol* 29, 896-908 (2015). https://doi.org/10.1210/me.2014-1388

292 Siedlinski, M. *et al.* Vascular transcriptome profiling identifies Sphingosine kinase 1 as a modulator of angiotensin II-induced vascular dysfunction. *Scientific Reports* 7, 44131 (2017). https://doi.org/10.1038/srep44131

293 Cantalupo, A. *et al.* Nogo-B regulates endothelial sphingolipid homeostasis to control vascular function and blood pressure. *Nature Medicine* 21, 1028-1037 (2015). https://doi.org/10.1038/nm.3934

294 Camm, J., Hla, T., Bakshi, R. & Brinkmann, V. Cardiac and vascular effects of fingolimod: Mechanistic basis and clinical implications. *American Heart Journal* 168, 632-644 (2014). https://doi.org/https://doi.org/10.1016/j.ahj.2014.06.028

295 Tölle, M. *et al.* Immunomodulator FTY720 Induces eNOS-Dependent Arterial Vasodilatation via the Lysophospholipid Receptor S1P3. *Circulation Research* 96, 913-920 (2005). https://doi.org/10.1161/01.RES.0000164321.91452.00

296 Skoura, A. *et al.* Sphingosine-1-phosphate receptor-2 function in myeloid cells regulates vascular inflammation and atherosclerosis. *Arterioscler Thromb Vasc Biol* 31, 81-85 (2011). https://doi.org/10.1161/atvbaha.110.213496

297 Keul, P. *et al.* Sphingosine-1-phosphate receptor 3 promotes recruitment of monocyte/macrophages in inflammation and atherosclerosis. *Circ Res* 108, 314-323 (2011). https://doi.org/10.1161/circresaha.110.235028

298 Nofer, J. R. *et al.* FTY720, a synthetic sphingosine 1 phosphate analogue, inhibits development of atherosclerosis in low-density lipoprotein receptor-deficient mice. *Circulation* 115, 501-508 (2007). https://doi.org/10.1161/circulationaha.106.641407

299 Galvani, S. *et al.* HDL-bound sphingosine 1-phosphate acts as a biased agonist for the endothelial cell receptor S1P1 to limit vascular inflammation. *Sci Signal* 8, ra79 (2015). https://doi.org/10.1126/scisignal.aaa2581

300 Gaengel, K. *et al.* The Sphingosine-1-Phosphate Receptor S1PR1 Restricts Sprouting Angiogenesis by Regulating the Interplay between VE-Cadherin and VEGFR2. *Developmental Cell* 23, 587-599 (2012). https://doi.org/https://doi.org/10.1016/j.devcel.2012.08.005

301 Igarashi, J., Bernier, S. G. & Michel, T. Sphingosine 1-Phosphate and Activation of Endothelial Nitric-oxide Synthase: DIFFERENTIAL REGULATION OF Akt AND MAP KINASE PATHWAYS BY EDG AND BRADYKININ RECEPTORS IN VASCULAR ENDOTHELIAL CELLS*. *Journal of Biological Chemistry* 276, 12420-12426 (2001). https://doi.org/https://doi.org/10.1074/jbc.M008375200

302 Keul, P. *et al.* Potent anti-inflammatory properties of HDL in vascular smooth muscle cells mediated by HDL-S1P and their impairment in coronary artery disease due to lower HDL-S1P: a new aspect of HDL dysfunction and its therapy. *Faseb j* 33, 1482-1495 (2019). https://doi.org/10.1096/fj.201801245R

303 Keul, P. *et al.* Sphingosine-1-Phosphate (S1P) Lyase Inhibition Aggravates Atherosclerosis and Induces Plaque Rupture in ApoE(-/-)Mice. *Int J Mol Sci* 23 (2022). https://doi.org/10.3390/ijms23179606

304 Surendran, A., Zhang, H., Stamenkovic, A. & Ravandi, A. Lipidomics and cardiovascular disease. *Biochimica et Biophysica Acta (BBA) - Molecular Basis of Disease* 1871, 167806 (2025). https://doi.org/https://doi.org/10.1016/j.bbadis.2025.167806

305 Martin, S. S. *et al.* 2024 Heart Disease and Stroke Statistics: A Report of US and Global Data From the American Heart Association. *Circulation* 149, e347-e913 (2024). https://doi.org/10.1161/cir.0000000000001209

306 Mensah, G. A., Fuster, V., Murray, C. J. L. & Roth, G. A. Global Burden of Cardiovascular Diseases and Risks, 1990-2022. *J Am Coll Cardiol* 82, 2350-2473 (2023). https://doi.org/10.1016/j.jacc.2023.11.007

307 Laaksonen, R. *et al.* Plasma ceramides predict cardiovascular death in patients with stable coronary artery disease and acute coronary syndromes beyond LDL-cholesterol. *Eur Heart J* 37, 1967-1976 (2016). https://doi.org/10.1093/eurheartj/ehw148

308 Campbell, M. K., Chew, N. W. S. & Mehta, A. Beyond Cholesterol: Unraveling Residual Lipidomic Risk in Cardiovascular Health. *Current Atherosclerosis Reports* 27, 37 (2025). https://doi.org/10.1007/s11883-025-01284-0

309 Poss, A. M. *et al.* Machine learning reveals serum sphingolipids as cholesterol-independent biomarkers of coronary artery disease. *The Journal of Clinical Investigation* 130, 1363-1376 (2020). https://doi.org/10.1172/JCI131838

310 Zhu, D. *et al.* Lipidomics Profiling and Risk of Coronary Artery Disease in the BioHEART-CT Discovery Cohort. *Biomolecules* 13 (2023). https://doi.org/10.3390/biom13060917

311 Hilvo, M. *et al.* Development and validation of a ceramide- and phospholipid-based cardiovascular risk estimation score for coronary artery disease patients. *Eur Heart J* 41, 371-380 (2020). https://doi.org/10.1093/eurheartj/ehz387

312 Hilvo, M. *et al.* Prediction of Residual Risk by Ceramide-Phospholipid Score in Patients With Stable Coronary Heart Disease on Optimal Medical Therapy.

Journal of the American Heart Association 9, e015258 (2020). https://doi.org/10.1161/JAHA.119.015258

313 Wittenbecher, C. *et al.* Lipid Profiles and Heart Failure Risk: Results From Two Prospective Studies. *Circ Res* 128, 309-320 (2021). https://doi.org/10.1161/circresaha.120.317883

314 Nurmohamed, N. S. *et al.* Proteomics and lipidomics in atherosclerotic cardiovascular disease risk prediction. *European Heart Journal* 44, 1594-1607 (2023). https://doi.org/10.1093/eurheartj/ehad161

315 Shoghli, M. *et al.* The Novel Ceramide- and Phosphatidylcholine-Based Risk Score for the Prediction of New-Onset of Hypertension. *Journal of Clinical Medicine* 12, 7524 (2023).

316 Leiherer, A. *et al.* Coronary Event Risk Test (CERT) as a Risk Predictor for the 10-Year Clinical Outcome of Patients with Peripheral Artery Disease. *J Clin Med* 12 (2023). https://doi.org/10.3390/jcm12196151

317 Ekroos, K., Jänis, M., Tarasov, K., Hurme, R. & Laaksonen, R. Lipidomics: a tool for studies of atherosclerosis. *Curr Atheroscler Rep* 12, 273-281 (2010). https://doi.org/10.1007/s11883-010-0110-y

318 Meeusen, J. W. *et al.* Plasma Ceramides. *Arteriosclerosis, Thrombosis, and Vascular Biology* 38, 1933-1939 (2018). https://doi.org/10.1161/ATVBAHA.118.311199

319 Vasile, V. C. & Jaffe, A. S. An enhanced ceramide-based approach for primary prevention of atherosclerotic events. *Eur Heart J Open* 1, oeab016 (2021). https://doi.org/10.1093/ehjopen/oeab016

320 Vasile, V. C. *et al.* Ceramide Scores Predict Cardiovascular Risk in the Community. *Arteriosclerosis, Thrombosis, and Vascular Biology* 41, 1558-1569 (2021). https://doi.org/10.1161/ATVBAHA.120.315530

321 Huang, H. *et al.* Plasma Lipidomics Identifies Unique Lipid Signatures and Potential Biomarkers for Patients With Aortic Dissection. *Front Cardiovasc Med* 8, 757022 (2021). https://doi.org/10.3389/fcvm.2021.757022

322 Xie, T. *et al.* Plasma Lipidomics Analysis Reveals the Potential Role of Lysophosphatidylcholines in Abdominal Aortic Aneurysm Progression and Formation. *Int J Mol Sci* 24 (2023). https://doi.org/10.3390/ijms241210253

323 Zhou, X. *et al.* Identification of Lysophosphatidylcholines and Sphingolipids as Potential Biomarkers for Acute Aortic Dissection via Serum Metabolomics. *Eur J Vasc Endovasc Surg* 57, 434-441 (2019). https://doi.org/10.1016/j.ejvs.2018.07.004

324 Saito, K. *et al.* Lipidomic signatures of aortic media from patients with atherosclerotic and nonatherosclerotic aneurysms. *Scientific Reports* 9, 15472 (2019). https://doi.org/10.1038/s41598-019-51885-4

325 Moxon, J. V. *et al.* Comparison of the Serum Lipidome in Patients With Abdominal Aortic Aneurysm and Peripheral Artery Disease. *Circulation: Cardiovascular Genetics* 7, 71-79 (2014). https://doi.org/10.1161/CIRCGENETICS.113.000343

326 Brinkmann, V., Cyster, J. G. & Hla, T. FTY720: Sphingosine 1-Phosphate Receptor-1 in the Control of Lymphocyte Egress and Endothelial Barrier Function. *American Journal of Transplantation* 4, 1019-1025 (2004). https://doi.org/https://doi.org/10.1111/j.1600-6143.2004.00476.x

327 Au - Lu, H. *et al. JoVE*, e53191 (2015). https://doi.org/doi:10.3791/53191

328 Ott, W. H. Antipyridoxine activity of 2,4-dimethyl-3-hydroxy-5-hydroxymethylpyridine in the chick. *Proc Soc Exp Biol Med* 61, 125-127 (1946). https://doi.org/10.3181/00379727-61-15247

329 Krege, J. H., Hodgin, J. B., Hagaman, J. R. & Smithies, O. A noninvasive computerized tail-cuff system for measuring blood pressure in mice. *Hypertension* 25, 1111-1115 (1995). https://doi.org/10.1161/01.hyp.25.5.1111

330 Chamberlain, C. M. *et al.* Perforin-independent extracellular granzyme B activity contributes to abdominal aortic aneurysm. *Am J Pathol* 176, 1038-1049 (2010). https://doi.org/10.2353/ajpath.2010.090700

331 Cao, R. Y., Amand, T., Ford, M. D., Piomelli, U. & Funk, C. D. The Murine Angiotensin II-Induced Abdominal Aortic Aneurysm Model: Rupture Risk and Inflammatory Progression Patterns. *Front Pharmacol* 1, 9 (2010). https://doi.org/10.3389/fphar.2010.00009

332 Daugherty, A., Manning, M. W. & Cassis, L. A. Antagonism of AT2 receptors augments angiotensin II-induced abdominal aortic aneurysms and atherosclerosis. *Br J Pharmacol* 134, 865-870 (2001). https://doi.org/10.1038/sj.bjp.0704331

333 Grynkiewicz, G., Poenie, M. & Tsien, R. Y. A new generation of Ca2+ indicators with greatly improved fluorescence properties. *Journal of Biological Chemistry* 260, 3440-3450 (1985). https://doi.org/https://doi.org/10.1016/S0021-9258(19)83641-4

334 Sensken, S.-C. *et al.* Redistribution of Sphingosine 1-Phosphate by Sphingosine Kinase 2 Contributes to Lymphopenia. *The Journal of Immunology* 184, 4133-4142 (2010). https://doi.org/10.4049/jimmunol.0903358

335 Saraff, K., Babamusta, F., Cassis, L. A. & Daugherty, A. Aortic Dissection Precedes Formation of Aneurysms and Atherosclerosis in Angiotensin II-Infused, Apolipoprotein E-Deficient Mice. *Arteriosclerosis, Thrombosis, and Vascular Biology* 23, 1621-1626 (2003). https://doi.org/doi:10.1161/01.ATV.0000085631.76095.64

336 Trachet, B. *et al.* Angiotensin II infusion into ApoE-/- mice: a model for aortic dissection rather than abdominal aortic aneurysm? *Cardiovasc Res* 113, 1230-1242 (2017). https://doi.org/10.1093/cvr/cvx128

337 Sawada, H., Lu, H. S., Cassis, L. A. & Daugherty, A. Twenty Years of Studying AngII (Angiotensin II)-Induced Abdominal Aortic Pathologies in Mice: Continuing Questions and Challenges to Provide Insight Into the Human Disease. *Arteriosclerosis, Thrombosis, and Vascular Biology* 42, 277-288 (2022). https://doi.org/doi:10.1161/ATVBAHA.121.317058

338 Manning, M. W., Cassis, L. A., Huang, J., Szilvassy, S. J. & Daugherty, A. Abdominal aortic aneurysms: fresh insights from a novel animal model of the disease. *Vascular Medicine* 7, 45-54 (2002). https://doi.org/10.1191/1358863x02vm413ra

339 Meissner, A. *et al.* Sphingosine-1-phosphate signalling-a key player in the pathogenesis of Angiotensin II-induced hypertension. *Cardiovasc Res* 113, 123-133 (2017). https://doi.org/10.1093/cvr/cvw256

340 Seto, S. W. *et al.* Impaired Acetylcholine-Induced Endothelium-Dependent Aortic Relaxation by Caveolin-1 in Angiotensin II-Infused Apolipoprotein-E (ApoE−/−) Knockout Mice. *PLOS ONE* 8, e58481 (2013). https://doi.org/10.1371/journal.pone.0058481

341 Yang, Q. & Hori, M. Characterization of Contractile Machinery of Vascular Smooth Muscles in Hypertension. *Life* 11, 702 (2021).

342 White, J. V., Haas, K., Phillips, S. & Comerota, A. J. Adventitial elastolysis is a primary event in aneurysm formation. *J Vasc Surg* 17, 371-380; discussion 380-371 (1993). https://doi.org/10.1067/mva.1993.43023

343 Campa, J. S., Greenhalgh, R. M. & Powell, J. T. Elastin degradation in abdominal aortic aneurysms. *Atherosclerosis* 65, 13-21 (1987). https://doi.org/10.1016/0021-9150(87)90003-7

344 Menashi, S., Campa, J. S., Greenhalgh, R. M. & Powell, J. T. Collagen in abdominal aortic aneurysm: Typing, content, and degradation. *Journal of Vascular Surgery* 6, 578-582 (1987). https://doi.org/https://doi.org/10.1016/0741-5214(87)90274-6

345 Wamhoff, B. R., Lynch, K. R., Macdonald, T. L. & Owens, G. K. Sphingosine-1-phosphate receptor subtypes differentially regulate smooth muscle cell phenotype. *Arterioscler Thromb Vasc Biol* 28, 1454-1461 (2008). https://doi.org/10.1161/atvbaha.107.159392

346 Lorenz, J. N., Arend, L. J., Robitz, R., Paul, R. J. & MacLennan, A. J. Vascular dysfunction in S1P2 sphingosine 1-phosphate receptor knockout mice. *Am J Physiol Regul Integr Comp Physiol* 292, R440-446 (2007). https://doi.org/10.1152/ajpregu.00085.2006

347 Allen, B. G. & Walsh, M. P. The biochemical basis of the regulation of smooth-muscle contraction. *Trends in Biochemical Sciences* 19, 362-368 (1994). https://doi.org/https://doi.org/10.1016/0968-0004(94)90112-0

348 Ikebe, M. Regulation of the function of mammalian myosin and its conformational change. *Biochemical and Biophysical Research Communications* 369, 157-164 (2008). https://doi.org/https://doi.org/10.1016/j.bbrc.2008.01.057

349 Spijkers, L. J., Alewijnse, A. E. & Peters, S. L. FTY720 (fingolimod) increases vascular tone and blood pressure in spontaneously hypertensive rats via inhibition of sphingosine kinase. *Br J Pharmacol* 166, 1411-1418 (2012). https://doi.org/10.1111/j.1476-5381.2012.01865.x

350 Cantalupo, A. *et al.* S1PR1 (Sphingosine-1-Phosphate Receptor 1) Signaling Regulates Blood Flow and Pressure. *Hypertension* 70, 426-434 (2017). https://doi.org/10.1161/hypertensionaha.117.09088

351 Ailawadi, G. *et al.* Smooth muscle phenotypic modulation is an early event in aortic aneurysms. *The Journal of Thoracic and Cardiovascular Surgery* 138, 1392-1399 (2009). https://doi.org/https://doi.org/10.1016/j.jtcvs.2009.07.075

352 Hla, T. Sphingosine 1-phosphate receptors. *Prostaglandins & Other Lipid Mediators* 64, 135-142 (2001). https://doi.org/https://doi.org/10.1016/S0090-6980(01)00109-5

353 Brinkmann, V. Sphingosine 1-phosphate receptors in health and disease: Mechanistic insights from gene deletion studies and reverse pharmacology. *Pharmacology & Therapeutics* 115, 84-105 (2007). https://doi.org/https://doi.org/10.1016/j.pharmthera.2007.04.006

354 Soltau, I. *et al.* Serum-Sphingosine-1-Phosphate Concentrations Are Inversely Associated with Atherosclerotic Diseases in Humans. *PLOS ONE* 11, e0168302 (2016). https://doi.org/10.1371/journal.pone.0168302

355 Sattler, K. *et al.* HDL-Bound Sphingosine 1-Phosphate (S1P) Predicts the Severity of Coronary Artery Atherosclerosis. *Cellular Physiology and Biochemistry* 34, 172-184 (2014). https://doi.org/10.1159/000362993

356 Edvinsson, C. *et al.* Sphingosine-1-Phosphate, a Marker of Endothelial Injury and Disease Severity in Preeclampsia. *Hypertension* 82, 914-925 (2025). https://doi.org/10.1161/HYPERTENSIONAHA.124.24118

357 Daugherty, A., Manning, M. W. & Cassis, L. A. Angiotensin II promotes atherosclerotic lesions and aneurysms in apolipoprotein E-deficient mice. *J Clin Invest* 105, 1605-1612 (2000). https://doi.org/10.1172/jci7818

358 Keul, P. *et al.* The Sphingosine-1-Phosphate Analogue FTY720 Reduces Atherosclerosis in Apolipoprotein E–Deficient Mice. *Arteriosclerosis, Thrombosis, and Vascular Biology* 27, 607-613 (2007). https://doi.org/10.1161/01.ATV.0000254679.42583.88

359 Meissner, A. *et al.* Sphingosine-1-phosphate signalling—a key player in the pathogenesis of Angiotensin II-induced hypertension. *Cardiovascular Research* 113, 123-133 (2016). https://doi.org/10.1093/cvr/cvw256

360 Kurano, M. & Yatomi, Y. Sphingosine 1-Phosphate and Atherosclerosis. *J Atheroscler Thromb* 25, 16-26 (2018). https://doi.org/10.5551/jat.RV17010

361 Siedlinski, M. *et al.* Vascular transcriptome profiling identifies Sphingosine kinase 1 as a modulator of angiotensin II-induced vascular dysfunction. *Sci Rep* 7, 44131 (2017). https://doi.org/10.1038/srep44131

362 Cassis, L. A. *et al.* ANG II infusion promotes abdominal aortic aneurysms independent of increased blood pressure in hypercholesterolemic mice. *Am J Physiol Heart Circ Physiol* 296, H1660-1665 (2009). https://doi.org/10.1152/ajpheart.00028.2009

363 Golledge, J. & Norman, P. E. Atherosclerosis and abdominal aortic aneurysm: cause, response, or common risk factors? *Arterioscler Thromb Vasc Biol* 30, 1075-1077 (2010). https://doi.org/10.1161/atvbaha.110.206573

364 Argraves, K. M. *et al.* High density lipoprotein-associated sphingosine 1-phosphate promotes endothelial barrier function. *J Biol Chem* 283, 25074-25081 (2008). https://doi.org/10.1074/jbc.M801214200

365 Goetzl, E. J. & Gräler, M. H. Sphingosine 1-phosphate and its type 1 G protein-coupled receptor: trophic support and functional regulation of T lymphocytes. *J Leukoc Biol* 76, 30-35 (2004). https://doi.org/10.1189/jlb.1103567

366 Langenskiöld, M., Smidfelt, K., Nordanstig, J., Bergström, G. & Tivesten, Å. Leukocyte subsets and abdominal aortic aneurysms detected by screening in men. *J Intern Med* 288, 345-355 (2020). https://doi.org/10.1111/joim.13040

367 Li, Y. *et al.* Single-Cell Transcriptome Analysis Reveals Dynamic Cell Populations and Differential Gene Expression Patterns in Control and Aneurysmal Human Aortic Tissue. *Circulation* 142, 1374-1388 (2020). https://doi.org/10.1161/circulationaha.120.046528

368 Hofmann, M., Brinkmann, V. & Zerwes, H. G. FTY720 preferentially depletes naive T cells from peripheral and lymphoid organs. *Int Immunopharmacol* 6, 1902-1910 (2006). https://doi.org/10.1016/j.intimp.2006.07.030

369 Koch, A. E. *et al.* Enhanced production of the chemotactic cytokines interleukin-8 and monocyte chemoattractant protein-1 in human abdominal aortic aneurysms. *American Journal of Pathology* 142, 1423-1431 (1993).

370 Hance, K. A., Tataria, M., Ziporin, S. J., Lee, J. K. & Thompson, R. W. Monocyte chemotactic activity in human abdominal aortic aneurysms: Role of elastin degradation peptides and the 67–kD cell surface elastin receptor. *Journal of Vascular Surgery* 35, 254-261 (2002). https://doi.org/https://doi.org/10.1067/mva.2002.120382

371 Asghar, M. Y., Kemppainen, K., Lassila, T. & Törnquist, K. Sphingosine 1-phosphate attenuates MMP2 and MMP9 in human anaplastic thyroid cancer C643 cells: Importance of S1P2. *PLOS ONE* 13, e0196992 (2018). https://doi.org/10.1371/journal.pone.0196992

372 Keul, P., Heusch, G. & Levkau, B. Sphingosine-1-phosphate (S1P) inhibits TNFA-induced MMP-9 expression (TIME) through S1P2-mediated activation

of PTEN. *Atherosclerosis* 241, e76-e77 (2015). https://doi.org/10.1016/j.atherosclerosis.2015.04.267

373 Wang, C., Qian, X., Sun, X. & Chang, Q. Angiotensin II increases matrix metalloproteinase 2 expression in human aortic smooth muscle cells via AT1R and ERK1/2. *Exp Biol Med (Maywood)* 240, 1564-1571 (2015). https://doi.org/10.1177/1535370215576312

374 Yaghooti, H., Firoozrai, M., Fallah, S. & Khorramizadeh, M. R. Angiotensin II Differentially Induces Matrix Metalloproteinase-9 and Tissue Inhibitor of Metalloproteinase-1 Production and Disturbs MMP/TIMP Balance. *Avicenna J Med Biotechnol* 2, 79-85 (2010).

375 MacSweeney, S. T., Powell, J. T. & Greenhalgh, R. M. Pathogenesis of abdominal aortic aneurysm. *Br J Surg* 81, 935-941 (1994). https://doi.org/10.1002/bjs.1800810704

376 Neptune, E. R. *et al.* Dysregulation of TGF-beta activation contributes to pathogenesis in Marfan syndrome. *Nat Genet* 33, 407-411 (2003). https://doi.org/10.1038/ng1116

377 Lindsay, M. E. & Dietz, H. C. Lessons on the pathogenesis of aneurysm from heritable conditions. *Nature* 473, 308-316 (2011). https://doi.org/10.1038/nature10145

378 Li, W. *et al.* Tgfbr2 disruption in postnatal smooth muscle impairs aortic wall homeostasis. *J Clin Invest* 124, 755-767 (2014). https://doi.org/10.1172/jci69942

379 Xin, C. *et al.* Sphingosine 1-Phosphate Cross-activates the Smad Signaling Cascade and Mimics Transforming Growth Factor-β-induced Cell Responses *. *Journal of Biological Chemistry* 279, 35255-35262 (2004). https://doi.org/10.1074/jbc.M312091200

380 Kono, Y. *et al.* Sphingosine kinase 1 regulates differentiation of human and mouse lung fibroblasts mediated by TGF-beta1. *Am J Respir Cell Mol Biol* 37, 395-404 (2007). https://doi.org/10.1165/rcmb.2007-0065OC

381 Riemma, M. A. *et al.* Sphingosine-1-phosphate/TGF-β axis drives epithelial mesenchymal transition in asthma-like disease. *British Journal of Pharmacology* 179, 1753-1768 (2022). https://doi.org/https://doi.org/10.1111/bph.15754

382 Lee, C. Y. *et al.* Blockade of TGF-β (Transforming Growth Factor Beta) Signaling by Deletion of Tgfbr2 in Smooth Muscle Cells of 11-Month-Old Mice Alters Aortic Structure and Causes Vasomotor Dysfunction—Brief Report. *Arteriosclerosis, Thrombosis, and Vascular Biology* 42, 764-771 (2022). https://doi.org/10.1161/ATVBAHA.122.317603

383 Lockman, K. *et al.* Sphingosine 1-Phosphate Stimulates Smooth Muscle Cell Differentiation and Proliferation by Activating Separate Serum Response Factor Co-factors*. *Journal of Biological Chemistry* 279, 42422-42430 (2004). https://doi.org/https://doi.org/10.1074/jbc.M405432200

384 Kluk, M. J. & Hla, T. Role of the Sphingosine 1-Phosphate Receptor EDG-1 in Vascular Smooth Muscle Cell Proliferation and Migration. *Circulation Research* 89, 496-502 (2001). https://doi.org/doi:10.1161/hh1801.096338

385 Medlin, M. D., Staus, D. P., Dubash, A. D., Taylor, J. M. & Mack, C. P. Sphingosine 1-phosphate receptor 2 signals through leukemia-associated RhoGEF (LARG), to promote smooth muscle cell differentiation. *Arterioscler Thromb Vasc Biol* 30, 1779-1786 (2010). https://doi.org/10.1161/atvbaha.110.209395

386 Yang, S. *et al.* Myeloid-derived growth factor suppresses VSMC dedifferentiation and attenuates postinjury neointimal formation in rats by activating S1PR2 and its downstream signaling. *Acta Pharmacologica Sinica* 45, 98-111 (2024). https://doi.org/10.1038/s41401-023-01155-x
387 Majesky, M. W. Developmental Basis of Vascular Smooth Muscle Diversity. *Arteriosclerosis, Thrombosis, and Vascular Biology* 27, 1248-1258 (2007). https://doi.org/10.1161/ATVBAHA.107.141069
388 Haimovici, H. & Maier, N. FATE OF AORTIC HOMOGRAFTS IN CANINE ATHEROSCLEROSIS. 3. STUDY OF FRESH ABDOMINAL AND THORACIC AORTIC IMPLANTS INTO THORACIC AORTA: ROLE OF TISSUE SUSCEPTIBILITY IN ATHEROGENESIS. *Arch Surg* 89, 961-969 (1964). https://doi.org/10.1001/archsurg.1964.01320060029006
389 Haimovici, H. The role of arterial tissue susceptibility in atherogenesis. *Tex Heart Inst J* 18, 81-83 (1991).
390 Liu, Y. *et al.* Edg-1, the G protein-coupled receptor for sphingosine-1-phosphate, is essential for vascular maturation. *Journal of Clinical Investigation* 106, 951-961 (2000). https://doi.org/10.1172/JCI10905
391 Pan, G. *et al.* Inhibition of Sphingosine-1-Phosphate Receptor 2 Prevents Thoracic Aortic Dissection and Rupture. *Front Cardiovasc Med* 8, 748486 (2021). https://doi.org/10.3389/fcvm.2021.748486
392 Sawada, H., Beckner, Z. A., Ito, S., Daugherty, A. & Lu, H. S. β-Aminopropionitrile-induced aortic aneurysm and dissection in mice. *JVS Vasc Sci* 3, 64-72 (2022). https://doi.org/10.1016/j.jvssci.2021.12.002
393 Pitman, M. R. *et al.* The sphingosine 1-phosphate receptor 2/4 antagonist JTE-013 elicits off-target effects on sphingolipid metabolism. *Scientific Reports* 12, 454 (2022). https://doi.org/10.1038/s41598-021-04009-w
394 Salomone, S. *et al.* Analysis of sphingosine 1-phosphate receptors involved in constriction of isolated cerebral arteries with receptor null mice and pharmacological tools. *British Journal of Pharmacology* 153, 140-147 (2008). https://doi.org/https://doi.org/10.1038/sj.bjp.0707581
395 Shimizu, T. *et al.* Sphingosine-1-phosphate receptor 3 promotes neointimal hyperplasia in mouse iliac-femoral arteries. *Arterioscler Thromb Vasc Biol* 32, 955-961 (2012). https://doi.org/10.1161/atvbaha.111.241034
396 Rembold, C. M. *et al.* Cooperative attachment of cross bridges predicts regulation of smooth muscle force by myosin phosphorylation. *American Journal of Physiology-Cell Physiology* 287, C594-C602 (2004). https://doi.org/10.1152/ajpcell.00082.2004
397 Kimura, K. *et al.* Regulation of myosin phosphatase by Rho and Rho-associated kinase (Rho-kinase). *Science* 273, 245-248 (1996). https://doi.org/10.1126/science.273.5272.245
398 Uehata, M. *et al.* Calcium sensitization of smooth muscle mediated by a Rho-associated protein kinase in hypertension. *Nature* 389, 990-994 (1997). https://doi.org/10.1038/40187
399 Milewicz, D. M. *et al.* Altered Smooth Muscle Cell Force Generation as a Driver of Thoracic Aortic Aneurysms and Dissections. *Arterioscler Thromb Vasc Biol* 37, 26-34 (2017). https://doi.org/10.1161/atvbaha.116.303229
400 Meister, T. A. *et al.* Increased Arterial Responsiveness to Angiotensin II in Mice Conceived by Assisted Reproductive Technologies. *Int J Mol Sci* 23 (2022). https://doi.org/10.3390/ijms232113357

401 Leloup, A. J. A. *et al.* Short-Term Angiotensin II Treatment Affects Large Artery Biomechanics and Function in the Absence of Small Artery Alterations in Mice. *Front Physiol* 9, 582 (2018). https://doi.org/10.3389/fphys.2018.00582
402 Rodrigues-Diez, R. *et al.* Resolvin D2 prevents vascular remodeling, hypercontractility and endothelial dysfunction in obese hypertensive mice through modulation of vascular and proinflammatory factors. *Biomedicine & Pharmacotherapy* 174, 116564 (2024). https://doi.org/https://doi.org/10.1016/j.biopha.2024.116564
403 Villalobos-Molina, R., Uc, M., Hong, E. & García-Sáinz, J. A. Correlation between phosphatidylinositol labeling and contraction in rabbit aorta: effect of alpha-1 adrenergic activation. *J Pharmacol Exp Ther* 222, 258-261 (1982).
404 Wu, D., Katz, A., Lee, C. H. & Simon, M. I. Activation of phospholipase C by alpha 1-adrenergic receptors is mediated by the alpha subunits of Gq family. *J Biol Chem* 267, 25798-25802 (1992).
405 Hartmann, H. A., Mazzocca, N. J., Kleiman, R. B. & Houser, S. R. Effects of phenylephrine on calcium current and contractility of feline ventricular myocytes. *Am J Physiol* 255, H1173-1180 (1988). https://doi.org/10.1152/ajpheart.1988.255.5.H1173
406 de Gasparo, M., Catt, K. J., Inagami, T., Wright, J. W. & Unger, T. International Union of Pharmacology. XXIII. The Angiotensin II Receptors. *Pharmacological Reviews* 52, 415-472 (2000). https://doi.org/https://doi.org/10.1016/S0031-6997(24)01458-3
407 Griendling, K. K., Ushio-Fukai, M., Lassègue, B. & Alexander, R. W. Angiotensin II Signaling in Vascular Smooth Muscle. *Hypertension* 29, 366-370 (1997). https://doi.org/10.1161/01.HYP.29.1.366
408 Machida, T., Matamura, R., Iizuka, K. & Hirafuji, M. Cellular function and signaling pathways of vascular smooth muscle cells modulated by sphingosine 1-phosphate. *Journal of Pharmacological Sciences* 132, 211-217 (2016). https://doi.org/https://doi.org/10.1016/j.jphs.2016.05.010
409 Panta, C. R. *et al.* Sphingosine-1-Phosphate Enhances α(1)-Adrenergic Vasoconstriction via S1P2-G(12/13)-ROCK Mediated Signaling. *Int J Mol Sci* 20 (2019). https://doi.org/10.3390/ijms20246361
410 Pulli, I., Asghar, M. Y., Kemppainen, K. & Törnquist, K. Sphingolipid-mediated calcium signaling and its pathological effects. *Biochimica et Biophysica Acta (BBA) - Molecular Cell Research* 1865, 1668-1677 (2018). https://doi.org/https://doi.org/10.1016/j.bbamcr.2018.04.012
411 Sandoo, A., van Zanten, J. J., Metsios, G. S., Carroll, D. & Kitas, G. D. The endothelium and its role in regulating vascular tone. *Open Cardiovasc Med J* 4, 302-312 (2010). https://doi.org/10.2174/1874192401004010302
412 Furchgott, R. F. & Zawadzki, J. V. The obligatory role of endothelial cells in the relaxation of arterial smooth muscle by acetylcholine. *Nature* 288, 373-376 (1980). https://doi.org/10.1038/288373a0
413 Shatanawi, A. *et al.* Angiotensin II-induced vascular endothelial dysfunction through RhoA/Rho kinase/p38 mitogen-activated protein kinase/arginase pathway. *Am J Physiol Cell Physiol* 300, C1181-1192 (2011). https://doi.org/10.1152/ajpcell.00328.2010
414 Camerer, E. *et al.* Sphingosine-1-phosphate in the plasma compartment regulates basal and inflammation-induced vascular leak in mice. *J Clin Invest* 119, 1871-1879 (2009). https://doi.org/10.1172/jci38575
415 Weigel, C., Bellaci, J. & Spiegel, S. Sphingosine-1-phosphate and its receptors in vascular endothelial and lymphatic barrier function. *Journal of*

Biological Chemistry 299, 104775 (2023). https://doi.org/https://doi.org/10.1016/j.jbc.2023.104775

416 Komarova, Y. A., Mehta, D. & Malik, A. B. Dual regulation of endothelial junctional permeability. *Sci STKE* 2007, re8 (2007). https://doi.org/10.1126/stke.4122007re8

417 Shikata, Y., Birukov, K. G. & Garcia, J. G. S1P induces FA remodeling in human pulmonary endothelial cells: role of Rac, GIT1, FAK, and paxillin. *J Appl Physiol (1985)* 94, 1193-1203 (2003). https://doi.org/10.1152/japplphysiol.00690.2002

418 Nofer, J.-R. *et al.* HDL induces NO-dependent vasorelaxation via the lysophospholipid receptor S1P3. *The Journal of Clinical Investigation* 113, 569-581 (2004). https://doi.org/10.1172/JCI18004

419 Theilmeier, G. *et al.* High-density lipoproteins and their constituent, sphingosine-1-phosphate, directly protect the heart against ischemia/reperfusion injury in vivo via the S1P3 lysophospholipid receptor. *Circulation* 114, 1403-1409 (2006). https://doi.org/10.1161/circulationaha.105.607135

420 Salomone, S. *et al.* S1P3 receptors mediate the potent constriction of cerebral arteries by sphingosine-1-phosphate. *Eur J Pharmacol* 469, 125-134 (2003). https://doi.org/10.1016/s0014-2999(03)01731-x

421 Gajofatto, A., Turatti, M., Monaco, S. & Benedetti, M. D. Clinical efficacy, safety, and tolerability of fingolimod for the treatment of relapsing-remitting multiple sclerosis. *Drug, Healthcare and Patient Safety* 7, 157-167 (2015). https://doi.org/10.2147/DHPS.S69640

422 Brinkmann, V. *et al.* The Immune Modulator FTY720 Targets Sphingosine 1-Phosphate Receptors*. *Journal of Biological Chemistry* 277, 21453-21457 (2002). https://doi.org/https://doi.org/10.1074/jbc.C200176200

423 Paugh, S. W., Payne, S. G., Barbour, S. E., Milstien, S. & Spiegel, S. The immunosuppressant FTY720 is phosphorylated by sphingosine kinase type 2. *FEBS Lett* 554, 189-193 (2003). https://doi.org/10.1016/s0014-5793(03)01168-2

424 Mullershausen, F. *et al.* Persistent signaling induced by FTY720-phosphate is mediated by internalized S1P1 receptors. *Nat Chem Biol* 5, 428-434 (2009). https://doi.org/10.1038/nchembio.173

425 Gräler, M. H. & Goetzl, E. J. The immunosuppressant FTY720 down-regulates sphingosine 1-phosphate G protein-coupled receptors. *The FASEB Journal* 18, 551-553 (2004). https://doi.org/https://doi.org/10.1096/fj.03-0910fje

426 Mandala, S. *et al.* Alteration of lymphocyte trafficking by sphingosine-1-phosphate receptor agonists. *Science* 296, 346-349 (2002). https://doi.org/10.1126/science.1070238

427 Uchida, H. A. *et al.* Total lymphocyte deficiency attenuates AngII-induced atherosclerosis in males but not abdominal aortic aneurysms in apoE deficient mice. *Atherosclerosis* 211, 399-403 (2010). https://doi.org/10.1016/j.atherosclerosis.2010.02.034

428 Tölle, M. *et al.* Immunomodulator FTY720 Induces eNOS-dependent arterial vasodilatation via the lysophospholipid receptor S1P3. *Circ Res* 96, 913-920 (2005). https://doi.org/10.1161/01.Res.0000164321.91452.00

429 Cantalupo, A. & Di Lorenzo, A. S1P Signaling and De Novo Biosynthesis in Blood Pressure Homeostasis. *The Journal of Pharmacology and Experimental Therapeutics* 358, 359-370 (2016). https://doi.org/https://doi.org/10.1124/jpet.116.233205

430 Aslanidou, L. *et al.* Early Morphofunctional Changes in AngII-Infused Mice Contribute to Regional Onset of Aortic Aneurysm and Dissection. *J Vasc Res* 57, 367-375 (2020). https://doi.org/10.1159/000509545
431 Wang, X. *et al.* The TRPM7 chanzyme in smooth muscle cells drives abdominal aortic aneurysm in mice. *Nature Cardiovascular Research* 4, 216-234 (2025). https://doi.org/10.1038/s44161-025-00613-5
432 Zemann, B. *et al.* Sphingosine kinase type 2 is essential for lymphopenia induced by the immunomodulatory drug FTY720. *Blood* 107, 1454-1458 (2006). https://doi.org/10.1182/blood-2005-07-2628
433 Gräler, M. H. & Goetzl, E. J. The immunosuppressant FTY720 down-regulates sphingosine 1-phosphate G-protein-coupled receptors. *Faseb j* 18, 551-553 (2004). https://doi.org/10.1096/fj.03-0910fje
434 Sykes, D. A. *et al.* Investigating the molecular mechanisms through which FTY720-P causes persistent S1P1 receptor internalization. *Br J Pharmacol* 171, 4797-4807 (2014). https://doi.org/10.1111/bph.12620
435 Bravo, G., Cedeño, R. R., Casadevall, M. P. & Ramió-Torrentà, L. Sphingosine-1-Phosphate (S1P) and S1P Signaling Pathway Modulators, from Current Insights to Future Perspectives. *Cells* 11 (2022). https://doi.org/10.3390/cells11132058
436 Zhou, X. *et al.* Identification of Lysophosphatidylcholines and Sphingolipids as Potential Biomarkers for Acute Aortic Dissection via Serum Metabolomics. *European Journal of Vascular and Endovascular Surgery* 57, 434-441 (2019). https://doi.org/https://doi.org/10.1016/j.ejvs.2018.07.004
437 Allen-Redpath, K. *et al.* Phospholipid membranes drive abdominal aortic aneurysm development through stimulating coagulation factor activity. *Proceedings of the National Academy of Sciences* 116, 8038-8047 (2019). https://doi.org/doi:10.1073/pnas.1814409116
438 Tsimikas, S. & Witztum, J. L. Oxidized phospholipids in cardiovascular disease. *Nature Reviews Cardiology* 21, 170-191 (2024). https://doi.org/10.1038/s41569-023-00937-4
439 Cao, J. *et al.* Spatial Metabolomics Identifies LPC(18:0) and LPA(18:1) in Advanced Atheroma With Translation to Plasma for Cardiovascular Risk Estimation. *Arteriosclerosis, Thrombosis, and Vascular Biology* 44, 741-754 (2024). https://doi.org/doi:10.1161/ATVBAHA.123.320278
440 Paapstel, K. *et al.* Inverse relations of serum phosphatidylcholines and lysophosphatidylcholines with vascular damage and heart rate in patients with atherosclerosis. *Nutrition, Metabolism and Cardiovascular Diseases* 28, 44-52 (2018). https://doi.org/https://doi.org/10.1016/j.numecd.2017.07.011
441 Choi, R. H., Tatum, S. M., Symons, J. D., Summers, S. A. & Holland, W. L. Ceramides and other sphingolipids as drivers of cardiovascular disease. *Nature Reviews Cardiology* 18, 701-711 (2021). https://doi.org/10.1038/s41569-021-00536-1
442 Zhao, F. *et al.* Sphingolipid metabolites involved in the pathogenesis of atherosclerosis: perspectives on sphingolipids in atherosclerosis. *Cellular & Molecular Biology Letters* 30, 18 (2025). https://doi.org/10.1186/s11658-024-00679-2
443 Lucke, S. & Levkau, B. Endothelial functions of sphingosine-1-phosphate. *Cell Physiol Biochem* 26, 87-96 (2010). https://doi.org/10.1159/000315109
444 Nussbaum, C. *et al.* Sphingosine-1-phosphate receptor 3 promotes leukocyte rolling by mobilizing endothelial P-selectin. *Nat Commun* 6, 6416 (2015). https://doi.org/10.1038/ncomms7416

445 Yu, F. C. *et al.* Protective effect of sphingosine-1-phosphate for chronic intermittent hypoxia-induced endothelial cell injury. *Biochem Biophys Res Commun* 498, 1016-1021 (2018). https://doi.org/10.1016/j.bbrc.2018.03.106
446 Liu, W., Liu, B., Liu, S., Zhang, J. & Lin, S. Sphingosine-1-phosphate receptor 2 mediates endothelial cells dysfunction by PI3K-Akt pathway under high glucose condition. *European Journal of Pharmacology* 776, 19-25 (2016). https://doi.org/https://doi.org/10.1016/j.ejphar.2016.02.056
447 Weigel, C., Bellaci, J. & Spiegel, S. Sphingosine-1-phosphate and its receptors in vascular endothelial and lymphatic barrier function. *Journal of Biological Chemistry* 299 (2023). https://doi.org/10.1016/j.jbc.2023.104775
448 Takahashi, C. *et al.* Vehicle-dependent Effects of Sphingosine 1-phosphate on Plasminogen Activator Inhibitor-1 Expression. *J Atheroscler Thromb* 24, 954-969 (2017). https://doi.org/10.5551/jat.37663
449 Doppler, C. *et al.* Metabolomic profiling of ascending thoracic aortic aneurysms and dissections - Implications for pathophysiology and biomarker discovery. *PLOS ONE* 12, e0176727 (2017). https://doi.org/10.1371/journal.pone.0176727
450 Qu, Z., Cheuk, B. L. & Cheng, S. W. Differential expression of sphingosine-1-phosphate receptors in abdominal aortic aneurysms. *Mediators Inflamm* 2012, 643609 (2012). https://doi.org/10.1155/2012/643609
451 Witoslawska, A. *et al.* Ceramide and phosphatidylcholine lipids-based risk score predicts major cardiovascular outcomes in patients with heart failure. *Eur J Clin Invest* 55, e14359 (2025). https://doi.org/10.1111/eci.14359
452 Sonkusare, S. *et al.* Vascular calcium channels and high blood pressure: pathophysiology and therapeutic implications. *Vascul Pharmacol* 44, 131-142 (2006). https://doi.org/10.1016/j.vph.2005.10.005
453 Józefczuk, E. *et al.* Cardiovascular Effects of Pharmacological Targeting of Sphingosine Kinase 1. *Hypertension* 75, 383-392 (2020). https://doi.org/10.1161/HYPERTENSIONAHA.119.13450
454 Britten, C. D. *et al.* A Phase I Study of ABC294640, a First-in-Class Sphingosine Kinase-2 Inhibitor, in Patients with Advanced Solid Tumors. *Clinical Cancer Research* 23, 4642-4650 (2017). https://doi.org/10.1158/1078-0432.Ccr-16-2363
455 Ding, X. *et al.* Antitumor effect of the novel sphingosine kinase 2 inhibitor ABC294640 is enhanced by inhibition of autophagy and by sorafenib in human cholangiocarcinoma cells. *Oncotarget* 7, 20080-20092 (2016). https://doi.org/10.18632/oncotarget.7914
456 Hong Choi, O., Kim, J.-H. & Kinet, J.-P. Calcium mobilization via sphingosine kinase in signalling by the FcεRI antigen receptor. *Nature* 380, 634-636 (1996). https://doi.org/10.1038/380634a0
457 Quintana, R. A. & Taylor, W. R. Cellular Mechanisms of Aortic Aneurysm Formation. *Circ Res* 124, 607-618 (2019). https://doi.org/10.1161/circresaha.118.313187
458 Peng, Z. *et al.* Association between high-density lipoprotein cholesterol and risk of abdominal aortic aneurysm among males and females aged 60 years and over. *J Vasc Surg* 81, 894-904.e896 (2025). https://doi.org/10.1016/j.jvs.2024.12.004
459 Ya'ar Bar, S., Pintel, N., Abd Alghne, H., Khattib, H. & Avni, D. The therapeutic potential of sphingolipids for cardiovascular diseases. *Front Cardiovasc Med* 10, 1224743 (2023). https://doi.org/10.3389/fcvm.2023.1224743

460 SenthilKumar, G. *et al.* Ying and Yang of Ceramide in the Vascular Endothelium. *Arteriosclerosis, Thrombosis, and Vascular Biology* 44, 1725-1736 (2024). https://doi.org/10.1161/ATVBAHA.124.321158
461 Akhiyat, N. *et al.* Plasma Ceramide Levels Are Elevated in Patients With Early Coronary Atherosclerosis and Endothelial Dysfunction. *J Am Heart Assoc* 11, e022852 (2022). https://doi.org/10.1161/jaha.121.022852
462 Watts, J. D., Gu, M., Patterson, S. D., Aebersold, R. & Polverino, A. J. On the complexities of ceramide changes in cells undergoing apoptosis: lack of evidence for a second messenger function in apoptotic induction. *Cell Death & Differentiation* 6, 105-114 (1999). https://doi.org/10.1038/sj.cdd.4400472
463 Zietzer, A., Düsing, P., Reese, L., Nickenig, G. & Jansen, F. Ceramide Metabolism in Cardiovascular Disease: A Network With High Therapeutic Potential. *Arteriosclerosis, Thrombosis, and Vascular Biology* 42, 1220-1228 (2022). https://doi.org/10.1161/ATVBAHA.122.318048
464 Busch, A. *et al.* Translating mouse models of abdominal aortic aneurysm to the translational needs of vascular surgery. *JVS Vasc Sci* 2, 219-234 (2021). https://doi.org/10.1016/j.jvssci.2021.01.002
465 Shannon, A. H. *et al.* Porcine Model of Infrarenal Abdominal Aortic Aneurysm. *J Vis Exp* (2019). https://doi.org/10.3791/60169

8. Appendix

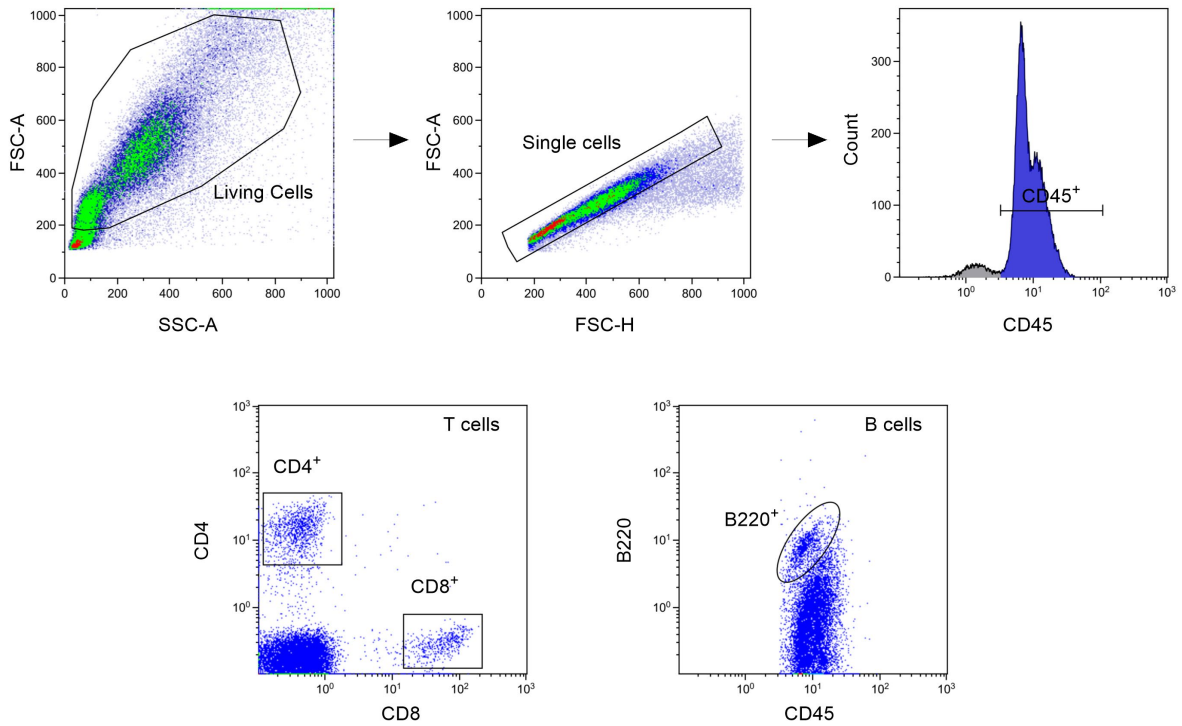

Figure S 1: Representative flow cytometric gating strategy to determine lymphocytes in whole blood. Whole blood was stained with fluorochrome-conjugated antibodies to identify $CD4^+$ and $CD8^+$ T-cells or B-cells. Living cells were selected on a forward-scatter area (FSC-A) versus side-scatter area (SSC-A) excluding cellular depris. Singlets were identified by plotting FSC-A against FSC height (FSC-H). Total leukocytes were identified as $CD45^+$ events. Within the $CD45^+$ gate, $CD4^+$ and $CD8^+$ T-cells were identified. B-cells were identified as $B220^+$ in the $CD45^+$ gate.

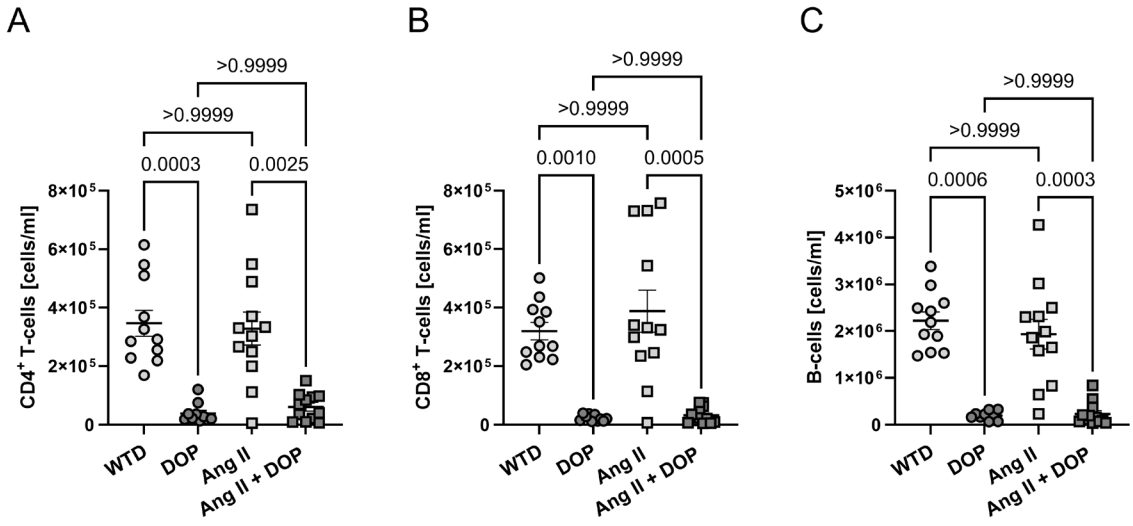

Figure S 2: Peripheral lymphopenia induced by pharmacological inhibition of the S1P lyase. Quantification of lymphocyte subsets in peripheral blood of mice fed a western-type diet (WTD), DOP-treated, Ang II-infused, or receiving a combination of DOP and Ang II for 28 days. (A) $CD4^+$ T cells (B) $CD8^+$ T cells and (C) B cells were quantified by flow cytometry. Data are presented as mean ± SEM (n = 10-12). Statistical analysis was performed using one-way ANOVA followed by multiple comparison testing.

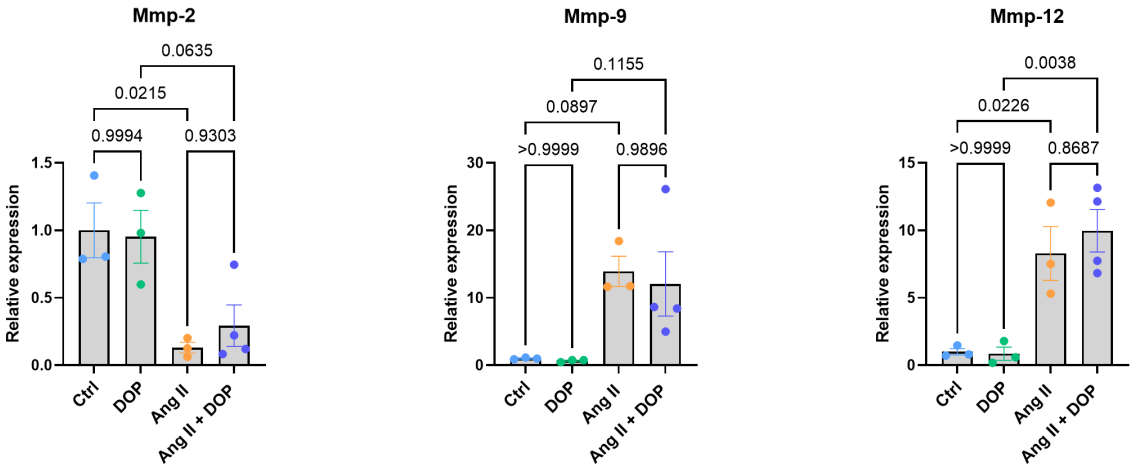

Figure S 3 Gene expression of matrix metalloproteinases (MMPs). Relative mRNA expression of Mmp-2, Mmp-9, Mmp-12 3 measured by qPCR in aortic tissue of ApoE$^{-/-}$ mice that received either a western-type diet (WTD), DOP (S1P lyase inhibitor, 30 mg/L in drinking water), Ang II (1,000 ng/kg/min for 28 days), or a combination of both treatments. (n= 3-4 per group) Data are presented as mean ± SEM. Only statistically significant differences relevant to the biological interpretation are displayed. Statistical analysis was performed using one-way ANOVA with multiple comparisons test.

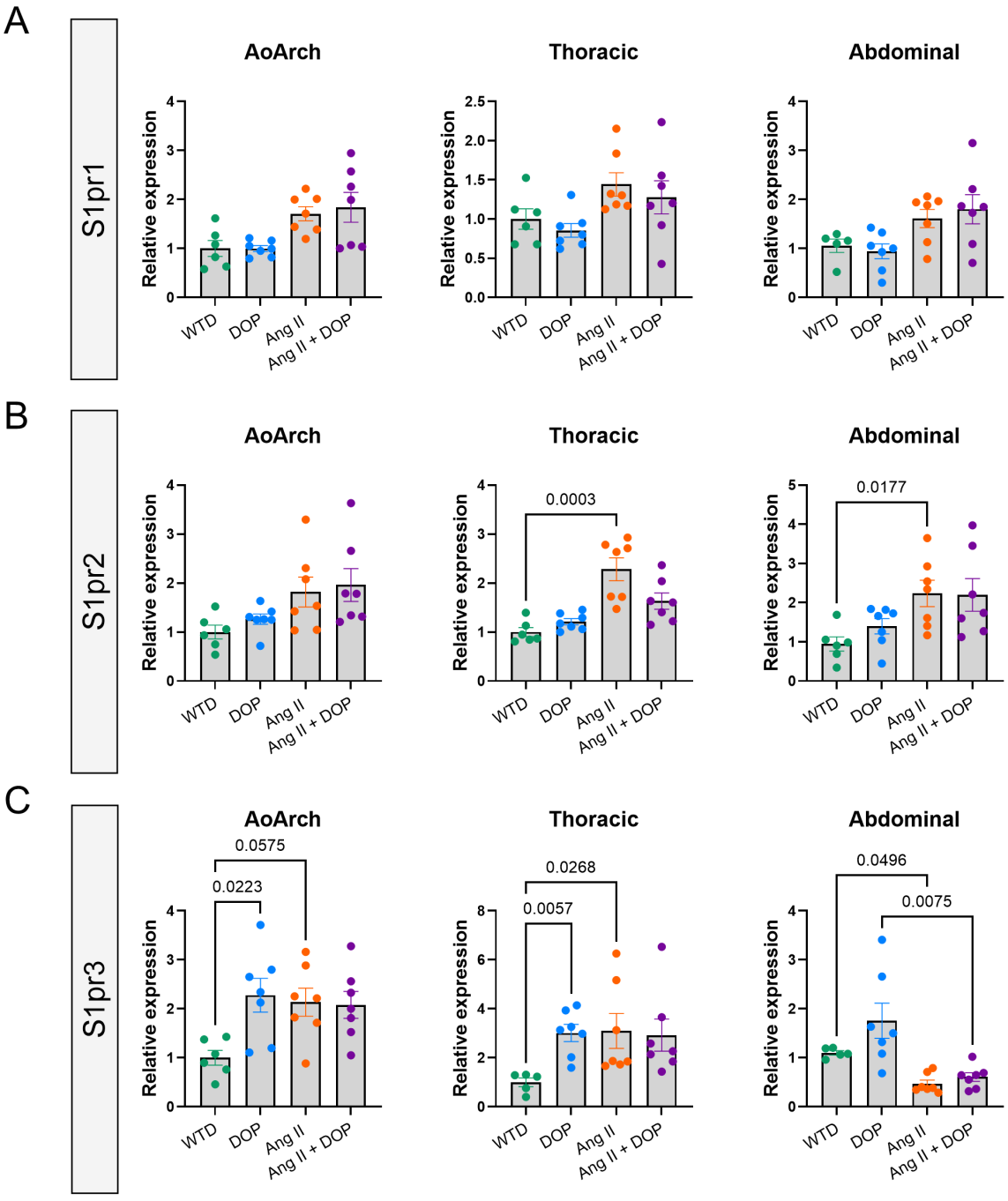

Figure S 4: Altered S1PR expression under Ang II infusion combined with pharmacological inhibition of the S1P lyase. Relative mRNA expression of (A) S1pr1, (B) S1pr2, and (C) S1pr3 was measured by qPCR in different aortic regions (aortic arch, thoracic aorta, and abdominal aorta) of ApoE$^{-/-}$ mice that received either a western-type diet (WTD), DOP (S1P lyase inhibitor, 30 mg/L in drinking water), Ang II (1,000 ng/kg/min for 28 days), or a combination of both treatments (n = 5-7 per group). Data are presented as mean ± SEM. Only statistically significant differences relevant to the biological interpretation are displayed. Statistical analysis was performed using one-way ANOVA with multiple comparisons test.

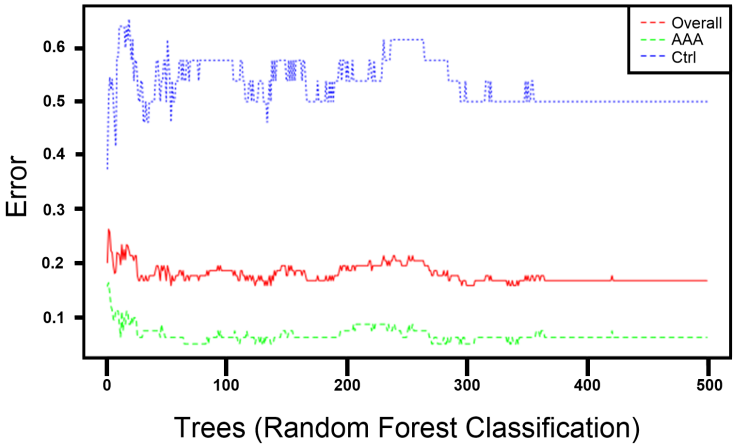

The OOB error is 0.167

	AAA	Ctrl	Class. error
AAA	77	5	0.061
Ctrl	13	13	0.5

Figure S 5: Random forest classification performance for distinguishing AAA patients from controls based on plasma lipid profiles. Out-of-bag (OOB) error rates are shown for the overall model (red), abdominal aortic aneurysm (AAA) group (green), and control (Ctrl) group (blue) as a function of the number of trees in the random forest. The model was trained using lipidomic data to classify samples as AAA or Ctrl. The table indicates the confusion matrix and class-specific error rates, with an overall OOB error rate of 0.167.

Table S 1 Sphingolipid levels in murine plasma

	WTD (A)	DOP (B)	Ang II (C)	Ang II+DOP (D)	p-value
Sph (d18:1)	22.13 ± 3.75	54.8 ± 5.22	42.61 ± 13.69	76.43 ± 12.03	ns
Cer (d18:1/14:0)	33.3 ± 3.11	152.5 ± 22.74	48.13 ± 4.45	257 ± 56.79	A vs B =0.0344 C vs D <0.0001
Cer (d18:1/16:0)	929.5 ± 125.1	3590 ± 616.6	1467 ± 187.50	8800 ± 1731	C vs D <0.0001 B vs D =0.0010
Cer (d18:1/18:0)	35.2 ± 7.31	144.7 ± 34.81	70.2 ± 12.61	313.5 ± 62.74	C vs D =0.0001 B vs D =0.0086
Cer (d18:1/22:0)	69.25 ± 19.32	230 ± 86.80	81.73 ± 16.27	141.2 ± 47.87	ns
Cer (d18:1/24:0)	99.2 ± 29.61	201.7 ± 71.60	118.1 ± 25.55	150.5 ± 39.39	ns
Cer (d18:1/24:1)	189.6 ± 31.64	1113 ± 252.6	343.3 ± 32.85	1259 ± 311.10	A vs B =0.0092 C vs D =0.0098

Table S 2 Sphingolipid levels in murine aortic tissue

	WTD (A)	DOP (B)	Ang II (C)	Ang II+DOP (D)	p-value
Sph (d18:1)	1.30 ± 0.29	20.08 ± 6.56	4.32 ± 1.11	54.56 ± 8.43	ns
Cer (d18:1/14:0)	0.37 ± 0.06	0.71 ± 0.23	0.58 ± 0.11	0.74 ± 0.14	A vs B =0.0344 C vs D <0.0001
Cer (d18:1/16:0)	9.09 ± 1.32	23.00 ± 5.77	22.68 ± 3.89	30.18 ± 7.85	C vs D <0.0001 B vs D =0.0010
Cer (d18:1/18:0)	2.72 ± 0.48	5.54 ± 1.85	4.92 ± 0.93	3.19 ± 0.37	C vs D =0.0001 B vs D =0.0086
Cer (d18:1/22:0)	7.99 ± 1.72	6.40 ± 1.73	16.60 ± 3.03	6.23 ± 1.33	ns
Cer (d18:1/24:0)	12.97 ± 2.61	10.04 ± 2.70	28.27 ± 5.10	10.27 ± 1.64	ns
Cer (d18:1/24:1)	21.82 ± 4.31	19.54 ± 4.55	44.02 ± 7.48	23.68 ± 6.55	A vs B =0.0092 C vs D =0.0098

Table S 3 Definitions of device parameters for blood pressure measurement

Preliminary Cycles	Preliminary cycles are cycles that serve to acclimatize the mouse before the actual measurement.
Measurement Cycles	Measurement cycles are the experimental consecutive number of cycles from which the final blood pressure is determined at the end.
Movement Detection	The algorithm for detecting movement distinguishes between large signals attributable to movement and those resulting from normal pulse amplitude. Should any motion be detected, the measurement process is consistently interrupted, restarting only if no further activity is recorded.
Minimum Pulse Amplitude	Lowest level of pulse signal that must be present before a pulse can be detected.
Number of Consecutive Peaks	The number of consecutive peaks defines the number of pulse peaks that must be detected before a pulse is declared and the actual measurement starts.
Maximum Pressure	Highest blood pressure value, which can be detected.
Pulse Timeout	Pulse timeout is the time span in which a pulse must be detected. If no pulse is detected, a new measuring cycle is started.
Measurement Timeout	Measurement timeout is the time span in which a pulse must be detected. If no pulse is detected, a new measuring cycle is started.
Time between Measurements	Time span between measurement cycles
Systolic Threshold	The systolic threshold is the percentage of the average pulse amplitude that must be reached for a systolic pressure reading to be declared.
Diastolic Threshold	The diastolic threshold is the inversion of the systolic threshold as the system recognizes the point at which the pulse signal first begins to decrease. As a result, the threshold accounts for a large percentage of the signal amplitude and is typically set at 50% of the average signal value.
Platform temperature	Constant temperature of the platform

Table S 4 Patient demographics (plasma cohort)

Baseline characteristics	**Ctrl n=27**	**AAA n=82**	**p-value**
General parameter			
Male sex - no. (%)	17 (62.96%)	61 (76.25%)	0.3255
Age - mean ± SD	44.92 ± 14.17	73.52 ± 8.02	<0.0001
BMI - mean ± SD (kg/m²)	23.33 ± 3.71	28.40 ± 5.34	<0.0001
Aneurysm size			
Diameter - mean ± SD (mm)	/	54.33 ± 16.22	-
Pre-existing diseases of the aorta			
Familial predisposition - no. (%)	1 (3.70%)	6 (7.31%)	0.6759
Medical history			
Obesity - no. (%)	11 (40.74%)	20 (24.39%)	0.1395
Nicotine abuse - no. (%)	5 (18.52%)	44 (53.66%)	0.0016
Diabetes Mellitus - no. (%)	1 (3.70%)	9 (10.98%)	0.4457
Hypertension - no. (%)	6 (22.22%)	62 (75.61%)	<0.0001
Dyslipidemia - no. (%)	1 (3.7%)	25 (30.49%)	0.0036
COPD - no. (%)	1 (3.7%)	3 (3.66%)	>0.9999
Coronary heart disease - no. (%)	5 (18.52%)	15 (18.29%)	>0.9999
Chronic kidney disease – no. (%)	0 (0%)	1 (1.22%)	>0.9999

Table S 5 Patient demographics (aortic tissue cohort)

Baseline characteristics	**Ctrl n=14**	**AAA n=33**	**p-value**
General parameter			
Male sex - no. (%)	8 (57.14%)	26 (81.25%)	0.1430
Age - mean ± SD	52.29 ± 18.38	68.45 ± 7.67	0.0063
BMI -mean ± SD (kg/m²)	24.51 ± 5.38	27.09 ± 3.41	0.1155
Aneurysm size			
Diameter – mean ± SD (mm)	/	59.84 ± 22.08	-
Pre-existing diseases of the aorta			
Familial predisposition – no. (%)	1 (7.14%)	2 (6.25%)	>0.9999
Medical history			
Obesity - no. (%)	6 (42.85%)	14 (43.75%)	>0.9999
Nicotine abuse - no. (%)	6 (42.86%)	23 (71.88%)	0.0969
Diabetes Mellitus - no. (%)	1 (7.14%)	3 (9.09%)	>0.9999
Hypertension - no. (%)	6 (42.86%)	25 (75.76%)	0.0447
Dyslipidemia - no. (%)	1 (7.14%)	7 (21.21%)	0.4048
COPD - no. (%)	1 (7.14%)	0 (0%)	0.2979
Coronary heart disease – no. (%)	5 (35.71%)	2 (6.06%)	0.0184
Chronic kidney disease – no. (%)	0 (0%)	0 (0%)	>0.9999

Table S 6 Sphingolipid levels in human plasma

Lipid species	Ctrl	AAA	p-value
S1P (d18:1)	349.7 ± 23.89	751.3 ± 33.84	<0.0001
Sphingosine (d18:1)	37.17 ± 5.22	23.63 ± 1.55	0.0510
Sphinganine (d18:1)	14.84 ± 2.39	9.88 ± 0.70	0.1687
Cer (d18:1/16:0)	366.1 ± 55.19	358.7 ± 19.44	0.3508
Cer (d18:1/18:0)	120.8 ± 26.65	133.3 ± 6.83	0.0008
Cer (d18:1/20:0)	129.3 ± 20.69	145.8 ± 8.78	0.0144
Cer (d18:1/22:0)	1061 ± 150.8	1196 ± 108.2	0.4360
Cer (d18:1/24:0)	1779 ± 161.1	2496 ± 96.26	0.0003
Cer (d18:1/24:1)	2017 ± 439.1	1932 ± 144.9	0.2768
SM (d18:1/14:0)	25363 ± 3455	21056 ± 1092	0.1014
SM (d18:1/14:1)	1971 ± 515.6	1299 ± 70.24	0.0439
SM (d18:1/16:0)	25723 ± 1827	20551 ± 547.1	0.0091
SM (d18:1/16:1)	7457 ± 1184	5142 ± 219.5	0.0230
SM (d18:1/18:0)	22630 ± 1886	19752 ± 904.8	0.2064
SM (d18:1/18:1)	10716 ± 918	8292 ± 372	0.0234
SM (d18:1/18:2)	453.7 ± 80.82	371.4 ± 16.2	0.4278
SM (d18:1/20:0)	71520 ± 7487	48750 ± 1929	0.0006
SM (d18:1/20:2)	176.1 ± 31.23	164.4 ± 11.52	0.8206
SM (d18:1/22:0)	6627 ± 1135	6826 ± 450	0.2646
SM (d18:1/22:6)	2430 ± 145.1	2648 ± 147.4	0.9416
SM (d18:1/24:1)	4976 ± 412.6	5713 ± 229.3	0.1152
LPC (14:0)	618.1 ± 74.05	711.4 ± 37.46	0.1221
LPC (16:0)	32652 ± 2112	30288 ± 721.4	0.5459
LPC (16:1)	1882 ± 300.5	1656 ± 103.2	0.3805
LPC (18:0)	11683 ± 637.9	13264 ± 388.6	0.0582
LPC (18:1)	25707 ± 1942	25647 ± 806.9	0.2959
LPC (18:2)	43491 ± 3050	42191 ± 1276	0.6375
LPC (20:1)	167.1 ± 10.55	186.2 ± 7.62	0.3260
LPC (20:2)	338.0 ± 24.15	391.6 ± 17.67	0.2412
LPC (20:3)	3417 ± 270.1	4105 ± 176.5	0.0483
LPC (20:4)	9129 ± 706.8	10537 ± 373.4	0.0169
LPC (20:5)	1191 ± 124.8	1554 ± 121.0	0.0716
LPC (22:6)	40594 ± 3065	45533 ± 2069	0.1965
PC (28:1)	679.7 ± 37.61	856.5 ± 33.98	0.0115
PC (30:2)	1383 ± 92.08	1562 ± 58.50	0.1106
PC (32:0)	2568 ± 285	2521 ± 160.5	0.5694
PC (32:1)	5555 ± 1100	4531 ± 358.0	0.8588
PC (32:2)	789.2 ± 119.1	727.4 ± 42.06	0.8753

PC (34:0)	959.4 ± 104.7	1025 ± 66.36	0.9517
PC (34:1)	30232 ± 3963	30108 ± 1714	0.7141
PC (34:2)	78996 ± 7208	68529 ± 3543	0.1479
PC (34:4)	176.4 ± 21.77	213.1 ± 14.21	0.1059
PC (36:1)	9314 ± 1023	11311 ± 711.3	0.1965
PC (36:2)	40647 ± 3448	42861 ± 2501	0.6375
PC (36:3)	11730 ± 1076	14680 ± 794.3	0.0564
PC (36:4)	39620 ± 3648	42174 ± 2137	0.7298
PC (36:5)	4575 ± 682.8	5211 ± 465.3	0.3472
PC (38:3)	11023 ± 1058	15673 ± 829.3	0.0033
PC (38:4)	25326 ± 2416	33077 ± 1939	0.0823
PC (38:5)	12812 ± 1155	15754 ± 752.4	0.0536
PC (38:6)	30324 ± 3746	30541 ± 1642	0.5138
PC (40:4)	849.8 ± 117.3	1072 ± 91.17	0.2894
PC (40:5)	4667 ± 567.8	4738 ± 343.1	0.9028
PC (40:6)	11849 ± 1837	12743 ± 929	0.2706
PC (40:7)	1588 ± 243.2	1525 ± 118.2	0.7721
PC (40:8)	553.4 ± 63.74	487.7 ± 30.72	0.3365
PC (42:10)	86.34 ± 9.16	90.90 ± 5.577	0.6526
LPE (16:0)	779.9 ± 104.4	1054 ± 43.83	<0.0001
LPE (18:0)	850.2 ± 69.3	1446 ± 58.24	<0.0001
LPE (18:1)	590.7 ± 78.21	809.7 ± 33.75	0.0003
LPE (18:2)	731.8 ± 77.95	890.3 ± 40.82	0.0190
LPE (20:4)	450.6 ± 38.46	767.6 ± 31.24	<0.0001
LPE (22:6)	415.7 ± 66.30	559.9 ± 31.18	0.0013
PE (34:1)	265.5 ± 60.03	415.2 ± 359.9	0.0004
PE (34:2)	603.8 ± 109.6	797.6 ± 54.68	0.0082
PE (36:1)	160.4 ± 28.58	324.0 ± 27.26	<0.0001
PE (36:2)	559.3 ± 66.50	929.7 ± 70.07	0.0020
PE (36:4)	1718 ± 309.6	2442 ± 163.6	0.0030
PE (38:4)	1551 ± 211.9	2636 ± 198.6	0.0004
PE (38:5)	178.1 ± 35.40	317.0 ± 23.71	<0.0001
PE (38:6)	774.8 ± 169.8	923.7 ± 74.56	0.0298
PE (40:6)	275.6 ± 65.6	367.7 ± 35.95	0.0037
Cholesterol	1441509 ± 94825	1756558 ± 47158	0.0018

Table S 7 Sphingolipid levels in human aortic tissue

Lipid species	Ctrl	AAA	p-value
S1P (d18:1)	0.0168 ± 0.0028	0.2809 ± 0.0368	<0.0001
Sphingosine (d18:1)	0.6677 ± 0.1140	5.450 ± 1.431	<0.0001
Sphinganine (d18:1)	0.1199 ± 0.0142	0.8022 ± 0.2182	0.0006
Cer (d18:1/14:0)	0.1395 ± 0.0252	0.4406 ± 0.0717	<0.0001
Cer (d18:1/16:0)	5.934 ± 0.7923	31.36 ± 5.201	<0.0001
Cer (d18:1/18:0)	0.6006 ± 0.077	2.092 ± 0.2871	<0.0001
Cer (d18:1/20:0)	0.7079 ± 0.0886	2.338 ± 0.2834	<0.0001
Cer (d18:1/22:0)	3.511 ± 0.5554	11.66 ± 1.399	<0.0001
Cer (d18:1/24:0)	11.48 ± 1.769	32.12 ± 3.784	<0.0001
Cer (d18:1/24:1)	4.823 ± 0.6412	21.73 ± 2.271	<0.0001
dhCer (d18:0/16:0)	0.3379 ± 0.0402	1.417 ± 0.1710	<0.0001
dhCer (d18:0/18:0)	0.0998 ± 0.0282	0.5223 ± 0.0620	<0.0001
dhCer (d18:0/24:0)	0.1122 ± 0.033	0.7194 ± 0.079	<0.0001
dhCer (d18:0/24:1)	0.0695 ± 0.0167	0.5143 ± 0.08	0.0008
SM (d18:1/14:0)	74.33 ± 9.406	196.0 ± 18.01	<0.0001
SM (d18:1/14:1)	5.450 ± 0.7281	5.728 ± 0.5491	0.8451
SM (d18:1/16:0)	103.1±11.25	150.8 ± 20.57	0.4267
SM (d18:1/16:1)	17.77 ± 1.985	21.73 ± 2.228	0.4403
SM (d18:1/18:0)	95.64 ± 11.78	166.5 ± 13.85	0.0012
SM (d18:1/18:1)	37.69 ± 4.686	57.36 ± 5.067	0.0129
SM (d18:1/20:0)	19.38 ± 4.352	53.28 ± 5.836	0.0001
SM (d18:1/20:5)	0.1964 ± 0.0227	0.6108 ± 0.0830	<0.0001
SM (d18:1/22:0)	30.32 ± 4.004	77.18 ± 6.179	<0.0001
SM (d18:1/22:1)	18.39 ± 2.321	43.45 ± 3.769	<0.0001
SM (d18:1/22:6)	1.817 ± 0.2217	2.659 ± 0.3116	0.1172
SM (d18:1/24:0)	19.76 ± 2.123	39.67 ± 3.270	<0.0001
SM (d18:1/24:1)	19.28 ± 2.228	50.07 ± 4.403	<0.0001
LPC (14:0)	0.1694 ± 0.0311	0.7028 ± 0.0926	<0.0001
LPC (16:0)	20.81 ± 5.332	80.27 ± 7.704	<0.0001
LPC (18:0)	13.02 ± 3.986	56.51 ± 5.997	<0.0001
LPC (18:1)	6.595 ± 1.323	25.32 ± 3.077	<0.0001
LPC (18:2)	2.325 ± 0.5960	12.61 ± 2.191	<0.0001
LPC (20:0)	0.057 ± 0.0195	0.3754 ± 0.0398	<0.0001
LPC (20:1)	0.1400 ± 0.0331	0.6362 ± 0.067	<0.0001
LPC (20:2)	0.1240 ± 0.0356	0.5241 ± 0.0702	<0.0001
LPC (20:3)	0.3238 ± 0.0849	1.207 ± 0.1830	<0.0001
LPC (20:4)	0.9182 ± 0.1306	2.492 ± 0.2981	<0.0001
LPC (22:6)	1.466 ± 0.2908	5.328 ± 0.7414	<0.0001

PC (28:0)	0.2844 ± 0.035	0.6008 ± 0.0526	0.0005
PC (30:0)	5.295 ± 0.705	13.44 ± 1.459	<0.0001
PC (30:2)	24.78 ± 3.931	19.15 ± 2.131	0.2075
PC (32:0)	67.04 ± 6.439	126.8 ± 13.98	0.0104
PC (32:1)	23.73 ± 2.218	33.67 ± 3.994	0.1236
PC (34:1)	212.8 ± 18.44	206.6 ± 21.64	0.5730
PC (34:2)	94.10 ± 12.00	169.3 ± 15.24	0.0040
PC (34:4)	0.5098 ± 0.0539	0.8825 ± 0.1105	0.0378
PC (36:1)	62.07 ± 5.334	78.97 ± 7.908	0.3045
PC (36:2)	63.63 ± 7.138	121.4 ± 11.24	0.0016
PC (36:3)	11.15 ± 1.633	36.59 ± 3.706	<0.0001
PC (36:4)	106.8 ± 9.15	123.6 ± 14.28	0.3385
PC (36:5)	2.463 ± 0.3815	7.632 ± 1.267	0.0027
PC (38:1)	19.78 ± 2.621	27.19 ± 2.384	0.1118
PC (38:3)	14.04 ± 1.695	24.08 ± 2.727	0.0257
PC (38:4)	113.5 ± 8.643	139.9 ± 14.14	0.3155
PC (38:5)	7.652 ± 0.7383	13.04 ± 1.417	0.0204
PC (38:6)	20.34 ± 3.011	46.42 ± 6.057	0.0045
PC (40:4)	21.95 ± 2.047	14.37 ± 1.440	0.0053
PC (40:5)	13.30 ± 1.077	19.49 ± 1.890	0.0449
PC (40:6)	16.75 ± 1.801	30.65 ± 3.864	0.0271
PC (40:7)	2.608 ± 0.2295	7.191 ± 0.8711	0.0003
PC (40:8)	1.175 ± 0.1325	2.954 ± 0.3367	0.0007
PC (42:10)	0.2792 ± 0.024	0.5992 ± 0.0902	0.0251
Cholesterol	4889 ± 668.4	16210 ± 1561	<0.0001

Protocol 1: H&E

Detailed staining protocol for H&E:

Xylol	10 min
Xylol	10 min
Xylol	10 min
Xylol	1 min
100% EtOH	1 min
100% EtOH	1 min
96% EtOH	1 min
96% EtOH	1 min
70% EtOH	1 min
Aqua dest.	1 min
Mayer's hematoxylin	1 min

Rinsing under running tap water for 10 min to ensure bluing of the nuclei

Aqua dest.	1min
1% Eosin	1min
Aqua dest.	30 s
Aqua dest.	30 s
70% EtOH	30 s
70% EtOH	30 s
70% EtOH	1 min
96% EtOH	1 min
96% EtOH	1 min
100% EtOH	1 min
100% EtOH	1 min
Xylol	1 min

Mounting

Protocol 2: Elastica van Gieson

Detailed staining protocol for Elastica van Gieson:

Xylol	10 min
Xylol	10 min
Xylol	10 min
Xylol	1 min
100% EtOH	1 min
100% EtOH	1 min
96% EtOH	1 min
70% EtOH	1 min
Aqua dest.	1 min
Verhoeff's Solution	1 h
Rinsing under running tap	for 3 min
2% ferric chloride	2 min
Water	3x 1 min
5% Sodium thiosulfate	1 min
Rinsing under running tap	for 5 min
Van Gieson Solution	5 min
Aqua dest.	
70% EtOH	1 min
70% EtOH	1 min
96% EtOH	1 min
100% EtOH	1 min
100% EtOH	1 min
Xylol	1 min
Mounting	

Protocol 3: Vascular smooth muscle cells

Detailed staining protocol for vascular smooth muscle cells:

Xylol	10 min
Xylol	10 min
Xylol	10 min
Xylol	1 min
100% EtOH	1 min
100% EtOH	1 min
96% EtOH	1 min
96% EtOH	1 min
70% EtOH	1 min
Aqua dest.	1 min
PBS	5 min
3% Hydrogen peroxide	10 min
Washed in PBS (3x)	
3% Normal serum block	15 min
Washed in PBS (3x)	
Primary antibody incubation	overnight
Washed in PBS (3x)	
Secondary antibody incubation	1 h
Washed in PBS (3x)	
Streptavidin-conjugated horseradish peroxidase in PBS for 1 h	
Washed in PBS (3x)	
DAB working solution	10 min
Washed in PBS (3x)	
Mayer’s hematoxylin	5 min
Rinsing under running tap for 15 min	
70% EtOH	1 min
96% EtOH	1 min
96% EtOH	1 min
100% EtOH	1 min
100% EtOH	1 min
Xylol	1 min
Mounting	

8.1. Curriculum vitae

PERSONAL DETAILS

Name:	Nathalie Hannelore Schröder
Date of birth:	16/10/1992
Place of birth:	Kyritz
E-Mail:	nathaliehannelore.schroeder@med.uni-duesseldorf.de
Nationality:	German

RESEARCH AND PROFESSIONAL EXPERIENCE

10/2018 – present	Heinrich-Heine University Düsseldorf Institute for Molecular Medicine III PhD thesis: The role of sphingosine-1-phosphate signaling in aortic aneurysm formation Supervisor: Prof. Dr. Bodo Levkau
10/2016 – 10/2018	Friedrich Schiller University Jena Course of studies: Molecular Medicine (M.Sc.) Master thesis: The effect of low dose epirubicin on neutrophils Supervisor: Prof. Dr. Markus H. Gräler
10/2012 – 09/2016	Friedrich Schiller University Jena Course of studies: Biochemistry/Molecular Biology (B.Sc.) Bachelor thesis: Die protektive Rolle der DNA-Schadensantwort nach genotoxischem Stress unter inflammatorischen Bedingungen Supervisor: Prof. Dr. Markus H. Gräler

EDUCATION

08/2005 – 06/2012	Gymnasium Wittstock (Dosse) Qualification: A-level

Düsseldorf, October 25 _____

PUBLICATIONS

1. Benkhoff M, Vogt J, **Schröder NH**, Hu H, Dannenberg L, Keul P, Mourikis P, Zeus T, Wollnitzke P, Kelm M, Levkau B, Polzin A. S1P-Loading of CAD-HDL Restored Impaired HDL-Mediated Cardioprotection. Circ Res. 2025 Oct 3. doi: 10.1161/CIRCRESAHA.125.327041. Epub ahead of print. PMID: 41042164.

2. Weske S, Nowak MK, Zaufel A, Esser L, Peter C, Walz L, Kühn H, Wolde T, Hoppe J, **Schröder NH**, Buschmann T, Wollnitzke P, Levkau B. Intracellular Sphingosine-1-Phosphate Induces Lipolysis Through Direct Activation of Protein Kinase C Zeta. FASEB J. 2025 Apr 15;39(7):e70528. doi: 10.1096/fj.202403272R. Erratum in: FASEB J. 2025 Jun 15;39(11):e70692. doi: 10.1096/fj.202501754. PMID: 40193069; PMCID: PMC11975168.

3. Duse DA, **Schröder NH**, Srivastava T, Benkhoff M, Vogt J, Nowak MK, Funk F, Semleit N, Wollnitzke P, Erkens R, Kötter S, Meuth SG, Keul P, Santos W, Polzin A, Kelm M, Krüger M, Schmitt J, Levkau B. Deficiency of the sphingosine-1-phosphate (S1P) transporter Mfsd2b protects the heart against hypertension-induced cardiac remodeling by suppressing the L-type-Ca2+ channel. Basic Res Cardiol. 2024 Oct;119(5):853-868. doi: 10.1007/s00395-024-01073-x. Epub 2024 Aug 7. PMID: 39110173; PMCID: PMC11461684.

4. Wille A, Weske S, von Wnuck Lipinski K, Wollnitzke P, **Schröder NH**, Thomas N, Nowak MK, Deister-Jonas J, Behr B, Keul P, Levkau B. Sphingosine-1-phosphate promotes osteogenesis by stimulating osteoblast growth and neovascularization in a vascular endothelial growth factor-dependent manner. J Bone Miner Res. 2024 Apr 19;39(3):357-372. doi: 10.1093/jbmr/zjae006. PMID: 38477738; PMCID: PMC11240155.

5. Thomas N, **Schröder NH***, Nowak MK, Wollnitzke P, Ghaderi S, von Wnuck Lipinski K, Wille A, Deister-Jonas J, Vogt J, Gräler MH, Dannenberg L, Buschmann T, Westhoff P, Polzin A, Kelm M, Keul P, Weske S, Levkau B. Sphingosine-1-phosphate suppresses GLUT activity through PP2A and counteracts hyperglycemia in diabetic red blood cells. Nat Commun. 2023 Dec 14;14(1):8329. doi: 10.1038/s41467-023-44109-x. PMID: 38097610; PMCID: PMC10721873.
   *contributed equally

6. Polzin, A., Dannenberg, L., Benkhoff, M.; **Schröder NH** et al. Revealing concealed cardioprotection by platelet Mfsd2b-released S1P in human and murine myocardial infarction. Nat Commun 14, 2404 (2023). https://doi.org/10.1038/s41467-023-38069-5

7. Keul P, Peters S, von Wnuck Lipinski K, **Schröder NH**, Nowak MK, Duse DA, Polzin A, Weske S, Gräler MH, Levkau B. Sphingosine-1-Phosphate (S1P) Lyase Inhibition Aggravates Atherosclerosis and Induces Plaque Rupture in ApoE−/− Mice. International Journal of Molecular Sciences. 2022; 23(17):9606. doi.org/10.3390/ijms23179606

8. A Polzin, L Dannenberg; **NH Schröder** et al. Impaired Cardioprotection by HDL in CAD and Diabetes in Ischemia/Reperfusion Injury: role of S1P and SR-BI, European Heart

Journal, Volume 43, Issue Supplement_2, October 2022, ehac544.2913, https://doi.org/10.1093/eurheartj/ehac544.2913

9. Weigel C, Hüttner SS, Ludwig K, Krieg N, Hofmann S, **Schröder NH**, Robbe L, Kluge S, Nierhaus A, Winkler MS, Rubio I, von Maltzahn J, Spiegel S, Gräler MH. S1P lyase inhibition protects against sepsis by promoting disease tolerance via the S1P/S1PR3 axis. EBioMedicine. 2020 Aug; 58:102898. doi: 10.1016/j.ebiom.2020.102898. Epub 2020 Jul 22. PMID: 32711251; PMCID: PMC7381498.

10. **NH Schröder**, C Weigel, MH Graeler. The protective role of sphingosine 1-phosphate in genotoxic stress induced DNA damage response in inflammation. "8th international congress “sepsis and multiorgan dysfunction”." Infection 45(1): 1-66.

SCIENTIFIC PRESENTATIONS AND INVITED TALKS

Invited talks

2025 Sphingosine-1-phosphate in abdominal aortic aneurysms, DGK Herztage, Hamburg, Germany

Selected oral presentations

2025 Sphingosine-1-phosphate in aortic aneurysm disease: a biomarker and therapeutic target, FASEB Conference Lipid Mediators: Advancements and Approaches, Malahide, Ireland

Sphingosine-1-phosphate in the pathogenesis of human and mouse aneurysms: a biomarker and causal player, 91st Annual Conference of the German Society of Cardiologists (DGK), Mannheim, Germany

2023 Tonic Sphingosine-1-phosphate (S1P)/S1P receptor 3 signaling in vascular smooth muscle cells promotes aortic aneurysm rupture, FASEB Conference Lysophospholipids and related mediators, Melbourne, Florida, USA

Tonic Sphingosine-1-phosphate (S1P)/S1P receptor 3 signaling in vascular smooth cells promotes aortic dissection and rupture, 89th Annual Conference of the German Society of Cardiologists (DGK), Mannheim, Germany

2019 Dissection and rupture of aortic aneurysms after inhibition of Sphingosine 1-phosphate lyase, FASEB Conference Lysophospholipids and Related Mediators: From Bench to Clinic, Lisbon, Portugal

Dissection and rupture of aortic aneurysms after inhibition of Sphingosine 1-phosphate lyase, 85th Annual Conference of the German Society of Cardiologists (DGK), Mannheim, Germany

Selected poster presentations

2024 Tonic Sphingosine-1-phosphate receptor 3 signaling in vascular smooth muscle cells promotes aortic aneurysm rupture, International Vascular Biology Meeting (IVBM), Amsterdam, Netherlands

Sphingosine-1-phosphate receptor 3 (S1PR3) signaling in vascular smooth muscle cells as a target to stabilize aortic aneurysm and dissection, 90th Annual Conference of the German Society of Cardiologists (DGK), Mannheim, Germany

2023 Tonic Sphingosine-1-phosphate (S1P)/S1P receptor 3 signaling in vascular smooth muscle cells promotes aortic aneurysm rupture, FASEB Conference Lysophospholipids and related mediators, Melbourne, Florida, USA

2022 Sphingosine-1-phosphate signaling in aortic aneurysm formation and dissection, 88th Annual Conference of the German Society of Cardiologists (DGK), Mannheim, Germany

2019 Dissection and rupture of aortic aneurysms after inhibition of Sphingosine 1-phosphate lyase, FASEB Conference Lysophospholipids and Related Mediators: From Bench to Clinic, Lisbon, Portugal

2017 The protective role of sphingosine 1-phosphate in genotoxic stress induced DNA damage response in inflammation, 8th International Congress Sepsis and Multiorgan Dysfunction, Weimar, Germany

AWARDS & GRANTS

2025 Young Investigator Award, FASEB Conference Lipid Mediators: Advancements and Approaches, Malahide, Ireland

2025 Rising Star Award, TRR259, DFG-funded; 10,000 €

Travel Award, 91st Annual Conference of the German Society of Cardiologists (DGK)

2024 Starting Grant for Female Scientists, TRR259, DFG-funded, 10,000 €

Poster Award, 90th Annual Conference of the German Society of Cardiologists (DGK)

Travel Award, 90th Annual Conference of the German Society of Cardiologists (DGK)

2023 Poster Award, FASEB Conference Lysophospholipids and related mediators

Travel Award, FASEB Conference Lysophospholipids and related mediators

2022 Abstract Award for Clinical Lipid Research of the German Society of Cardiologists (DGK), 88th Annual Conference of the German Society of Cardiologists (DGK)

2019 Travel Award, 85th Annual Conference of the German Society of Cardiologists (DGK)

Düsseldorf, October 25 _____

8.2. Contributions

Nathalie Hannelore Schröder was responsible for the planning, execution, analysis and interpretation of the experimental work within this thesis, under the supervision and guidance of Prof. Dr. Bodo Levkau. This included the development of the experimental strategy, execution of all *in vitro* and *in vivo* experiments, data analysis, and preparation of figures and manuscripts. The results presented in this dissertation are currently being implemented into a manuscript, and selected figures and data will be included in the forthcoming publication.

An overview of individual contributions and collaborations is provided below:

- Vascular reactivity studies: Equally performed by Dr. Dragos A. Duse and Nathalie Hannelore Schröder
- Immunohistochemistry: Tissue processing and staining by Rabia Taskesen; EvG staining and analysis by Klaus Kaiser, microscopic imaging and analysis by Nathalie Hannelore Schröder.
- RNA Sequencing: RNA isolation and sample preparation by Nathalie Hannelore Schröder; library preparation, sequencing, and initial data processing, by the Genomics & Transcriptomics Laboratory of Heinrich-Heine-University Düsseldorf; downstream analysis and interpretation by Nathalie Hannelore Schröder.
- Proteomics: Sample processing, mass spectrometry analysis and quantification by the Molecular Proteomics Laboratory of the Biomedical Research Center (BMFZ) of the Heinrich-Heine-University Düsseldorf; downstream analysis and interpretation by Nathalie Hannelore Schröder.
- LC/MS-MS Measurements: Sample preparation by Nathalie Hannelore Schröder; measurement and initial analysis by Dr. Philipp Wollnitzke and Dr. Hannah Siera; final data analysis and interpretation by Nathalie Hannelore Schröder.
- Human sample collection: Conduced and processed by staff members of the Clinic for Thoracic and Vascular Surgery (University Hospital Düsseldorf), the Clinic for Cardiovascular Surgery (University Hospital Düsseldorf) or the Section for Vascular and Endovascular Surgery (University Hospital Essen).

Stylistic assistance using AI-based tools (ChatGPT, Grammarly) was limited to language editing. All scientific ideas and reasoning presented in this thesis are the author's own.

Düsseldorf, October 25 _____

8.3. Affidavit

I hereby declare under oath that I prepared this dissertation independently and without unauthorized assistance from third parties, in accordance with the Principles for the Safeguarding of Good Scientific Practice at Heinrich Heine University Düsseldorf. I further confirm that this dissertation has neither been submitted, in whole or in part, in identical or similar form, to any other university or examination authority. Moreover, I have not previously made any unsuccessful attempt to obtain a doctoral degree.

Düsseldorf, October 25 _____

8.4. Acknowledgements

I would like to express my deepest gratitude to my supervisor Prof. Dr. Bodo Levkau, who offered me the opportunity to work on that project, and for his unwavering support throughout my PhD journey. His critical insights, scientific guidance and thoughtful advice have greatly shaped the way of my scientific thinking and working. Thank you for being such a supportive mentor.

I am also very thankful to Prof. Dr. Hubert Schelzig for being part of my thesis committee and for the opportunity to present and discuss my project in his clinical environment. I truly want to thank you for your constant willingness to offer your support.

A heartfelt thank you goes to Dr. Dragos A. Duse, whose selfless commitment and support have shaped this project in many important ways. You not only introduced me to the wire myograph and helped me master it with great patience, but also dedicated your time and expertise to this project with remarkable selflessness; something I truly value and will always be grateful for. Thank you for all that I was able to learn from you: for your patience, your clarity in solving problems, and for the many thoughtful discussions we had while making sense of our data together. I'm especially grateful for the way you always found the right words to encourage me when things became difficult. Your support has meant a great deal to me; both on a scientific and personal level.

Grateful thanks to the TRR259 consortium for the opportunity to be part of this outstanding scientific network. Being included in this collaborative environment has allowed me to learn from many inspiring researchers, and I am deeply thankful for the numerous opportunities and generous support that have accompanied me throughout this stage of my career.

I would like to thank Dr. Elvira Weber, Dr. Wiebke Ibing, and Martin Lainka for providing essential biological samples of aortic aneurysm patients. Your generous contribution laid the foundation for key parts of this study and greatly enhanced its scientific depth and relevance.

Many thanks go to Dr. Philipp Wollnitzke, Hannah Siera, and Nina Semleit for performing the mass spectrometry analyses. Their careful and precise work formed a critical foundation for key findings in this thesis.

I would like to sincerely thank Dr. Petra Keul and Dr. Sarah Weske for their constant support, helpful advice, and honest feedback on my work.

To Nadine, Annalena, Melissa, Jenni, Julia, Tobias and Alex; thank you for sharing this PhD journey with me. Your encouragement, teamwork, and empathy have been invaluable. I am truly grateful for the time we spent together and the many ways in which we supported each other along the way. There are so many moments I'm thankful for. You made so many things lighter and easier than they would have been otherwise.

I would also like to thank Kerstin Putzke and Rabia Taskesen for their indispensable technical support and commitment, which contributed greatly to the practical realization of this project.

Finally, I owe my deepest gratitude to my family and friends for their unconditional support, patience, and belief in me throughout the entire years. Thank you all for your encouragement and understanding.